

Tectono-sedimentary history of the Forlandsundet Graben

New insights from Sarsøyra, Western Spitsbergen

Niklas Wilko Schaaf



Master Thesis

Geosciences

60 credits

Department of Geosciences

Faculty of Mathematics and Natural Sciences

UNIVERSITY OF OSLO

in cooperation with

Department of Arctic Geology

THE UNIVERSITY CENTRE IN SVALBARD

December 2018

Tectono-sedimentary history of the Forlandsundet Graben

New insights from Sarsøyra, Western Spitsbergen

Niklas Wilko Schaaf

supervised by

Per Terje Osmundsen

and

Kim Senger



View from Dahltoppen onto Sarsøyra, Forlandsundet and Prins Karls Forland. Image courtesy Erik Kuschel.

© Niklas Wilko Schaaf

2018

Tectono-sedimentary history of the Forlandsundet Graben

Niklas Wilko Schaaf

<http://www.duo.uio.no/>

Print: Reprosentralen, Universitetet i Oslo

Abstract

The Forlandsundet Graben is an understudied Paleogene sedimentary basin, located between the islands Spitsbergen and Prins Karls Forland that belong to the Svalbard Archipelago. It represents a unique opportunity to study the evolution of the western Svalbard margin from a transpressional fold-and-thrust belt into a sharply tapered transform margin during the Cenozoic. The basin is bound by a N-S trending fault zone in the east and exhibits a half-graben to graben geometry. The bounding lineaments crosscut the structures of the Paleocene-Eocene West Spitsbergen fold-and-thrust-belt, suggesting an Oligocene age for at least parts of the Forlandsundet Graben, albeit age-relationships are debated.

This thesis is based on sedimentological and structural field data collected during two field seasons on Sarsøyra, a strandflat along the eastern basin boundary. Here, the two youngest sedimentary units of the Forlandsundet Graben, namely the Sarsbukta and Sarstangen Formations, are exposed. In total, 370 m of to date largely undescribed sedimentary sections were measured and a detailed assessment of the sedimentary architecture is provided. Also, the contact relationships between the sedimentary basin fill and the adjacent metamorphic basement were documented. The structural database includes kinematic measurements (~500) from basement and the sedimentary units. The field observations are supplemented with subsurface data and discussed in the light of low temperature geochronology and paleolimnology data collected under the project and kindly provided by the respective authors.

The results are used to construct a tectono-sedimentary model of Sarsøyra and suggest that reverse faulting affected the eastern basin boundary at 53.5 Ma followed by oblique normal faulting. The sedimentary units on Sarsøyra were deposited during two phases of oblique, northwest directed rifting. The Sarsbukta Formation records interfingering of alluvial fans and fluvial deposits that were affected by transtensional folding as well as faulting. Afterwards, the Sarstangen Formation was deposited along a major intrabasinal normal fault as fan delta succession. New paleolimnological analyses suggest an Early to Middle Oligocene age for the Sarstangen Formation.

The findings are synthesized into two tectono-thermal end-member models for the evolution of the Forlandsundet Graben as a whole. The first model considers that the Forlandsundet Graben experienced a multiphase deformation history, consisting of contraction followed by transtension. The second model explores whether the Forlandsundet Graben could have formed in a purely transtensional setting along with the exhumation of a metamorphic core complex on Prins Karls Forland.

Further research is suggested to better constrain the evolution of the Forlandsundet Graben as it represents a rare onshore analogue to the offshore basins of the Svalbard margin and transform margins elsewhere.

Acknowledgements

This project initiated on a scientific cruise in the Forlandsundet area, conducted by personnel of the Norwegian Geological Survey in summer 2016. I would like to acknowledge the people and institutions that have since then supported my work:

First and foremost, I want to thank my supervisors Per Terje Osmundsen and Kim Senger for their guidance and mentorship. Their input and support made this project possible and improved my work significantly.



Per Terje teaching how to take fieldnotes like a pro. Image curtesy Erik Kuschel.

A huge ‘thank you’ goes to my dear friends Julian Janocha, Kristine Larsen, Tim Hake and Erik Kuschel that not only assisted with the data acquisition in the field but also took care of the meal preparation and polar bear protection.

Without Jan Peachar, the staff of the Czech „Josef Svoboda Station“, Jurek Róžański and their respective sailing vessels, access to the field area would have been much harder. UNIS Logistics and, especially Sara Mollie Cohen, are acknowledged for the supply with equipment and their helpful advice.

Also, I would like to thank the scientists that contributed with their analyses and sample preparations to this thesis; namely, Roelant van der Lelij, Jasmin Schönenberger, Olaf Lenz, Tim Redfield and Salahalldin Akhavan.

I am grateful to the Svalbard Science Forum that provided the primary funding for both field campaigns through Arctic Field Grants. In addition, the University of Oslo, the Research Centre for Arctic Petroleum Exploration and the Geological Survey of Norway supported the project. At this point, I would also like to thank the institutions that sponsored my studies through scholarships.

To the wonderful friends I have made during the last six years of studying geology: Thank you for the great time! I am amazed by the warm welcome, every time I return to Potsdam, and with the Svalbardpirates I will always connect the adventures of a lifetime. That Kristine x2 and Gøystein also ended up writing their theses on Svalbard was the ‘icing on the cake’.

Thanks to Kik for cheering me up during the past months and lending me a second pair of eyes on the hunt for typos and missing commas.

Most importantly, I want to thank my family, especially my parents, for their loving support.

Table of Content

| | |
|---|-----------|
| ABSTRACT..... | IV |
| ACKNOWLEDGEMENTS..... | V |
| TABLE OF CONTENT | VIII |
| 1 INTRODUCTION..... | 1 |
| 1.1 AIMS AND OBJECTIVES | 3 |
| 1.2 GEOLOGICAL BACKGROUND | 4 |
| 1.2.1 <i>Passive margins</i> | 4 |
| 1.2.2 <i>Geological evolution of Svalbard</i> | 6 |
| 1.2.3 <i>Opening of the north Atlantic and the Eureka orogeny</i> | 9 |
| 1.2.4 <i>Geological setting of the Forlandsundet Graben</i> | 13 |
| 1.2.5 <i>The Forlandsundet Graben</i> | 14 |
| 1.2.6 <i>Field area</i> | 17 |
| 2 DATA AND METHODS..... | 22 |
| 2.1 DATA COLLECTION IN THE FIELD | 22 |
| 2.2 THIN SECTION ANALYSIS | 23 |
| 2.3 PALEOLIMNOLOGY | 23 |
| 2.4 K-AR DATING OF THE FAULT GOUGE..... | 24 |
| 2.5 SUBSURFACE DATA..... | 24 |
| 3 SEDIMENTOLOGY | 26 |
| 3.1 SARSBUKTA FORMATION | 26 |
| 3.1.1 <i>Lithofacies</i> | 26 |
| 3.1.2 <i>Lithofacies associations</i> | 34 |
| 3.1.3 <i>Summary</i> | 46 |
| 3.2 SARSTANGEN FORMATION | 47 |
| 3.2.1 <i>Lithofacies</i> | 47 |
| 3.2.2 <i>Lithofacies associations</i> | 51 |
| 3.3 PALEOFLOW INDICATORS..... | 58 |
| 3.4 PALEOLIMNOLOGY | 59 |
| 4 STRUCTURAL GEOLOGY..... | 60 |
| 4.1 DESCRIPTION OF THE BASIN-BOUNDING FAULT ZONE | 60 |
| 4.1.1 <i>Contact zone in central Sarsøyra</i> | 61 |
| 4.1.2 <i>Contact zone in northern Sarsøyra</i> | 64 |
| 4.1.3 <i>K-Ar ages of the fault gouge</i> | 69 |
| 4.2 STRUCTURAL DATA FROM THE PALEOGENE SEDIMENTS | 69 |
| 4.2.1 <i>Fractured clasts</i> | 69 |
| 4.2.2 <i>Faulting</i> | 70 |
| 4.2.3 <i>Folding</i> | 71 |
| 4.3 INTERPRETATION | 72 |
| 5 SUBSURFACE DATA | 76 |
| 5.1.1 <i>7811/5-1 Sarstangen petroleum exploration well</i> | 76 |
| 5.1.2 <i>Gravity and magnetic anomalies</i> | 76 |

| | | |
|----------|---|------------|
| 5.1.3 | <i>Seismic data</i> | 77 |
| 6 | DISCUSSION | 82 |
| 6.1 | TECTONO-SEDIMENTARY EVOLUTION OF SARSØYRA..... | 82 |
| 6.1.1 | <i>Tectono-sedimentary constrains</i> | 84 |
| 6.1.2 | <i>Deformation sequence</i> | 88 |
| 6.1.3 | <i>Updated tectono-sedimentary model of Sarsøyra</i> | 90 |
| 6.2 | EVOLUTION OF THE FORLANDSUNDET GRABEN..... | 93 |
| 6.2.1 | <i>Model for the tectono-thermal evolution of the Forlandsundet Graben</i> | 100 |
| 6.2.2 | <i>Multi-stage model</i> | 101 |
| 6.2.3 | <i>Purely transtensional model</i> | 103 |
| 6.2.4 | <i>Comparison of the basin models</i> | 107 |
| 6.2.5 | <i>Regional Implications</i> | 108 |
| 6.2.6 | <i>The Forlandsundet Graben in the context of (transform) rifted margin evolution</i> | 109 |
| 7 | CONCLUSIONS | 111 |
| | REFERENCES | 112 |
| | APPENDIX | 129 |
| | LOGS (NORTHERN BEACH) | 129 |
| | <i>Northeastern log</i> | 129 |
| | <i>Middle log</i> | 141 |
| | <i>Southwestern log</i> | 150 |
| | PALEOLIMNOLOGY..... | 153 |
| | K-AR DATING OF THE FAULT GOUGE | 165 |
| | APATITE AND ZIRCON FISSION TRACK | 168 |
| | COMPOSITE LOG OF THE 7811/5-1 SARSTANGEN PETROLEUM EXPLORATION WELL..... | 169 |
| | ABSTRACT NGF WINTERMEETING 2019..... | 173 |

1 Introduction

Following the evolution of the West Spitsbergen Fold and Thrust Belt (WSFB), the opening of the Greenland Sea initiated the formation of the Barents Sea and Svalbard margins during the Cenozoic (Braathen et al., 1999; Buitter and Torsvik, 2014; CASE Team, 2001; Dallmann, 2015; Faleide et al., 2008; Piepjohn et al., 2016; Tessensohn and Piepjohn, 2000). The transform margin of Svalbard and the Barents Sea developed along the De Geer Zone megashear system during late Cretaceous-Paleocene rifting and breakup of the northernmost Atlantic (Faleide et al., 2008). With 1500 km length it is one of the longest transform margin segments in the world (Blinova et al., 2009). The tectonic events of the Cenozoic era left a lasting imprint in the structural and sedimentary records of Svalbard's geology that is not yet fully understood (Dallmann, 2015). Especially, the geological history of the Forlandsundet Graben remains enigmatic.

The Forlandsundet Graben is the exposed part of an array of basins that are banked against the transform margin of the Western Barents Sea (Blinova et al., 2009; Eidvin et al., 2014; Faleide et al., 2008, 1993; Kristensen et al., 2017; Ritzmann et al., 2004). Therefore, it represents a rare onshore analogue for these offshore basins, as well as, other basins that evolved in the necking domains of a transform margins elsewhere.

The Forlandsundet Graben with surrounding structures and basement rocks is exposed at the western edge of the Svalbard archipelago, about 100 km east from the Knipovitch and Molloy Ridge segments. The site represents a critical location for the reconstruction of the west Svalbard margin evolution from a transpressional fold-and-thrust belt to a sharply tapered rifted margin (Braathen et al., 1999; Gabrielsen et al., 1992; Kleinspehn and Teyssier, 2016, 1992; Ritzmann et al., 2004; Steel et al., 1985). The Forlandsundet Graben presents a series of unresolved structural, sedimentological and geochronological problems that so far received limited scientific attention. With one or two exceptions, the few existing studies are mostly older than 20 years, as well as inconsistent with respect to their interpretation of age, deformation history and sedimentological evolution.

The tectonic and sedimentary evolution of the Eocene-Oligocene Forlandsundet Graben and its relation to the WSFB is complex. It has been proposed that it formed as a much broader basin in an unknown tectonic setting (Kleinspehn and Teyssier, 2016, 1992). The present half-

graben geometry and cross-cutting relationships to the WSFB (Hjelle et al., 1999; Ritzmann et al., 2004) are interpreted to be associated with crustal thinning related to the final stages of opening in the Norwegian-Greenland Sea (Gabrielsen et al., 1992; Kleinspehn and Teyssier, 2016, 1992; Steel et al., 1985). However, contractional structures have been identified within the basin (Blinova et al., 2009; Gabrielsen et al., 1992; Lepvrier, 1990; Rye-Larsen, 1982; von Gosen and Peach, 2001). This highlights the necessity to explain the coexistence of contractional and extensional structures (Gabrielsen et al., 1992; Kleinspehn and Teyssier, 1992; Steel et al., 1985). It has been suggested that parts of the basin formation overlapped with the formation of the WSFB and thus in part with foreland basin deposition in central Spitsbergen (Kleinspehn and Teyssier, 2016; Steel et al., 1985; von Gosen and Peach, 2001). But due to poor and inconsistent age constraints on the sedimentary deposits, as well as structures, the nature and sequence of tectonic events remains largely unresolved. The proposed depositional ages range from Eocene to Late Oligocene (Čepek, 2001; Eidvin et al., 2014, 1998; Feyling-Hanssen and Ulleberg, 1984; Lehmann et al., 1978; Livsic, 1992, 1974, Manum, 1962, 1960; Manum and Throndsen, 1986) but Eidvin et al. (2014) suggested that Eocene fossils reported by Manum and Throndsen (1986) were redeposited, indicating a large uncertainty in the depositional ages.

The Moho rises sharply under western Spitsbergen and westwards towards the Knipovitch and Molloy Ridges (Faleide et al., 2008; Ritzmann et al., 2004) and implies that the area of the Forlandsundet Graben represents the inner edge of a so-called necking domain, the part of rifted margins where the continental crust is thinned the most (cf. Peron-Pinvidic et al., 2013). Osmundsen and Péron-Pinvidic (2018) documented that crustal scale normal faulting can induce the exhumation of metamorphic core complexes within the necking domain of passive margins (see also Kapp et al., 2008). Kleinspehn and Teyssier (1992) speculated that Prins Karls Forland represents a metamorphic core complex but this possibility has not been investigated by later work. However, recent publications by Barnes and Schneider (2018) and Schneider et al. (2018) offer new insights into the thermal and exhumation history of basement rocks from Prins Karls Forland and should be discussed against the existing basin models.

1.1 Aims and objectives

This study focuses on the sedimentological and structural characterization of the youngest basin infill of the Forlandsundet Graben. The strata are exposed in the Sarsøyra area along the eastern basin margin. On the basis of field data, supplemented with subsurface and new geochronological data, the study provides an improved documentation of the sedimentology and structural geology on Sarsøyra, as well as a better understanding of the tectono-sedimentary evolution of the Forlandsundet Graben as a whole. Hence, the thesis aims to:

- Document the Paleogene sedimentary successions on Sarsøyra and their contact relationship to the adjacent basement rocks.
- Characterize the structural geology and deformation sequence on Sarsøyra.
- Integrate the existing seismic and well data from the Forlandsundet Graben.
- Develop a tectono-sedimentary model for the sedimentary successions on Sarsøyra.
- Compare the deformation pattern between the eastern and the western side of the basin.
- Discuss the results of this study against previously published results, and discuss their implications with respect to conceptual basin evolution models of the Forlandsundet Graben.

In the next section, an introduction to geological concepts, the geological history of Svalbard and the Forlandsundet Graben is provided, followed by a brief description of the utilized methods. Subsequently, the results from the field campaigns on Sarsøyra and the interpretation of subsurface data are presented. The thesis concludes with a discussion of the results and a summary of the key findings.

1.2 Geological background

1.2.1 Passive margins

Passive margins develop when continental rifts extend so far that the continental crust breaks and oceanic crust is formed. While rifting continues in the oceanic domain, a continental margin prevails on either side of the rift (Franke, 2013; Peron-Pinvidic et al., 2013).

Two end-members of passive margins can be distinguished, orthogonal rifted margins and transform margins. Orthogonal rifted margins characterizes that the extension direction is oriented perpendicular to the strike of the margin. Transform margins, on the other hand, are associated with strike-slip faults that cut upper and lower crust, so called transform faults (Wilson, 1985 as cited in Basile, 2015), and extension parallel to the strike of the margin. Naturally, a large portion of passive margins fall between the two end-members and so called oblique rifted margins occur where the extension direction is neither perpendicular nor parallel to the margin strike (Agostini et al., 2009; Brune et al., 2018; Corti, 2012; Heine and Brune, 2014). Oblique rifted margins can be classified according to the angle between the extension direction and the margin strike, also termed divergence angle (Fossen, 2010; Fossen et al., 2013).

In the following, characteristic elements of the passive margin end-members are briefly introduced.

Orthogonal rifted margin architecture

Rifted margins can also be distinguished according to their forming processes into magma-poor or magma-rich. During the evolution of magma-rich rifted margins, extension coincides with extensive extrusive magmatism related to a mantle plume. Magma-poor rifted margins exhibit a large degree of crustal extension with only little and systematically delayed post-breakup magmatism (Franke, 2013). The north Atlantic margin is considered as magma-rich, however, it probably underwent a period of magma-poor pre-breakup extension (Mosar, 2003; Peron-Pinvidic and Osmundsen, 2018; Skogseid et al., 2000).

Peron-Pinvidic et al. (2013) mapped out structural similarities from three pairs of conjugate rifted margins, including both magma-poor and magma-rich ones. Based on their observations

they established a ‘life cycle’ model for a rift that transitions into seafloor spreading. Peron-Pinvidic et al. (2013) suggest a distinction of rifted margins into five structural domains that correspond to distinct phases in the ‘life cycle’ of a rift.

Transform margin architecture

Based on the concept of transform faults as strike-slip faults that cut upper and lower crust (Wilson, 1985 as cited in Basile, 2015), transform continental margins are defined as continental margins associated with such a transform fault (Basile, 2015). Mercier De Lépinay et al. (2016) compiled an overview of the worlds transform margins which make up 16% of the cumulated length of continental margins.

The formation of transform margins is commonly explained with a three stage model (Basile, 2015). The stages are established based on the position of the active transform fault in relation to the lithosphere adjacent to it (Fig. 1).

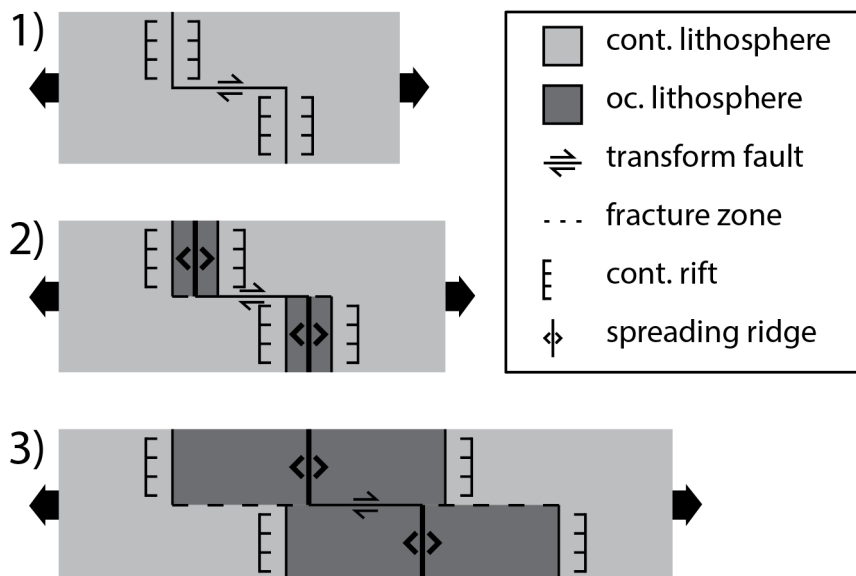


Fig. 1: Illustration of the three stage model for transform margin evolution. 1) Intra-continental transform fault. 2) active transform margin. 3) passive transform margin. Note the location of the transform fault. Simplified after Basile (2015).

Bird (2001) discussed the main characteristics that distinguish a transform margin from a passive one. Accordingly, a sheared margin exhibits an abrupt change in crustal thickness from over 20 km to less than 10 km at the transition from continental to oceanic crust. This resembles a sharply tapered necking domain following the classification of Peron-Pinvidic et al. (2013) for the architecture of rifted margins. The formation of complex rift basins along

the continental side of the margin is common and structural complexity can be introduced by normal, wrench and strike-slip faults as well as folding. The dominant direction of crustal extension approximately lines up with the margin. High standing marginal ridges, rising 1-3 km over the abyssal seafloor (50-100 km wide), form parallel to the transform margin and the adjacent oceanic fracture zone.

Basin formation and deformation along transform margins have for a long time received little scientific attention. Kristensen et al. (2017) and Seiler et al. (2010) conducted comprehensive studies on basins that formed in in association with transform and oblique rifted margins. They found that strain partitioning plays an important role in the evolution of these basins and can lead to the coeval formation of contractional and extensional structures (Fig. 2). The initiation of thrusts requires low divergence angles (e.g. Kristensen et al., 2017), whereas transtensional folding already occurs at higher divergence angles (cf. Fossen et al., 2013; Venkat-Ramani and Tikoff, 2002).

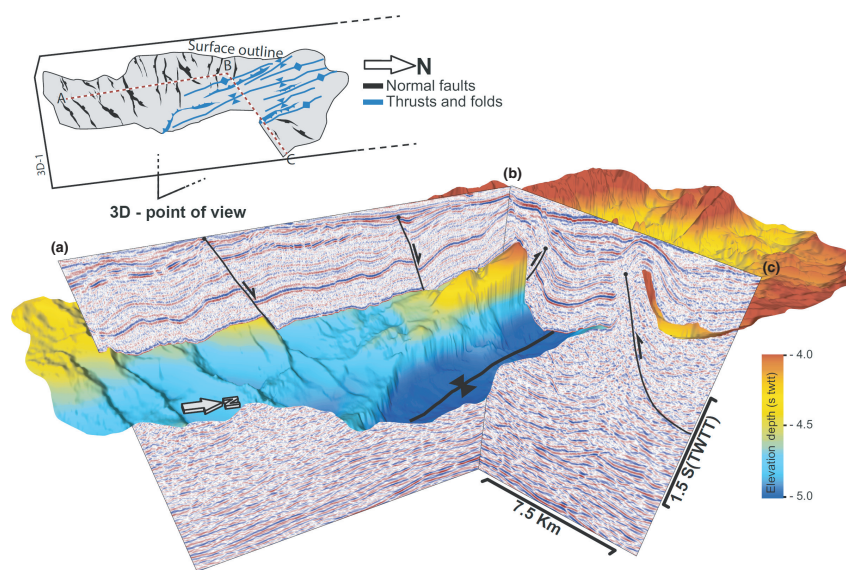


Fig. 2: Illustration of contractional thrusts and extensional normal faults that evolved coevally within the Sørvestsnaget basin. The Sørvestsnaget basin is located adjacent to the Senja Fracture Zone (Fig. 3). Figure from Kristensen et al. (2017).

1.2.2 Geological evolution of Svalbard

Svalbard is an Arctic archipelago comprising all islands located between 74° to 81° north and 10° to 35° east. It is confined by the Greenland Sea to the west, the Arctic ocean to the north

and the Barents Sea to the east (Fig. 3). Geologically, Svalbard represents the uplifted northwestern corner of the Barents Shelf (Dallmann, 2015; Henriksen et al., 2011).

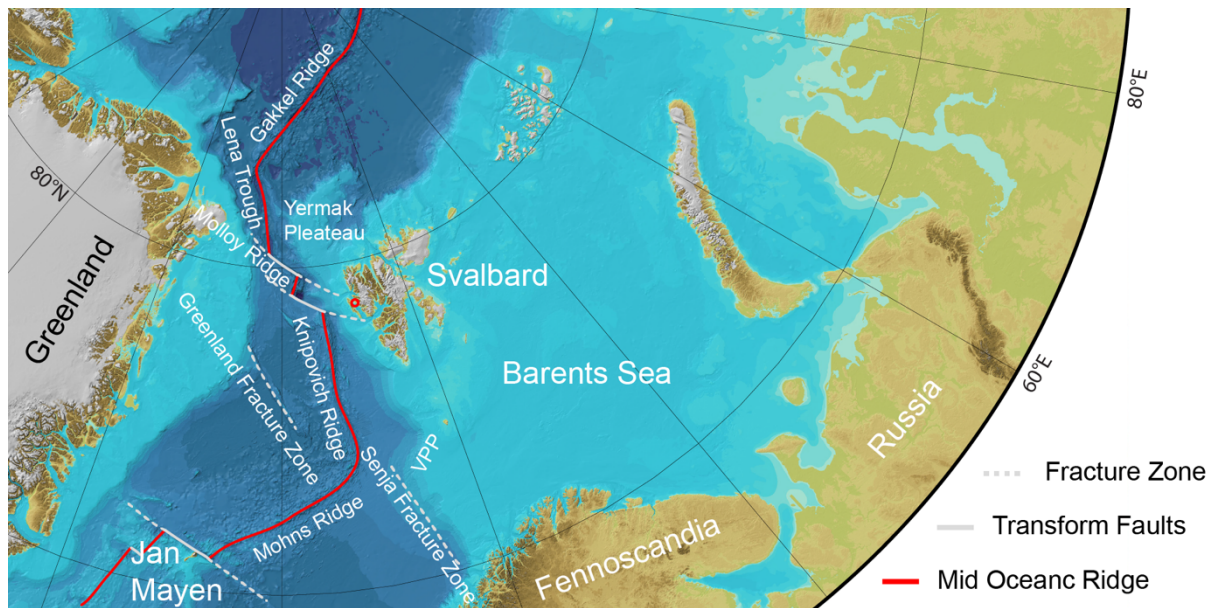


Fig. 3: Location and present day tectonic setting of Svalbard. Modified from IBCAO V3 and supplemented with tectonic elements from Dallmann (2015) and Faleide et al. (2008). VPP – Vestbakken Volcanic Province, red circle marks the study area.

Svalbard’s rock record covers the timespan from Archean to Quaternary (Fig. 4). It includes evidence of (i) the Caledonian orogeny and older events (Johansson et al., 2005; Ohta, 1994), (ii) strike slip movement along major fault zones and crustal-scale extension with subsequent contraction during the Devonian (Braathen et al., 2018; Manby and Lyberis, 1992; Piepjohn, 2000), (iii) Carboniferous rifting on a smaller scale which turned into (iv) a long lasting period of stable platform sedimentation continuing into the Mesozoic (Worsley, 2008), (v) mafic intrusions during the early Cretaceous (Senger et al., 2014) and (vi) the Eurekan orogeny in the Cenozoic with the subsequent establishment of a transform plate margin (Braathen et al., 1999; Faleide et al., 2008; Piepjohn et al., 2016). In the recent past, (vii) the Barents Sea region, including Svalbard, experienced significant amounts of uplift and glacial erosion (Dimakis et al., 1998; Dörr et al., 2013; Steel and Worsley, 1984; Worsley, 2008).

The Eurekan orogeny and the opening of the Greenland Sea (vi) are the most important tectonic events in the contexts of this study. Therefore, the regional tectonic evolution of the northeast Atlantic rift system will be assessed further in the following section (1.2.3).

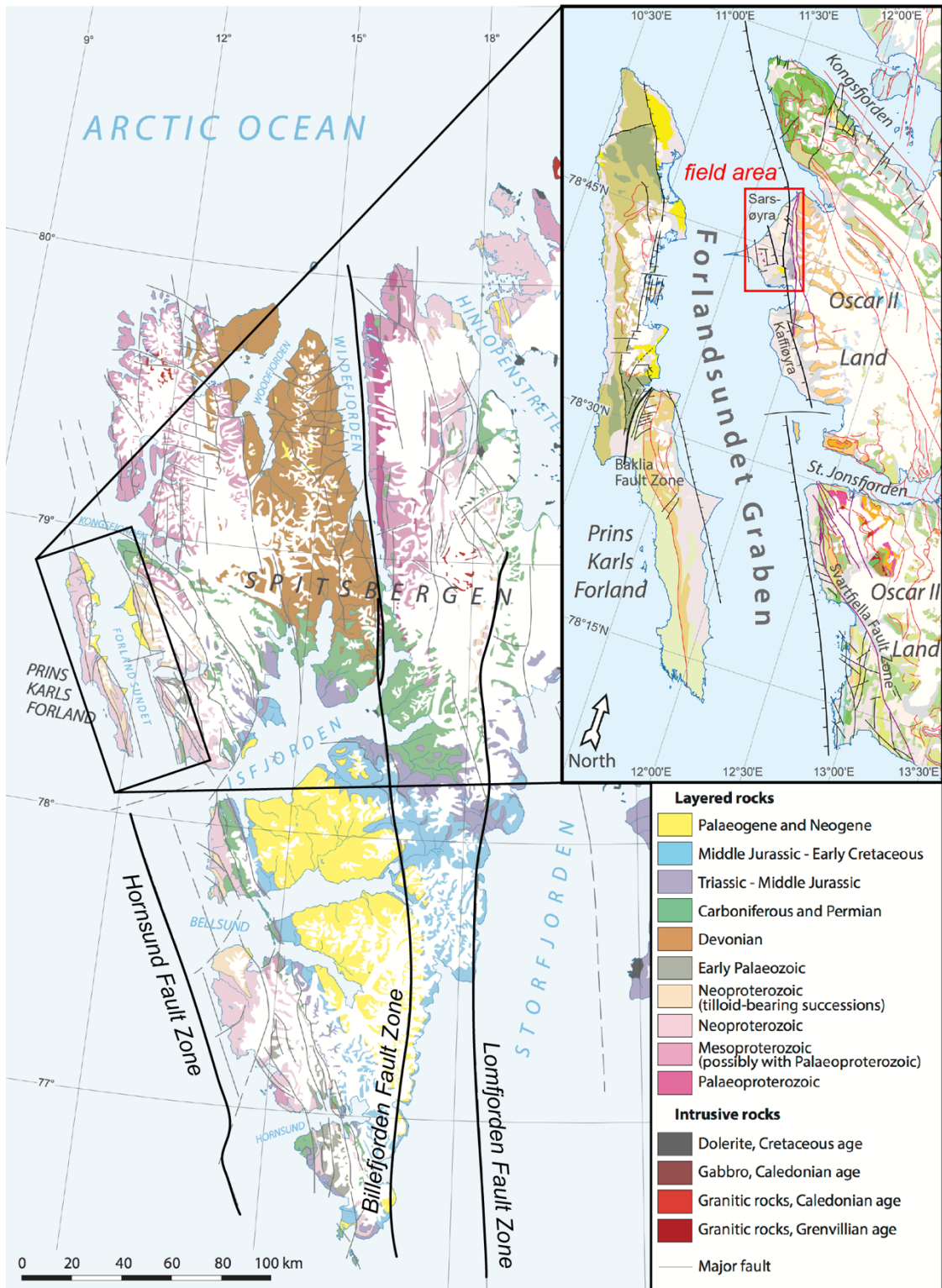


Fig. 4: Maps illustrating the geological setting of Svalbard and the Forlandsundet Graben (upper right) and the location of the field area. Modified from Dallmann (2015).

1.2.3 Opening of the north Atlantic and the Eurekan orogeny

The Cenozoic evolution of Svalbard's geology was controlled by plate motions that were introduced by the opening of the Norwegian-Greenland Sea, i.e. the north Atlantic. The northeast Atlantic rift system developed along preexisting (pre-) Caledonian structures that facilitated lithospheric extension from Late Devonian time (Skogseid et al., 2000). Rifting followed the northeasterly orientation of the Caledonides between Norway and Greenland (cf. Faleide et al., 2008). Towards the north it connected through the western transform margin of the Barents Sea with the rift system of the Arctic ocean (Fig. 3 and Fig. 5c).

The final rifting episode occurred from Paleocene to Oligocene and can be divided into three stages as illustrated in Fig. 5 and Fig. 6 (Blinova et al., 2009; Faleide et al., 2008, 2015; Piepjohn et al., 2016):

1) *Paleocene (until anomaly 24 / 53 Ma) – Pre-Eurekan stage*

Before the opening of the Norwegian-Greenland Sea, Greenland and the Eurasian plate were connected through a land bridge, spanning between Svalbard and North Greenland (Fig. 6) (Talwani and Eldholm, 1977; Tessensohn and Piepjohn, 2000). Deformation of the continental bridge began in the Late Cretaceous (88 – 80 Ma) as the Labrador Sea-Baffin Bay opening advanced northwards (Døssing et al., 2013; Hosseinpour et al., 2013; Kleinspehn and Teyssier, 2016). At that time, rifting and seafloor spreading associated with the propagation of the Atlantic rift system were concentrated west of Greenland (Piepjohn et al., 2016). Seafloor spreading started in the Labrador Sea during Early Paleocene at anomaly 27 (~61 Ma) and reached Baffin Bay between anomalies 25 and 24 (57-54 Ma) (Hosseinpour et al., 2013; Oakey and Chalmers, 2012). This movement occurred highly oblique to Ellesmere Island with a strike-slip component localized along the Nares Strait. As a result, Greenland drifted towards the northeast (Blinova et al., 2009; Oakey and Stephenson, 2008; Srivastava, 1985; Tessensohn and Piepjohn, 2000). At the same time, the Norwegian-Greenland Sea experienced an episode of rifting and dextral wrench movements along the De Geer Zone (Hornsund Fault Zone), an inherited zone of weakness (Faleide et al., 1993; Oakey and Chalmers, 2012).

2) *Eocene (anomalies 24 – 13 / 53 – 34 Ma) – Eurekan stage*

At anomaly 24, the tectonic plates in the north Atlantic and the Arctic underwent a major reorganization (Fig. 6). The propagation of seafloor spreading into Baffin Bay

and the beginning of seafloor spreading in the Norwegian-Greenland Sea and the Eurasian Basin mark the beginning of this period (Hosseinpour et al., 2013; Mosar et al., 2002; Oakey and Chalmers, 2012; Oakey and Stephenson, 2008; Tessensohn and Piepjohn, 2000). South of Greenland, the spreading systems of the Labrador Sea/Baffin Bay and Norwegian-Greenland Sea formed a triple junction with the Mid-Atlantic Ridge and Greenland's movement shifted to a northern direction. Greenland collided with both NE Canada and Svalbard. As a consequence, the WSFB developed (Braathen et al., 1997; CASE Team, 2001; Leever et al., 2011; Piepjohn et al., 2016; Tessensohn and Piepjohn, 2000).

The evolution of the WSFB is a matter of active dispute that centers around whether the structures of the WSFB formed under dextral transpression (Fig. 5) or orthogonal compression with subsequent dextral strike slip motion (Fig. 6).

Bergh et al. (2000), Braathen and Bergh (1999), Faleide et al. (2015, 2008) and Leever et al. (2011) argued that strain partitioning of a single transpressional event explains best the geometries of the WSFB structures (Fig. 5). CASE Team (2001), Piepjohn et al. (2016) and Tessensohn and Piepjohn (2000), however, suggested two separate stages of deformation (Fig. 6). The first was characterized by northwards movement of Greenland, lasting from anomaly 24 to 21, where Greenland and Svalbard experienced approx. orthogonal compression. The second stage spans from anomaly 21 to 13 when Greenland moved NNW. This change in motion caused dextral strike-slip along the De Geer Fracture Zone and other fault zones on Svalbard (Billefjorden, Lomfjorden) (Fig. 6).

The discussion is relevant for the evolution of the Paleogene basins on Svalbard, including the Forlandsundet Graben, as their formation is closely associated with the WSFB (Bergh et al., 1997; Helland-Hansen, 1990; Leever et al., 2011; Müller and Spielhagen, 1990; Steel et al., 1985, 1981).

3) *Oligocene – present (from anomaly 13 / 34 Ma) – Post-Eurekan stage*

This phase was characterized by continued seafloor spreading in the Norwegian-Greenland Sea and the Eurasian Basin while the generation of oceanic crust between Greenland (Faleide et al., 2015, 2008) and north America stopped (Hosseinpour et al., 2013). Greenland was again part of the north American plate and the opening of the Atlantic ocean continued east of Greenland, as north America and Eurasia drifted apart (Fig. 6). Along the Barents Sea and northeast Greenland conjugate sheared margins,

dextral movements most likely continued (Engen et al., 2008). In the Svalbard region, the tectonic regime has been suggested to switch from dextral transpression or strike slip motion to dextral transtension, affecting the Lomfjorden Fault Zone and the Forlandsundet Graben (Faleide et al., 2008, 2015; Piepjohn et al., 2016). During this period, Greenland and Svalbard separated and drifted to their present locations (Fig. 6) and the ultraslow Knipovich and Molloy spreading ridges formed (Curewitz et al., 2010; Dick et al., 2003; Engen et al., 2008).

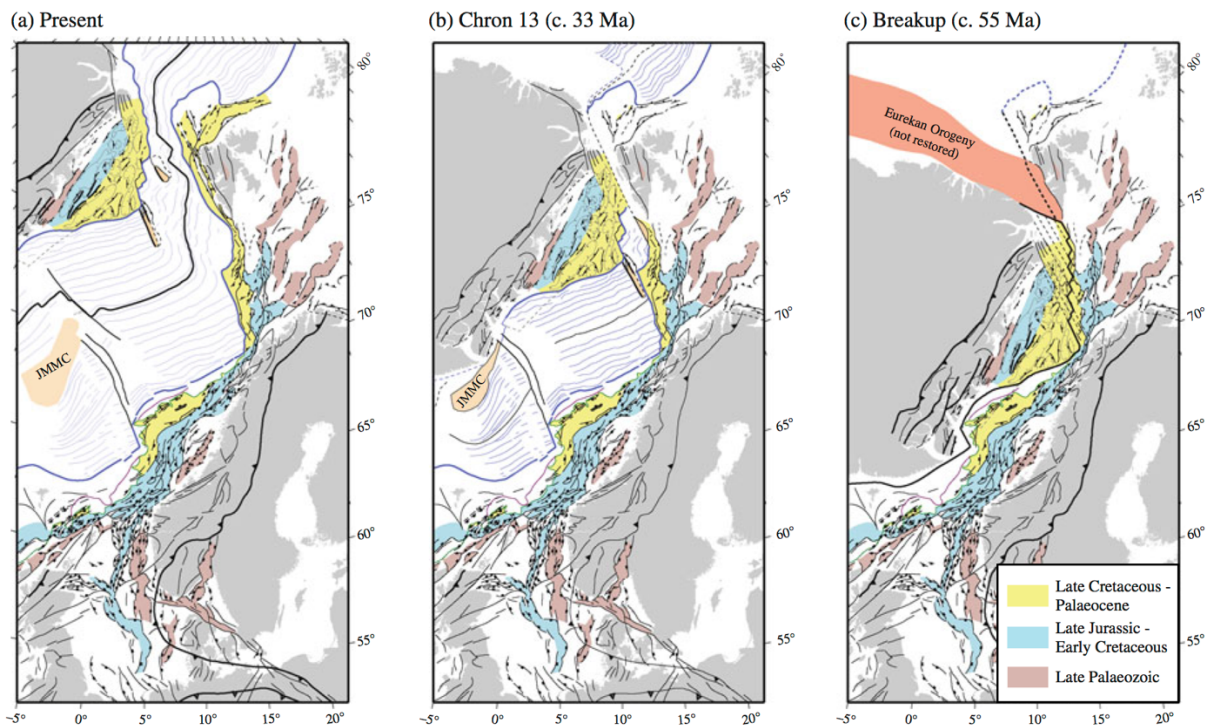


Fig. 5: Plate tectonic reconstructions of the north Atlantic according to Faleide et al. (2015). The Western Barents Sea developed in a transform margin setting. c) Breakup in the Norwegian Sea and development of the transpressional WSFB on Svalbard during the Eurekan orogeny at 55 Ma. b) Plate reorganization introducing dextral transtension along the western Svalbard margin at 33 Ma. a) Plate configuration at present.

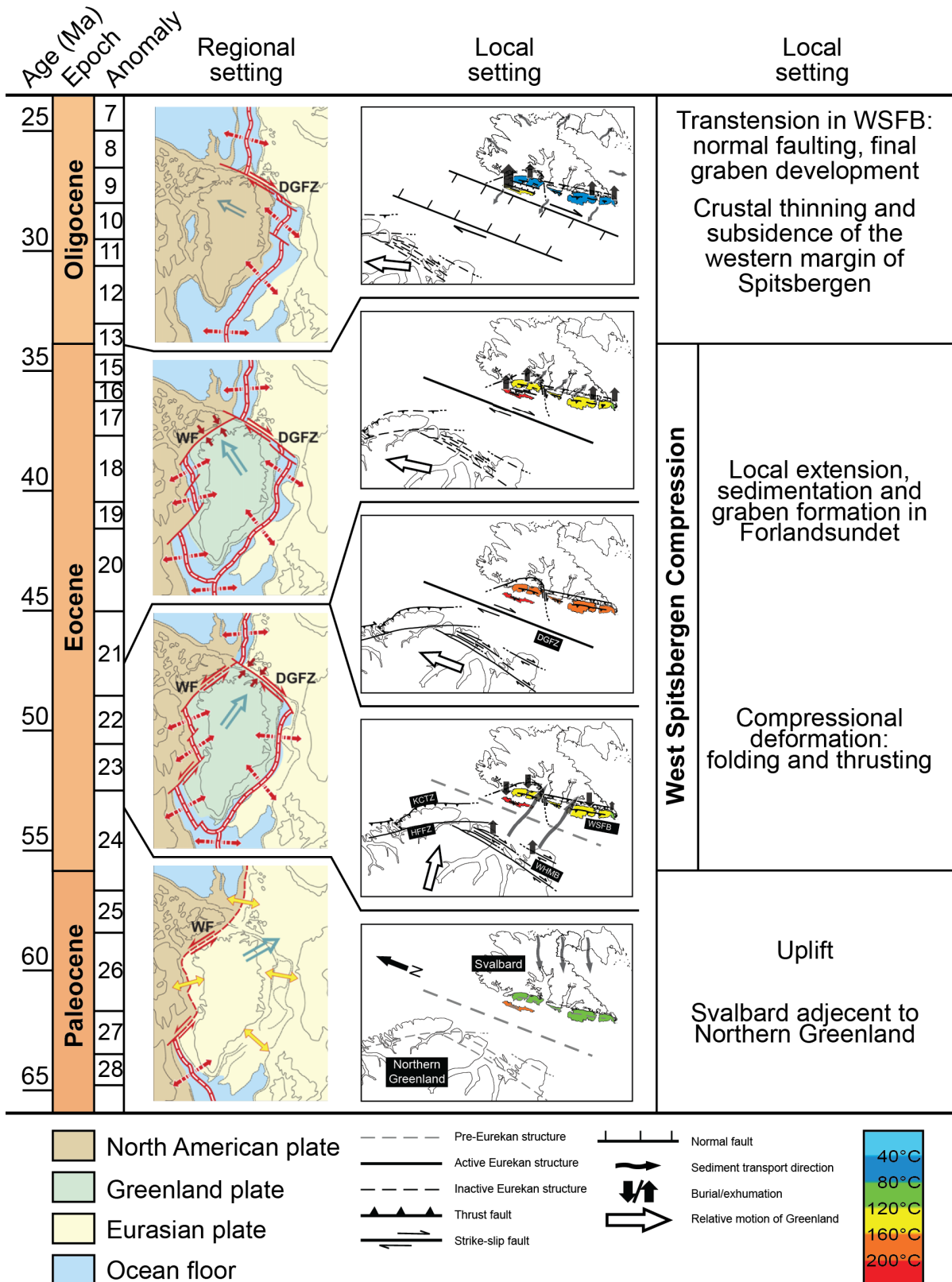


Fig. 6: Summary of the tectonic evolution of the north Atlantic (left) and Svalbard (middle and right) during the Paleogene. Note the differences in thermal and burial/uplift history between the west coast of Spitsbergen and Prins Karls Forland (middle). Figure compiled from Barnes (2016), Blinova et al. (2009) and Piepjohn et al. (2016).

1.2.4 Geological setting of the Forlandsundet Graben

Svalbard transform margin

The Forlandsundet Graben is located along the western Svalbard margin and was therefore affected by the evolution of the transform margin of the western Barents Sea (Faleide et al., 2008). The Barents Sea margin consists of two large transform segments that are separated by a rift segment: The transform Senja Fracture Zone in the south, the rifted Vestbakken Volcanic Province, and the transform Svalbard margin to the north (Fig. 3).

The Svalbard margin exhibits a sharply tapered necking domain (Fig. 7) (*sensu* Peron-Pinvidic et al., 2013). That corresponds to the zone where the crustal basement thins from more than 30 km to less than 10 km over a horizontal distance of approx. 100 km (Fig. 7).

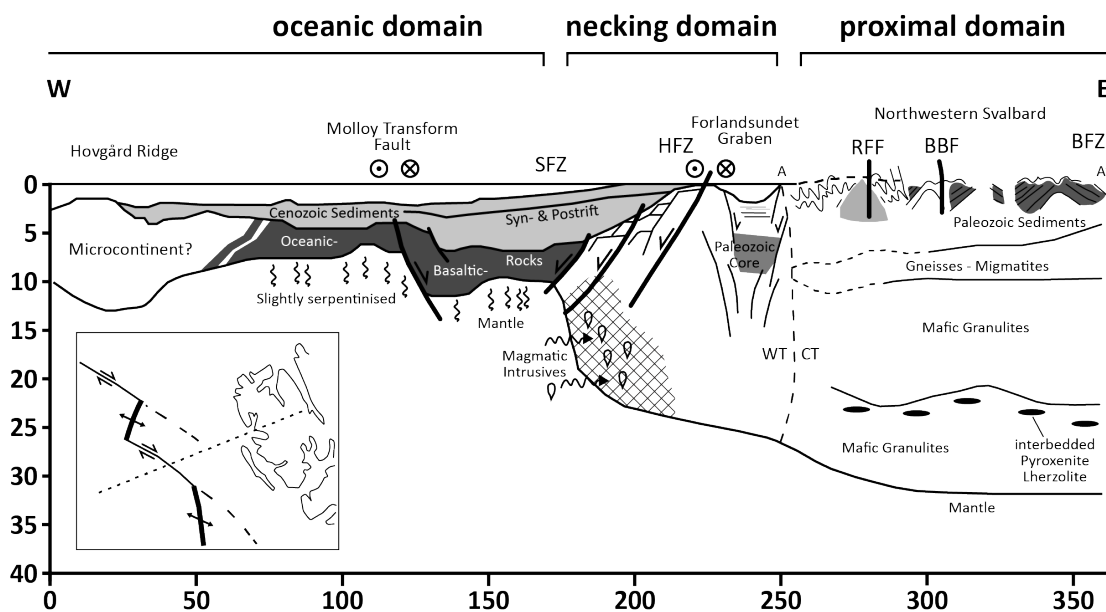


Fig. 7: Detailed interpretation of a seismic refraction data (OBS) across the Svalbard Margin with an indication of the structural domains following Peron-Pinvidic et al. (2013). Note that the structures of the Forlandsundet Graben crosscut those of the WSFB. Modified after Ritzmann et al. (2004).

Paleogeography and lithostratigraphy

During the Paleogene, Svalbard was located at 80° N, almost at its present latitude (Fig. 8A) (Faleide et al., 2008; Worsley, 1986). Despite its position in the high north, the climate was

warm and humid in Early Paleogene (Sewall and Sloan, 2004). Towards the Late Paleogene, the climate gradually cooled down and became drier (Fig. 9) (Spielhagen and Tripathi, 2009).

Svalbard comprises a rich record of Paleogene sedimentary rocks onshore and offshore (Fig. 4) (Dallmann, 2015). The strata were deposited in two sedimentary basins, the Central Spitsbergen Basin (CSB) and the Forlandsundet-Bellsund Graben (Fig. 8B) (Steel et al., 1985).

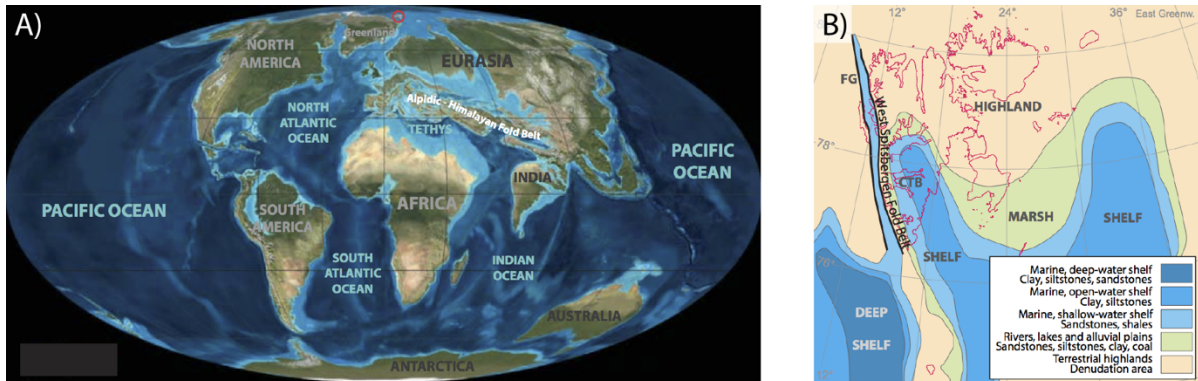


Fig. 8: A) Reconstruction of the global paleogeography during the Paleogene (Eocene, ca. 50 Ma). Svalbard, indicated by the red circle, was located off the margin of Greenland and north America on a similar latitude as today (80° N). B) Configuration of Svalbard’s sedimentary basins during the Eocene (ca. 40-50 Ma). At the time, two depositional areas were active, the Central Spitsbergen Basin (CTB) as part of the Barents Sea and the Forlandsundet Graben (FG) which constituted a segment of the initial rift basin of the north Atlantic ocean. Figures modified from Dallmann (2015): A) Based on R. Blakey, Colorado Plateau Geosystems Inc. B) Modified from Smelror et al. (2009).

The CSB covers the central and southern part of Spitsbergen (Fig. 4). It evolved as a foreland basin associated with the WSFB (Helland-Hansen, 1990; Müller and Spielhagen, 1990). The sedimentary units in the CSB make up the Van Mijenfjorden Group (Fig. 9) (Dallmann, 1999; Steel et al., 1985) and comprise sandstones, siltstones, shales as well as subordinate coals and conglomerates. The total thickness of Paleogene sedimentary rocks deposited was around 2900 m. Today, approx. 1900 m of stratigraphy are preserved with the remaining 1000 m being eroded (Steel et al., 1985). Basin remnants at Øyrlandsodden, southern Spitsbergen and on Brøggerhalvøya, Kongsfjorden are considered to be genetically linked to the CSB (Fig. 9) (Dallmann, 2015).

1.2.5 The Forlandsundet Graben

The Forlandsundet Graben is located at the western Svalbard margin between the west coast of Spitsbergen and the island Prins Karls Forland (Fig. 4 and Fig. 8). Together with the

Bellsund Graben it makes up a basin structure of approx. 150 km length (Fig. 4). The Forlandsundet Graben has been described as a half-graben basin by Blinova et al. (2009) and Gabrielsen et al. (1992). It is bounded by steep normal faults that cross-cut the structures of the WSFB (Fig. 7) (Gabrielsen et al., 1992; Hjelle et al., 1999; Kleinspehn and Teyssier, 2016, 1992; Lepvrier, 1990; Ritzmann et al., 2004; Steel et al., 1985; von Gosen and Peach, 2001).

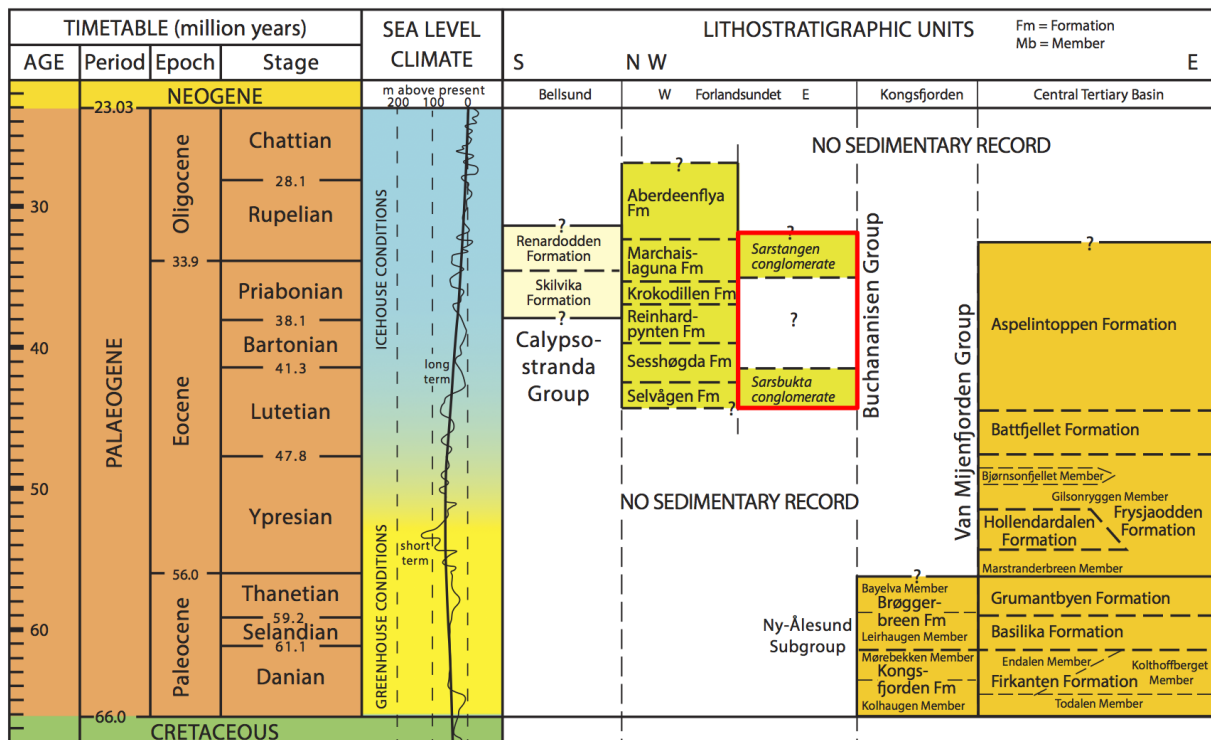


Fig. 9: Summary of the sedimentary units deposited in basins on Svalbard during Paleogene, modified from Dallmann (2015). Scope of this study are the Sarsbukta and Sarstangen Formations (red rectangle) from the eastern Forlandsundet margin. The figure includes a timetable as well as global sea level and climate data.

Paleogene sediments are exposed onshore on both sides of the Forlandsundet strait (Fig. 4) while most of the strata are submerged (Blinova et al., 2009; Gabrielsen et al., 1992). The stratigraphy exhibits fundamental differences compared to the infill of the CSB. Therefore, it has been described as a separate lithostratigraphic unit, called Buchananisen Group (Fig. 9) (Dallmann, 2015; Rye-Larsen, 1982). The Buchananisen Group is made up from conglomerates, sandstones, siltstones and shales (Dallmann, 1999). In the following section, the stratigraphy of the Buchananisen Group is presented in more detail.

The clastic sediments of the Calypsostranda Group (Fig. 9) might represent a distal equivalent of the Buchananisen Group comprising 265 m of stratigraphy that are exposed in the Renarodden Fault Block south of Bellsund (Fig. 4) (Dallmann, 2015).

The Buchananisen Group

The sedimentary rocks of the Buchananisen Group were first mentioned by workers in the early 20th century (Rye-Larsen, 1982 and references therein). Later, Atkinson (1962) divided the strata into two units, the basal **Selvågen Conglomerate** and the overlying **McVitie Formation**, dominated by an arenite/pelite sequence. The units rest unconformably on metamorphic basement, partly with a depositional, partly with a fault contact. Since then, the stratigraphy has been revised by Livsic (1974) to provide a higher resolution and subsequently updated by Manby (1978), as cited in von Gosen and Peach (2001) and Rye-Larsen (1982). The cumulative thickness of the exposed stratigraphy exceeds 4000 m (Dallmann, 2015) but the true sediment thickness in the basin is probably around 3000 m (Sellevoll et al., 1991). The Buchananisen Group consists of eight formations (Fig. 10) (Dallmann, 1999; Rye-Larsen, 1982) and is summarized in Table 1.

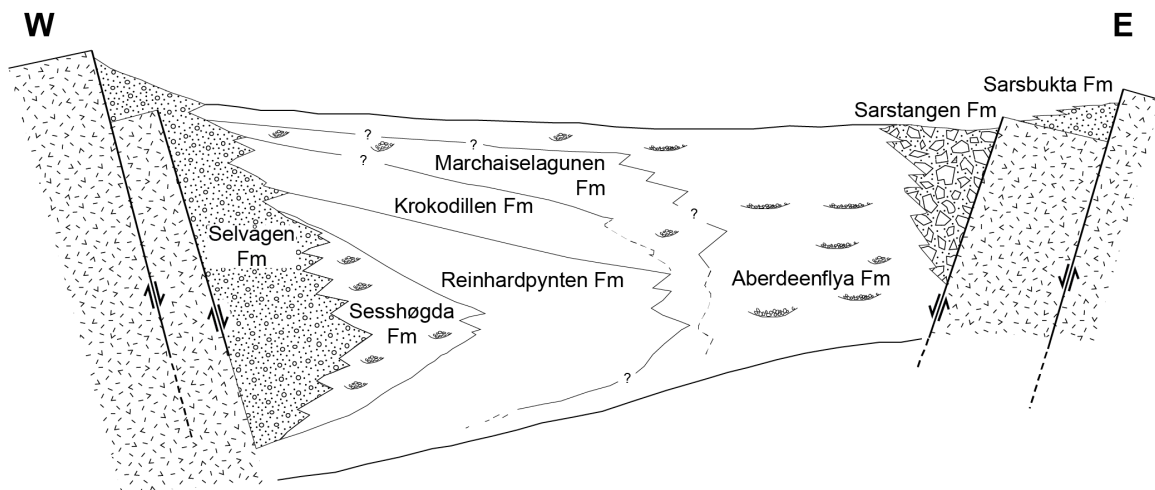


Fig. 10: Schematic W - E cross section through the Forlandsundet Graben illustrating the stratigraphical units. Recent observations challenge this simple stratigraphic model. Modified after Gabrielsen et al. (1992) and Rye-Larsen (1982).

Table 1: Formations of the Buchananisen Group according to Dallmann (1999) and Rye-Larsen (1982). Stratigraphic thicknesses from Dallmann (1999).

| Name | Thickness | Sedimentology |
|---|------------------------|--|
| Sarstangen Formation | >1600 m (?) | Very proximal basin margin fan conglomerates and sedimentary breccias. |
| Sarsbukta Formation | | Basin margin alluvial fan conglomerates and floodplain deposits. |
| Aberdeenflya Formation | >2800 m (?) | Submarine turbidite fan deposits with sandstone, shale and conglomerates, no marine fossils. |
| Marchaiselaguna Formation | >600 m (?) | Shallow-marine arenite with pelite intercalations, no marine fossils. This formation is very similar to the Aberdeenflya Formation and is only considered an individual formation because the stratigraphic relationships are not exposed. |
| Krokodillen Formation | 400 m (?) | Shallow-marine pelite with arenite intercalations, no fossils. |
| Sesshøgda Formation and Reinhardpynten Formation | 120 m and >210 m | Delta fan sandstone, conglomerate and siltstone with poor marine fauna (Livsic, 1974). |
| Selvågen Formation | 170 m | Basin margin alluvial fan conglomerate, almost no fossils. |

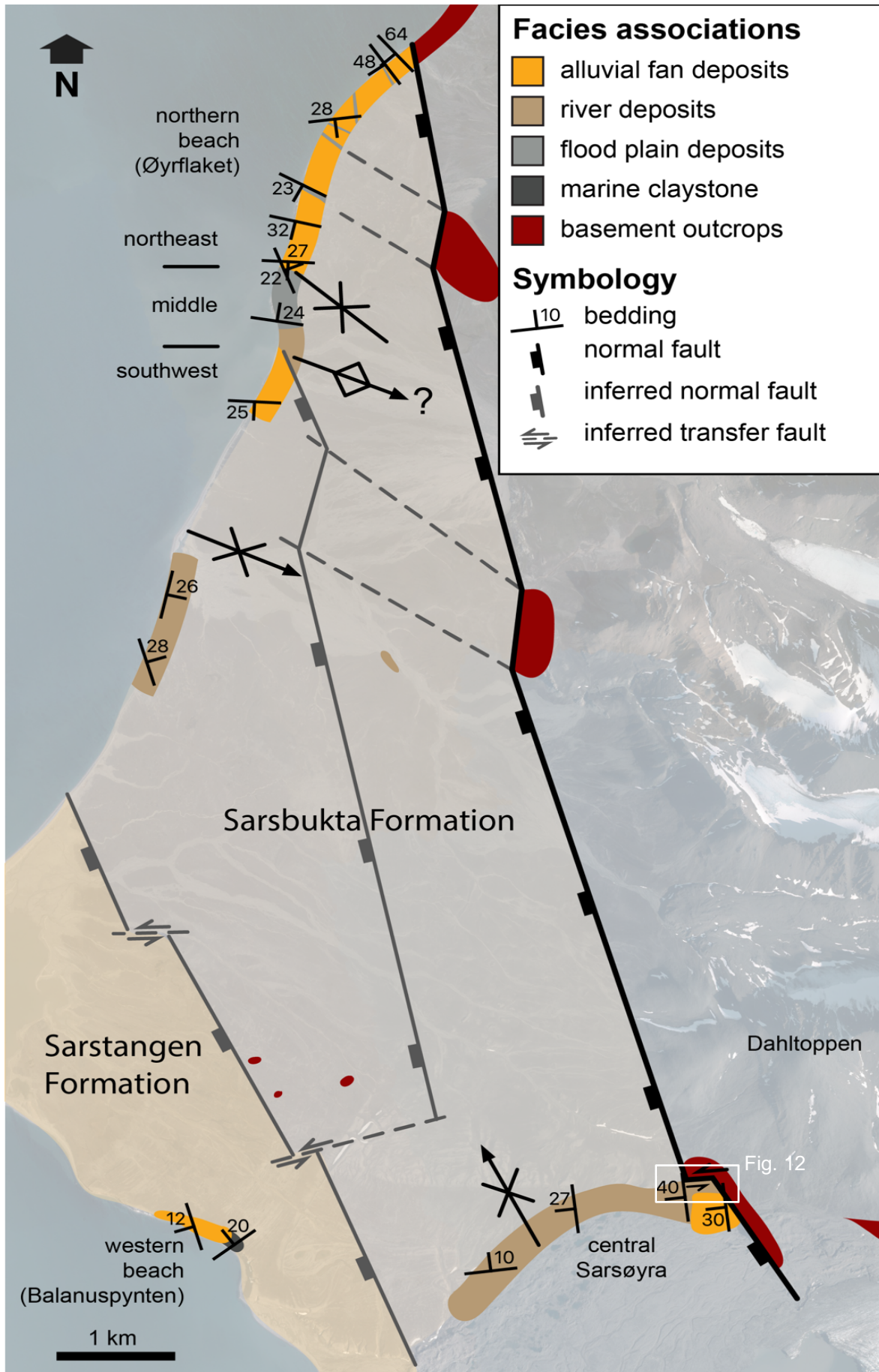
1.2.6 Field area

The study area, Sarsøyra (Fig. 4), was named after the Norwegian zoologist and professor Michael Sars (Norwegian Polar Institute, 2018). It is located on the eastern margin of the Forlandsundet Graben approx. 20 km south of the research community Ny-Ålesund. The study area is 5 km wide (E-W) and 13 km long (N-S), covering an area of approx. 41 km²

(Fig. 4). It is bordered by a mountain range, more than 600 m high, to the east. Towards the west, the prominent Sarstangen spit stretches some 5 km into the Forlandsundet strait. The north-western part of the area is flat and gently rises from a 3 to 5 m high beach cliff to a plateau of approx. 30 m elevation in the central part of Sarsøyra. Rivers, fed from the nearby glaciers, incise the plateau. In central Sarsøyra, two smaller plateaus at roughly 50 m and 100 m of elevation are located in between the mountains and the lower plateau. The 100 m high plateau is made up of a carbonate cliff that probably resembles the fault scarp of the Forlandsundet Graben boundary fault (Gabrielsen et al., 1992). To the south, an extensive area is covered by moraine deposits of the Aavatsmarkbreen glacier.

The Paleogene deposits on Sarsøyra comprise of the older Sarsbukta Formation and the younger Sarstangen Formation (Fig. 9) (Rye-Larsen, 1982). The outcrops in the study area are scattered and of varying quality. Fig. 11 gives a general overview of the localities and the distribution of Paleogene and basement exposures on Sarsøyra.

Fig. 11 (next page): Overview map of the field area displaying the visited outcrops color-coded according to their facies association. Bedding and major structures are also indicated. Inferred structures (grey) are based on a surface magnetic survey by Krasilscikov et al. (1995). Note the occurrence of alluvial plain deposits within alluvial fan deposits at the northern beach. Also, pay attention to the basement exposures in the center of Sarsøyra. The location of the map is indicated in Fig. 4. Background satellite imagery courtesy of the Norwegian Polar Institute.



Exposures of the Sarsbukta Formation

Exposures of the Sarsbukta Formation are located in central Sarsøyra and along the northern beach (Fig. 11). The outcrops in central Sarsøyra (Fig. 12) represent the type section of the Sarsbukta Formation where Rye-Larsen (1982) logged 80 m of alluvial fan derived conglomerates. In this location, 46 m of stratigraphy were logged and sedimentary architectures were documented with photomosaics as well as 2D drawings from well exposed outcrops.

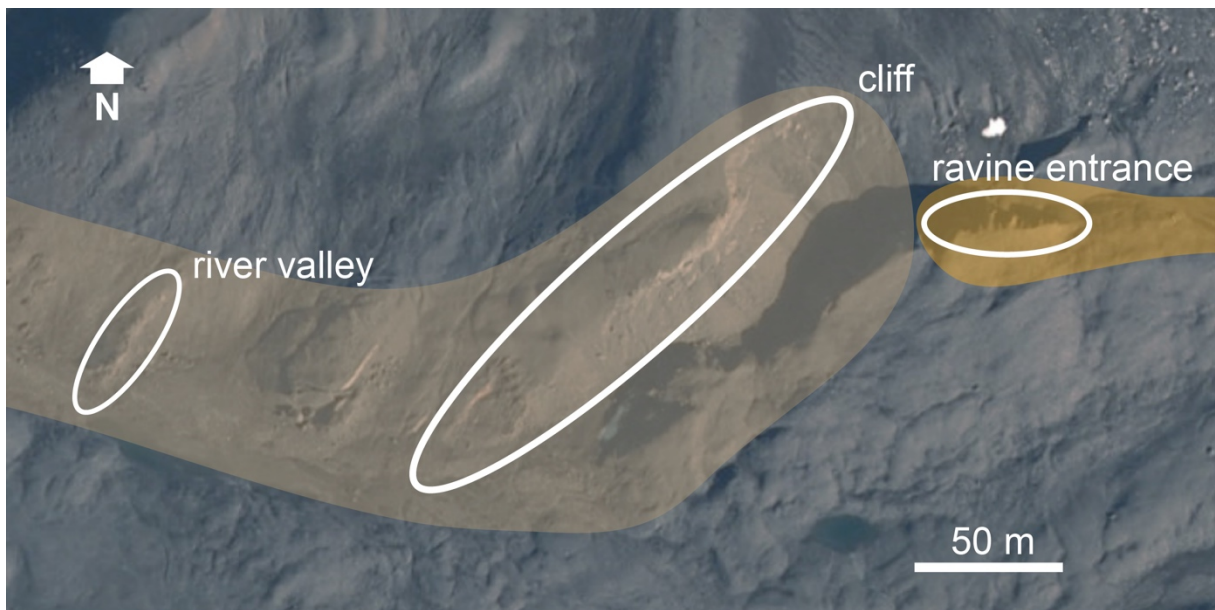


Fig. 12: Overview of the outcrop locations in central Sarsøyra. The location of this map is indicated in Fig. 11. Imagery from toposvalbard.npolar.no.

Along the northern beach (Fig. 11), approx. 200 m of stratigraphy were logged from well exposed beach cliffs. These sections were mentioned by Kesper (1986), Kleinspehn and Teyssier (2016), Rye-Larsen (1982) and Sperling (1990), but a detailed documentation was missing. Some of the well preserved costal outcrops allowed for detailed assessment of the sedimentary architecture. It has to be mentioned that the exposures along the northern beach are highly affected by wave activity and costal erosion since the outcrops changed significantly from the first field season to the second.

Other exposures of the Sarsbukta Formation are reported from Kaffiøyra (Rye-Larsen, 1982) but were not visited for this study (Fig. 4).

Exposures of the Sarstangen Formation

The Sarstangen Formation only crops out at the western beach of Sarsøyra, close to Balanuspynten (Fig. 11). The exposed section accounts for approx. 22 m of stratigraphy (Rye-Larsen, 1982 and this study). Also at this locality, the database includes logs and 2D documentation of the outcrops. Especially, the 2D assessment of the sedimentary architecture represents an improved documentation of the Sarstangen Formation.

In addition, it was probably encountered in the 7811/5-1 Sarstangen petroleum exploration well drilled by Norsk Polar Navigasjon AS on Sarstangen in 1974 (section 5.1.1).

In the following, the methods (chapter 2) utilized for this study are presented, followed by the description of the sedimentology (chapter 3) and structural geology (chapter 4) of the field area.

2 Data and methods

This chapter presents the methods used in this study such as the collection of sedimentary and structural geological field data as well as thin section and geochronological analysis. Furthermore, the subsurface datasets that were available are described.

2.1 Data collection in the field

Sedimentological data were gathered in the form of sedimentary logs, as well as line drawings and photomosaics. Sedimentary logging was carried out in 1:50 scale and sedimentary structures as well as biogenic content were indicated. The resolution of 1:50 allowed for a recognition of layers down to 5 cm thickness. Thinner features were noted down or drawn into the logs. The bed thickness was measured with a measuring stick perpendicular to bedding. Smaller scree-covered sections were measured directly while in some longer sections, the covered stratigraphy was calculated using horizontal distance and prevailing dip. In fair weather, millimeter paper was preferred above “Rite in the Rain” field books.

To document the 2D sedimentary architecture, scale drawings and photomosaics of well exposed outcrops were produced. Often, sedimentary logging and 2D assessment were combined to provide a thorough documentation of the exposures. For the photographs, a Nikon COOLPIX AW130 digital camera with a resolution of 16 megapixel was used.

Lithofacies were defined for the sedimentological data collected in the field, following Miall (1985, 1978, 1977). Based on the lithofacies, lithofacies associations and their corresponding depositional environments were reconstructed.

Bedding, paleo flow indicators and structural measurements were measured with a SILVA or Krantz Geologist’s compass and subsequently corrected for the declination of +7°. Planes were measured as strike and dip according to the right-hand-rule. If possible, the plunge of striations and the kinematic sense were added to fault plane measurement. Visualization of the structural and kinematic data was carried out with Stereonet and FaultKin software (Allmendinger et al., 2013). Fold axes were calculated in Stereonet applying the Bingham axial distribution to the bedding measurements.

The kinematic database consists of fault plane measurements, the plunge of the lineation and the sense of motion if retrievable. The plunge was noted with a positive algebraic sign when it was directed along the strike, otherwise it was marked with a minus. In order to import this data into FaultKin, the Aki Richards convention had to be used. The following equations illustrate the calculations that were implemented into Excel to convert the data:

First, the rake was calculated. For plunges with the strike (+):

$$rake = \arcsin\left(\frac{\sin(plunge)}{\sin(dip)}\right)$$

For plunges against the strike (-):

$$rake = 180 + \arcsin\left(\frac{\sin(plunge)}{\sin(dip)}\right) \text{ since } \sin(plunge) \text{ is negative}$$

Subsequently, the rake was converted according to the Aki Richards convention:

For reverse faults: *Aki Richards* = 180 – rake

For normal faults: *Aki Richards* = –rake

2.2 Thin section analysis

The samples for thin sections include sedimentary, basement and fault rocks. A total of 18 thin sections were prepared from 14 samples at the thin section laboratory of the University of Oslo. The samples were not treated with stained epoxy in the process.

The thin sections were scanned at a resolution of 4200 dpi with a flatbed scanner to provide good orientation while interpreting. The interpretation itself was carried out with a Nikon ECLIPSE 50iPOL transmitted light microscope under unpolarized and cross-polarized light.

2.3 Paleolimnology

Paleolimnology is a method to determine the stratigraphical age of sedimentary rocks based on the analysis of pollen (palynomorphs) (Appendix 4). The palynomorphs themselves, as well as their distribution and abundance, change over time due to biological evolution and the composition of the paleovegetation. Thus, characteristic palynomorph assemblages can be

assigned to certain geological times and regions (Traverse, 2007). Fine grained sandstones and siltstones, as well as, coals were sampled for this method.

In connection with this study, 10 samples were analyzed by the lab of the Institute for Applied Geosciences at the University of Darmstadt in Germany. PD Dr. Olaf Lenz prepared the samples, analyzed them and composed a report with the results (Appendix 4).

2.4 K-Ar dating of the fault gouge

K-Ar low temperature geochronology was used to date illite growth within a fault gouge. The analysis was conducted by Roelant van der Lelij from the laboratory of the Norwegian Geological Survey (NGU). The formation of authigenic illite in fault gouges can be correlated with the episodes of movement along a fault (Bense et al., 2014; Kralik et al., 1987; Lyons and Snellenburg, 1971).

In addition, the samples were analyzed with the x-ray diffraction method (Vrolijk and Van Der Pluijm, 1999) by Jasmin Schönenberger, also staff at the NGU laboratory, to confirm that the measured grain fractions correspond to authigenic illite.

2.5 Subsurface data

The 2D seismic data analyzed in this study were recorded by Statoil in 1985 and the Svalex academic expedition managed by the University of Bergen in 2001. Overall, 21 lines were available for this study. The quality of the data varies greatly and especially the Svalex data are poorly processed. Therefore, only the best lines were chosen for interpretation, including the lines interpreted by Gabrielsen et al. (1992). In total 5 lines were interpreted. The lines are all oriented across the basin, approx. E – W, and allow for an interpretation of the overall basin geometry.

In addition, the data from a composite log of an exploration well drilled at Sarstangen by Norsk Polar Navigasjon AS in 1974 was integrated into the project. The well data and additional archive material was kindly provided by Asbjørn Skotte, the executor of Norsk Polar Navigasjon AS's inheritance.

Interpretation of the seismic data was carried out with the Petrel E&P software package provided by Schlumberger.

3 Sedimentology

The following sections describe the sedimentological units on Sarsøyra. For each of the two formations, lithofacies and lithofacies associations are defined and interpreted based on the field data. The field data comprises c. 370 m of logs, 5 detailed outcrop drawings, as well as high-resolution photographs and bedding measurements.

3.1 Sarsbukta Formation

The Sarsbukta Formation is characterized based on the outcrops in central Sarsøyra at the foot of Dahltoppen and along the northern beach, called Øyrflaket (Fig. 11 and Fig. 12). Rye-Larsen (1982) was the first to describe the Sarsbukta Formation based on the exposures in central Sarsøyra. He logged 85 m of stratigraphy that he interpreted as alluvial fan and fluvial deposits (Rye-Larsen, 1982). Kleinspehn and Teyssier (2016) incorporated observations from the northern beach and concluded that the Sarsbukta Formation represents the deposits of a fluvio-deltaic gravelly meandering-channel. However, their study lacks a well-founded documentation of the stratigraphy and does not include any measured sections.

This thesis assesses the sedimentology of the Sarsbukta Formation with the concept of lithofacies (sensu Miall, 1977b). The lithofacies are then combined into lithofacies associations that represent depositional systems. Strip logs and detailed outcrop sketches are presented to fill the gap left by previous workers.

3.1.1 Lithofacies

Table 2: Lithofacies of the Sarsbukta Formation. The color code is used to mark the facies in the logs.

| Code | Lithofacies | Description | Sedimentary structures | Interpretation |
|------|-------------------------------|--|------------------------------------|--|
| Gm | Massive and stratified gravel | Sub-angular to well-rounded clasts, clast supported, sandy matrix | Massive to stratified, imbrication | Debris flows, high energy stream flows |
| Gp | Planar cross-bedded gravel | Well-rounded clasts, clast supported, can contain very coarse sand | Planar cross-bedding | Channel fills and bars |

| | | | | |
|-----|----------------------------------|---|--|--|
| Sm | Massive sandstone | Coarse to medium fine sand | Massive | Channel fills, hyperconcentrated flow deposits |
| Smr | Sandstone with rootlets | Fine to coarse sandstone with rootlets | Massive with rootlets | Seatearth |
| St | Trough cross-bedded sandstone | Medium to very coarse, may be pebbly | Trough cross-bedding | Dunes, lower flow regime |
| Sp | Planar cross-bedded sandstone | Medium to very coarse, may be pebbly | Planar cross-bedding | Lingoid or transverse bars, dunes in the lower flow regime |
| Sh | Horizontally laminated sandstone | Very fine to coarse sand | Horizontal lamination | Planar bed flow, in the upper and lower flow regime |
| Sr | Sandstone with current ripples | Very fine to coarse sandstone with ripples | Ripples, horizontal lamination | Ripples in the lower flow regime |
| Fl | Very fine sand- to siltstone | Heterolithic silt to very fine sandstones | Horizontal lamination, ripples, planar cross-bedding | Overbank or waning flood deposits |
| C | Coal | Coal stringers and coalified plant remains | Burial of peat | Swamp deposits |
| P | Paleosol | Fine grained sediment horizon with greenish color alterations | Soil formation | Soil formation during subaerial exposure |

Gm – massive to stratified gravel

Description – Facies Gm makes up a large portion of the Sarsbukta Formation. The facies is well exposed in the outcrops of central Sarsøyra (Fig. 23, Fig. 26, Fig. 20 and Fig. 21) and along the northeastern part of the northern beach (Fig. 22 and Fig. 11). The beds commonly appear as massive but some exhibit horizontal stratification (Fig. 23) and imbrication. The bases of the beds are commonly erosive but within thicker packages of facies Gm, the boundaries are often indistinct. The facies consists of poorly sorted, clast supported gravels with clasts ranging in size from granule to large cobble with better sorted beds occurring

locally. The clast composition is polymictic and derived from basement lithologies with a high fraction of vein quartz. Coal fragments, as well as rounded coal pebbles are present. Most clasts are rounded to sub-rounded but can also be sub-angular (Fig. 23), especially at the southwestern outcrops at the northern beach. Lithification of the facies is generally poor. However, a few beds and sections in proximity to faults can exhibit a higher degree in lithification. Fig. 13 shows examples of facies Gm.

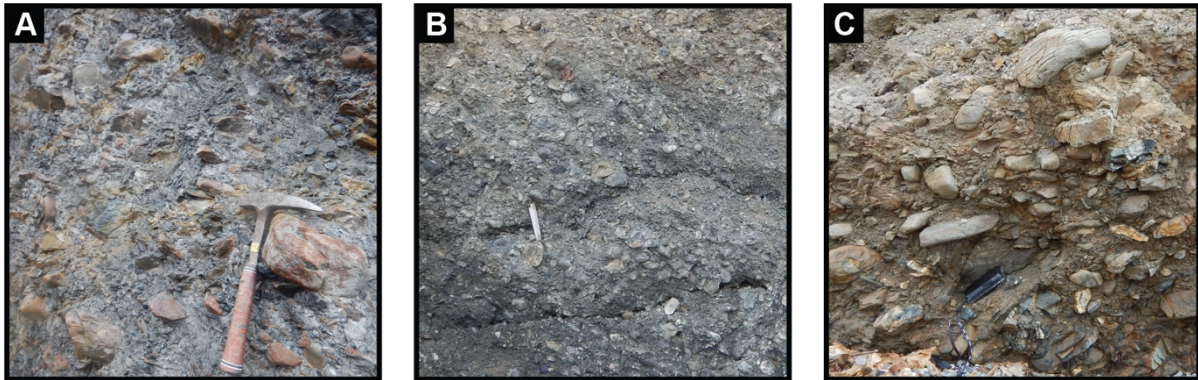


Fig. 13: Examples of facies Gm. A) Facies Gm in the outcrop at the ravine entrance in central Sarsøyra (hammer for scale). B) Facies Gm at the northeastern part of the northern beach (Fig. 11). Note the erosive bed boundaries (measuring stick, 10 cm, for scale). C) Facies Gm in the southwestern section of the northern beach (compass for scale).

Interpretation – Conglomerates similar to facies Gm are common in (proximal) alluvial fan (Blair and McPherson, 1994; DeCelles et al., 1991; Nemeč and Steel, 1984; Nilsen, 1982) as well as braided river deposits (DeCelles et al., 1991; Leleu et al., 2009; Miall, 1977b; Orton and Reading, 1993; Steel and Thompson, 1983). The depositional processes include debris and high energy stream flows (Blair, 2000; Blair and McPherson, 1994; Nilsen, 1982). Within braided rivers, facies Gm can constitute bars as well as bedload as lag or sieve deposits (DeCelles et al., 1991; Leleu et al., 2009; Miall, 1977b; Smith, 1974).

Gp – planar cross-bedded gravel

Description – This facies is present in most localities of the Sarsbukta Formation (Fig. 22, Fig. 26 and Fig. 25) and consists of planar cross-bedded gravel. The beds often exhibit erosive bases. Facies Gp comprises well sorted, clast supported gravels in a sandy matrix. The clasts are rounded and exhibit a polymictic composition. This facies is characterized by planar cross-beds either internally or in alternation with sandy units (Fig. 24 and Fig. 25).

Interpretation – Facies Gp is likely to be deposited by a fluvial system in the form of channel fills (Fig. 25), linguoid bars or deltaic growth from older bar remnants (Fig. 24) (Best et al., 2003; DeCelles et al., 1991; Leleu et al., 2009; Miall, 1977b; Orton and Reading, 1993).

Sm – massive sandstone

Description – Facies Sm comprises all fine to very coarse sandstones that appear structureless in the field. Facies Sm occurs in contact with all other facies of the Sarsbukta Formation but especially with sandstone facies St, Sp and Sh. The beds of facies Sm are 10 to 100 cm thick, commonly with sharp, conformable lower boundaries but locally also with erosive bases. Fig. 14A presents an outcrop example of facies Sm. Thin sections of samples of facies Sm have a quartzitic composition and are carbonate cemented (Fig. 15).

Coalified leaf imprints of *Metasequoia* and deciduous tree leaves can be found in the sandstones of the Sarsbukta Formation (Fig. 14B and C).

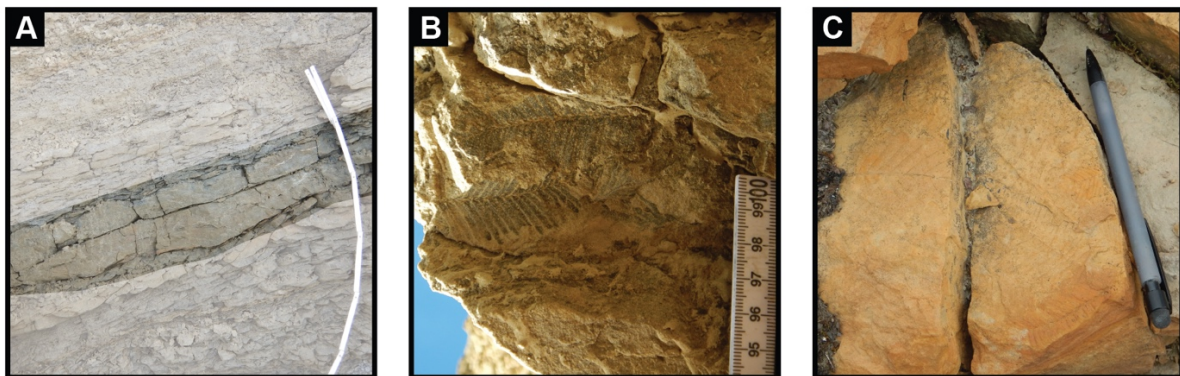


Fig. 14: Appearance and fossil content of facies Sm. A) Massive sandstone bed (middle) with sharp erosive base (measuring stick for scale, one segment is 20 cm). B) Coalified leaf imprints of *Metasequoia* (scale is in cm). C) Leaf imprints of deciduous trees and *Metasequoia* (pencil for scale).

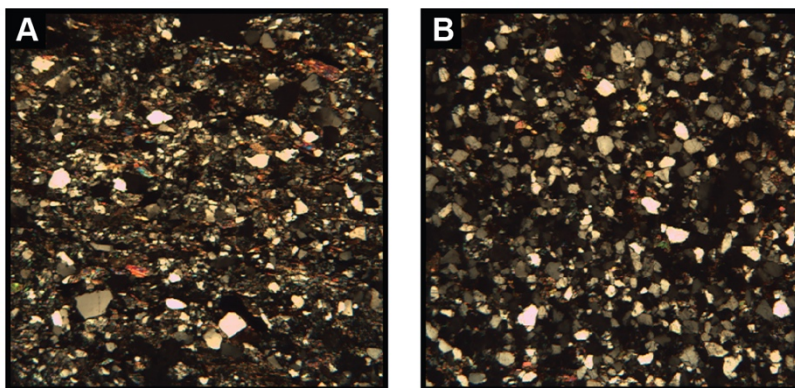


Fig. 15: Thin sections under cross polarized light of sandstones from central Sarsøyra (A) and the northern beach (B). The composition of the angular sand grains is generally quartzitic, cemented with carbonate. Unfortunately, no scale can be given due to limited facilities available.

Interpretation – The occurrence of coalified leaf imprints and coal suggests a terrestrial depositional environment for facies Sm. Massive sandstone facies are common in fluvial deposits (Martin and Turner, 1998; Walker and Cant, 1984) and facies Sm was probably deposited from suspension under hyperconcentrated flow conditions (e.g. Martin and Turner, 1998).

Smr – massive sandstone with rootlets

Description – Facies Sr is made up by fine to coarse sandstones that contain rootlets (Fig. 16). The rootlets often initiate in a thin organic rich layer that overlies the sandstones (Fig. 16B). Apart from the presence of rootlets, these units resemble the massive sandstones of facies Sm.

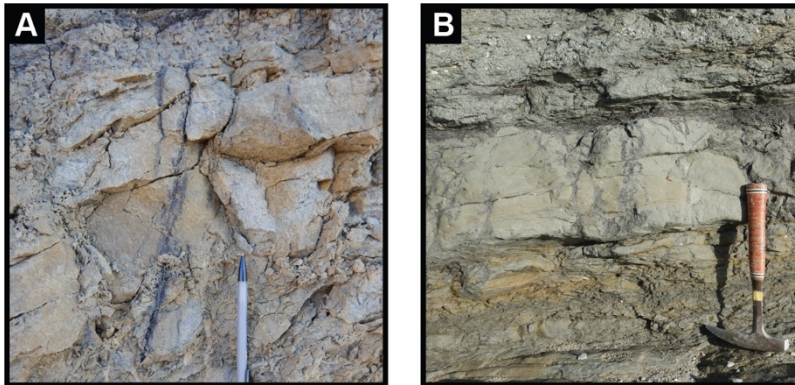


Fig. 16: Example of rootlets in sandstones of the Sarsbukta Formation. A) Close-up of a coalified rootlet (pencil for scale). B) Sandstone bed with rootlets that are probably linked to the overlying organic rich horizon (hammer for scale).

Interpretation – These sandstone beds are interpreted as seatearth (Miall, 1977a, 1977b). After their deposition, soils were formed on top of the beds and plants rooted into the sand bodies. This process is common in a floodplain setting (Reinfelds and Nanson, 1993).

St – trough cross-bedded sandstone

Description – Facies St is made up by medium to coarse grained, trough cross-bedded sandstones. The trough cross-beds occur on cm to dm scale while bed thicknesses reach up to 1 m and the bed boundaries are sharp with conformable bases. Facies St is mostly found in the exposures along the northern beach (Fig. 22).

Interpretation – Trough cross beds are formed by migration of dunes with sinuous crests in the lower flow regime of a unidirectional current (Walker and Cant, 1984). Unidirectional currents occur in fluvial channels and coastal environments (Boggs, 2011; Boyd et al., 1992;

Walker and Cant, 1984). Based on terrestrial fossils and the coal content, facies St is interpreted as fluvial channel deposit (Miall, 1985, 1977b).

Sp – planar cross-bedded sandstone

Description – Facies Sp is characterized by planar cross-bedded sandstones with grain sizes ranging from medium to very coarse, and may contain granules to pebbles (Fig. 17). It is common in the exposures along the northern beach but also in central Sarsøyra (Fig. 21 and Fig. 22). Bed thicknesses range between c. 10 and c. 100 cm. The planar cross-beds often affect only parts of a bed that otherwise appears as massive or horizontally laminated. Still, some beds are cross stratified over their entire thickness (Fig. 25).

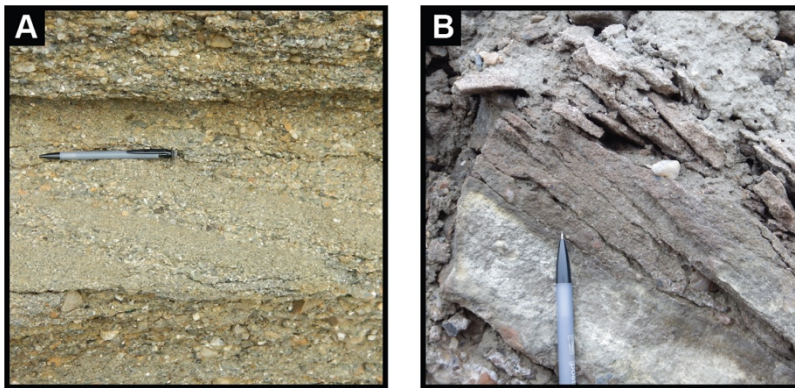


Fig. 17: Example of planar cross-bedding (facies Sp) in sandstones of the Sarsbukta Formation. A) Very coarse sandstone planar cross-bedded with granules (pencil for scale). B) Planar cross-beds in coarse sandstone (pencil for scale).

Interpretation – Facies Sp may represent different modes of deposition. It can form due to the migration of dunes with straight crests in the lower flow regime, but can also be the result of deltaic growth of linguoid bars, transverse bars or sand flats (Miall, 1985, 1977b, 1977a; Walker and Cant, 1984). Thus, in the present context, facies Sp is interpreted as fluvial channel deposit.

Sh – horizontally laminated sandstone

Description – Facies Sh consists of horizontally laminated fine to coarse sand and may be pebbly. The boundaries are sharp with conformable and seldom erosive bases. Bed thicknesses are variable and reach more than 3 m.

Interpretation – Horizontally laminated sandstones form by bedload deposition in fluvial channels (Miall, 1985, 1977b, 1977a; Walker and Cant, 1984). Facies Sh is considered to result from planar bed flow.

Sr – rippled sandstone

Description – Facies Sr is made up by very fine to medium sand and contains asymmetrical ripples. Often, horizontal lamination is also present in beds containing ripples.

Interpretation – The rippled sandstone beds are interpreted to result from the formation of ripples in the lower flow regime of a river channel (Miall, 1985, 1977b).

F1 – fine sand to claystone

Description – Facies F1 comprises the very fine grained deposits of the Sarsbukta Formation and is most abundant in the middle section of the northern beach (Fig. 22). It consists of clay to silt stones with silt to fine sand interbeds (Fig. 18C). The appearance is generally dark grey with less frequent light brown beds and the units appear ashorizontally laminated or massive with occasional ripples or planar cross-beds. Beds can reach thicknesses of up to 4 m and have sharp, conformable boundaries. Facies F1 commonly occurs between sandstone units of facies Sm and Sh, and is commonly associated with organic rich horizons, paleosols and thin (<5 mm) coal stringers as well as larger coal fragments.

Interpretation – Facies F1 characterizes sedimentation from suspension during flooding events or in lakes (Walker and Cant, 1984). In the present case, it is therefore interpreted as overbank deposit (Benvenuti, 2003; Miall, 1977b, 1977a; Reinfelds and Nanson, 1993).

C – Coal

Description – The coal within the Sarsbukts Formation occurs as stringers of up to 10 cm thickness, coalified wood fragments and detrital coal clasts (Fig. 18). The coal stringers are commonly discontinuous but occasionally extend over entire outcrops (Fig. 18A). Within the finer grained units of the Sarsbukta Formation, coalified remains of tree trunks and branches are abundant (Fig. 18B and C). They vary in size but can reach >30 cm in diameter. Some of the fragments are very well preserved and growth rings are still distinguishable. One bed within facies Gm contains well-rounded coal clasts.

Interpretation – Coal stringers are the result of peat burial. Peat can form in abandoned channels, oxbow lakes and floodplain depressions (Cameron et al., 1989; Fielding, 1986; Miall, 1977b). The coalified wood fragments were probably deposited as driftwood during

flooding and subsequently buried by fine grained sediments (Dill et al., 2004). Detrital coal clasts were most likely eroded from coal bearing strata that are much older than the infill of the Forlandsundet Graben (Kleinspehn and Teyssier, 2016).

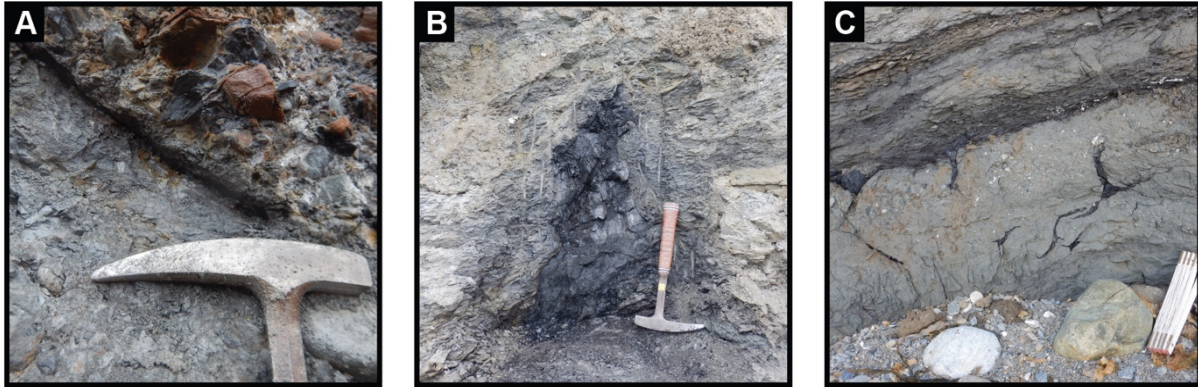


Fig. 18: Examples of coal within the Sarsbukta Formation. A) Thin coal seam within conglomerates of facies Gm (hammer for scale). B) Coalified tree trunk (hammer for scale). C) Coal fragments within sandstone. Note the geometry of the coal features that is probably related to fluid escape (measuring stick for scale, length of the segments 20 cm).

P – Paleosol

Description – Paleosols appear as distinct greenish or bleached horizons within fine grained sedimentary strata. The color alterations indicate that the sediments were oxidized and weathered. They are up to 10 cm thick. Within thick conglomerate packages of facies Gm (Fig. 23), paleosols can form the base of coarsening upwards sequences.



Fig. 19: Paleosol surface at the base of a fine sandstone within a conglomerate succession (hammer for scale). This photograph shows the lower paleosol surface indicated in Fig. 23.

Interpretation – Facies P is interpreted to have formed as soil on alluvial fan lobes and/or floodplains. Soil formation requires longer phases of inactivity or areas that are protected from the main transport corridors (Blair, 2000; Bown and Kraus, 1981; Pimentel, 2002).

3.1.2 Lithofacies associations

This section introduces lithofacies associations (FA) based on the previously presented lithofacies and represent depositional systems. Table 3 gives an overview over the defined lithofacies associations, subsequently the lithofacies associations are described in detail.

Table 3: Lithofacies associations of the Sarsbukta Formation.

| Code | Name | Facies | Description | Interpretation |
|-------------|--------------|-------------------------------------|--|--|
| A | Alluvial fan | Gm, Gp, Sm, P, C | Dominated by thick conglomerate beds of facies Gm | Debris and high energy stream flow deposits on alluvial fans |
| R | River | Sm, St, Sp, Sh, Sr, Gp, P, C, Gm | Dominated by sandstone facies with interbedded conglomerates | Deposition by fluvial channels |
| F | Floodplain | Fl, S, P, C | Dominated by facies Fl and subordinate sandstone facies | Floodplain deposits |

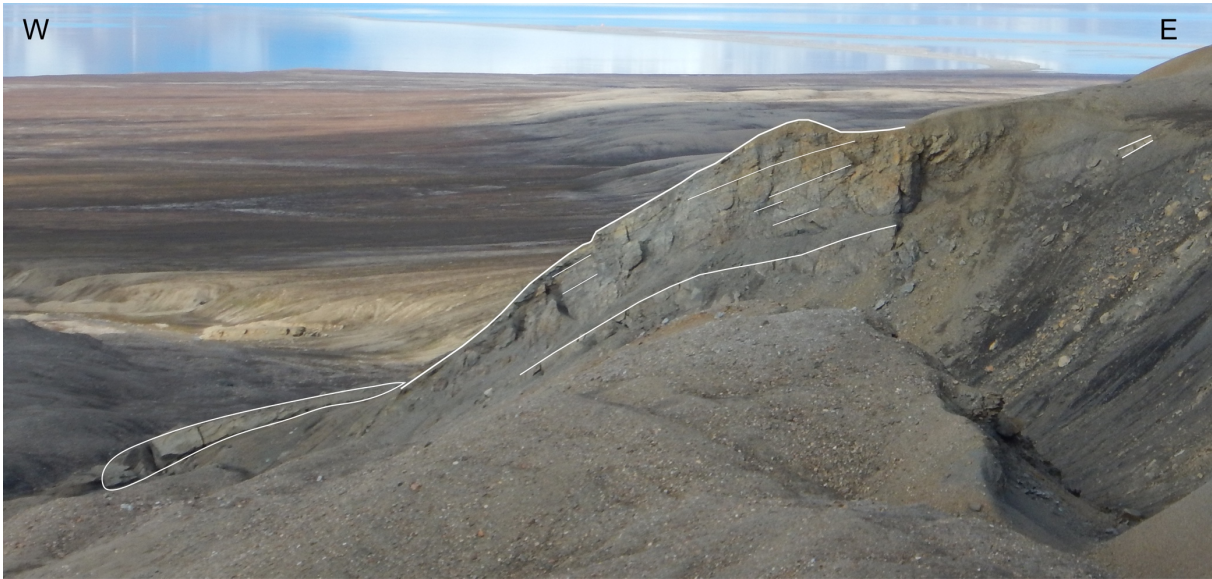


Fig. 20: Picture of the largest outcrop at the type section of the Sarsbukta Formation in central Sarsøyra, oriented W-E. Layer contacts are indicated, as well as, a wedge-shaped feature in the background. The layers are dipping towards the west (Fig. 11) and steepen into the basin. The wedge-shaped feature documented in Fig. 24 is located directly behind (north) the wedge indicated in this figure.

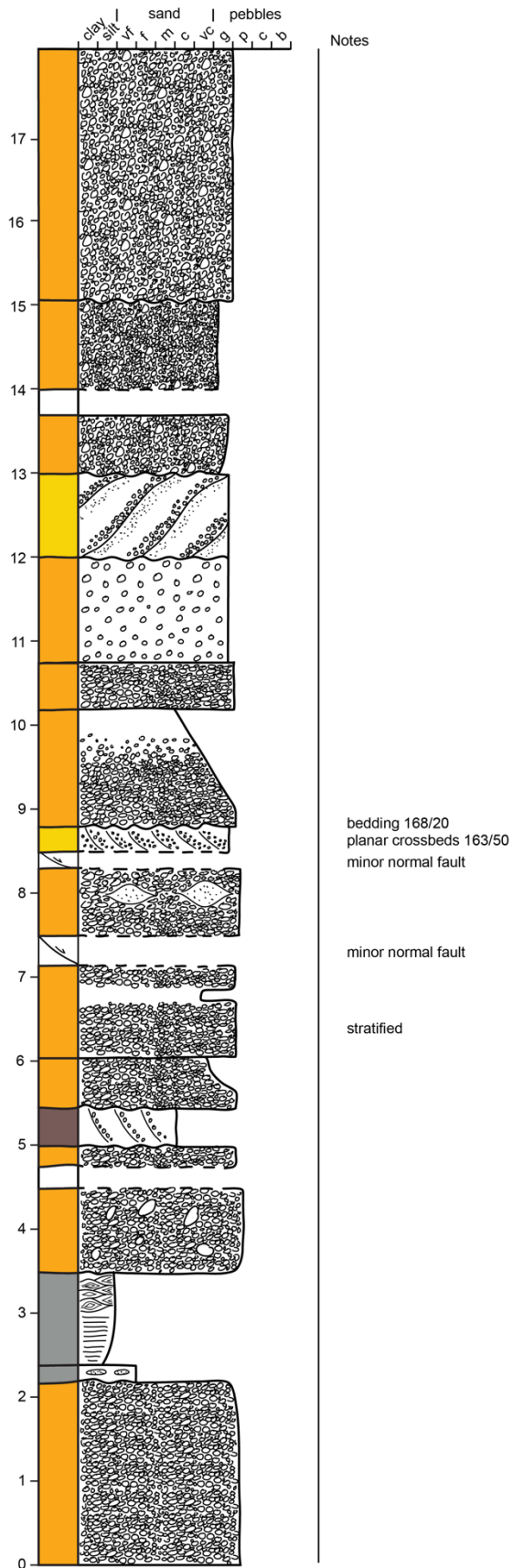


Fig. 21: Sedimentary log through the succession of the outcrop shown in Fig. 20.

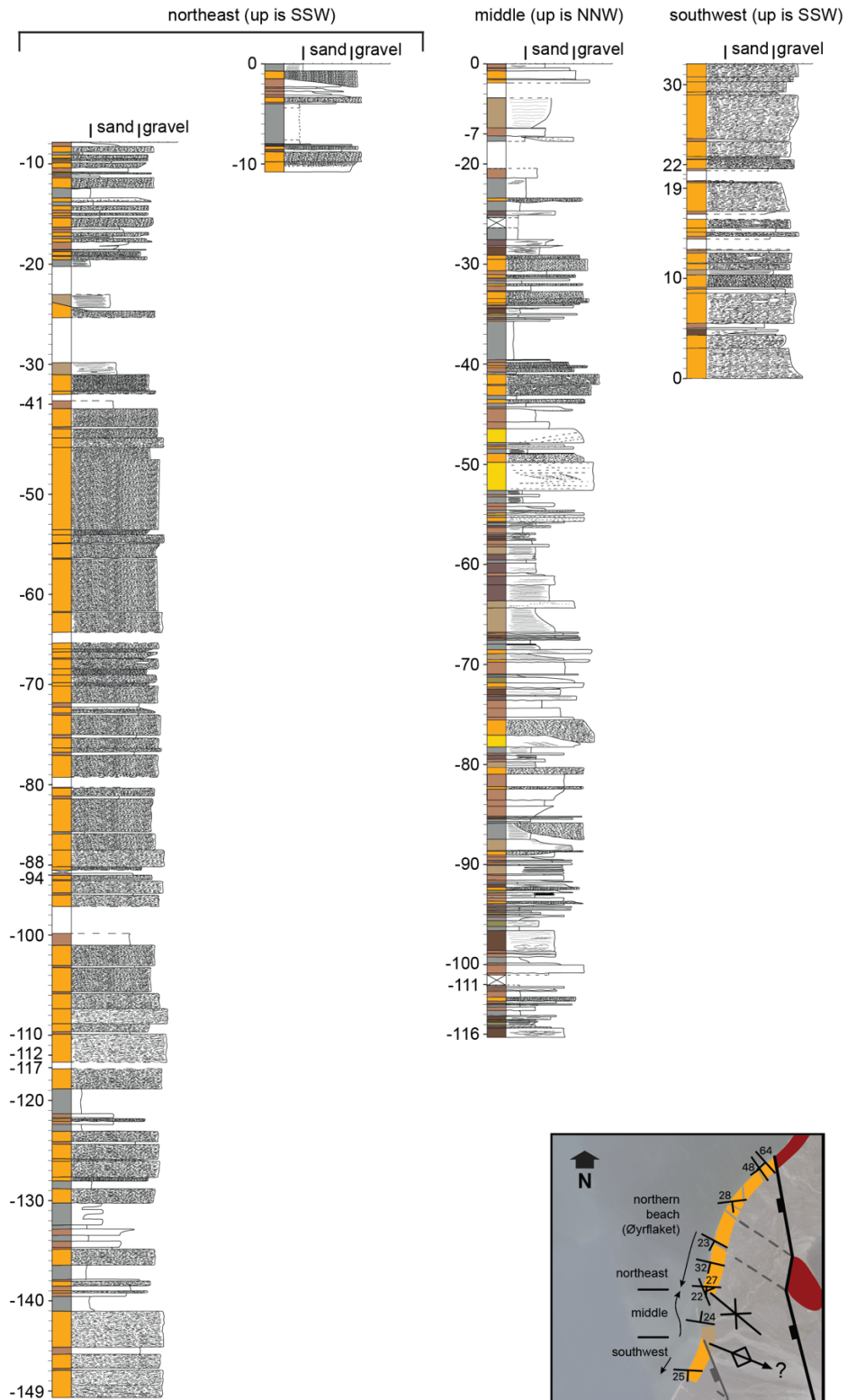


Fig. 22: Sedimentary logs from the northern beach, scale is in meters. The map shows the position and logging direction of logs (arrows point stratigraphically up). For the location of the northern beach locality the reader is referred to Fig. 11. The logging direction is given in parenthesis and changes between the logs according to the prevailing layer dip. The northeastern and middle logs start at the same stratigraphic level in the center of a syncline. The stratigraphic position of the southwestern log is uncertain as it might be separated by a fault from the rest of the stratigraphy (Fig. 11). More detailed versions of the logs in 1:50 scale are presented in Appendix 1, Appendix 2 and Appendix 3.

A – Alluvial fan & proximal river

Description – Facies association A contains thick successions of facies Gm with thinner beds of facies Gp, Sm and Fl as subordinate lithologies. Paleosols (facies P), as well as coal (facies C), are present in interbedded finer grained deposits (Fig. 23). The conglomerates are coarse with clasts of pebble to cobble size and poorly sorted. Most of the beds are massive but some exhibit sedimentary structures like horizontal stratification, planar cross-bedding (Fig. 24) and clast imbrication. The bases of facies Gm are often erosive while the sandstones overlie the conglomerates conformably. Facies association A is exposed in central Sarsøyra (Fig. 23 and Fig. 12) and along the northeastern part of the northern beach (Fig. 11 and Fig. 22). At the northern beach, facies association A interfingers with facies association F (Fig. 11). The large-scale stratigraphic architecture is difficult to assess since the available outcrops only cover some 10s of meters along the strike of the bedding.

Interpretation – The presence of paleosols and coal suggests that facies association A was deposited in a terrestrial environment. Thick conglomerate dominated succession, like facies association A (Fig. 22 and Fig. 23), are commonly associated with alluvial fans (Blair and McPherson, 1994; Gloppen and Steel, 1981; Nemeč and Postma, 1993; Nemeč and Steel, 1984; Nilsen, 1982). The clast size dominating facies Gm points towards high-energy depositional processes (Blair and McPherson, 1994). Since much of the clast rounding may occur close to the source area (Mills, 1979), the roundness of the clasts does not rule out a proximal sediment source. However, the roundness of the clasts does suggest that bedrock cliff failure processes had little importance during deposition or occurred in a more proximal location. Hence, facies association A was deposited on a mature alluvial fan (Blair and McPherson, 1994; Nemeč and Postma, 1993). According to Blair and McPherson (1994) alluvial fans can be classified into debris flow dominated and sheetflood dominated. Sheetflood deposits are characterized by relatively thin planar couplets and the development of low-angle cross-beds as well as transverse ribs (Blair, 2000; Rahn, 1967). These structures have not been observed in outcrops but that does not rule out that sheetfloods were active on the fan.

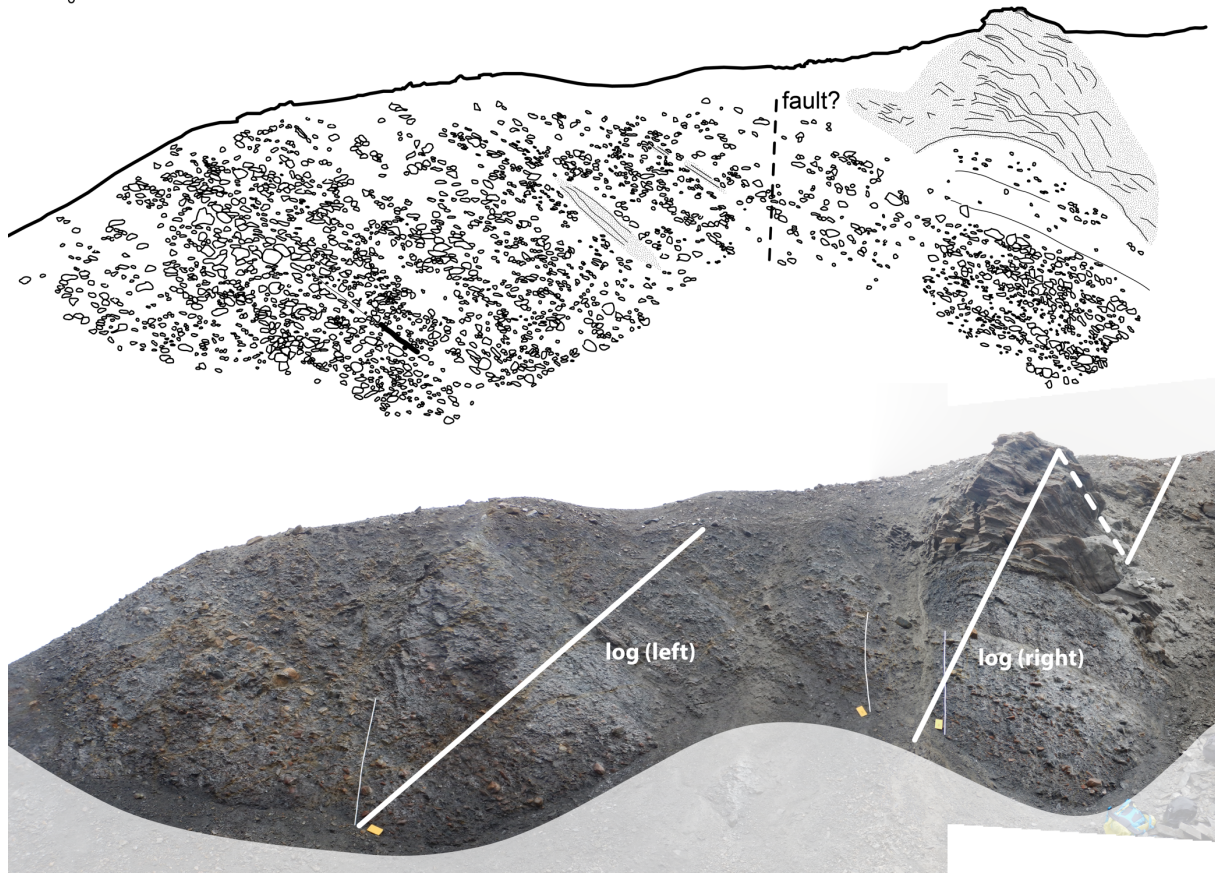
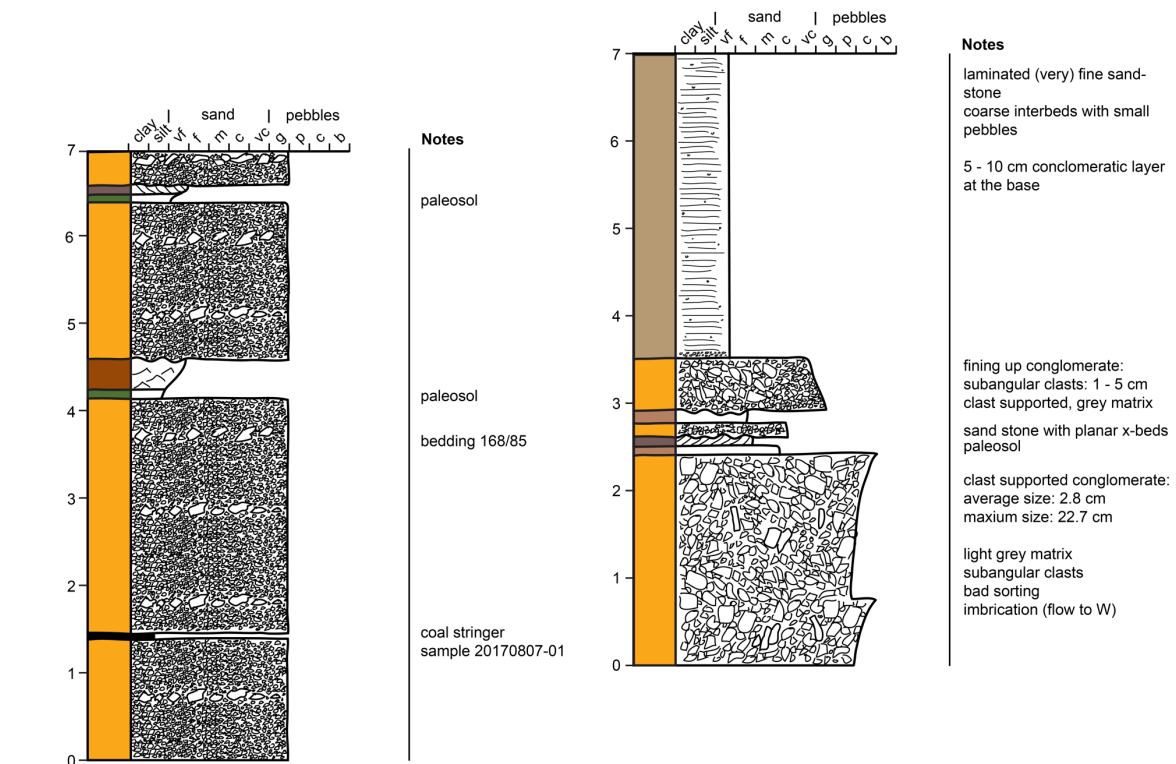


Fig. 23: Detailed documentation of the outcrop at the ravine entrance (Fig. 12). Facies association A makes up the larger part of the exposure with some interbedded fines. The conglomerate succession is overlain by a very fine sandstone (see also Fig. 26). For the location see Fig. 12.

Sedimentary structures like inverse grading (Fig. 23) and bed thicknesses over 2 m (Fig. 22) are attributed to debris flows (Blair and McPherson, 1994; Gloppen and Steel, 1981; Nemeč and Postma, 1993). The poor sorting and clast supported texture also point towards deposition by debris-flow mechanisms. However, erosional boundaries at the base of conglomerate packages as well as clast imbrication, are not commonly associated with debris flows (Blair and McPherson, 1994; Nemeč and Steel, 1984) but high energy stream flows or secondary processes are more likely to have caused these structures (Blair and McPherson, 1994). Stream flows on alluvial fans commonly deposit lag and bar gravels (Blair and McPherson, 1994; Miall, 1977b). Also, the few existing sandy beds (Fig. 22) are probably related to stream flows. An exposure in the river valley (Fig. 24) in central Sarsøyra (Fig. 12) shows downlap of facies Gp and Sp on a conglomerate body of facies Gm. The outcrop contains high angle planar cross-bedding, of alternating conglomerates and sandstones, as well as small scale planar cross-bedding within sandstone beds and sandstone relics. Remnants of a siltstone (facies Fl) exist between the conglomerate body and the downlapping strata. These structures could represent the progradation or deltaic growth of a longitudinal bar within a stream flow on the mid fan section (Allen, 1981; Best et al., 2003; Miall, 1977b, 1977a; Nilsen, 1982). That the planar cross-beds were induced by sheetfloods, is considered unlikely due to the high angled nature of the structures (Fig. 24) (e.g. Blair, 2000). The combination of massflow dominated (Fig. 23) and proximal stream flow dominated (Fig. 24) deposits within facies association A is justified because they show a similar transport direction (Fig. 33), oriented away from the uplifted footwall that was probably located to the east (section 6.1). Also, the scale of the sedimentary structures and the pebbly grain size in Fig. 24 differ significantly from the interpreted fluvial deposits exposed at the northern beach (Fig. 25) and the fine grained sandstones overlying the alluvial fan conglomerates in central Sarsøyra (Fig. 23 and Fig. 26).

The development of paleosols (Fig. 23) indicates that at least parts of the fan experienced longer periods of inactivity. On debris flow dominated fans it is common that the active lobe is only depositing on parts of the fan, leaving the rest of it undisturbed. The position of the active depositional lobe on the fan changes in a cyclic manner to maintain the semiconical shape (Denny, 1967 as cited in Blair and McPherson, 1994).

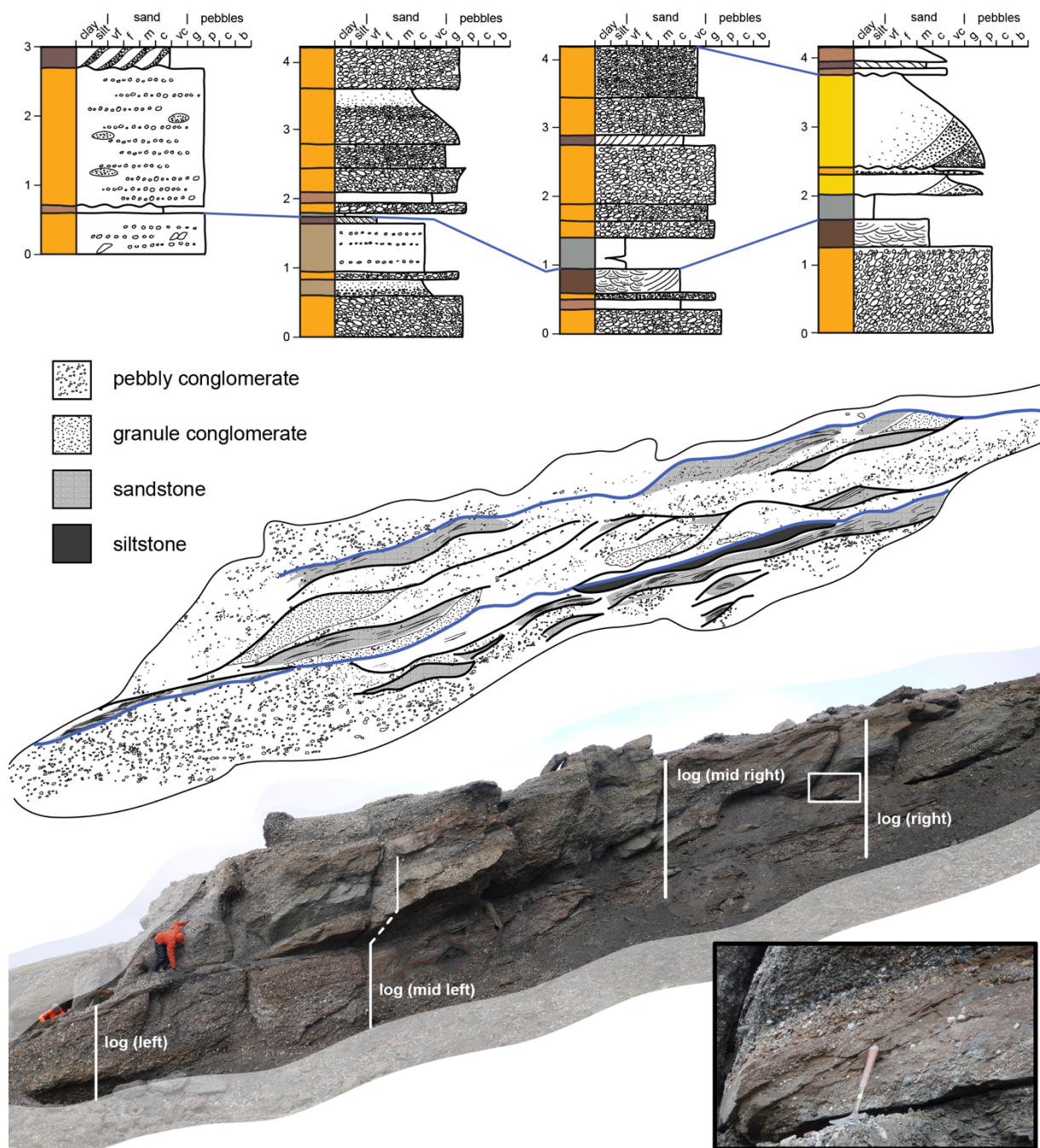


Fig. 24: Detailed assessment of a wedge-shaped sedimentary body in the river valley. It is located behind the wedge-shaped feature indicated in Fig. 20. Note the downlap of the planar cross-bedded conglomerates and sandstones in the upper part onto the conglomeratic body below. Blue lines mark major bounding surfaces in outcrop and logs.

R – river

Description – Facies association R comprises a variety of lithofacies. It is dominated by sandstones of facies Sm, St, Sp, Sh and Sr but also includes facies Gm and Gp with clast size pebble and smaller. Beds are 5 cm to approx. 1 m thick and contain planar as well as trough

cross-bedding as the most important sedimentary structures. Leaf imprints, coal (Fig. 14B and C), rootlets (Fig. 16) and paleosols attribute to biogenic activity. Facies association R is exposed in central Sarsøyra (Fig. 26 and Fig. 21), along the northern beach (Fig. 22 and Fig. 25) and in a small present-day river cut between those localities (Fig. 12).

Headlands at the northern beach give the opportunity to study the sedimentary architecture perpendicular to the prevailing dip. Fig. 25 showcases the best exposure. It consists of a channel that cuts into a horizontally laminated and partly planar cross-bedded fine-grained sandstone (facies Sh/Sp). The fill of the downcutting channel consists of pebbles at the base grading into granule conglomerates (facies Gm) and sandstones (facies Sm). Within the sandstone, horizons pebbles and granule bodies occur. Some of them exhibit planar cross-bedded geometries (facies Sp). The succession is overlain by a coarse pebbly sandstone with planar cross-beds on bed-scale.

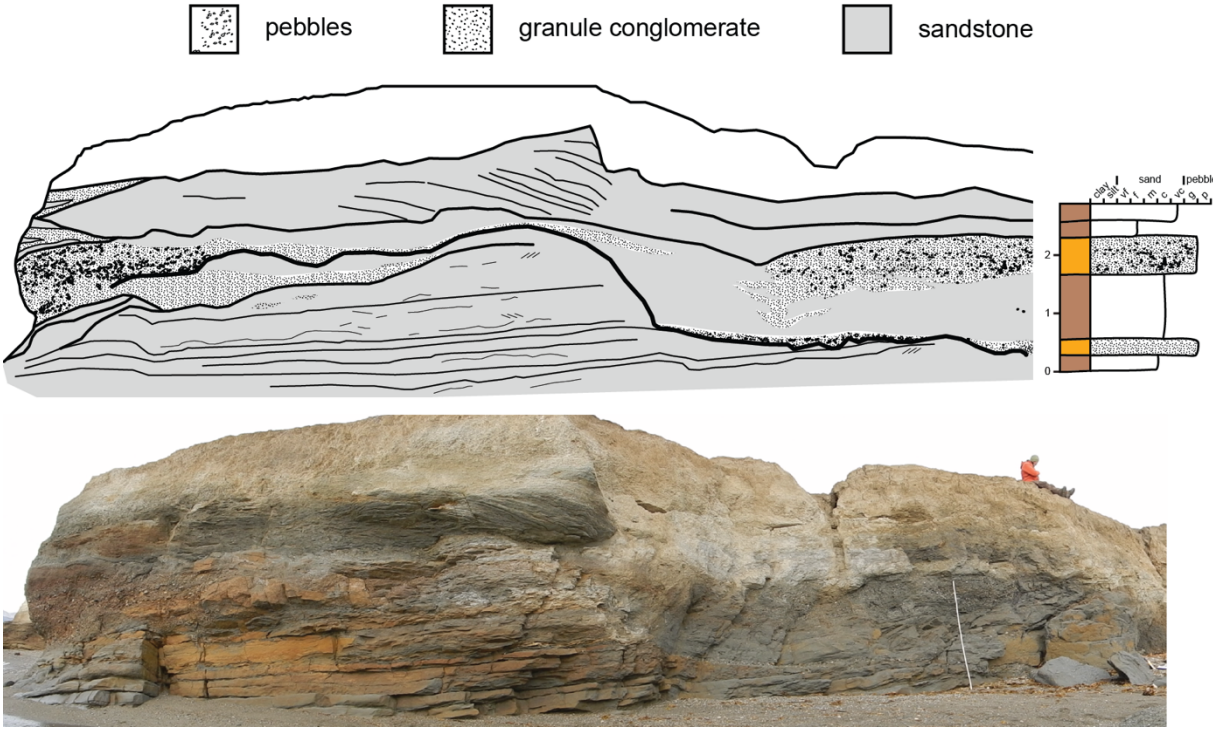


Fig. 25: Best outcrop of facies association R showing the sedimentary architecture of amalgamated fluvial channels. The exposures are located in headlands along the northern beach. The thick black line marks the main bounding surface / channel base.

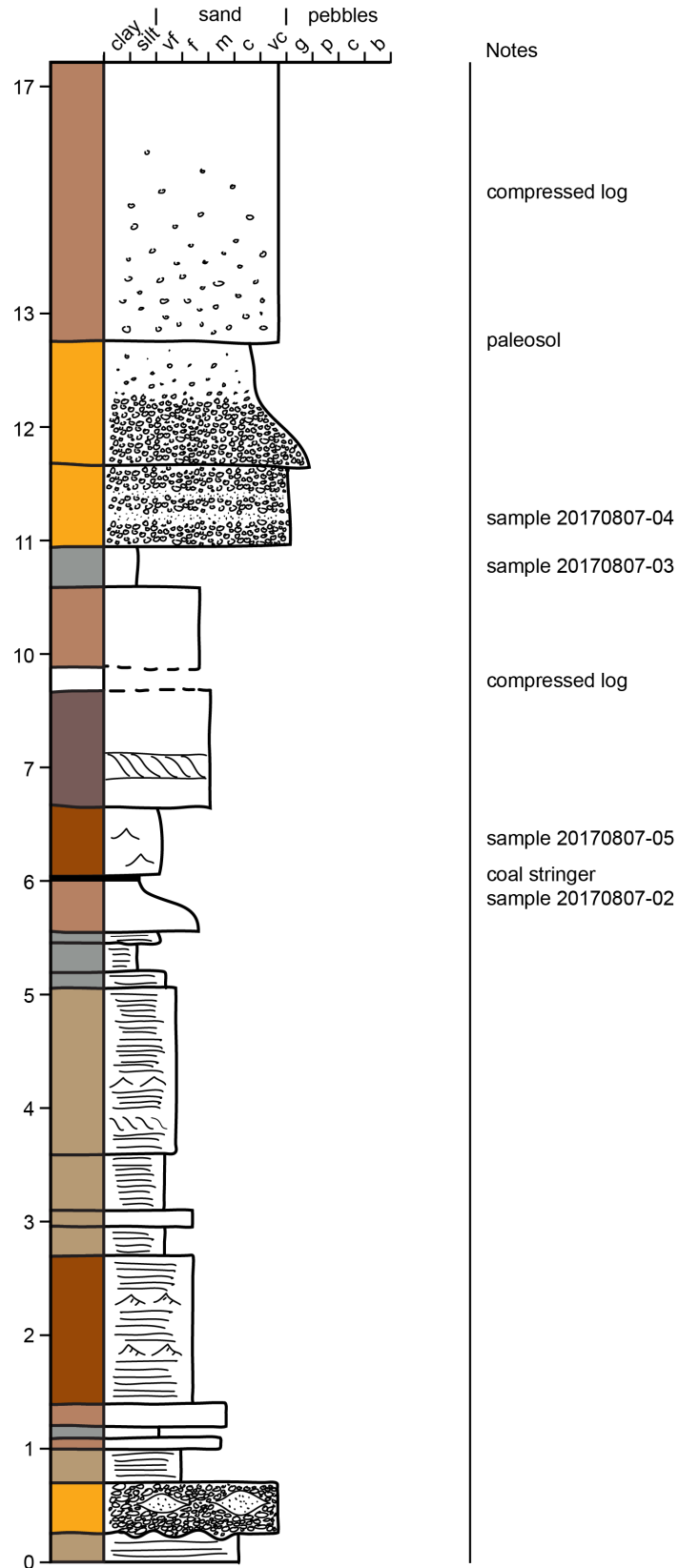


Fig. 26: Log of the sedimentary succession at the ravine entrance in central Sarsøyra. This section is dominated by facies association R made up from fluvial sandstones with some subordinate conglomerates. Interlayered beds of facies F1 indicate remnants of floodplain deposition (FA F). This log connects to top of the right log in Fig. 23.

Interpretation – The occurrence of coal, paleosols and rootlets is a clear indicator for subaerial exposure in a continental environment. Planar and trough cross-bedding in sandy units suggest unidirectional flow in a fluvial system. The two most important river types are meandering and braided fluvial systems (Miall, 1985; Walker and Cant, 1984): Meandering rivers deposit a sequence that fines upwards from trough cross-bedded channel deposits into fine grained overbank sediments (Reinfelds and Nanson, 1993; Smith, 1987; Walker and Cant, 1984). A meandering river model for the Sarsbukta Formation was previously suggested by Kleinspehn and Teyssier (2016). Braided rivers on the other hand are characterized by changes in flow intensity and deltaic bar growth (Blum et al., 2005; Bourquin et al., 2009; Miall, 1985, 1977b, 1977a). Due to this dynamic behavior they show a greater variety in lithofacies and a complex interaction between them. Facies association R appears to exhibit characteristics of both a meandering and a braided river (Fig. 22, Fig. 26 and Fig. 25).

Cannibalization and amalgamation of channel bodies are typical features of braided river deposition and are well illustrated in Fig. 25 from the northern beach (Miall, 1977a; Rust, 1972). Fig. 25 shows how a channel cuts into a horizontally laminated sandstone that was probably deposited in the lower flow regime of an earlier channel (Miall, 1977b, 1977a). A pebbly lag deposit at the base of the newly established channel forms a well pronounced bounding surface (Fig. 25) (Rust, 1977a; Walker and Cant, 1984), while the sandy to granule channel fill above consists of bedload deposits (Martin and Turner, 1998). The outcrop is capped by a sand bed that contains planar cross-beds over its entire thickness (Fig. 25).

Planar cross-bedded textures of this magnitude can be associated with sandbars in the river bed (Rust, 1977a; Walker and Cant, 1984). High-angle planar cross-beds as shown in Fig. 25 are most likely attributed to downstream or lateral accretion of bars (Best et al., 2003; Blum et al., 2005; Smith, 1974). Thereby, sediment transported over the bar accumulates on the slipface. Since the cross-beds are oriented approx. parallel to the trend of the channel, it can be assumed that they formed sub-parallel to the flow direction of the stream. Therefore, the planar cross-bedded layer is interpreted to represent lateral accretion of a lingoid bar (Best et al., 2003; Lunt and Bridge, 2004; Walker and Cant, 1984). This mode of deposition requires at least seasonal bar-top flow and therefore develops preferentially in fluvial systems with high variations in discharge (Blum et al., 2005; McLelland et al., 1999). Interlayered granule and sand structures that pinch out (Fig. 25, upper left) are interpreted as trough cross-stratification deposited by dunes along the bar flanks (cf. Best et al., 2003).

Especially the up to 4 m thick intervals of facies association F indicate that substantial floodplain sediments were accumulated and lead to the conclusion that the fluvial channels had a rather high sinuosity (e.g. Boggs, 2011; Rosgen, 1994; Rust, 1977b).

F – floodplain

Description – Facies association F consists of facies F1 with subordinate sandstones. The silt to clay intervals reach thicknesses of several meters while sandstone thicknesses do not exceed 50 cm (Fig. 22). Commonly, the deposits are horizontally laminated. However, they occasionally show small scale current ripple lamination. Coal stringers as well as larger coal fragments are common in this facies association. Facies association F is exposed in the middle section of the northern beach (Fig. 22) and interfingers with the deposits of facies association A towards the northeast (Fig. 11 and Fig. 22).

Interpretation – Coal stringers and fragments are strong arguments for a terrestrial deposition of facies association F. The fine grain size and the horizontal lamination advocate for sedimentation from suspension and thus, a low energy transport mechanism. However, the occasional ripples indicate some unidirectional flow. Such fine grained facies can form as overbank deposits during flood events (Miall, 1977b, 1977a; Nanson and Croke, 1992; Reinfelds and Nanson, 1993; Walker and Cant, 1984). In the context of fluvial system (FA R), such depositional processes are expected. The thickness of the overbank deposits is significantly lower than the thickness of the river sediments (FA R) (Fig. 22 and Fig. 26). This relationship is established because the fine grained facies are easily eroded by high energy fluvial currents which is common for braided rivers (Nanson and Croke, 1992; Reinfelds and Nanson, 1993; Walker and Cant, 1984). Thus, facies association F is often only preserved as a thin and discontinuous layer. The logs in Fig. 22 and Fig. 26 show this characteristic in many places but also significantly thicker intervals that would point more towards meandering channel deposition (e.g. Reinfelds and Nanson, 1993; Smith, 1987; Walker and Cant, 1984). Facies association F is therefore interpreted as floodplain deposits that evolved in association with a sinuous (braided) river that allowed the establishment of extensive floodplains (e.g. Miall, 1977b, 1985; Reinfelds and Nanson, 1993; Rust, 1977a; Walker and Cant, 1984).

3.1.3 Summary

In summary, the Sarsbukta Formation is interpreted as marginal alluvial fans that interfinger with floodplain and fluvial deposits. This conception is based on some key observations that stand against the interpretation of the Sarsbukta Formation as purely gravelly meandering river deposit by Kleinspehn and Teyssier (2016). The existence of two different depositional systems is apparent from the paleocurrent data at the northern beach. The widely varying paleoflow directions, as reported by Kleinspehn and Teyssier (2016), were not found in this study. Instead, the paleocurrent data clearly show that sediment transport was directed towards the northeast (section 3.3). Within a single depositional system, the grain size would be expected to decrease with the transport direction (e.g. Dade et al., 1998). Along the northern beach, however, sedimentary logging revealed a substantial increase of the dominating grain size with the transport direction from sand dominated to pebble and cobble dominated deposits (Fig. 22). As presented in the lithofacies associations chapter (section 3.1.2) these systems are interpreted as alluvial fan and a river system.

The sand and pebble dominated strata show signs of bar formation (Fig. 25) and the general facies assemblage would fit well with a braided river system (Miall, 1985, 1977a, 1977b). Also, the often thin and discontinuous floodplain deposits would complement this picture. However, thicker intervals of floodplain sediments account for intervals of up to 4 m (Fig. 22). Together with roots, coals and paleosols they suggest that substantial amounts floodplain sediments could accumulate adjacent to the river bed and that some channels were abandoned (Nanson and Croke, 1992; Rosgen, 1994; Walker and Cant, 1984). Thick floodplain deposits are commonly associated with fining upwards cycles in meandering river systems where they can account for up to two thirds of the sedimentary succession (Nanson and Croke, 1992; Walker and Cant, 1984). This characteristic, as well as point bar accretion (e.g. Smith, 1987), has not been recognized in the field (section 3.1). However, the thick fluvial plain deposits indicate that the fluvial channel showed a high sinuosity (e.g. Boggs, 2011; Rosgen, 1994; Rust, 1977b). Thus, the fluvial deposits of the Sarsøyra Formation exhibit characteristics of a braided river, e.g. lateral bar formation and amalgamation, as well as of a meandering river, e.g. extensive floodplain deposition and formation of paleosols. Therefore, the deposits are interpreted as an intermediate river type, e.g. a sinuous braided river.

3.2 Sarstangen Formation

3.2.1 Lithofacies

The Sarstangen Formation is only exposed at the western beach of Sarsøyra (Fig. 12). Fig. 30 and Fig. 31 document the type section of the succession. The rocks of the Sarstangen Formation are barely lithified and especially the finer grained facies appear as unconsolidated sediments.

The Sarstangen Formation was first described by Rye-Larsen (1982) as marine ‘debris wedge’. Kleinspehn and Teyssier (2016) interpreted the deposits as alluvial fan/marine fan delta succession.

Table 4: Lithofacies of the Sarstangen Formation. The colors correspond to the ones used to mark the lithofacies in the logs.

| Code | Lithofacies | Description | Sedimentary structures | Interpretation |
|------|-------------------------------|---|-----------------------------|--|
| B | Sedimentary breccia | Poorly sorted angular boulders in very coarse matrix | Stratification, Imbrication | Debris flow and rock fall deposits |
| Gm | Massive rounded conglomerate | Polymictic conglomerate made up from well-rounded pebbles | Erosive base | Stream flow or coastal deposit |
| St | Trough cross-bedded sandstone | Medium to fine sandstone with coal streaks | Trough cross-bedding | Fluvial or coastal deposit |
| M | Marine claystone | Dark silty clay stone with rounded pebbles | Horizontal lamination | Distal (fan) delta to basin floor deposits |

B – sedimentary breccia

Description – Facies B is made up from poorly sorted angular to sub-rounded clasts in a matrix of very coarse sand. The angularity of the basement derived clasts increases with their size and boulders reach diameters of up to 4 m (Fig. 32). The clasts are largely derived from basement lithologies such as schists and quartzite and some mud clasts are also present (Fig. 27). The base of facies B is undulating and cuts into the underlying sedimentary units, forming an angular unconformity (Fig. 30). The breccia is largely clast supported, stratified (Fig. 32) and exhibits clast imbrication. A matrix consisting of very coarse sand is abundant. Facies B makes up a package of at least 15 m (Rye-Larsen, 1982 and this study).



Fig. 27: Mud clast (middle) within basement cobbles. Segment of the measuring stick corresponds to 20 cm.

Interpretation – Facies B is interpreted as a very proximal fan deposit. The sedimentary structures of facies B suggest that debris flows, sheetfloods and rock falls were active depositional processes (Blair, 2000; Blair and McPherson, 1994). Mud clasts can form in a variety of fluvial and shallow marine environments (Li et al., 2017). Facies B could have been deposited in an alluvial fan or as (subaerial) part of a fan delta (Benvenuti, 2003; Blair, 2000; Gloppen and Steel, 1981).

Gm – massive rounded conglomerate

Description – Facies Gm of the Sarstangen Formation is similar to facies Gm of the Sarsbukta Formation. It consists of a clast supported massive conglomerate that is made up from poorly sorted, rounded pebbles and granules. Some of the beds exhibit normal grading (Fig. 32). The clast composition is polymictic, containing a variety of basement lithologies. Erosive boundaries are present within the package.

Interpretation – Due to the limited exposure it is difficult to pinpoint the exact depositional environment and processes. However, normal grading suggest that the gravel was rather deposited by stream flow than mass flow processes (e.g. Miall, 1985, 1977b; Rust, 1972). Another alternative would be the deposition as a deltaic or coastal conglomerate (e.g. Boyd et al., 1992; Nemec and Steel, 1984; Rohais et al., 2007).

St – trough bedded sandstone

Description – Facies St overlies Facies M and consists of an approx. 30 cm thick bed of trough cross-bedded sandstone (Fig. 28B). The sand has the grain size medium to fine that contains thin (<3 mm) and discontinuous coal stringers (Fig. 28C) and streaks of granules

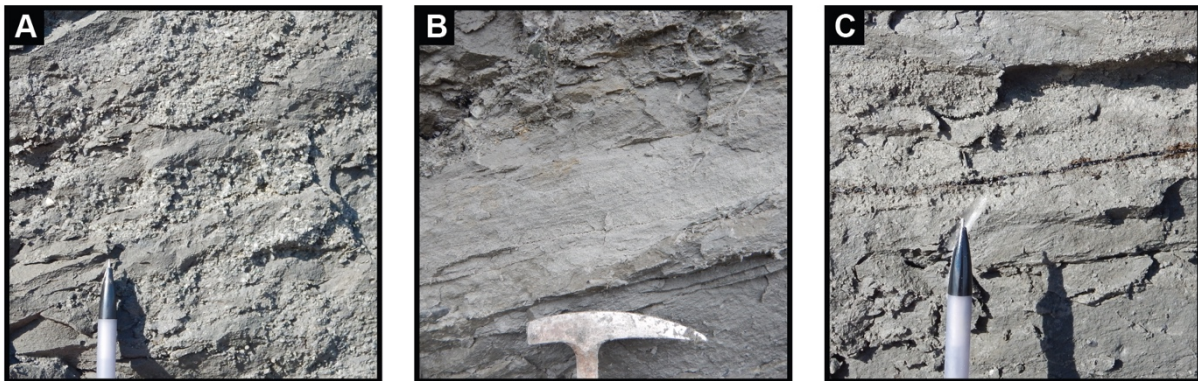


Fig. 28: Facies St in the Sarstangen Formation. A) Granules in medium sandstone (pencil for scale). B) Trough cross-bedding in medium sandstone (hammer for scale). C) Thin coal streak in medium sandstone (pencil for scale).

(Fig. 28A).

Interpretation – The cross-beds in facies St suggest unidirectional flow during deposition while granule streaks hint towards changes in flow intensity. The thin coal stringers are clearly autochthonous and argue towards deposition under terrestrial conditions. Facies St could therefore represent a fluvial deposit (e.g. Miall, 1985, 1977b; Walker and Cant, 1984). However, unidirectional flow and coal formation can also occur in coastal settings. For example, in tidal marshes, tidal channels or deltas (e.g. Arthur L. Bloom, 1964; Boggs, 2011; Boyd et al., 1992).

M – marine claystone

Description – Facies M is made up from dark silty clay and contains some rounded granules to pebbles (Fig. 29). The appearance is massive to horizontally laminated and the sediments

contain marine foraminifera as well as a variety of pollen (section 2.3) (see also Feyling-Hanssen and Uilleberg, 1984).

Interpretation – Due to the occurrence of marine foraminifera, facies M is interpreted as a marine claystone. The grain size and the massive to horizontally laminated texture suggest that facies M was deposited offshore on the basin floor. This could occur in the very distal part of a (fan) delta (Benvenuti, 2003; Gloppen and Steel, 1981). The rounded pebbles within facies M are interpreted as dropstones.



Fig. 29: Rounded pebble in the marine claystone of facies M (pencil for scale).

3.2.2 Lithofacies associations

The facies associations (FA) of the Sarstangen Formation essentially correspond to the defined lithofacies. This is due to the fact that each facies only makes up one package in the outcrop (Fig. 30 and Fig. 31). Therefore, the assessment of facies relationships is very limited. Overall, the succession at Balanuspynten is interpreted as a prograding fan delta (Kleinspehn and Teyssier, 2016; Rye-Larsen, 1982).

Table 5: Lithofacies associations of the Sarstangen Formation.

| Code | Name | Facies | Description | Interpretation |
|-------------|-------------------------|---------------|---|--|
| F | Fan | B | Dominated by thick sedimentary breccia | Debris flow deposits on a (subaerial) fan |
| R | River | Gm, St | Well-rounded conglomerate beds on trough cross-bedded sandstone | Deposition in a fluvial, deltaic or coastal system |
| M | Marine offshore deposit | M | Marine claystone with well-rounded pebbles | Very distal fan delta or basin floor deposits |

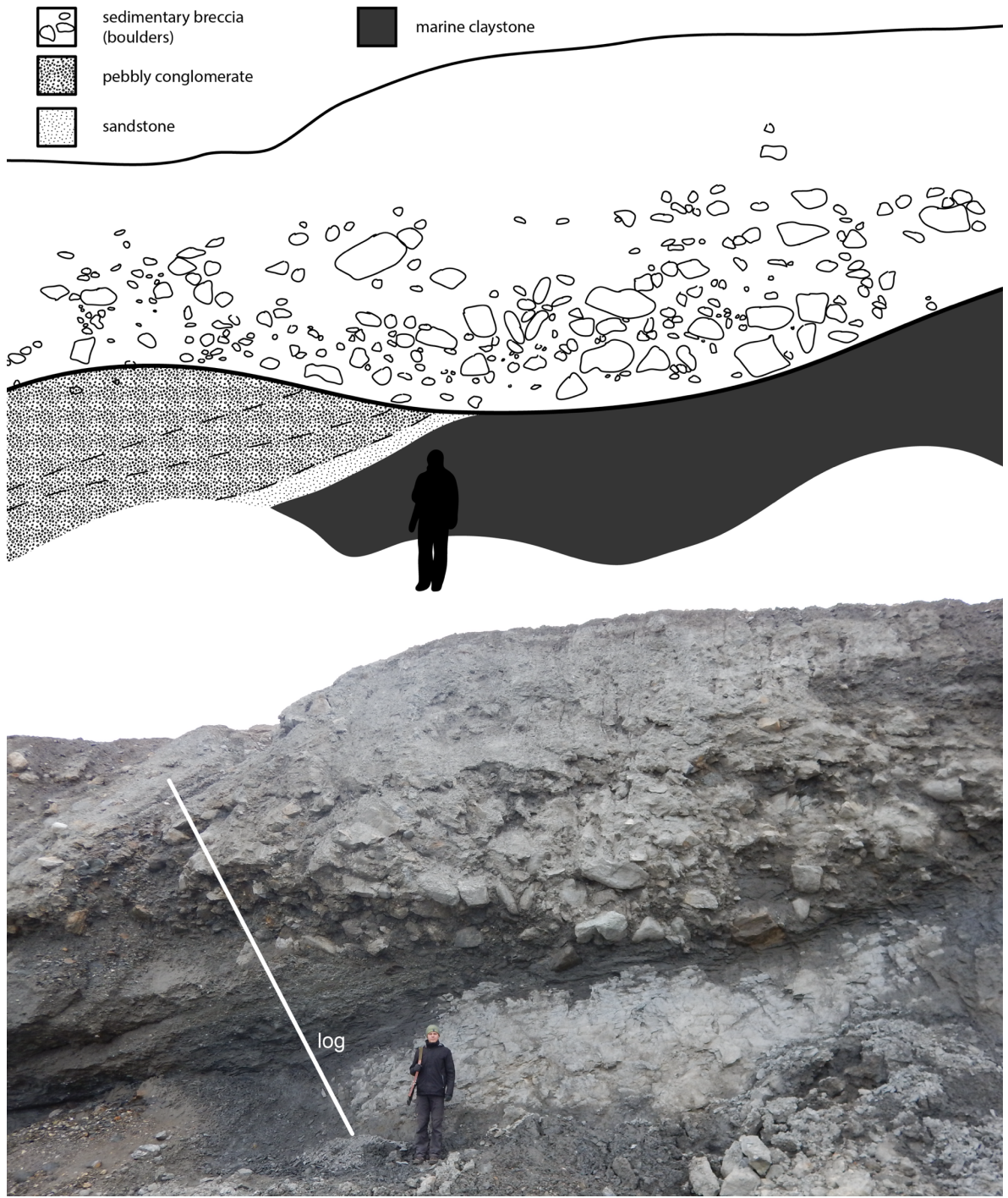
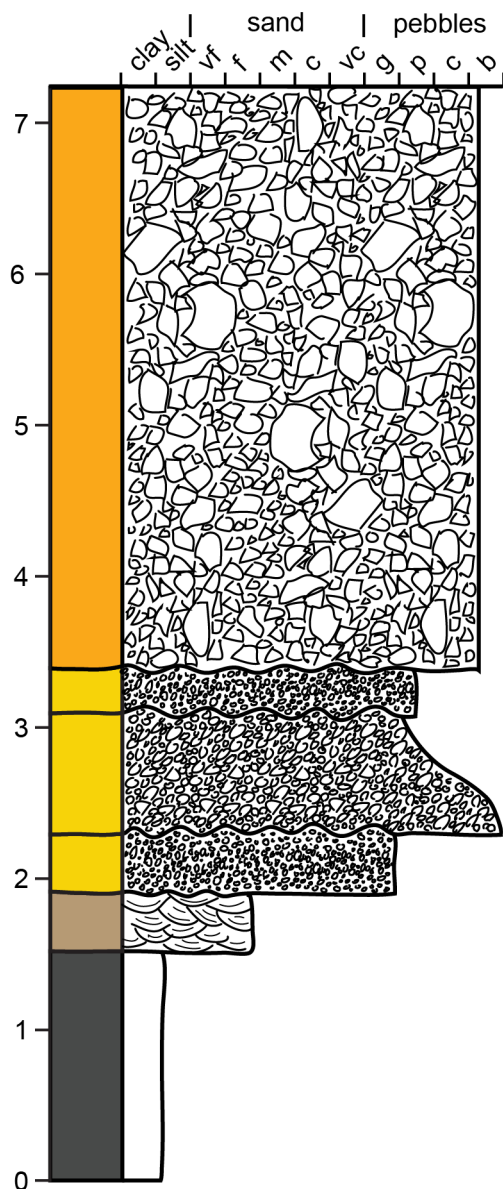


Fig. 30: Type section of the Sarsbukta Formation at Balanuspynten consisting of a sedimentary breccia eroding into a well-rounded conglomerate, sandstone and marine claystone succession. The underlying strata dips $233/20$ while the sedimentary breccia dips at $163/12$ (Fig. 32), forming an angular unconformity (see also Fig. 11). The log is presented in Fig. 31. It is oriented perpendicular to the lower beds.



Notes

bedding 223/20

sample 20180809-02

Fig. 31: Stratigraphy of the Sarstangen Formation at Balanuspynten (Fig. 30). The thickness of the lowermost and uppermost unit is unknown but probably exceeds the measured thicknesses by far. The overlying conglomerates are displayed in more detail in Fig. 32.

F – fan

Description – Facies association F is entirely made up by facies B and exhibits an erosive contact to the underlying sediments. It consists of chaotic (Fig. 30) as well as stratified (Fig. 32) conglomerate beds containing large angular outsize boulders.

Interpretation – Within facies association F, the most striking features are angular boulders with a diameter of up to 4 m (Fig. 32). Blair and McPherson (1994) outline three processes

that can deposit angular breccias: 1) Rockfalls, 2) rockslides and, 3) rock avalanches. They occur when parts of a bedrock cliff fail under their own gravitational load. Rockslides involve the destabilization of large rock volumes along preexisting weaknesses. They occur on several scales and successively disintegrate during transport (Weidinger et al., 2014). Similar to rock avalanches, they produce angular detritus across all grain sizes (Blair and McPherson, 1994). A characteristic that is not shared by facies association F since the angularity decreases for smaller clasts and a sandy matrix is present. Rock slides and avalanches therefore only played a minor role, if any, during deposition (Blair and McPherson, 1994). Rockfalls, however, could be responsible for the deposition of angular gravels (cf. Tanner and Hubert, 1991; Watkins, 1992). Particularly boulders bounce and roll to their deposition site after they detached off steep cliffs (Blair and McPherson, 1994). Hence, rockfalls are a likely cause for the emplacement of angular boulders into sediments accumulated by other processes. The steep topography that is required for this depositional process could be generated by the offset of a fault (cf. Blair and McPherson, 1994). The existence of a major structural feature in proximity to Balanuspynten is suggested by surface magnetic anomalies (Krasilschikov et al., 1995) as well as the difference in the top basement level between central Sarsøyra (sea level, Fig. 11) and the exploration well 5 km to the west on Sarstangen (1046 m depth, see section 5.1.1) (see also Kleinspehn and Teyssier, 2016). The boulders could also have been derived from steep intramontane valleys and subsequently transported by high density debris flows onto the fan (Nemec and Postma, 1993; Rodine and Johnson, 1976). However, transport within the valleys would probably have involved rounding of the boulders which was not observed in facies B (Mills, 1979; Rodine and Johnson, 1976).

As mentioned, rockfall is only one out of several processes that were active during the deposition of facies association B. Commonly, rockfall deposits are associated with sedimentation in talus cones and alluvial fans (Blair and McPherson, 1994). Notable is the well-developed stratification of dm thick conglomerate beds in facies association B (Fig. 32). Planar stratification, in so-called couplets, is a distinctive feature of sheetflood deposits, so is a poorly sorted, clast supported texture (Blair, 2000). Conversely, other common sedimentary structures of sheetflood deposits, such as low-angle cross-beds or transverse ribs (cf. Blair and McPherson, 1994), are absent. Kleinspehn and Teyssier (2016) suggest that the dip of the layers, represents the original depositional slope. A dip of 12° to 17° (Fig. 11) appears steep for a sheetflood dominated fan. Dip angles between 2° and 8° would rather be expected (Blair

and McPherson, 1994). This suggests that the layers either experienced rotation after deposition or other processes are responsible for the deposition facies association F.

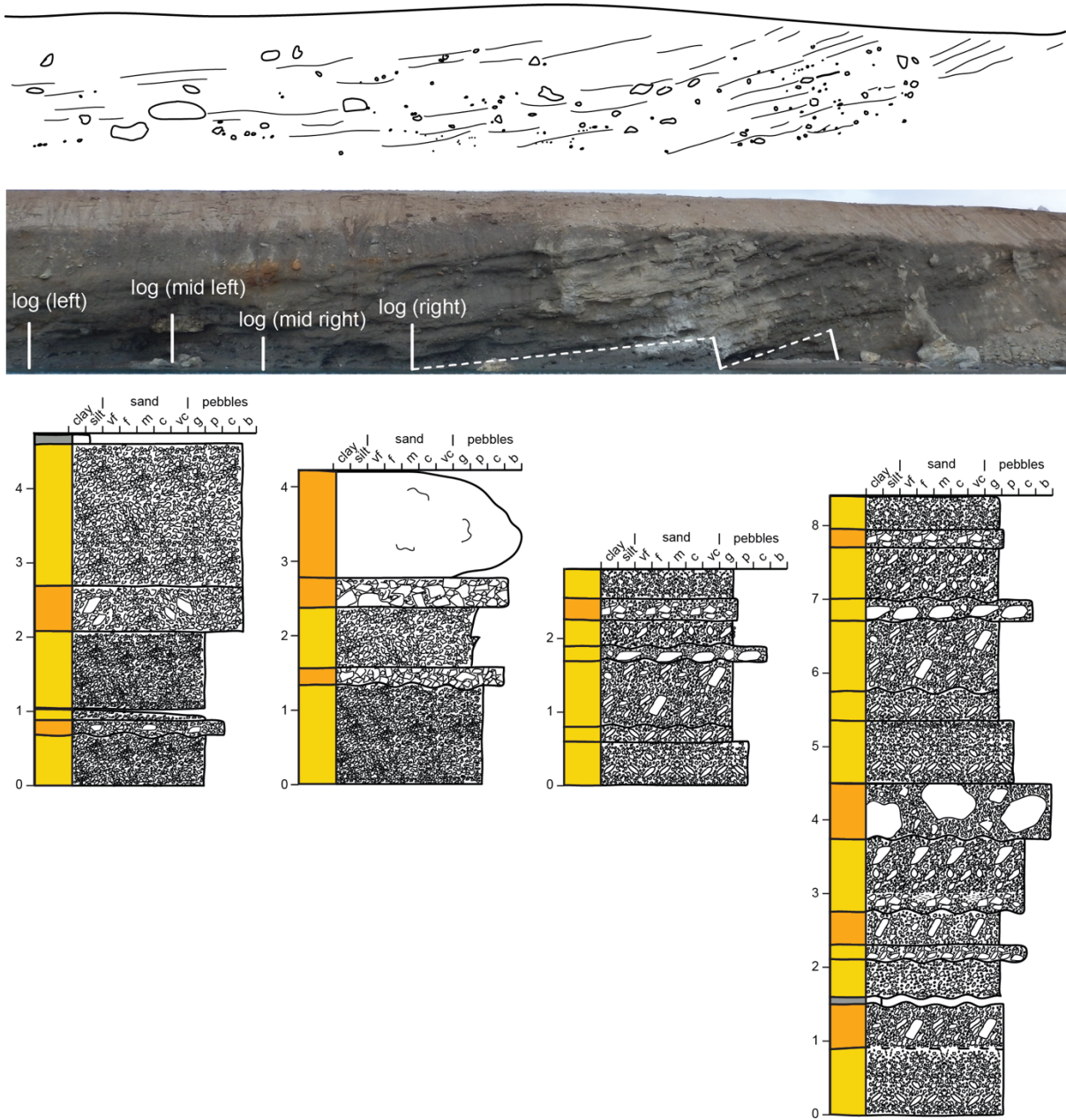


Fig. 32: Logs through the Sarstangen fanglomerates at Balanuspynten dipping at 163/12 to 173/17. Locations of the logs are indicated in the picture.

Debris flow dominated fans usually exhibit steeper slopes of 5° to 15° (Blair and McPherson, 1994) and can reach over 20° near the fan apex (Nemec and Postma, 1993). Sheet-like deposits, such as observed in facies association F, can be generated by amalgamation of several debris flows into a single layer (Sohn et al., 1999). Some beds exhibit inverse grading (Fig. 32) which is also characteristic for debris flows (Nemec and Postma, 1993; Nemec and

Steel, 1984). Sharp and erosive bed boundaries can be formed during surging of debris flows (Rickenmann and Weber, 2003), by secondary processes that erode the surface of the strata before the next depositional event occurs or by stream flow activity (Blair and McPherson, 1994; Nemeč and Steel, 1984). The presence of stream flows appears likely as some of the erosive bed boundaries coincide with normal grading and clast imbrication (Fig. 32) (cf. Nemeč and Steel, 1984).

Another way to explain a high depositional dip is that the exposed part of the ancient fan resembles an early or transitional stage of fan evolution (cf. Blair and McPherson, 1994). At that point, the fan has not established its final geometry and is characterized by steep slopes due to a large offset between the feeder channel and the basin floor that is not yet backfilled with sediments. Such fans are likely to exhibit an increased amount of cliff failure deposits (rock falls and avalanches), as seen in facies association F (Blair and McPherson, 1994; Nemeč and Postma, 1993).

An angular unconformity between is formed between facies association F and the underlying succession (Fig. 32). The underlying beds exhibit a dip of 20° towards the northwest (Fig. 32) while facies association F dips between 12° and 17° to the west (Fig. 32). While the beds of facies association F might have maintained their depositional dip (Kleinspehn and Teyssier, 2016), the finer grained lower beds were probably deposited sub-horizontally. Consequently, the underlying succession was tilted prior to the deposition of the sedimentary breccia. Causes for the folding could be displacement gradients or drag along the proposed normal fault and will be discussed in further detail in chapter 6 (see also Kleinspehn and Teyssier, 2016; Krasilscikov et al., 1995).

Whether facies association F was deposited under subaerial or submarine conditions is not certain (Gloppen and Steel, 1981; Leeder and Gawthorpe, 1987; Nemeč and Steel, 1984). The occurrence of mud clasts does not suggest to a certain environment. They were probably eroded by gravity flows from the underlying marine clay stone (facies M) (Li et al., 2017). Due to the angularity of the mud clasts (Fig. 27) and the direct contact between facies M and B (Fig. 30), they were probably not transported far (Smith, 1972). This could imply that facies association F was deposited into a marine environment. However, the underlying sandstones of facies St contain coal fragments and advocate for a terrestrial setting (Fig. 31). Either way, the erosional contact with the underlying strata could represent a major unconformity (Fig. 30), which would prohibit a direct correlation of the deposits.

Since facies association F exhibits an erosional contact with the underlying, at least partly marine succession, it appears most feasible that it was deposited as (subaerial) part of a debris flow dominated fan delta (e.g. Blair and McPherson, 1994; Gloppen and Steel, 1981; Nemeč and Postma, 1993). Foraminifera have been found in the deposits of facies association F

R – river (delta)

Description – Facies association R comprises facies Gm and St. The layer boundaries within facies association R are erosive while the contact to the underlying marine claystone is sharp but conformable (Fig. 31).

Interpretation – Facies St holds most information about the depositional environment of facies association R. Trough cross-bedding is a clear indicator of unidirectional flow in a deeper channel (Blair and McPherson, 1994; Miall, 1977b, 1977a; Walker and Cant, 1984) while coal fragments suggest deposition in a terrestrial setting or tidal marsh (cf. Bloom, 1964). Therefore, facies association R is placed in a fluvial to deltaic environment. Deposition within a fluvio-deltaic system also fits with the well-rounded, clast supported texture of the conglomeratic units of facies G (Bourquin et al., 2009; Rust, 1977a). The limited exposure prohibits a reliable conclusion concerning the type of river or delta. However, due to the difference in depositional energy between the overlying breccia and the underlying marine claystone (Fig. 30 and Fig. 31), a high relief can be expected. This would favor a braid or fan delta environment since they are more common in areas with a lot of topography (e.g. Blair and McPherson, 1994; Miall, 1985, 1977b, 1977a; Walker and Cant, 1984).

M – marine offshore deposits

Description – Facies association M is made up from facies M, a marine claystone that contains some well-rounded pebbles.

Interpretation – Facies association M contains marine foraminifera (see section 3.4) and is interpreted as a marine offshore deposit. Claystones make up around 50% of the sedimentary strata worldwide (Boggs, 2011). Their primary locus of deposition is close to continents below the storm wave base. Here, the supply of fine grained sediment is abundant and the conditions are calm enough for sedimentation from suspension (Boggs, 2011).

As previously mentioned, the pebbles are interpreted as dropstones. Drop stones are traditionally associated with transport by ice rafts (Spielhagen and Tripathi, 2009) but can also be transported by wooden logs or kelp (Vogt and Parrish, 2012). Facies M was dated to an Oligocene age (see section 3.4) and at that time the climate had already cooled significantly (Fig. 9) and seasonal ice covers as well as ice bergs can be expected (Moran et al., 2006). Therefore, ice rafts appear as the likely transport mechanism for the drop stones. However, turbidity currents are known to deposit pebbly claystones as well (Crowell, 1957; Postma et al., 1988).

3.3 Paleoflow indicators

A total of 114 measurements of paleo flow indicators were obtained in the field and plotted at their respective location (Fig. 33). The data scatter, but show a clear trend of flow away from central Sarsøyra. Cross-beds from the fine grained unit in the north (middle) also shows flow to the NE. When interpreting these data, it is important to be aware of the fact that the measurements reflect the flow directions at the time of deposition. It is not certain if the measurements within the Sarsbukta Formation represent similar stratigraphic levels and whether the data from the Sarstangen Formation embody the same time period. Thus, the measurements could also indicate a change in transport direction over time.

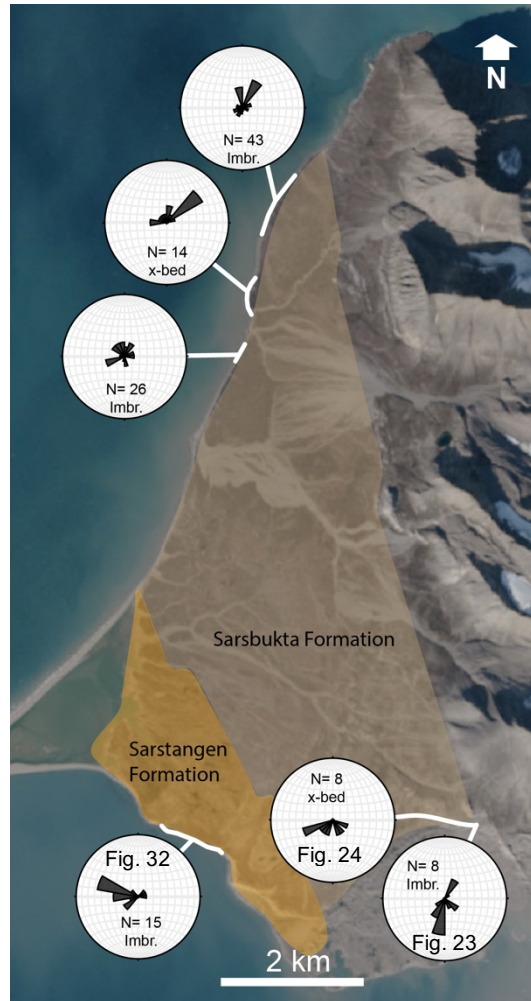


Fig. 33: Paleoflow directions from imbricated clasts and cross-beds. Flow is in the direction of the roset diagram. Note that the paleoflow was directed away from central Sarsøyra. Figures are referenced for the measurements that were taken from the respective feature.

3.4 Paleolimnology

Despite the generally high organic content, only one (OSL-17-21) of the ten analyzed samples contained a sufficient number of well preserved palynomorphs. The sample was taken from fine grained sediments below the Sarstangen conglomerates at Balanuspynten (Fig. 11) and dated Lower to Middle Oligocene (Appendix 4).

A second coal sample (OSL-17-16) from the Sarsbukta Formation in central Sarsøyra contains poorly preserved pollen and diatom fragments. The findings might indicate an Upper Paleocene to Upper Eocene age but are highly uncertain due to the badly preserved microfossils (Appendix 4).

4 Structural Geology

The structural data recorded for this study consist of measurements from the basin-bounding fault zone as well as from the Cenozoic basin fill. Along the basin bounding fault zone, fault kinematic data (~200) have been recorded in basement units and exposed fault rocks. Qualitative outcrop descriptions have been prepared to illustrate the prevailing tectono-stratigraphy and an exposure of the basin-bounding fault zone. Also, the results of K-Ar Illite dating of a fault gouge, conducted by staff at the NGU, are presented (Schönenberger et al., 2019).

Within the Paleogene basin fill, structural data include fault kinematics (~250), measurements of intraclast fracture planes (~50) and fold axes (4) constructed from bedding readings.

4.1 Description of the basin-bounding fault zone

The basin bounding fault zone is partly exposed along the northern beach of Sarsøyra (Fig. 34 and Fig. 11), whereas the degraded fault scarp crops out in several places along the eastern basin boundary (Fig. 34). Measurements and outcrop descriptions have been obtained at the northern beach and are supplemented by data acquired during a scientific cruise in 2016 (Osmundsen et al., 2017).

The contact zone of basement lithologies to the basin fill contains several very deformed rock units. Therefore, a short overview of the host rock tectono-stratigraphy is provided before the fault rocks themselves are described.

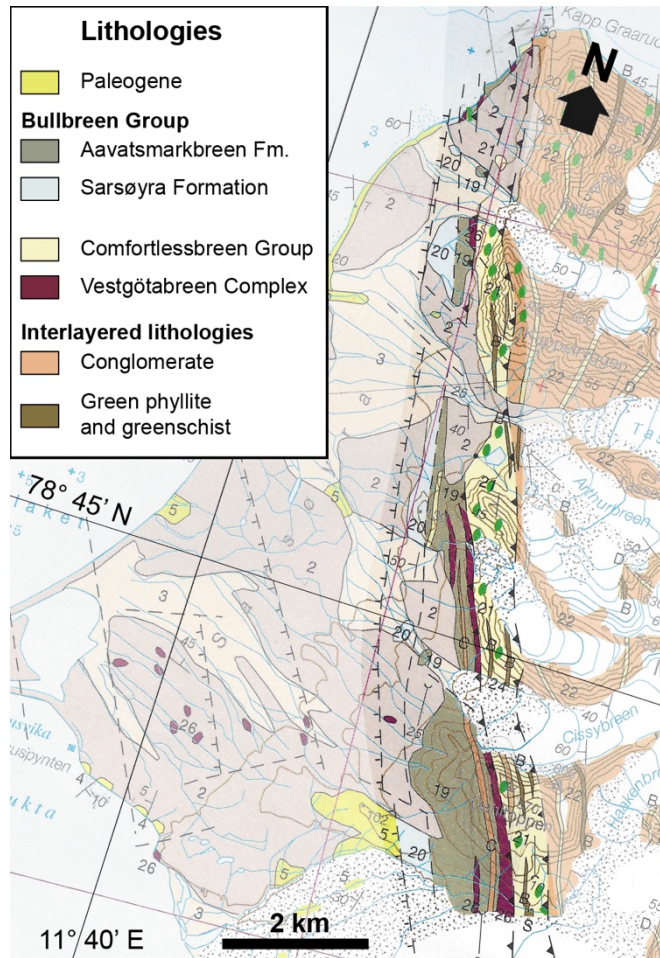


Fig. 34: Tectono-stratigraphy of the basement rocks along the eastern margin of the Forlandsundet Graben on Sarsøyra. Modified from Hjelle et al. (1999).

4.1.1 Contact zone in central Sarsøyra

Tectono-stratigraphy

The basement units along the eastern basin margin are exposed in central Sarsøyra (Fig. 34 and Fig. 11). Adjacent to the Paleogene exposures, **light grey marbles** of the Sarsøyra Formation crop out in an exposure that likely represents the degraded fault scarp (Kanat and Morris, 1988). They are considered to be of Early Paleozoic in age (Hjelle et al., 1999).



Fig. 35: Photograph of the degraded fault scarp (middle) in central Sarsøyra made up from marbles of the Sarsøyra Formation. To the left, Paleogene sedimentary units are exposed in a ravine. Note persons for scale.

Roughly 500 m to the east, distinct zones of metasedimentary basement lithologies were observed (Fig. 34). The rocks show ductile deformation and a foliation oriented 326/80. Overall, 6 lithologies were distinguished; from west to east (Fig. 36):

1. Foliated **black schist** with some discontinuous quartzite lenses. Some parts of the outcrop appear more deformed and weather in a rusty color (Fig. 36). Outcrop width 27 m.

2. Shattered **light grey carbonate**. The unit is probably silicified as it is very brittle and scratches the hammer. Outcrop width 4 m.

3. Well foliated **greenish-quartz schist** containing chlorite, reddish mineral alterations and quartz veins. It includes some small (~5 mm) pyrite nodules and weathers light brown (Fig. 36). Outcrop width 6 m. The previous units are assigned to the Aavatsmarkbreen Formation. Together with the Sarsøyra Formation it constitutes the Late Ordovician to Middle Silurian Bullbreen Group (Hjelle et al., 1999; Kanat and Morris, 1988).

4. A 4 m wide **Carbonate-serpentinite association** is considered to be part of the Vestgötabreen Complex (Kanat and Morris, 1988). The Vestgötabreen Complex is considered to be of Late Proterozoic age (Hjelle et al., 1999).

5. **Grey phyllite** that covers an outcrop width of several tens to hundreds of meters. This grey phyllite makes up the larger part of the Aavatmarkbreen Formation. It is well foliated and can be interlayered with conglomerates, quartzites and marbles (Hjelle et al., 1999; Kanat and Morris, 1988).

6. Even further to the east, a several hundred meter thick **quartzite** unit is exposed. It makes up the Annabreen Formation (Harland et al., 1979), corresponding to the upper part of the

Vendian Comfortlessbreen Group (Hjelle et al., 1999; Kanat and Morris, 1988). These metasedimentary units appear to be protoliths for the deformed lithologies within the brittle fault zone at the northern beach (see section 4.1.2).

A limited number of fault planes (6) could be measured in the basement units (Fig. 36 lower left). They plot in three sets; one consisting of NW-SE-striking low-angle reverse faults indicating top-to-the NE dip slip. The second set is also oriented NW-SE but experienced top-to-the east oblique slip. The third set strikes E-W and shows striae with a high rake on conjugated planes but no interpretation of the slip direction was made due to a lack of kinematic indicators.

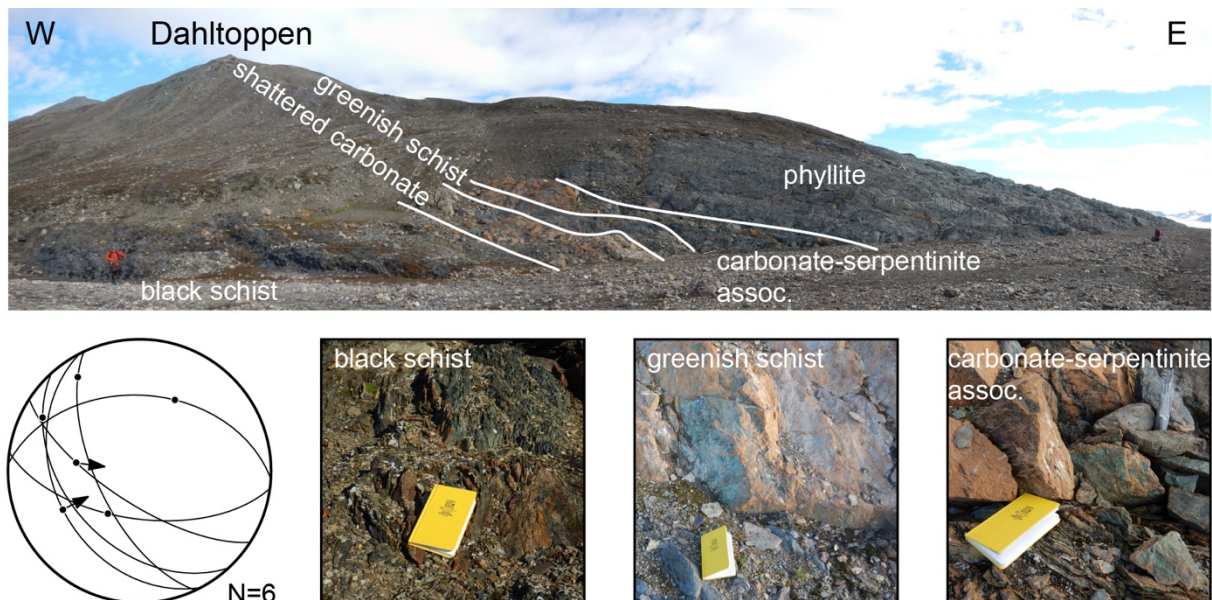


Fig. 36: Photograph of the basement outcrop 500m east of the fault scarp (top), kinematic measurements from faults (lower left) and closeups of the exposed lithologies (lower middle and right).

Kinematic measurements from the fault scarp

From central Sarsøyra to the north, parts of the degraded fault scarp (Fig. 35) are exposed along the basin margin (Fig. 34). The remnants of the fault scarp form small mounts mapped as grey marbles of the Sarsøyra Formation (Hjelle et al., 1999). These are often shattered and always rich in fault planes. Carbonate growth fibers, growth in pressure shadows and steps are abundant on the fault planes providing clear indication of the slip direction (Fig. 37C). Fig. 37 (A and B) illustrates the results from fault plane measurements acquired during a scientific

cruise in 2016 by Osmundsen et al. (2017). Most of the faults appear to have formed under NW-SE extension with some faults indicating NE-SW strike-slip movement.

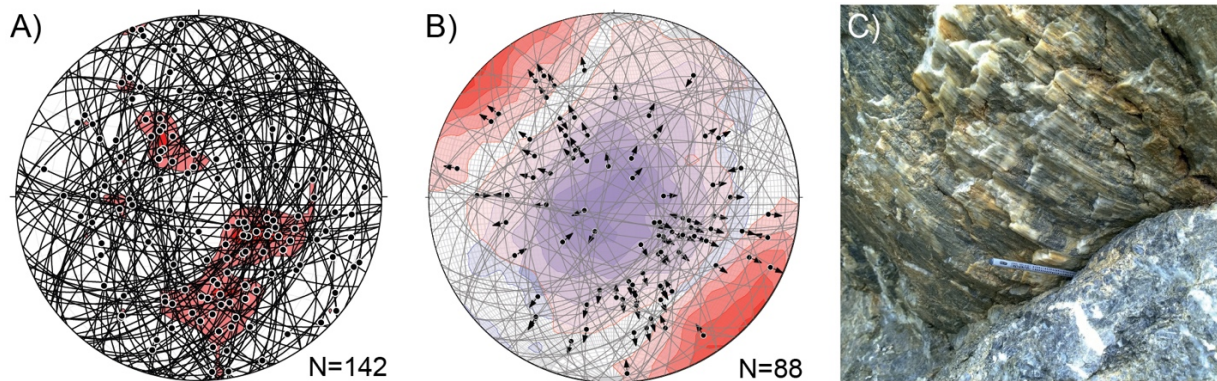


Fig. 37: Fault plane measurements with striae (A) and plot of the data with unidirectional kinematic indicators (B) from the exposed fault scarp in central Sarsøyra. In B), the arrows indicate the hanging-wall slip direction while red contours indicate the tension axes and blue contours the pressure axes calculated with FaultKin based on all available unidirectional kinematic data. The measurements indicate NW-SE extension and NE-SW strike slip movement. C) shows an example of a fault plane with calcite growth fibers from the fault scarp (Fig. 35). Data from Osmundsen et al. (2017).

4.1.2 Contact zone in northern Sarsøyra

The outcrop of the basin bounding fault zone at the northern beach stretches over approx. 250 m in a SW – NE direction (Fig. 41). The direct contact between the basement and the sedimentary basin fill is covered by a 160 m wide zone of Quaternary fluvial deposits and scree.

Lithologies associated with the fault zone

The fault zone can be divided into five different zones according to deformation and lithology (Fig. 41). The lithologies are very likely to correspond to the units presented in section 4.1.1, and are, from west to east;

- 1. Black breccia** with brecciated white carbonate lenses. It mainly consists of quartz, mica and calcite. The rock can be classified as a crackle breccia since most of the fragments exceed 2 mm in thin section (Fig. 38B) (sensu Woodcock and Mort, 2008). As the sample for the thin section was obtained from a lens of less deformed breccia, most of the exposed rock might actually exhibit a higher degree of fragmentation. Over the entire width of the outcrop a cataclastic foliation has been superimposed over the older ductile fabric. At the contact to the

gouge in the east a c. 20 cm wide zone is tightly folded containing some carbonate clasts (Fig. 38C). In proximity to the gouge, the cataclastic foliation is oriented subparallel to the contact, dipping at 70° to the NE. Towards the west the orientation of the foliation changes and it starts to dip with 75° towards WSW. Also, the habitus of enclosed carbonate lenses differs. In the eastern part, a lens is offset by reverse shear (Fig. 41C) whereas lenses further west are elongated subparallel to the cataclastic foliation (Fig. 41D). The sigmodal shape of the lenses (Fig. 41D) indicates top-to-the west normal movements in this part of the outcrop (cf. Passchier and Simpson, 1986).

The protoliths for this unit were probably the black shale (1.) and the shattered carbonate (2.) exposed further south. Width is 16.5 m in the outcrop.

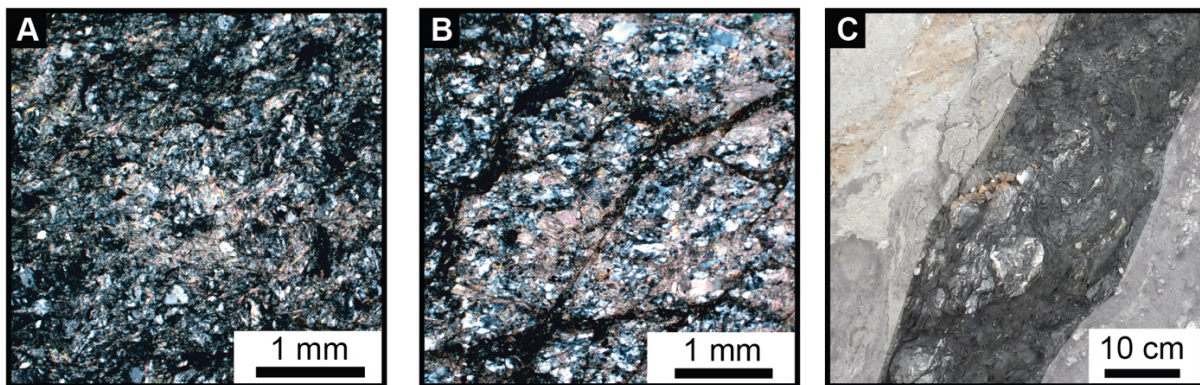


Fig. 38: Photomicrographs under cross-polarized light showing the black schist (A) in its undeformed state at the locality in central Sarsøyra and as black breccia (B) in the fault zone at the northern beach. C) shows a close up of the contact between the black breccia (right) and the gouge (left) that is intensely folded, see also Fig. 41.

2. A 5.7 m wide zone consisting mainly of clay minerals could be related to preferential weathering of a weak lithology (Fig. 41B). In the context of the surrounding rocks and the internal structure of the zone it is however interpreted as **fault gouge** (Fig. 41). The zone exhibits dark grey, green and red color variations that are probably related to the mineral composition of different protoliths or weathering. Within the clay gouge sits a large lens of black schist that appears elongated and sheared from east to west (Fig. 41B). The geometry resembles shearband boudins which are associated with synthetic drag in shear zones (e.g. Goscombe and Passchier, 2002; Passchier and Trouw, 2005). Only the angle of the shearband towards the boundaries of the fault gouge is steeper than commonly expected (e.g. Goscombe and Passchier, 2002). This feature was probably caused by continued fault movement after the establishment of the boudin. Hence, the internal structure of the gouge is considered to have formed as the result of synthetic shear. This observation suggests a significant component of

top-to-the west reverse displacement for the gouge. Smaller reverse faults in adjacent rocks that terminate at the contact to the gouge are interpreted as antithetic faults and support the interpretation (Fig. 41). In 2017, only a small part of this gouge was exposed and sampled. It was dated with the K-Ar method (sections 2.4, 4.1.3 and Appendix 5) (Schönenberger et al., 2019).

3. A grey carbonate unit probably corresponds to the shattered carbonate unit in central Sarsøyra (see section 4.1.1). At the northern beach, it is preserved as a 1 m wide sliver east of the gouge (Fig. 41). It is cut into two blocks by a westerly dipping thrust fault (Fig. 41B). The displacement of the thrust corresponds to c. 75 cm.

4. The greenish quartz-schist makes up 2 m in this outcrop. It is well foliated and was also affected by the thrust fault in the adjacent grey unit (Fig. 41). Thin section analysis shows that it consists of quartz, mafics, chlorite and veinous carbonate.

5. From this point to the northeast, a light brown to white **quartzitic unit** makes up the outcrop for 225 m. It is interrupted by zones of brecciated dark schist (Fig. 39A). Structural features include tectonic fabrics (Fig. 39A & C), folding (Fig. 39B) and reverse faulting (Fig. 39A & C). The protolith for this interval was probably the Aavatsmarkbreen Formation as it consists of phyllites with interbedded quartzites and marbles (Hjelle et al., 1999).

Fault plane measurements from the rocks east of the fault gouge (lithologies 3, 4 and 5) are presented in Fig. 41A and governed by a conjugate set of NNW-SSE striking thrusts (Fig. 39A & C). Kinematic data from the quartzitic unit some 30 m further east exhibit a set of NE-SW oriented strike slip faults (Fig. 40).

In the river valley behind the fault zone exposure, located approximately 110 m towards the south, grey marbles of the Sarsøyra Formation crop out. Therefore, this lithology might be situated between the black breccia and the Paleogene sediments but is eroded or scree covered in the coastal exposure. As further south, it might have constituted the fault scarp in this location also. However, the distance from the basin fill to the other basement lithologies is much less, attesting that the basin bounding fault is cutting obliquely into the preexisting tectono-stratigraphy described briefly at the beginning of this chapter. This interpretation is backed by the difference in deformation style and deformation intensity between the basement rock exposures in the field area. In central Sarsøyra, the basement rocks, with the exception of

the Sarsøyra Formation marbles, were almost exclusively affected by ductile deformation (Fig. 36). The same lithologies experienced severe brittle deformation that overprinted the previous ductile fabric at the northern beach (Fig. 41).

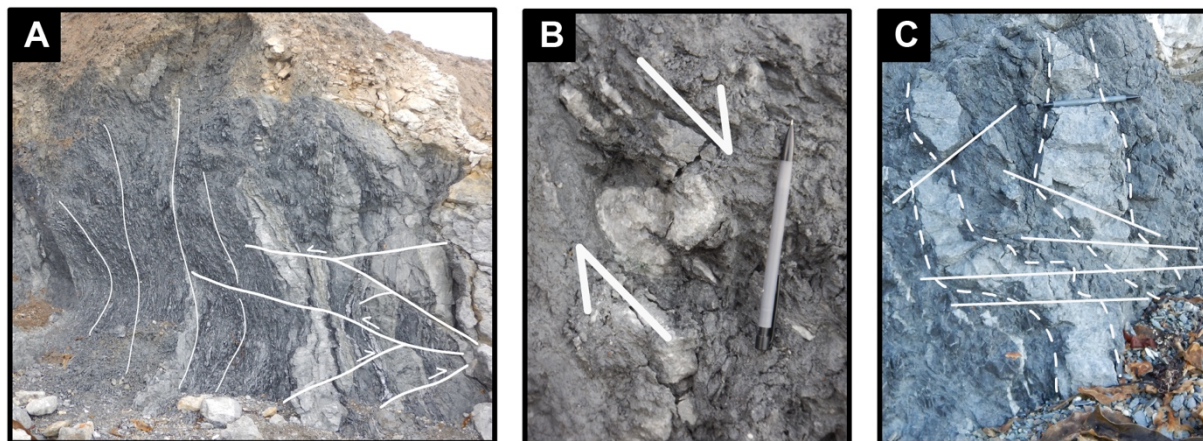


Fig. 39: Illustration of structural features found in the quartzitic unit: A) Conjugated reverse faults cutting the fabric of brecciated schist (29 to 32 m). B) Tight folding within a section of brecciated schist, indicating normal movement. C) Tectonic fabric (dashed), clearly offset by later reverse faulting (solid).

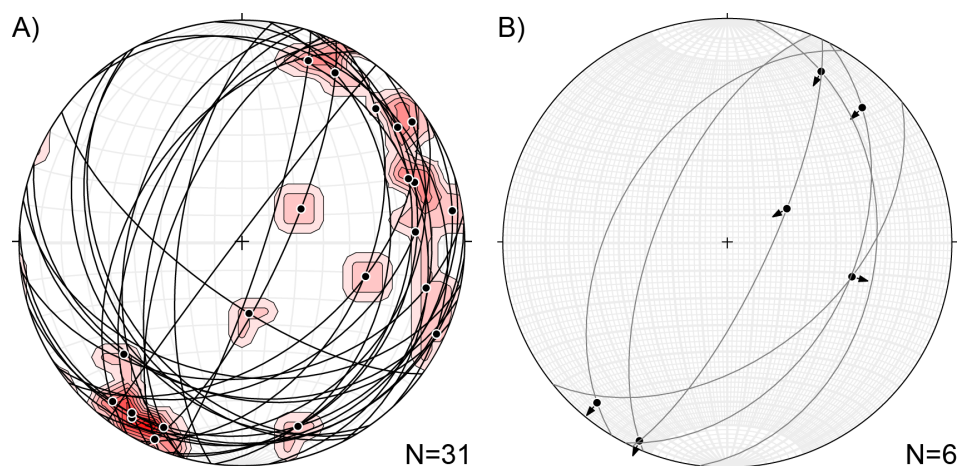
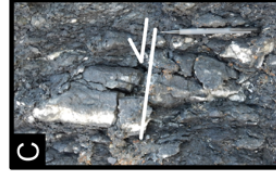
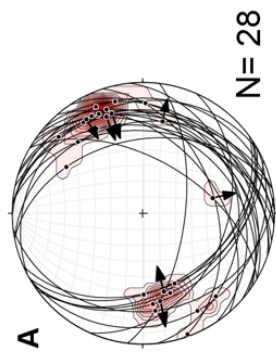
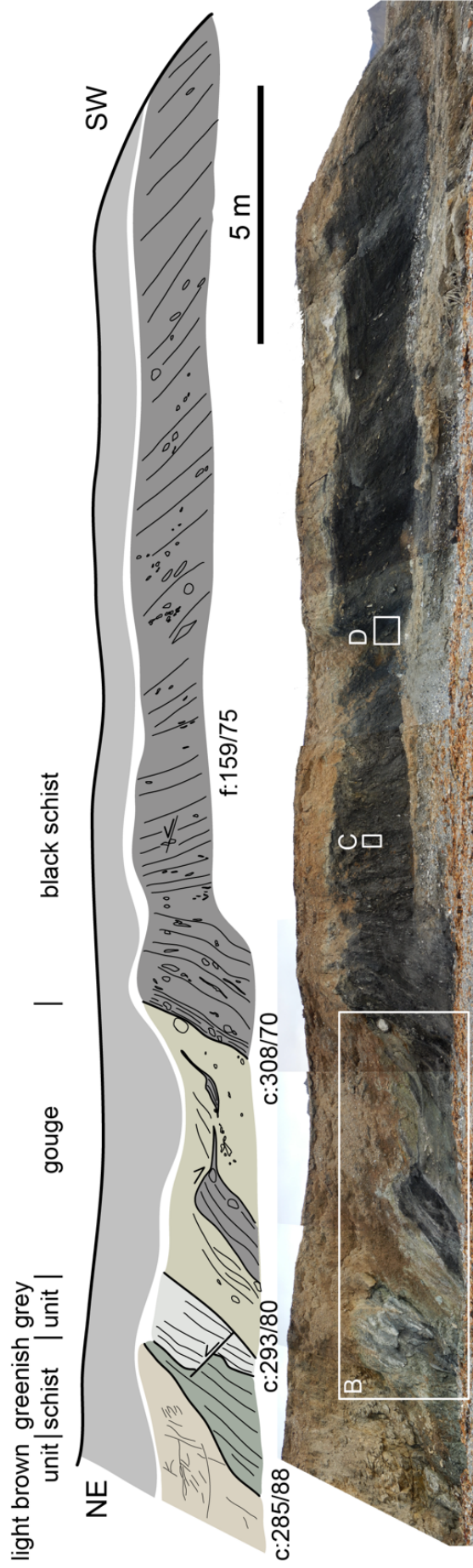


Fig. 40: A) Fault planes (lines), striae (poles) from faults within the quartzitic unit (63-72 m). B) Plot of the faults with unidirectional slip indicators. The data shows dextral and sinistral strike-slip movement on NNE-SSW oriented faults with varying dip.

Fig. 41 (next page): Photomosaic (middle) and schematic drawing (top) of the first 25 m of the basin bounding fault zone. The orientations of lithological contacts (c) and tectonic fabric (f) are given in between the photomosaic and the line drawing. Lower row: A) Fault planes (lines), striae (dots) and unidirectional kinematics (arrows) from the light brown unit (25 to 29 m). The kinematic indicators show dominant NNW-SSE oriented reverse faults with a dextral component but also NE-SW oriented reverse faults with a sinistral component and some normal faults with inconsistent orientations. B) Close up of top-to-the east reverse faults (left) that splay off an almost 6 m wide fault gouge. Smear out segments point towards top-to-the west normal faulting (center). C) Sheared clast within the black schist crosscutting the dominant foliation. D) Sigmoidal shaped lense in the black schist suggesting normal movement. The location of the features is indicated by the white boxes on the photomosaic.



4.1.3 K-Ar ages of the fault gouge

Staff from the NGU laboratory dated illite growth for different grain fractions using the K-Ar method (Schönenberger et al., 2019). The two smallest grain fractions yield ages of 83.0 Ma and 53.5 Ma and are considered to represent fault activity (Appendix 5) (Schönenberger et al., 2019). The 53.5 Ma age is most relevant for this study as it coincides with the beginning of breakup in the Norwegian Sea and the onset of mountain building in the WSFB (Engen et al., 2008; Faleide et al., 2015, 2008).

4.2 Structural data from the Paleogene Sediments

The structural data from the Paleogene sediments includes kinematic fault measurements as well as fold axes calculated from bedding measurements and data from fractured clasts.

4.2.1 Fractured clasts

Fractured conglomerate clasts as shown in Fig. 42, are most abundant in a distinct zone along the northern beach while they are much less frequent in central Sarsøyra. Fracturing of clasts occurs from macroscale (Fig. 42) to microscale (Fig. 43) and the clasts are cut by arrays of subparallel fractures that are filled with the surrounding matrix. Most clasts are elongated perpendicular to the fracture planes. Occasionally, the fragments are offset a few centimeters in a strike-slip manner (Fig. 42). These fractured cobbles were described by Kleinspehn and Teyssier (2016) who developed a model for their development. Accordingly, the fractures developed due to elevated hydraulic pressure before the matrix was lithified. Fracture plane measurements are presented in Fig. 42. The mean orientation of the fracture planes is 084/64. For tension fractures, also called joints, this corresponds to a stretching direction of 174° (Schultz and Fossen, 2008; Singhal and Gupta, 2010) which is in line with the clast elongation direction of 171° that Kleinspehn and Teyssier (2016) reported. The relevance of this feature is further assessed in the discussion (chapter 6).

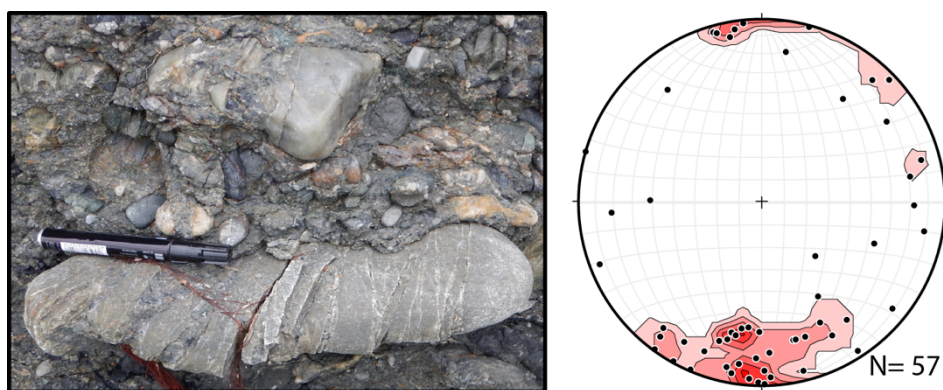


Fig. 42: Example of a fractured cobble (left) and poles to the fracture planes (right). The mean vector is 174/32.

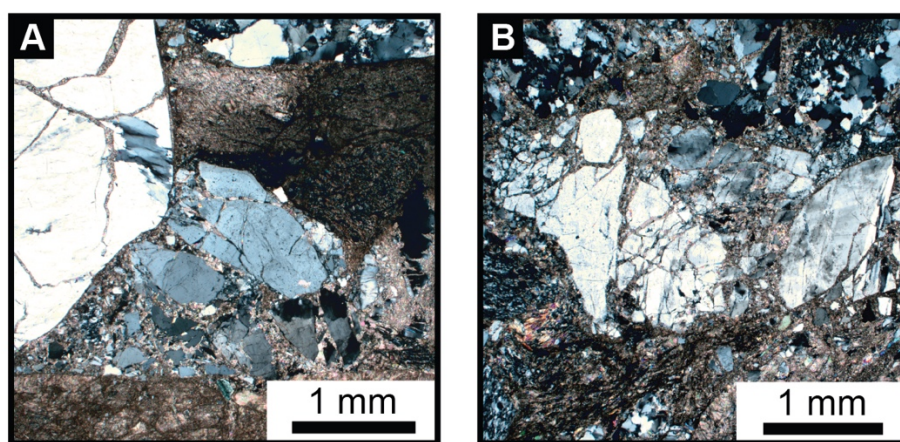


Fig. 43: Pictures of fractured grains under cross polarized light illustrating that fracturing also occurs on micro scale in coarse sandstone beds with granules at northern beach. The fractures are filled with the carbonate cement.

4.2.2 Faulting

Fault data from the Paleogene sediments were recorded within the Sarsbukta Formation at the northern beach and in central Sarsøyra (Fig. 11). The faulting consists mainly of oblique normal faults that strike NE-SW and E-W (Fig. 44A & C). Some fault planes oriented N-S to E-W indicate strike-slip kinematics. Despite striae being abundant on the fault planes in central Sarsøyra (Fig. 44A), only very few contain distinct indicators of the motion sense (Fig. 44B). In that respect, the data from the northern beach (Fig. 44C) are significantly better (Fig. 44D). Overall, the pressure (P) and tension (T) axes derived from both localities show that the tension axis was oriented NW-SE (Fig. 44B & D). The results are consistent with the measurements by Kleinspehn and Teyssier (2016).

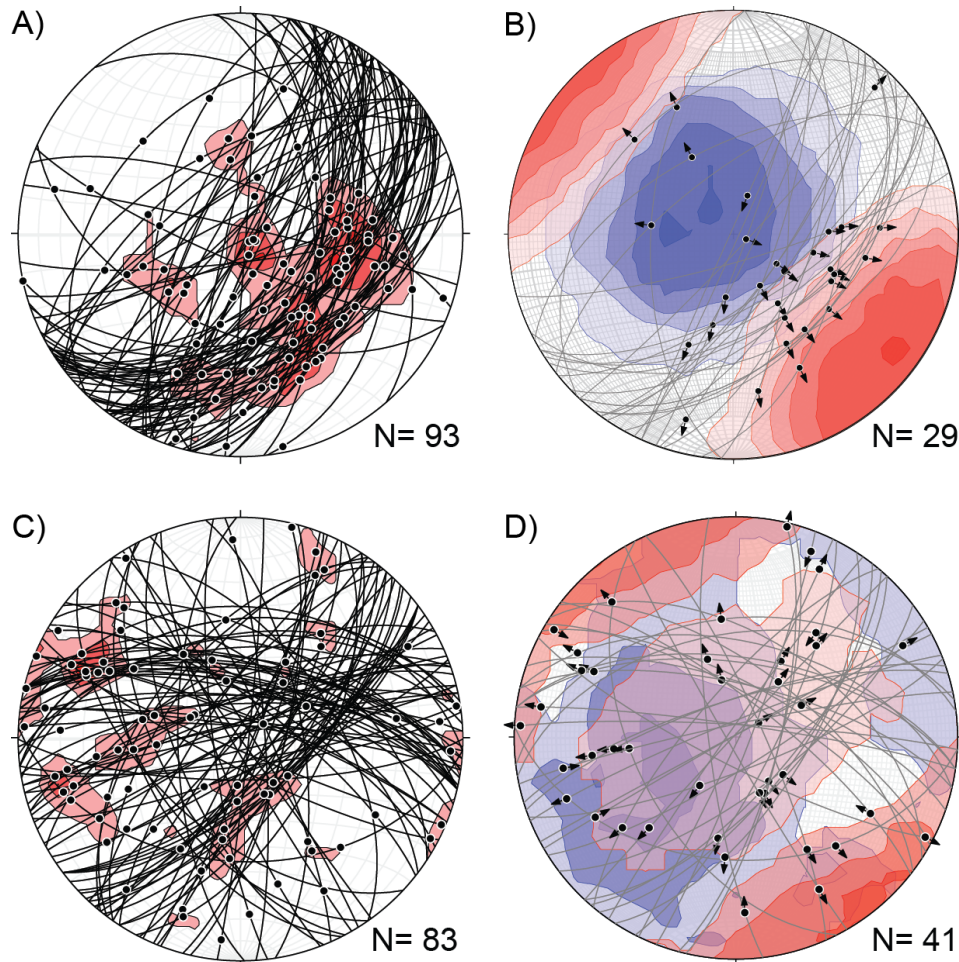


Fig. 44: Stereoplots illustrating the fault measurements from the Paleogene units as fault planes (lines), striae (poles) and kinematics (arrows). A) Measurements from central Sarsøyra showing NW-SE and NE-SW striking normal faults, as well as indication of N-S striking dextral strike slip faults with an oblique normal component. Data compiled from Osmundsen et al. (2017) and this study. B) Kinematics, as well as pressure axes (blue) and tension axes (red), derived from the fault measurements from central Sarsøyra. The tension axes suggest a NW-SE directed extension. Data was compiled from Osmundsen et al. (2017) and this study. All measurements with slip direction data were used to calculate the stress field. C) Measurements from the northern beach exhibiting NE-SW and E-W striking, highly oblique normal faulting and NW-SE oriented strike slip faults. D) Kinematics, as well as pressure axes (blue) and tension axes (red) derived from the fault measurements on the northern beach. The stress axes suggest a NW-SE directed extension. All measurements with slip direction data were used to calculate the stress field.

4.2.3 Folding

Folding in the Paleogene strata was observed along the northern beach as well as the river valley in central Sarsøyra (Fig. 11). At both localities, the bedding steepens towards the basin boundary; at the northern beach to dips over 60° and in central Sarsøyra to 40° (Fig. 11). Within the basin, gentle open folding with strata dipping below 30° was recognized (Fig. 45). The calculated fold axis of the syncline in central Sarsøyra plunges 10° to the NNW at 332°

(Fig. 45, yellow). Another syncline in the NE of the northern beach is oriented more NW-SE and plunges horizontally at 311° (Fig. 45, red). Southwest of the syncline, the bedding measurements suggest the existence of an anticline plunging slightly (1°) ESE at 112° (Fig. 45, green). However, the pebbly conglomerate beds (facies association Gm) contain sub-angular clasts derived from tightly folded phyllite in addition to the well-rounded, mainly quartzitic clasts that dominate the conglomerates in the northeastern part of the northern beach. This difference in clast composition could indicate that the change in dip along this section is caused by a fault (Fig. 11). The presence of a fault in this location was also suggested by Krasilscikov et al. (1995). Further southwest, the beds fold into another syncline plunging 16° to the SE at 133° (Fig. 45, blue).

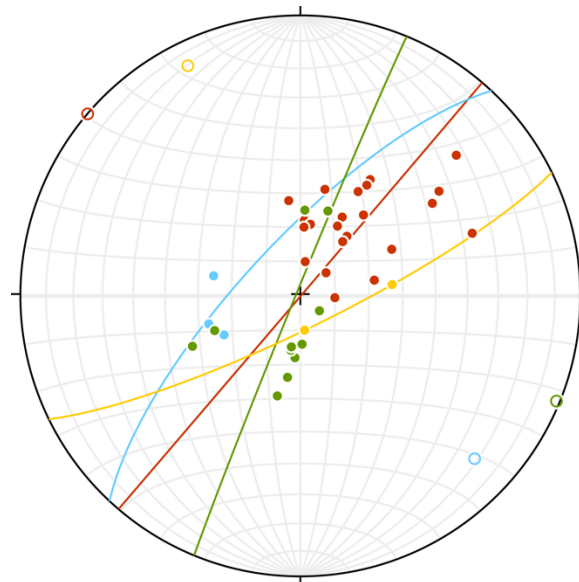


Fig. 45: Poles to bedding (dots), best-fit great circles (lines) and fold axes (circles) from folds on Sarsøyra. Syncline in central Sarsøyra in yellow. From the northern beach: northeastern syncline in red, anticline in green and southwestern syncline in blue. See also Fig. 11.

4.3 Interpretation

The arguably oldest structures documented in this study are found in the sheared basement lithologies in central Sarsøyra that constitute the protoliths for the fault rocks at the northern beach (section 4.1.1). Folds and tectonic foliations that dip steeply to the NE record ductile deformation at deeper crustal levels (Fig. 36). The deformation is attributed to events that long predate the tectonic processes during the Paleogene since the rocks formed before and during the Caledonian orogeny (Hirajima et al., 1988; Hjelle et al., 1999; Kanat and Morris, 1988; Labrousse et al., 2008; Ohta et al., 1995).

A conjugate set of reverse faults cuts through the tectonic fabric, recording ENE-WSW compression on NNW-SSE striking planes (Fig. 36, Fig. 41A and Fig. 39A). NNW-SSE striking thrusts characterize the main structural grain of the WSFB (Bergh et al., 1997; Bergh and Andresen, 1990; Braathen et al., 1997; Braathen and Bergh, 1995a; Lepvrier, 1992). The data from further east within the fault zone (Fig. 40), indicate NNE-SSW oriented strike slip kinematics with a slight reverse component. Comparable structures with a similar orientation have also been observed within the WSFB (Braathen and Bergh, 1995a). The faults are therefore interpreted to have formed along with the WSFB.

Smaller reverse faults splay off the gouge zone, indicating that the structures are genetically linked (Fig. 41B). The gouge itself exhibits top-to-the west reverse kinematics that are not commonly recognized within the WSFB, as it is traditionally associated with top-to-the east thrusting (Bergh and Andresen, 1990; Braathen et al., 1999; Braathen and Bergh, 1995a). However, the gouge zone might have primarily accommodated strike-slip displacement during the formation of the WSFB as a transpressional orogen (e.g. Leever et al., 2011). Indications for that are the rather high dip of 70° to 80° (Fig. 41) as well as the fact that there is no change in tectono-stratigraphy between the undisturbed southern outcrop (section 4.1.1) and the fault zone in the north (section 4.1.2). The tectono-stratigraphy is layered approx. parallel to the basin boundary (Fig. 34) but is expected to change with depth (Hjelle et al., 1999). Therefore, vertical displacement may have caused a change in lithology across the fault, especially because the thickness of the gouge suggest large amounts of displacement (cf. Scholz, 1987). Strike-slip movements on the other hand would be harder to recognize in the exposed section. The fault zone might represent a continuation or strand of the Svartfjella, Eidembukta and Daudmannsodden lineament (SEDL) (cf. Bergh et al., 2000, 1998; Maher et al., 1997). With the Hornsund lineament, the SEDL accommodated mainly strike-slip motion during the formation of the WSFB under decoupled transpression but also acted as a backthrust (Bergh et al., 2000; Braathen and Bergh, 1999; Leever et al., 2011; Maher et al., 1997). The K-Ar date suggests that the fault was active at 53.5 Ma which corresponds approximately to the time of break up in the northeast Atlantic. Normally, 55 Ma or 54 Ma are referred to as the time of breakup (Faleide et al., 2015, 2008) but 53 Ma have also been reported (Breivik et al., 2006; Engen et al., 2008; Piepjohn et al., 2016).

The black breccia that is exposed in between the gouge and the basin fill contains shear indicators that suggest top-to-the west normal faulting (Fig. 41D). The indicators are probably

related to the establishment of today's basin-bounding fault. The kinematics of the degraded fault scarp in central Sarsøyra (Fig. 37B) suggest that the oblique normal and strike slip faults formed under NW-SE directed extension. Similar tension axes can be derived from the kinematic measurements of faults in the basin fill (Fig. 44) suggesting that they formed in the same structural setting. As the boundaries of the Forlandsundet Graben strike NNW-SSE at c. 337° for the entire basin and at 350° for Sarsøyra locally, a NW-SE oriented extensional stress results in an highly oblique transtensional setting (sensu Fossen and Tikoff, 1998).

The axes of open folds trend approximately NW-SE (section 4.2.3) which lines up with the direction of bulk extension (sections 4.1.1 and 4.2.2). These folds may have evolved in a transtensional setting since transtensional folds are modeled to rotate into parallelism with the extensional stress (Fossen et al., 2013; Venkat-Ramani and Tikoff, 2002). Within the WSFB, NW-SE trending folds only occur locally and are associated with a more complex fold pattern (Bergh et al., 2000; Braathen et al., 1997; Braathen and Bergh, 1995a; CASE Team, 2001) that was not observed on Sarsøyra (section 4.2). Therefore, the folds are interpreted as transtensional folds in accordance with the results of Kleinspehn and Teyssier (2016).

The measurements from matrix filled intraclast fractures in the Sarsbukta Formation suggest they formed under approx. N-S oriented extension (see section 4.2.1). Kleinspehn and Teyssier (2016) present a model for the evolution of the fractured cobbles. Accordingly, the fractures were generated before the matrix lithified, tentatively shortly after deposition, and represent an episode of orogen parallel extension within the WSFB. Following their argument, the fractures would predate the transtensional faulting. It is, however, not certain that the Sarsbukta Formation was deposited during the orogeny of the WSFB. Therefore, alternative mechanisms for the evolution of the intraclast fractures will be discussed in section 6.

At this point, three separate deformation phases can be distinguished:

1. **Ductile deformation** that established the prevailing NE dipping tectonic fabric and folding of the metasedimentary rocks along the eastern basin boundary. The age of this deformation predates the Forlandsundet Graben, as well as the WSFB, and will not be discussed further here.

2. ENE-WSW **compression** and NE-SW directed **dextral strike slip movement** (Fig. 36, Fig. 39, Fig. 40 and Fig. 41) related to the formation of the WSFB. During this stage fault gouge became active at 53.5 Ma (section 4.1.2), possibly as part of the SEDL.
3. **NW-SE** oriented **transtension** causing oblique rifting as indicated by oblique-normal faulting, folding and sigmoidal shaped carbonate lenses within the black breccia (Fig. 41B and C, Fig. 44 and Fig. 45).

5 Subsurface Data

5.1.1 7811/5-1 Sarstangen petroleum exploration well

The 7811/5-1 Sarstangen petroleum exploration well by Norsk Polar Navigasjon AS (Fig. 46a) was drilled to a total depth of 1113.5 m after encountering basement at 1046.5 m (Appendix 7). According to the composite log, the sediments above consist of Quaternary (0 to 45 m) and Paleogene (45 to 1046.5 m) deposits. The Paleogene succession is made up from dark-grey to brown shale grading into fine silt alterations (Appendix 7). Thin beds of poorly sorted, coarse to granule sandstone and conglomerate layers derived from basement rocks disrupt the finer sediments. Foraminifera are present throughout the entire succession and traces of coal are found in the intervals from 145 to 205 m and 310 to 480 m. In between 394 and 396 m, a few calcite fragments were impregnated with live oil. Natural gas was found in the interval from 608 to 784 m and flow rates of up to 190 m³/h were measured. Three core samples obtained from the shale below 648.7 m exhibit abundant shear planes with slickensides. The sedimentary succession rests unconformably on weathered metamorphic basement, indicating a depositional contact. The correlation of the rock units with the onshore sedimentary successions are not entirely resolved. Kleinspehn and Teyssier (2016) suggest that an interval of conglomerate and coarse sandstone between 600 m and 640 m depth constitutes the distal equivalent of the Sarstangen Formation (Appendix 7).

5.1.2 Gravity and magnetic anomalies

Gravimetry and magnetic anomaly maps of Svalbard have been published in Dallmann (2015) and cutouts of the Forlandsundet area are displayed in Fig. 46 (b and c). The gravity anomaly map shows a clear increase towards the west (Fig. 46b). In the east, negative anomalies were interpreted overthickened crust of the WSFB, while the high positive anomalies west of Prins Karls Forland are probably related to Pliocene sediment packages that are not yet isostatically balanced (Dallmann, 2015). On the magnetic anomaly map, (Fig. 46c) the Forlandsundet Graben appears as a NNW-SSE trending area that is magnetically neutral in between highly magnetic basement blocks (Dallmann, 2015). Within the Forlandsundet Graben, only minor variabilities occur, for example a slight increase in the magnetic field in the area of Sarstangen (Fig. 46c).

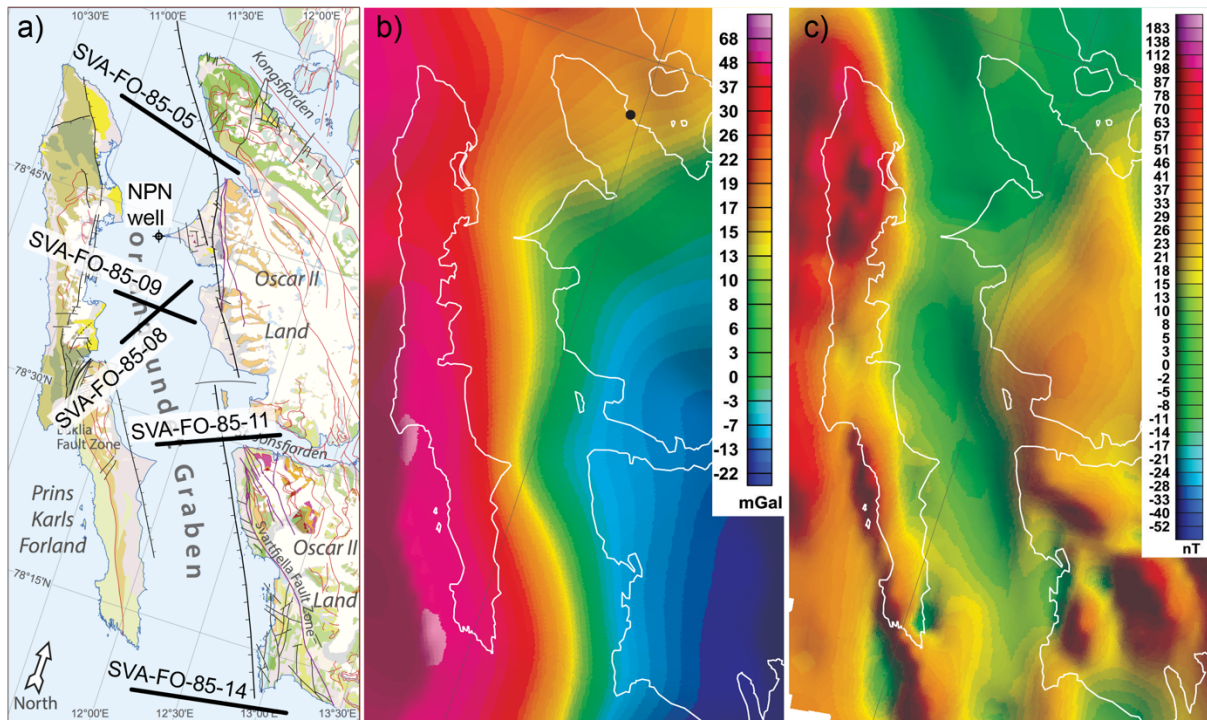


Fig. 46: a) Geological map of the Forlandsundet Graben with the position of the 7811/5-1 Sarstangen petroleum exploration well drilled by Norsk Polar Navigasjon AS and the seismic lines. Map modified from Dallmann (2015). b) Cutout from the Bouguer corrected gravity anomaly map as published in Dallmann (2015). Note the very high values along the western margin of the Forlandsundet Graben and an increase along the eastern margin north of Sarsøyra. c) Cutout from the magnetic anomaly map as published in Dallmann (2015). Note the high magnetic anomalies on Prins Karls Forland and the slight increase in the magnetic field in the Sarstangen area.

5.1.3 Seismic data

Five seismic lines from the Forlandsundet Graben (section 2.5) were chosen to interpret the overall basin geometry, if possible, and compare the results with previously published interpretations. They are crossing the basin approximately in an W-E direction (Fig. 46a). Due to the age of the seismic, the hard sea bottom and shallow waters around Svalbard, the quality of the data is limited. Often, the strongest reflectors turn out to be sea floor multiples. However, some elements of the basin can be identified, a steep normal fault at the eastern basin boundary, for example, is evident in the lines SVA-FO-05 (Fig. 51), SVA-FO-11 (Fig. 48) and SVA-FO-14 (Fig. 47). The western basin boundary is imaged in the southernmost line SVA-FO-14 (Fig. 47). Folding along the western basin margin can be observed in line SVA-FO-11 (Fig. 48) and is indicated towards the western edges of other lines. Unfortunately, SVA-FO-14 (Fig. 47) is the only line that gives a reflection of the basement under the basin fill. In the following, a more detailed interpretation of each line is presented (from S to N).

SVA-FO-14

Line SVA-FO-14 was acquired from south of Prins Karls Forland into Isfjorden (Fig. 46). It is the only line that crosses both basin boundaries (Fig. 47). To the east, the rift shoulder is exposed on the seafloor while the western equivalent is covered by sediments. A strong reflection in the hanging wall of the western fault is interpreted as basement. Unfortunately, the basement reflector is discontinuous and cannot be traced all the way to the eastern basin margin. In this section, the basin appears to have a symmetrical graben geometry. Within the basin, reflectors appear to dip towards the east. It is hard to determine whether those reflectors resemble the dip of the sedimentary strata, or if they are artefacts. Similar reflectors are present in all other seismic lines, although, they are dipping to the west in line SVA-FO-08 (Fig. 49).

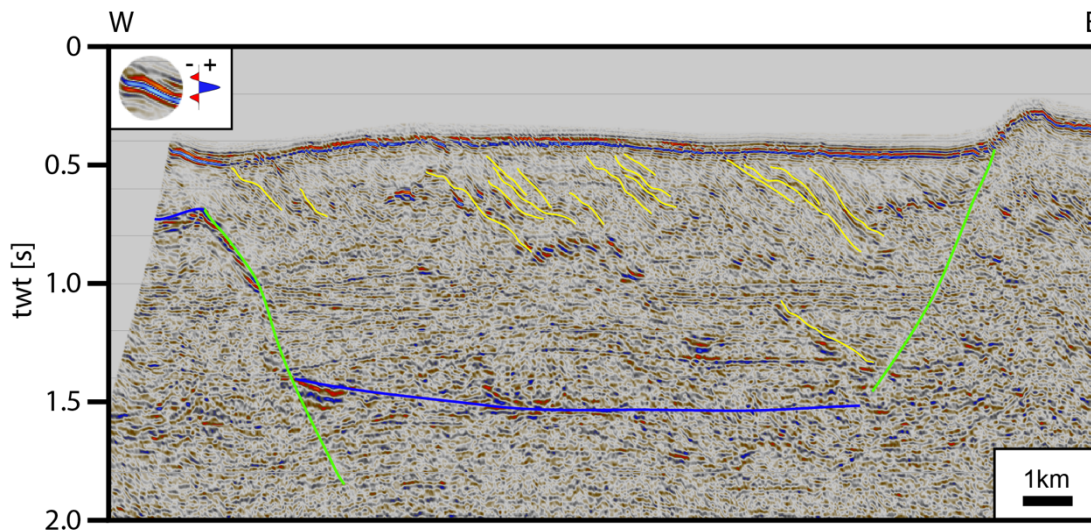


Fig. 47: Seismic line SVA-FO-14, showing both basin bounding faults (green) and reflectors that are dipping to the east (yellow). The blue lines mark the potential basement reflectors.

SVA-FO-11

Line SVA-FO-11 was shot from Brucebukta into St. Jonsfjorden (Fig. 46a). The location of the eastern boundary fault is clearly recognizable (Fig. 48). To the east, the fault scarp makes for distinct positive topography. As mentioned, the sedimentary infill is folded into an asymmetrical syncline at the western basin margin. The structure is cut by several minor normal faults (Fig. 48). In the center of the basin, the reflectors appear noisy. The topography of the seafloor and some deeper reflectors indicate a layer dip towards east. A normal fault

might separate the dipping layers from the anticline. In this section, the Forlandsundet Graben appears to have a half-graben geometry with a smaller graben structure in the basin center.

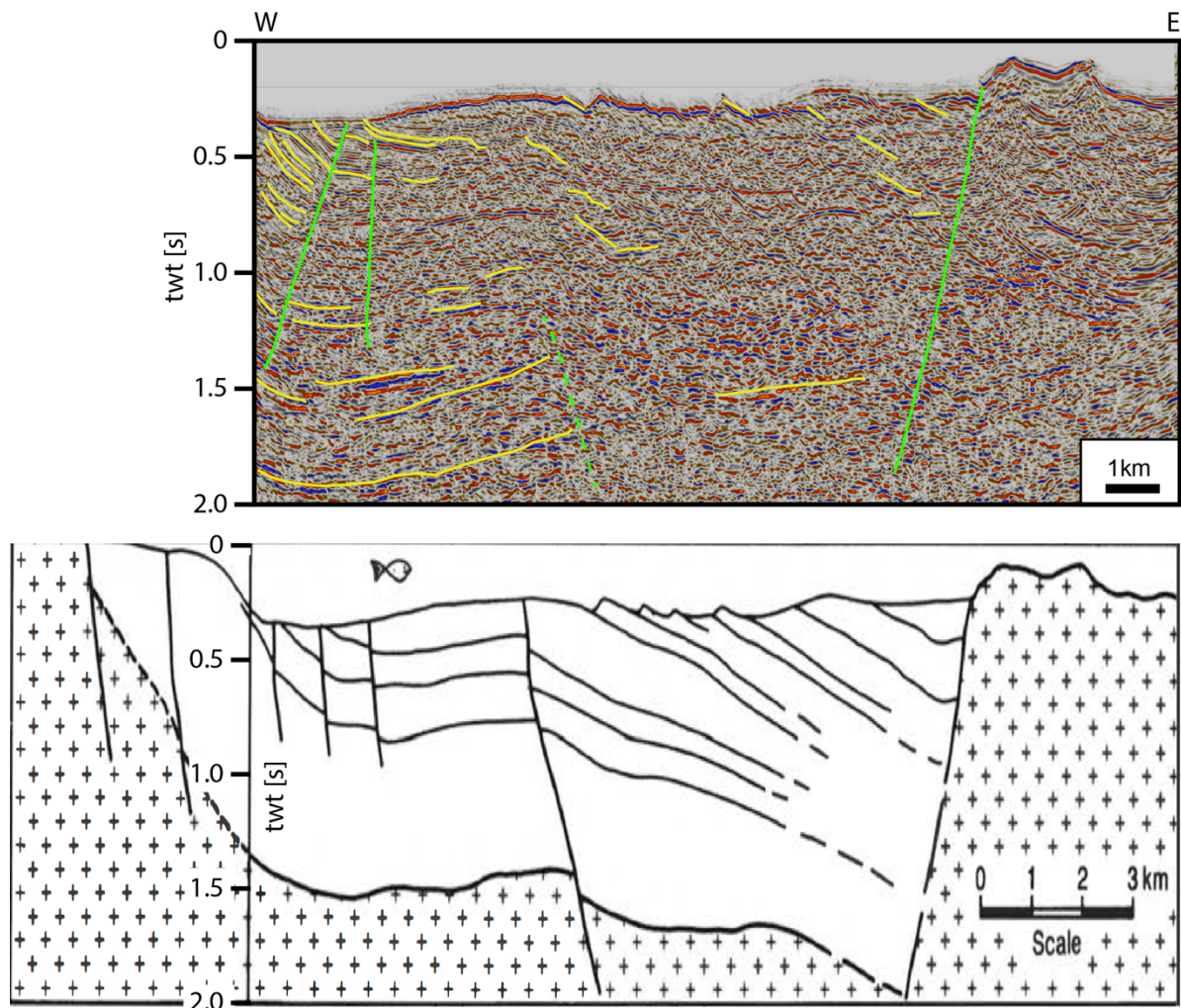


Fig. 48: Seismic line SVA-FO-11, seismic line from Brucebukta into St. Jonsfjorden. It shows the eastern boundary fault and folding of the sedimentary strata to the west. The lower drawing shows the interpretation from Gabrielsen et al. (1992).

SVA-FO-08

Line SVA-FO-08 was shot from Hornbækbukta to Selvågen (Fig. 46a). This line does not cover the basin margins or basin bounding faults (Fig. 49). The reflectors appear to dip to the west but observations from the crossing line SVA-FO-09 (Fig. 50), suggest that the layers actually dip towards the south. The apparent westward dip could be caused by the orientation of the seismic line towards the true layer dip. This feature could represent clinofolds of a southwards migrating delta front or an artefact related to the bad quality of the seismic. Some

reflectors in the middle of the line resemble sediment wedges and could be related to sub-basins with a half-graben geometry (Fig. 49).

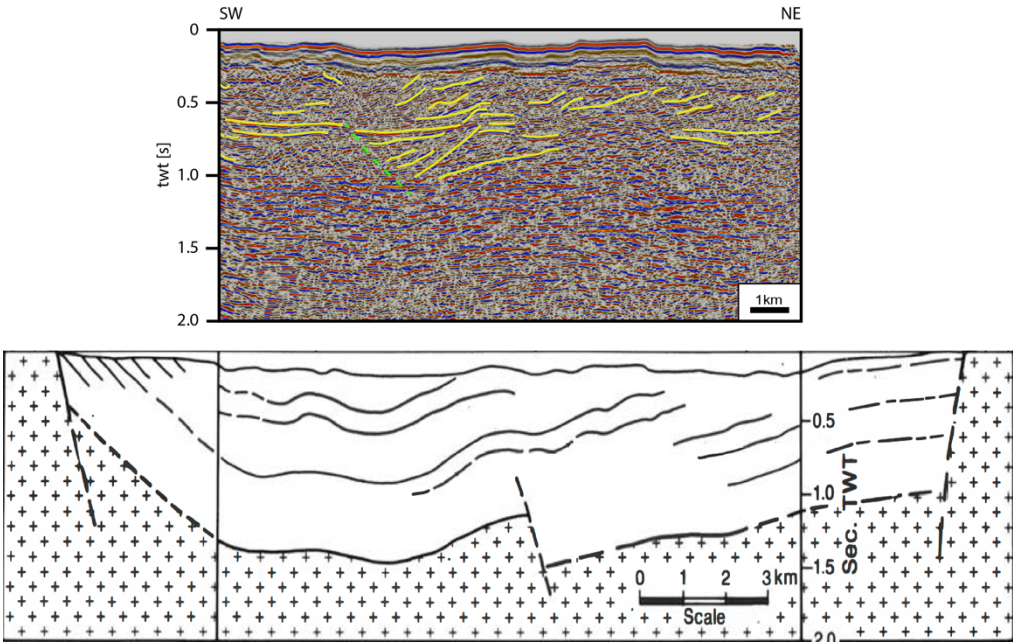


Fig. 49: Seismic live SVA-FO-08, shot from Hornbækbukta to Selvågen. The lower drawing shows the interpretation from Gabrielsen et al. (1992).

SVA-FO-09

Line SVA-FO-09 (Fig. 50), running from Kaffiøyra to Brebukta (Fig. 46a), is mainly included to illustrate the eastern dipping reflectors mentioned under line SVA-FO-08 (Fig. 49). Other than that the line does not contain any reliable reflectors that could be associated with basin structures.

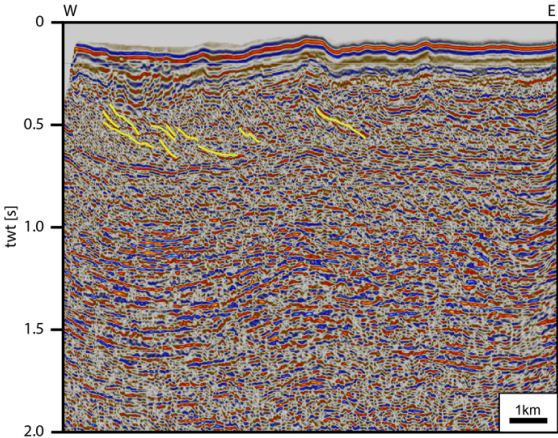


Fig. 50: Seismic line SVA-FO-09 from Kaffiøyra to Brebukta showing crude refelctors dipping to the east.

SVA-FO-05

Line SVA-FO-05 (Fig. 51) was shot from Engelsbukta to Aberdeenflya (Fig. 46a). Again, the eastern boundary fault is well imaged. The structures within the basin, however, appear more complex than in the southern lines. A large rotated fault block creates a half-graben to the east. In the center of the basin, a graben structure is bounded by the rotated fault block and a horst to the west. The graben structure contains smaller rotated fault blocks and a half-graben sub-basin. Further to the west lies another graben structure. Within this graben, the layers appear to be folded into a syncline. The western boundary fault is not imaged by the line.

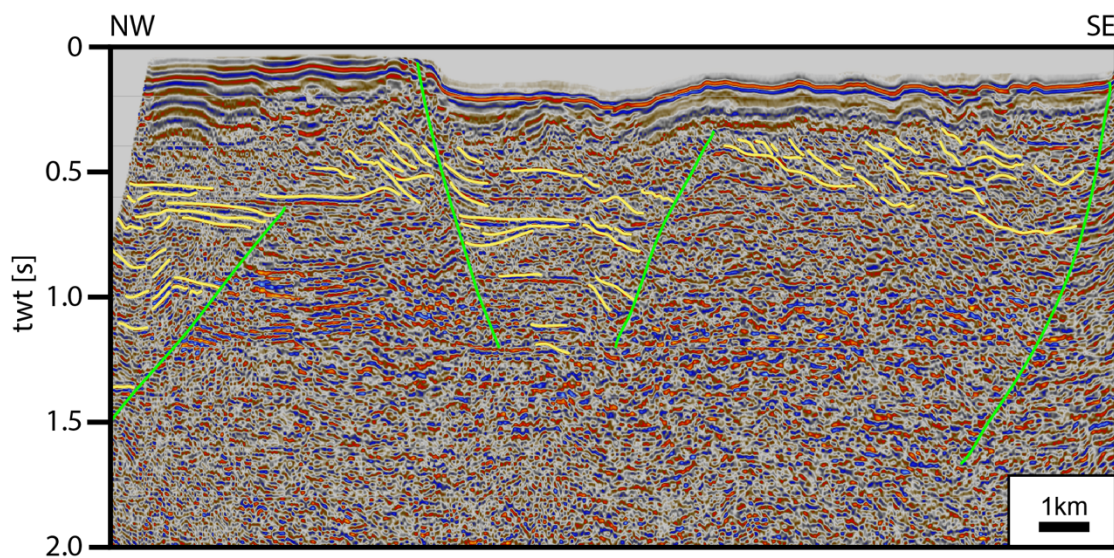


Fig. 51: Seismic line SVA-FO-05 shot from Engelsbukta to Aberdeenflya.

6 Discussion

This chapter debates the previously presented results in the context of the tectono-sedimentary evolution of Sarsøyra and the Forlandsundet Graben. Furthermore, the significance of the Forlandsundet Graben in respect to the formation of the west Svalbard margin and for the conception of passive margin evolution in general, will be assessed.

To better constrain the temporal evolution of the basin, a framework for the sequence of geological events is established based on the available literature. Accordingly, three events can be used as corner stones to constrain the formation of the Forlandsundet Graben:

1. Onset of reverse and strike-slip faulting along the west coast of Spitsbergen between 55 Ma and 53 Ma, forming the WSFB (CASE Team, 2001; Engen et al., 2008; Faleide et al., 2008, 2015; Piepjohn et al., 2016).
2. Deposition of sedimentary units in the Forlandsundet Graben from ~44 Ma (Mid Eocene) through ~28 Ma (Mid Oligocene) (Čepek, 2001; Čepek and Krutzsch, 2001; Feyling-Hanssen and Ulleberg, 1984; Kleinspehn and Teyssier, 2016; Lehmann et al., 1978; Livsic, 1992, 1974, Manum, 1962, 1960; Manum and Throndsen, 1986; Steel et al., 1985).
3. Onset of seafloor spreading at the Molloy Ridge segment at 22 Ma marks the end of rifting along the west coast of Spitsbergen (Engen et al., 2008; Kleinspehn and Teyssier, 2016).

6.1 Tectono-sedimentary evolution of Sarsøyra

Essentially two models have been proposed for the tectono-sedimentary evolution of the Paleogene successions on Sarsøyra; Gabrielsen et al. (1992), Rye-Larsen (1982) and Steel et al. (1985) interpreted the Sarsbukta and Sarstangen Formations as marginal alluvial fan sediments deposited within a graben structure that postdates the WSFB (Fig. 10). According to these models, the Sarsbukta Formation was deposited along the basin bounding fault on a rotated fault block. It was considered to overlie the Sarstangen Formation which was shed off the basinward fault scarp of the rotated fault block (Gabrielsen et al., 1992).

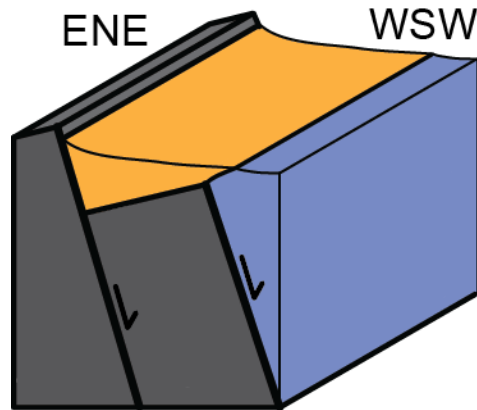


Fig. 52: Tectono-sedimentary model of Sarsøyra based on *Gabrielsen et al. (1992)* and *Rye-Larsen (1982)*. Deposition of the Sarsbukta Formation (orange) on top of the Sarstangen Formation (blue) as part of a half-graben basin.

Kleinspehn and Teyssier (2016) suggested that the Sarsbukta Formation represents gravelly meandering-channel fluvio-deltaic sediments that were deposited in a piggyback basin within the WSFB. With the initiation of the eastern boundary lineament during Oligocene transtension, the Sarsbukta Formation got deformed and downfaulted to its present position. At the same time, the deposition of the Sarstangen Formation began as a fan delta along a major normal fault within the graben structure. Kleinspehn and Teyssier (2016) consider the Sarstangen Formation as younger because it is not affected by internal faulting and shows a significant difference in clast habitus compared to the Sarsbukta Formation.

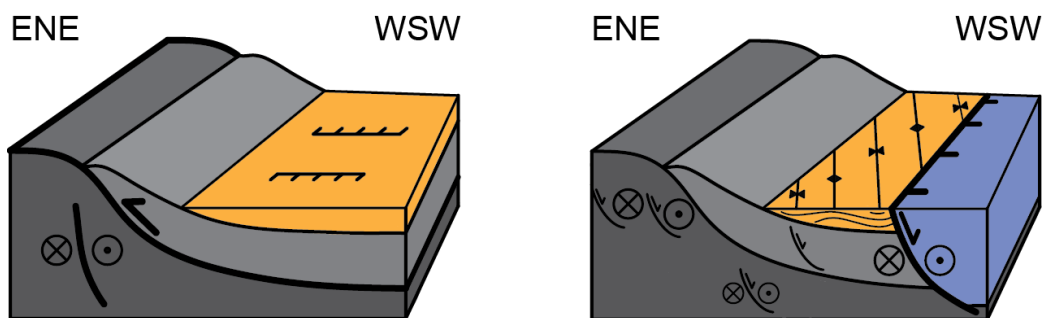


Fig. 53: Schematic model for the evolution of the Paleogene strata at Sarsøyra according to Kleinspehn and Teyssier (2016). Left: Deposition of the Sarsbukta Formation (orange) in a piggyback basin within the WSFB while experiencing orogen parallel extension. Right: Deposition of the Sarstangen Formation (blue) in a graben structure bound by a major oblique normal fault. The Sarsbukta Formation (orange) experiences transtensional folding and is also affected by oblique faulting.

The results of this study (chapter 3, 4 and 5) are not consistent with the existing models. Therefore, the models are updated to better assess the tectono-sedimentary evolution of Sarsøyra.

6.1.1 Tectono-sedimentary constrains

Sarsbukta Formation

The Sarsbukta Formation is interpreted as a sedimentary succession dominated by alluvial fan, fluvial and floodplain deposits (section 3.1). This interpretation is in accordance with Rye-Larsen (1982) who described the outcrops in central Sarsøyra as marginal alluvial fan succession. Kleinspehn and Teyssier (2016), on the other hand, suggested that the entire Sarsbukta Formation was deposited by gravelly meandering channels. As shown in section 3.1.3, a depositional system consisting of alluvial fans interfingering with a fluvial system and associated floodplain sediments matches the observations of this study better.

The interfingering of coarse conglomeratic units in the east with finer grained sedimentary units towards the west, indicates that a source of coarse clastics was localized to the east of today's basin boundary. Source areas for coarse clastics are commonly associated with topography, e.g. highlands. The interfingering architecture could be attributed to cyclic variations in the availability of coarse sediment, probably caused by changes in topographic relief. Therefore, it is likely that sedimentation was controlled by a fault and therefore occurred syn-tectonically (cf. Gawthorpe and Leeder, 2000; Leeder and Gawthorpe, 1987). This impression is further strengthened by the observation of a monocline in central Sarsøyra (section 3.1.2) (cf. Brandes and Tanner, 2014; Gawthorpe and Leeder, 2000; Leeder and Gawthorpe, 1987). The strata displayed in Fig. 20 probably extended further to the east, thereby covering the fault scarp at the time of deposition. Due to fault movement within the underlying basement rocks, the strata were bent into a monocline. The wedge shown in Fig. 24 is interpreted as a sediment package that prograded into the basin. Planar cross-beds within the feature suggest that the dominant transport direction was WSW (section 3.3). Thickening of strata into the basin away from the boundary fault, is a characteristic feature associated with extensional monoclines (Fig. 54) (Leeder and Gawthorpe, 1987; Withjack et al., 1990). Extensional monoclines are formed by sedimentary layers that are bent over a propagating normal fault (Leeder and Gawthorpe, 1987). The geometry of the monocline allows for a syn-tectonic sedimentary wedge to build out from the footwall into the basin (Fig. 54). With continued displacement, the fault cuts into the overlying strata and a typical half-graben

geometry is established. In a half-graben, the sedimentary units usually thicken towards the boundary fault but the oppositely wedging packages associated with the extensional monocline are preserved in the hanging wall.

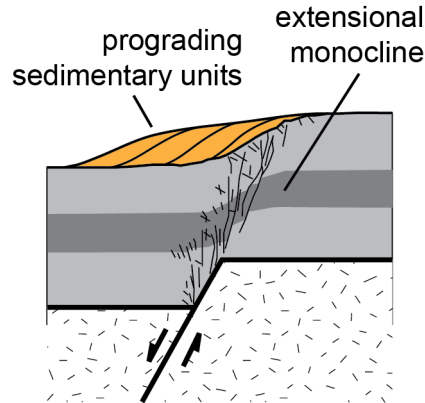


Fig. 54: Schematic drawing of an extensional monocline with a footwall derived sedimentary wedge. Modified from Gawthorpe and Leeder (2000).

The structural observations from the northern beach (section 4.1.2) show that there are two potential candidates that could have acted as boundary fault during the deposition of the Sarsbukta Formation. Either the backthrust of the WSFB (gouge), or the oblique normal fault, bounding the basin today, could have controlled the sedimentation. Their proximity to each other makes it difficult to distinguish which of them governed the deposition of the Sarsbukta Formation. Only reliable geochronological data on the Sarsbukta Formation and the activity of both faults will be able to answer this question.

The paleocurrent data suggest that the transport directions varied significantly within the Sarsbukta Formation (section 3.3). At the northern beach, the flow was directed between north and east while it covered westerly to southerly directions in central Sarsøyra. These differences could be attributed to either a drainage divide that was located between the localities or the spread in transport direction that depositional systems exhibit.

A drainage divide could have been provided by a high ground in between central Sarsøyra and the northern beach. Such topography would also explain the basement outcrops in that area (Fig. 11) and could have evolved in association with a metamorphic core complex (cf. Osmundsen and Péron-Pinvidic, 2018) or by a more ‘normal’ type of footwall uplift related to a large normal fault (cf. Jackson and McKenzie, 1983). During the exhumation of a metamorphic core complex, an anticline with two adjacent synclines develops in the footwall of the detachment, trending approximately perpendicular to the basin margin (e.g. Kapp et al.,

2008; Osmundsen and Péron-Pinvidic, 2018). That the Forlandsundet Graben could have formed in association with a metamorphic core complex has been mentioned by Kleinspehn and Teyssier (1992) and will be discussed further in section 6.2.3.

Alluvial fans may exhibit a spread in transport direction of 180° (e.g. Blair and McPherson, 1994) and could have caused the opposing paleoflow directions also. The axial and transverse depositional systems of a basin naturally exhibit different transport directions (e.g. Gawthorpe and Leeder, 2000; Leeder and Gawthorpe, 1987). At the northern beach, where alluvial fan conglomerates interfinger with river deposits (chapter 3), the fluvial sediments probably represent the axial drainage system, while the alluvial fan deposits make up the transverse drainage systems (e.g. Gawthorpe and Leeder, 2000; Leeder and Gawthorpe, 1987).

The paleocurrent data do not allow a differentiation of whether the coarse conglomerates along the eastern basin boundary belong to one big alluvial fan or if they were deposited by several smaller systems, in a so called bajada along the basin boundary (cf. Gawthorpe and Leeder, 2000; Nilsen, 1982). However, judging from the maximum extent of alluvial fan deposits at the northern beach, the fan radius was probably significantly less than 2 km. Thus, it is unlikely that a single fan spanned the distance of c. 10 km between the localities and it appears more feasible that parts of the Sarsbukta Formation were deposited by coalescent alluvial fans along the eastern basin boundary.

In tectonically active basins, the transverse and axial drainage system interact with each other (e.g. Alexander and Leeder, 1987; Gawthorpe and Leeder, 2000). These interactions can include toe trimming of the distal parts of alluvial fans by the river (sensu Harvey et al., 2005) but also deviation of the river by prograding alluvial fans. Hence, the northwesterly flow direction indicated by the fluvial sediments could be caused by the deviation of a generally northwards flowing axial river around an alluvial fan derived from the eastern footwall (cf. Reinfelds and Nanson, 1993). However, such specific interpretations are associated with a high uncertainty, as the number of measurements and the scattered outcrops limit the validity of the data (section 3.3). Furthermore, the fact that the measurements could only be taken at different stratigraphic levels, implies that the correlation of the individual data points may not be straightforward.

Sarstangen Formation

Traditionally, the Sarstangen Formation was considered to be the older unit on Sarsøyra (Gabrielsen et al., 1992; Rye-Larsen, 1982). This study places the Sarstangen Formation as the youngest sedimentary unit of the Forlandsundet Graben, as it lacks the deformation as well as lithification that characterizes the Sarsbukta Formation and represents a Lower to Middle Oligocene age (section 3.4) (see also Kleinspehn and Teyssier, 2016). The Sarstangen Formation is interpreted as a fan delta sequence consisting of an offshore marine to fluvio-deltaic succession overlain by a very proximal fan deposit (section 3.2), which is an interpretation broadly in line with earlier work (Kleinspehn and Teyssier, 2016; Rye-Larsen, 1982).

Despite the lack of faulting within the strata, the Sarstangen Formation does exhibit evidence of tectonic activity during its deposition. It is considered to have been deposited along a major normal fault, indicated by >1 km offset in top-basement from central Sarsøyra to the 7811/5-1 Sarstangen petroleum exploration well drilled by Norsk Polar Navigasjon AS on Sarstangen (section 5.1.1) (see also Kleinspehn and Teyssier, 2016; Krasilscikov et al., 1995). The existence of a high relief structure to the east is also supported by the transport direction of proximal fan deposits (section 3.3) (see also Kleinspehn and Teyssier, 2016, and this study). In addition, this study documents an angular unconformity within the sedimentary succession of the Sarstangen Formation (section 3.2.2). The stratigraphically lower sedimentary package dips at 20° to the northwest while the overlying strata preserved its depositional dip of 12° to 17° to west-northwest (Fig. 11). Consequently, the underlying strata must have been tilted prior to the deposition of the overlying sediments. The dip direction of the underlying deposits is almost perfectly parallel to the strike of a magnetic anomaly (Krasilscikov et al., 1995) that can be interpreted to represent the normal fault generating the subsidence for the deposition of the Sarstagen Formation (Kleinspehn and Teyssier, 2016 and this study). Therefore, it appears most likely that the lower sedimentary package was affected by transverse folding due to a northwards increasing displacement gradient along the normal fault in the style described by Brandes and Tanner (2014), Fossen and Rotevatn (2016) or Schlische (1995).

6.1.2 Deformation sequence

Transpression (53 Ma - ?)

The transpressional stage of the WSFB is reflected in the kinematics of faults in the basement adjacent to the basin. The kinematics clearly show that the deformation was dominated by ENE-WSW compression on NNW-SSE oriented thrusts and strike-slip motion on NE-SW oriented faults (section 4.1). Along the eastern basin boundary, top-to-the west reverse faulting at 53.5 Ma is manifested in a fault gouge (Schönenberger et al., 2019). The fault was interpreted as a backthrust within the WSFB that was associated with the SEDL (Bergh et al., 1998; Maher et al., 1997). This fault might have constituted the basin boundary during the deposition of the Sarsbukta Formation. In that case, the matrix filled tension fractures in the conglomerate clasts (section 4.2.1) could be attributed to orogen parallel extension, as proposed by Kleinspehn and Teyssier (2016). Although, additional contractional structures are absent in the basin fill, they prevent an unambiguous placement of the fractured clasts and the Sarsbukta Formation in a transpressional setting (section 4.2). Bergh et al. (1998) also suggest that the fractured clasts formed within the WSFB. However, they attribute the intraclast fractures to a shortlived phase of sinistral compression along the SEDL (Maher et al., 1997).

Early transtension (?)

A NW-SE oriented extensional stress field introduced a transtensional setting to the Forlandsundet Graben and initiated the dextral oblique normal fault that today bounds the basin to the east (section 4.1). Under this NW-SE oriented extension, oblique normal faults, strike slip faults and transtensional folding developed in the strata of the Sarsbukta Formation (section 4.2) (see also Kleinspehn and Teyssier, 2016). Consequently, the Sarsbukta Formation must have been deposited before or during this shift to transtensional deformation.

The elongation direction of the clasts has been used to place the deposition of the Sarsbukta Formation in the transpressional phase since it is oriented parallel to the NW-SE oriented extension direction, but appears to record a N-S oriented extension (Kleinspehn and Teyssier, 2016). However, Burg and Harris (1982) showed that tension fractures can initiate at oblique angles towards the direction of extensional stress and proposed that the formation of such structures can be viewed as analogue to the formation of so-called Lüders' bands (see also

Olsson, 2000). Lüders' bands are well known in material science from deformation experiments with thin metal plates (cf. Friedman and Logan, 1973). They correspond to a localized zone of plastic deformation that is characterized by intergranular deformation, intragranular fracturing and gliding flow (Friedman and Logan, 1973). The occurrence of Lüders' bands in rocks has been documented in laboratory experiments, as well as in the field (Burg and Harris, 1982; Friedman and Logan, 1973; Olsson, 2000) but some consider them a type of deformation band (Fossen et al., 2007; Olsson, 2000). Experiments show that Lüders' bands form before faults or shear fractures (Olsson, 2000) which corresponds to the deformation sequence suggested by Kleinspehn and Teyssier (2016) for the Sarsbukta Formation.

Burg and Harris (1982) argue that a rock layer can be approximated as a thin horizon within the surrounding rock masses. Therefore, extensional deformation could be accommodated analogous to Lüders' bands in thin metal plates (e.g. Burg and Harris, 1982). On Sarsøyra, fractured clasts occur preferentially in a rather small area along the northern beach (Kleinspehn and Teyssier, 2016 and this study). This part could represent a zone that facilitated large amounts of extensional deformation in a Lüders' band manner oblique to the main extension direction. A reason for this behavior could have been that the Sarsbukta Formation was not yet lithified and able to deform ductile in that area. The zone with the fractured clasts would have been thinned and stretched in the process. Analogous to Lüders' bands, the deformation would have been accommodated by ductile matrix flow and intergranular fracturing. Subsequently, faulting and folding became active. Unfortunately, the concept of Lüders' bands has not been modelled for features exceeding bed scale. But, Burg and Harris (1982) used the process in the Alps to explain the occurrence of fractures that did not initiate perpendicular to the orientation of the maximum extensional stress.

Lüders' bands show that there are alternative mechanisms that could have controlled the orientation of fractures in clasts. However, the orientation of the fractures could also be a local phenomenon.

Progressive transtension (?33 Ma – 22 Ma)

The Sarstangen Formation was probably deposited under the same transtensional stress field that affected (the deposition of) the Sarsbukta Formation. A major shift in the extension direction seems unlikely because the spreading direction of the Knipovich ridge today, 307°

(Curewitz et al., 2010), is close to the NE oriented extension direction derived from fault kinematics and transtensional fold axes (section 4.2) (see also Kleinspehn and Teyssier, 2016). The Sarstangen Formation was deposited along a normal fault that exhibited a throw of >1 km but was not affected by internal deformation like the Sarsbukta Formation. However, the results of this study indicate that sedimentation was contemporaneous with displacement along the fault as manifested by the angular unconformity shown in Fig. 30 (see section 6.1.1). The transition to a (partly) marine depositional environment suggests that subsidence provided by normal faults within the Forlandsundet Graben was higher than the sedimentation rate during the deposition of the Sarstangen Formation (section 3.2) (see also Kleinspehn and Teyssier, 2016).

During this progressive transtension, the strata of the Sarsbukta and Sarstangen Formations were buried and experienced maximum temperatures of <105 °C (cf. Barker and Pawlewicz, 1994) as indicated by vitrinite reflectance values (R_0) between 0.3 and 0.68 (Kleinspehn and Teyssier, 2016; Manum and Throndsen, 1986; Paech and Koch, 2001; Rye-Larsen, 1982). At today's geothermal gradient of 24°C/km at Sarstangen (Betlem et al., 2019, 2018), this would correspond to a maximum burial depth of c. 4 km.

The formation of the Svalbard margin terminated around 22 Ma when the first oceanic crust was formed between Greenland and Svalbard (Engen et al., 2008; Kleinspehn and Teyssier, 2016). Until then, progressive thinning of the lithosphere must have occurred and fault activity probably migrated from the Forlandsundet area to the west as proposed by the model developed by Peron-Pinvidic et al. (2013) (section 1.2.1).

6.1.3 Updated tectono-sedimentary model of Sarsøyra

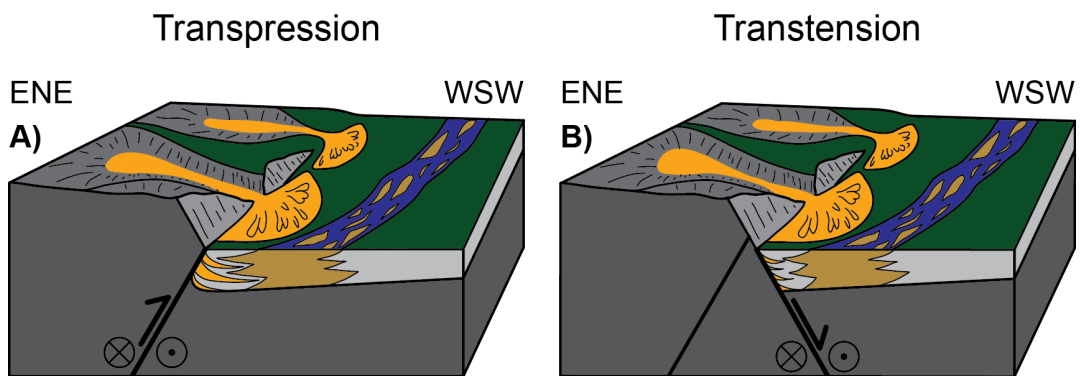
On the basis of the previously discussed observations, an updated model for the tectono-sedimentary evolution of Sarsøyra is proposed (Fig. 55). It aims to satisfy the following boundary conditions:

- Syn-tectonic deposition of the Sarsbukta Formation in the form of alluvial fans, braided river and floodplain sediments.
- Deformation of the Sarsbukta Formation under transtension.

- Deposition of the Sarstangen Formation along a major normal fault after the deposition of the Sarsbukta Formation.
- Angular unconformity within the Sarstangen Formation.

For the evolution of the Sarsbukta Formation two models were developed to allow for the two alternative basin-bounding fault types (Fig. 55A and B). In the first model, sedimentation is controlled by a backthrust of the WSFB (Fig. 55A). In the second model, an oblique normal fault governs the deposition and creates relief along the eastern basin boundary (Fig. 55B). In the following section, the strengths and limitations of each model will be discussed.

Sarsbukta Formation (Eocene?):



Sarstangen Formation (Lower to Middle Oligocene):

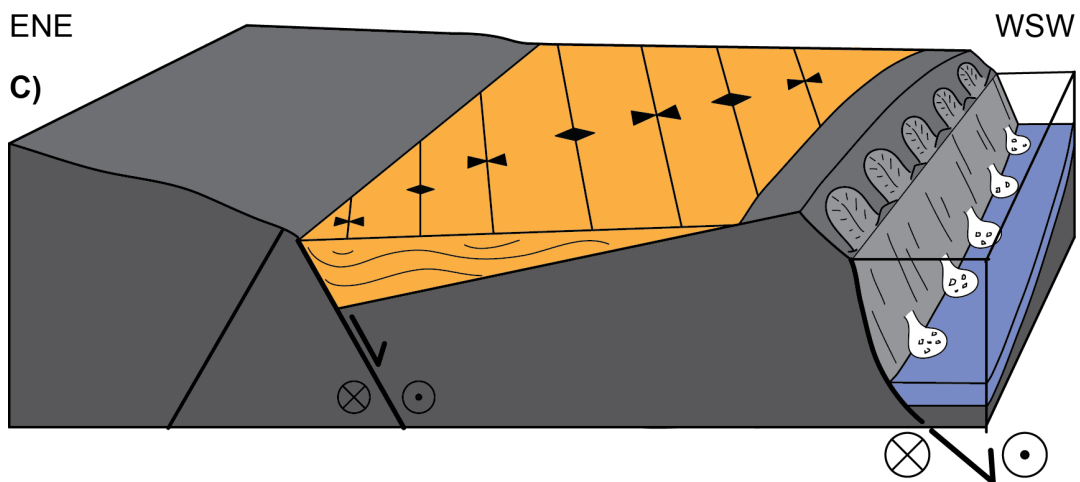


Fig. 55: Schematic models for the evolution of the Paleogene successions on Sarsøyra. At this point, a deposition of the Sarsbukta Formation in either a transpressional (A) or transtensional (B) setting has to be considered. Note the monocline in the models of the Sarsbukta Formation and the angular unconformity between basin floor deposits and footwall derived fans due to a northwards increasing displacement gradient of the normal fault that controlled the deposition of the Sarstangen Formation (C).

Deposition of the Sarsbukta Formation under transpression

The depositional model for the deposition of the Sarsbukta Formation within the WSFB (Fig. 55A) is similar to the model suggested by Kleinspehn and Teyssier (2016) (Fig. 53) since they share the same first order deformation sequence. However, this study documents a major reverse fault in direct proximity of today's basin-bounding oblique normal fault (section 4.1.2) as well as evidence for syn-tectonic deposition of the Sarsbukta Formation (section 6.1.1). Also, fault activity since the initiation of the WSFB at 53.5 Ma was documented (section 4.1.2) and the resulting high ground to the east could have supplied sediments to the western lowlands (Fig. 55). Therefore, the model considers the backthrust of the WSFB as basin bounding fault during the deposition of the Sarsbukta Formation (Fig. 55A).

This model has the potential to explain the approx. E-W striking fracture planes in the conglomerate clasts by orogen parallel shortening, as proposed by Kleinspehn and Teyssier (2016) (see section 6.1.2). Also, steepening of the strata towards the basin margin could be connected to drag along a reverse fault (Fig. 55A) (Tavani et al., 2015). However, the main problem with this model is that the preservation of the reverse fault, displacing basement against basement, within the footwall of today's basin-bounding normal fault, would result in the previously overriding basement block to be downfaulted into the basin (Fig. 55A). Consequently, the sedimentary succession should be in contact with the reverse fault, similarly to the basement configuration in Fig. 58, and not with the oblique normal fault for this model to work without further constrains.

Deposition of the Sarsbukta Formation under transtension

The model for the deposition of the Sarsbukta Formation under transtension assumes that the oblique normal fault bounding the basin today was active during sedimentation (Fig. 55B). In that context, the Sarsbukta Formation would postdate the compressional phase of the WSFB and the formation of intraclast fractures could not be attributed to orogen parallel extension, as suggested by Kleinspehn and Teyssier (2016). Instead, Lüders' bands or a local anomaly would be responsible for the clasts fracturing (section 6.1.2). Other structures observed in the Sarsbukta Formation are understood to have evolved under ongoing deposition. Steepening of the bedding towards the basin boundary can be caused by normal fault drag (Brandes and Tanner, 2014), while gentle open folds have been interpreted as transtensional (Kleinspehn and Teyssier, 2016 and this study). The fault kinematics within the Sarsbukta Formation

(section 4.2.2) match the kinematics from the fault scarp (section 4.1.1), suggesting that they formed in the same tectonic setting and possibly at a similar time. The model for the deposition of the Sarsbukta Formation under transtension is preferred in this study because it matches the field data better and appears more straightforward (Fig. 55B).

Deposition of the Sarstangen Formation

The (partly) marine environment suggests that subsidence rates were higher than sedimentation rates during the deposition of the Sarstangen Formation (Fig. 55C) while subsidence was controlled by normal faults within the basin (section 6.1.2). Sudden fault movement and the resulting displacement gradients are responsible for angular unconformities within the Sarstangen Formation (section 6.1.1). The high relief and seismicity that were probably associated with fault growth (e.g. Blair and McPherson, 1994; Fossen and Rotevatn, 2016) gave rise to rock failure processes. Therefore, oversized angular boulders can be found within the proximal fan delta deposits (section 3.2.2).

The Sarsbukta Formation was likely probably buried during the deposition of the Sarstangen Formation, as indicated by vitrinite reflectance values (section 6.1.2). The sediments of the Sarstangen Formation were probably derived from the footwall of a large normal fault. The clast were derived from basement lithologies (section 3.2), suggesting that basement rocks were exposed in the fault scarp (Fig. 55C). However, clasts from the Sarsbukta Formation could not be recognized by most workers (Kleinspehn and Teyssier, 2016, 1992; Rye-Larsen, 1982 and this study). Only Bergh et al. (1998) reported clasts from the Sarsbukta Formation within the Sarstangen Formation. That would be another argument for the deposition of the Sarstangen Formation after the Sarsbukta Formation.

6.2 Evolution of the Forlandsundet Graben

Previous studies suggest a multistage evolution of the Forlandsundet Graben (Gabrielsen et al., 1992; Kleinspehn and Teyssier, 2016, 1992; Lepvrier, 1990; Steel et al., 1985; von Gosen and Peach, 2001). Despite significant differences, the proposed models share a somewhat similar sequence:

1. The Forlandsundet Graben initiated as a sedimentary basin that extended across the current graben boundaries, at least to the west (Gabrielsen et al., 1992; Kleinspehn and

Teyssier, 1992). Many propositions have been made regarding the tectonic regime that the basin originated in. Some studies lean towards basin initiation in a strike slip setting due to the vicinity to the Hornsund Lineament (Gabrielsen et al., 1992; Lepvrier, 1990; von Gosen and Peach, 2001), while others suggest that the basin formed within the WSFB (Kleinspehn and Teyssier, 2016; Leever et al., 2011; Steel et al., 1985).

2. A period of transpression or compression that shortened the basin in an approximately N-S direction, inducing E-W oriented folds. And, a phase of approx. E-W oriented compression producing N-S trending reverse faults (Gabrielsen et al., 1992; Lepvrier, 1990; Rye-Larsen, 1982; von Gosen and Peach, 2001). The sequence of these two compressive phases is not clearly resolved in literature. This period was probably related to the formation of the WSFB and the structures could have evolved coevally in a transpressional setting (Faleide et al., 2008; Kleinspehn and Teyssier, 1992; Leever et al., 2011) or separately under compression with subsequent dextral strike slip (Piepjohn et al., 2016).
3. The present basin geometry developed after a shift towards northwest-directed transtension, during the establishment of the passive margin (Kleinspehn and Teyssier, 2016). Parts of the original basin got downfaulted into the graben structure while other parts were preserved in the western footwall on Prins Karls Forland. Sedimentation probably continued over the newly established fault scarps since the sediments along the eastern basin margin were not affected by the compressive deformation of the previous stage (Kleinspehn and Teyssier, 2016, 1992; Rye-Larsen, 1982; von Gosen and Peach, 2001). Kleinspehn and Teyssier (1992) speculated that Prins Karls Forland was exhumed as a metamorphic core complex during this transtensional phase.

The following section will discuss the impact of this and other recent studies on the understanding of the basin evolution. Subsequently, two conceptual models for the formation of the whole Forlandsundet Graben will be discussed.

Geometry and structural style of the basin

The large-scale geometry of the Forlandsundet Graben is controlled by NNW-SSE trending, steeply dipping normal faults that bound the basin to the east, and are documented from

surface and seismic mapping (see section 5.1.3) (Blinova et al., 2009; Dallmann, 2015; Gabrielsen et al., 1992; Hjelle et al., 1999; Rye-Larsen, 1982 and this study). Along the western margin, that is exposed on Prins Karls Forland, the Paleogene strata overlie the basement conformably and today's boundary faults cut through the basin fill (Kleinspehn and Teyssier, 1992; von Gosen and Peach, 2001).

The sedimentary rocks that are exposed on Prins Karls Forland exhibit different degrees of deformation. The strata in the northern part of Prins Karls Forland, consisting of the Aberdeenflya Formation, do not show signs of internal deformation (Gabrielsen et al., 1992; Magnus, 1986), while the sedimentary rocks in central Prins Karls Forland exhibit a complex deformation pattern. The deformation pattern includes folding on different scales, including reverse as well as normal faulting and even ductile fabrics (Gabrielsen et al., 1992; Kleinspehn and Teyssier, 1992; Lepvrier, 1990; von Gosen and Peach, 2001). Seismic scale folding of the basin fill along the western margin has also been recognized by Gabrielsen et al. (1992) and this study (Fig. 48). The sequence of deformation is not well constrained but broadly fits with the three stage basin evolution outlined in the previous section (Gabrielsen et al., 1992; Kleinspehn and Teyssier, 1992; Lepvrier, 1990; von Gosen and Peach, 2001).

Similar to the northern part of Prins Karls Forland, the sedimentary strata on Sarsøyra, respectively the eastern basin margin, are much less deformed compared to the central part of Prins Karls Forland. The structures are limited to NW-SE trending folds, normal and strike slip faults, and E-W trending tension fractures in the Sarsbukta Formation (section 4.2) (see also Kleinspehn and Teyssier, 2016; Rye-Larsen, 1982 and this study), and tilting of the bedding in the Sarstangen Formation (section 4.3). This study contemplates that the structures along the eastern basin margin are attributed to different stages of transtensional basin formation (section 6.1).

In summary, the sedimentary rocks within the Forlandsundet Graben exhibit a N-S and E-W gradient in structural complexity. The strata in central Prins Karls Forland experienced the highest degree of deformation, including contractional strain (Gabrielsen et al., 1992; Kleinspehn and Teyssier, 1992; Lepvrier, 1990; von Gosen and Peach, 2001). The Sarsbukta Formation at the eastern basin margin was probably only affected by transtensional deformation (section 6.1). The least deformation is evident in the Sarstangen Formation in the eastern part of the basin (section 6.1), as well as the Aberdeenflya Formation located in the north of Prins Karls Forland (Gabrielsen et al., 1992; Magnus, 1986; Rye-Larsen, 1982). They

only exhibit tilting and drag folding related to movement along normal faults and soft-sediment deformation (Gabrielsen et al., 1992; Kleinspehn and Teyssier, 2016; Magnus, 1986; Rye-Larsen, 1982 and this study).

Thermal history of the basin

The thermal imprint of the Forlandsundet Graben shows a similar trend in the deformation style. Vitrinite reflectance values (Fig. 56) are the highest in central Prins Karls Forland ($R_0 = 2.0$ to 4.3) and decrease towards the north ($R_0 = 0.9$ to 2.1), while the sedimentary rocks along the eastern margin exhibit the lowest coal rank ($R_0 = 0.3$ to 0.7) (Kleinspehn and Teyssier, 2016, 1992; Manum and Throndsen, 1986; Paech and Koch, 2001; Rye-Larsen, 1982; Sperling, 1990). The disparity across the basin corresponds to a difference in peak temperature of at least c. $85\text{ }^\circ\text{C}$ (east = $107\text{ }^\circ\text{C}$ for $R_0 = 0.7$, west = 192° for $R_0 = 2.0$), according to Barker and Pawlewicz (1994), and therefore a minimum difference in burial of c. 3.5 km assuming today's geothermal gradient of $24\text{ }^\circ\text{C/km}$ (Betlem et al., 2019, 2018).

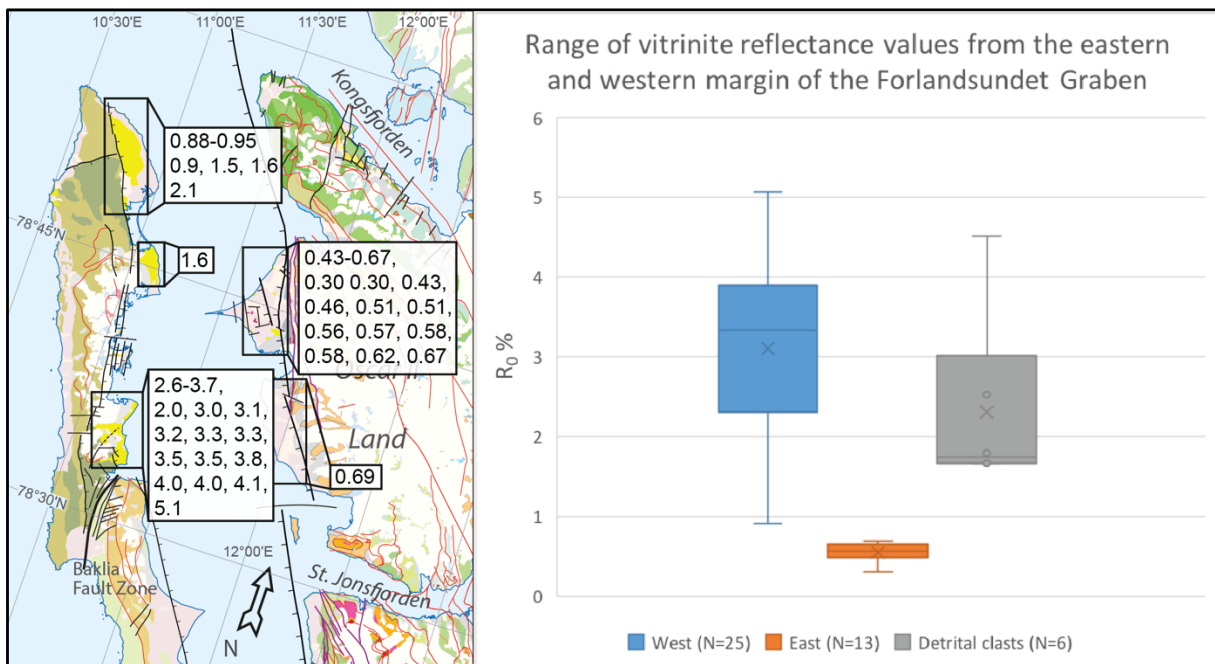


Fig. 56: Left: Vitrinite reflectance values (R_0) from Paleogene coals in the Forlandsundet Graben. The values are compiled from several studies (Kleinspehn and Teyssier, 2016; Manum and Throndsen, 1986; Paech and Koch, 2001; Rye-Larsen, 1982). The map was modified from Dallmann (2015). Right: Comparison of vitrinite reflectance values from the western and eastern basin margins, as well as detrital coal clasts. The western basin margin exhibits much higher vitrinite reflectance values compared to the eastern basin margin. Data was summarized from several studies (Kleinspehn and Teyssier, 2016; Manum and Throndsen, 1986; Paech and Koch, 2001; Rye-Larsen, 1982).

Similar results were reported by Barnes and Schneider (2018) based on zircon (U-Th)/He thermochronology (Fig. 57). They estimate that erosion was in the range of ~2.5-3.5 km since c. 47 Ma for the west coast of Spitsbergen and >4 km since c. 34 Ma for Prins Karls Forland. Accordingly, the exposures on Prins Karls Forland embody a deeper crustal level and experienced a more rapid exhumation than the ones along the west coast of Spitsbergen (Fig. 57) (Barnes and Schneider, 2018; Schneider et al., 2018).

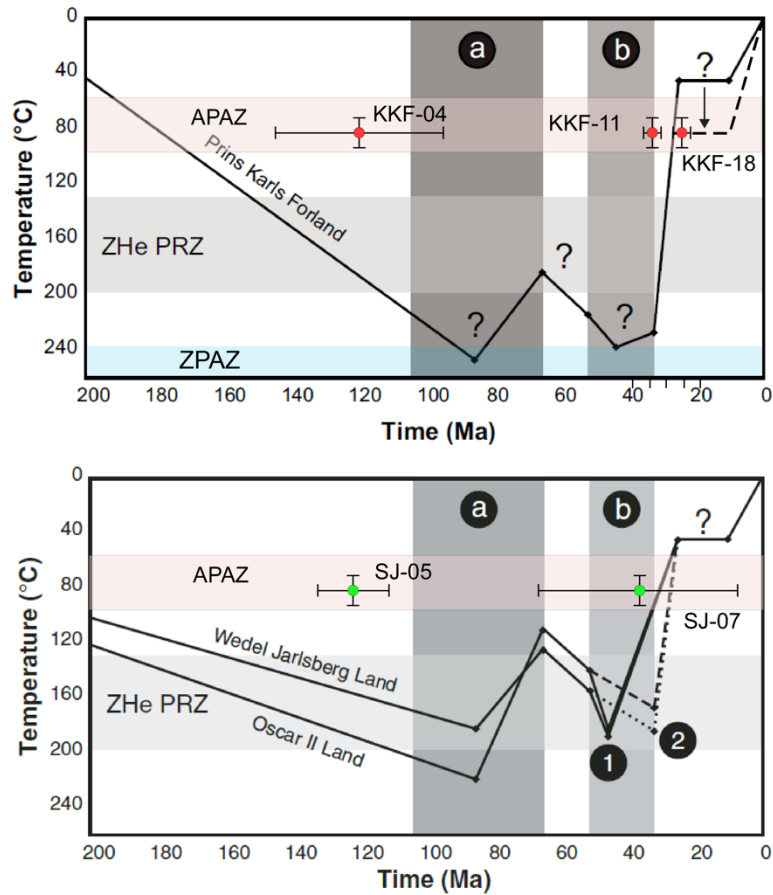


Fig. 57: Schematic time-temperature model (ZHe) by Barnes and Schneider (2018), indicating that Prins Karls Forland experienced higher temperatures for longer and subsequently faster uplift than Oscar II Land. For the Eurekan orogeny (b), two cases were modeled for each locality. Oscar II Land (solid line): max. 185 °C at 47 Ma cooling to 20 °C at 30 Ma. Oscar II Land (dashed line): max 175 °C at 34 Ma cooling to 20 °C at 32 Ma. Prins Karls Forland: max >200 °C cooling to ~45 °C at 26 Ma. Red and green dots mark apatite fission track ages with whiskers indicating the 95% certainty intervals supplied by Redfield (unpublished data). They are in line with a differential thermal history of Oscar II Land compared with Prins Karls Forland but do not entirely fit with the model by Barnes and Schneider (2018). A shift of the plateau around 20 Ma is suggested for the cooling history of Prins Karls Forland based on the data from Redfield (unpublished data). The figure is modified from Barnes and Schneider (2018).

In addition, thus far unpublished apatite (AFT) as well as zircon fission track (ZFT) data from metasedimentary rocks collected in St. Jonsfjorden and on Prins Karls Forland were provided

by Tim Redfield from the NGU (Fig. 57, Appendix 6). They are included to incorporate the latest results towards the thermal history of the basin. However, the quality of the measurements varies, mainly due to a low number of countable tracks or grains (Appendix 6). The age and length data presented here do not represent single unique thermal events. Thermal modelling could be used to extract a best-fit thermal history from the individual age/length pairs (Redfield, pers. comm.) but is not in the scope of this thesis. Therefore, the interpretation of the data will be limited to some basic key observations.

The ZFT ages from Prins Karls Forland (Appendix 6) all predate the proposed timing of the basin formation by far and suggest that the sedimentary successions did not experience temperatures above ~ 240 °C (Bernet, 2005; Gallagher et al., 1998). This maximum temperature can be used as an additional boundary condition to confine the time-temperature model by Barnes and Schneider (2018) (Fig. 57).

Two AFT ages from Prins Karls Forland (KKF-11 and KKF-18) exhibit acceptable results. The low mean track lengths indicate that the rocks were reheated or have resided in the apatite partial annealing zone (60 to 100 °C) (Gallagher et al., 1998) for an extended period during the latest exhumation event (Fig. 57). Therefore, it is suggested that cooling was slightly slower than proposed by Barnes and Schneider (2018), and the plateau they indicated is moved into the apatite partial annealing zone (Fig. 57) (Redfield, pers. comm.). However, due to poor statistics of the two KKF samples, this is a very unconstrained interpretation. Sample KKF-04 is disregarded because too few tracks were measured to justify a geological interpretation (Redfield, pers. comm.).

Sample SJ-05 from St. Jonsfjorden (Fig. 57) contained a sufficient number of measured grains and tracks to deliver a statistically viable age (Appendix 6). Since the sample was taken from a metagabbro, any inherited thermal history can be neglected (Redfield, pers. comm.). The age of 126 Ma implies that the rock did not experience temperatures above 120 °C (cf. Gallagher et al., 1998) while the medium track length indicates slow cooling (Appendix 6) (Redfield, pers. comm.). The age contradicts the measurements as well as the time-temperature model for Oscar II Land proposed by Barnes and Schneider (2018). However, many factors could have caused this discrepancy (Redfield, pers. comm.). The most obvious is that sample SJ-05 was collected 14 km inland from the Paleogene basin and over 6 km inland from the closest sample collected by Barnes and Schneider (2018). In between, several structures related to the WSFB cut the succession and possibly juxtaposed rocks with

different thermal histories. Since there were no other samples analyzed from localities in closer vicinity to the basin or the sample sites of Barnes and Schneider (2018), the spatial control is low which prevents a sound geological interpretation of the age (Redfield, pers. comm.). Sample JS-07 is ignored since the error associated with the age are extremely high.

These findings implicate that the sedimentary rocks on the eastern and the western side of the basin reflect different stages in the overall basin evolution. Barnes and Schneider (2018) suggested that the western margin of the Forlandsundet Graben was buried and exhumed along with the basement of Prins Karls Forland (see also Schneider et al., 2018). The results of Redfield (unpublished data) are consistent with the general interpretation of Barnes and Schneider (2018) since they support a difference in thermal history across the Forlandsundet Graben. Paech and Koch (2001) attributed the difference in thermal imprint to the circulation of hydrothermal fluids along the western boundary fault. It is possible that hydrothermal fluids contributed to the coalification of the sedimentary rocks. However, the results of Barnes and Schneider (2018) show that the basement rocks principally exhibit the same thermal history. Therefore, it appears more probable that the coalification pattern is associated with the burial and uplift history of the adjacent basement rocks.

The latest model for the evolution of the Forlandsundet Graben was presented by Kleinspehn and Teyssier (2016) and does not account for the difference in thermal history across the Forlandsundet Graben but focuses primarily on the differential deformation between the Sarsbukta and Sarstangen Formations. Based on the structural style, they argued for a major shift in the tectonic setting during the transition from the Sarsbukta Formation to the Sarstangen Formation, which are both located along the eastern side of the basin. This shift, however, is not reflected in the thermal evolution of the sedimentary rocks on Sarsøyra. It appears more reasonable that the a major shift in tectonic setting would also be reflected in the thermal history. Therefore, the differential thermal and structural imprint across the Forlandsundet Graben is considered more significant for the updated tectono-thermal models presented in the following sections.

6.2.1 Model for the tectono-thermal evolution of the Forlandsundet Graben

The previously presented findings supplement the results of this study and allow for the construction of an improved model for the evolution of the Forlandsundet Graben as a whole. The model aims to accommodate the following constrains:

- The constrains that were established for the tectono-sedimentary evolution of Sarsøyra (section 6.1.3), e.g. deposition of the Sarsbukta Formation under transtension and deposition of the Sarstangen Formation afterwards.
- A N-S and E-W gradient in structural style and thermal maturity.
- A differential uplift history for Prins Karls Forland and the westcoast of Spitsbergen.
- A steep eastern boundary fault, as indicated from seismic data.
- A depositional contact between the Paleogene strata and the basement rocks that extends over the basin bounding normal faults.

The constrains allow for a high degree of freedom in the construction of a basin model. Therefore, two end-member models for the tectono-thermal evolution of the entire Forlandsundet Graben are presented. The first model consists of multiple stages suggested by earlier studies and was summarized in the previous section (Gabrielsen et al., 1992; Kleinspehn and Teyssier, 2016, 1992; Lepvrier, 1990; Steel et al., 1985; von Gosen and Peach, 2001). It assumes that parts of the Paleogene strata were deposited during or before the WSFB and experienced heating as well as contractional strain as a consequence.

The second model investigates whether the Forlandsundet Graben and its associated structures could have evolved in a purely transtensional setting. As mentioned by Kleinspehn and Teyssier (1992), contractional and extensional structures could have evolved under strain partitioned transtension (see also Kristensen et al., 2017). The differential thermal imprint between the eastern and western basin margin is attributed to the exhumation of Prins Karls Forland as metamorphic core complex, as speculated about by Kleinspehn and Teyssier (1992).

In the following, the basin models will be presented and their aspects will be discussed.

6.2.2 Multi-stage model

The multi-stage model involves a transpressive or compressive deformation phase followed by a transtensional stress regime to explain the structures within the Forlandsundet Graben. As pointed out before, most studies suggest that parts of the Forlandsundet Graben strata were deposited in a broader basin prior or during the formation of the WSFB. The transpressional episode is required by the published models to explain the contractional structures along the eastern basin margin. An initially wider basin (in E-W direction) is suggested because Paleogene sedimentary rocks are preserved in the footwall of the basin-bounding fault to the west and exhibit a depositional contact to the underlying basement rocks. However, some studies also claim that the initial basin was shorter (in N-S direction), because no onshore Paleogene exposures are known in the southern part of Prins Karls Forland, even though the boundary fault is exposed (Gabrielsen et al., 1992; Kleinspehn and Teyssier, 1992; Steel et al., 1985).

Therefore, several propositions have been made regarding the initial geometry of the basin. The vicinity to the long-lived Hornsund Lineament led many workers to suggest a strike slip origin of the basin, for example as a classic pull apart basin of a right-stepping dextral strike-slip fault (Rye-Larsen, 1982; von Gosen and Peach, 2001 and references therein). A variety of other basin types can originate in association with strike slip zones (Kristensen et al., 2017) and are well summarized in Aksu et al. (2000). Steel et al. (1985) presented two possibilities how the Forlandsundet Graben could have evolved in a transpressive setting, either due to extension in lee of a wrench fault curvature caused by a resistant land mass in the northeast, or as the result of collapse in the axis of a flower structure (see also Sylvester, 1988). Leever et al. (2011) observed that such a depression forms in the axis of a transpressional fold-and-thrust belt during analogue modeling of the WSFB. Another possibility brought forward by Kleinspehn and Teyssier (2016) is that the Paleogene strata, with exception of the Sarstangen Formation, was deposited and deformed within a piggyback basin that was part of the WSFB.

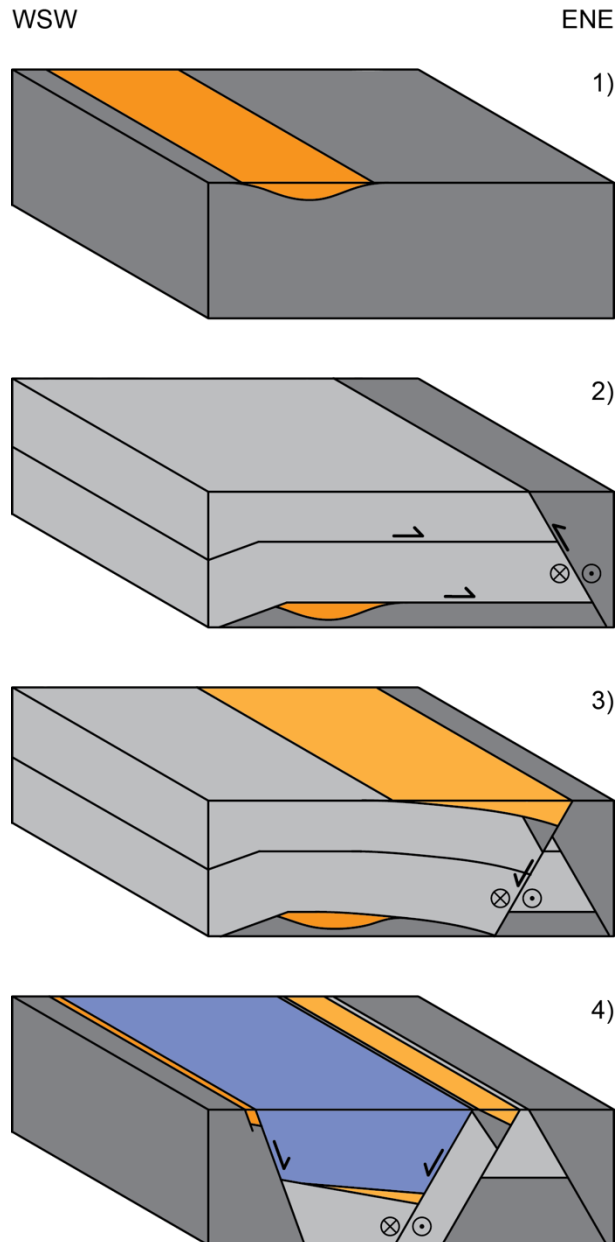


Fig. 58: Schematic multi-phase model for the evolution of the Forlandsundet Graben. Dark orange represents the sediments that are affected by high contractional deformation. Light orange is the Sarsbukta Formation and blue stands for the Sarstangen Formation at least along the eastern fault.

With the data available it is not possible to completely prove or disprove any of the suggested modes for the basin initiation. Therefore, the presented model does not assume the structural regime that the Forlandsundet Graben originated in. Instead, it features sediments deposited in a plain basement depression (Fig. 58). This ‘structureless’ basin serves as origin for the sedimentary rocks that experienced compressional strain and as a proxy for the alternative initiation modes.

To account for the high coal rank within the sedimentary rocks on central Prins Karls Forland and to comply with the thermal history of the adjacent basement modelled by Barnes and Schneider (2018), parts of the initial basin are considered to have been buried within a thrust stack of the WSFB (Fig. 58) (see also Maher et al., 1997). In the process, the sedimentary rocks were lithified and compressed. Folding as well as thrusting observed in the rocks along the western basin margin could have formed during this compressive period.

During subsequent oblique rifting in a transtensional setting, the present boundary faults were established and the sedimentary rocks in center and along the eastern basin margin were deposited (section 6.1). The basement rocks of Prins Karls Forland got exhumed as a horst structure along with some of the buried sedimentary rocks (Barnes and Schneider, 2018). As investigated in section 6.1, the transtensional phase can be subdivided into two episodes. The first episode corresponds to syn-tectonic deposition of the Sarsbukta Formation. At that time, subsidence was low and the transtensional strain was taken up by internal deformation in the Sarsbukta Formation (section 4.2). The second episode featured high subsidence along possibly oblique normal faults and the deposition of the Sarstangen Formation (see also Kleinspehn and Teyssier, 2016). Also, the Aberdeenflya Formation could have been deposited during the final rifting episode since it was only affected by tilting of the bedding and does not exhibit internal deformation.

6.2.3 Purely transtensional model

This study documents that the eastern boundary fault of the Forlandsundet Graben initiated under dextral transtension, and that the sedimentary successions on Sarsøyra were probably also deposited under transtension (section 6.1.3). Recent studies have shown that the occurrence of contractional and extensional structures in sedimentary basins can be associated with transtension (De Paola et al., 2005; Kristensen et al., 2017; Osmundsen and Andersen, 2001; Seiler et al., 2010). Consequently, it should be considered whether the structural complexity of the whole Forlandsundet Graben could have evolved under transtension. In a purely transtensional setting, however, the thermal history of Prins Karls Forland and the Paleogene sedimentary successions in the Forlandsundet Graben is not replicated straightforwardly. Therefore, the suggestion by Kleinspehn and Teyssier (1992) that Prins Karls Forland was exhumed along with a metamorphic core complex is included in the model.

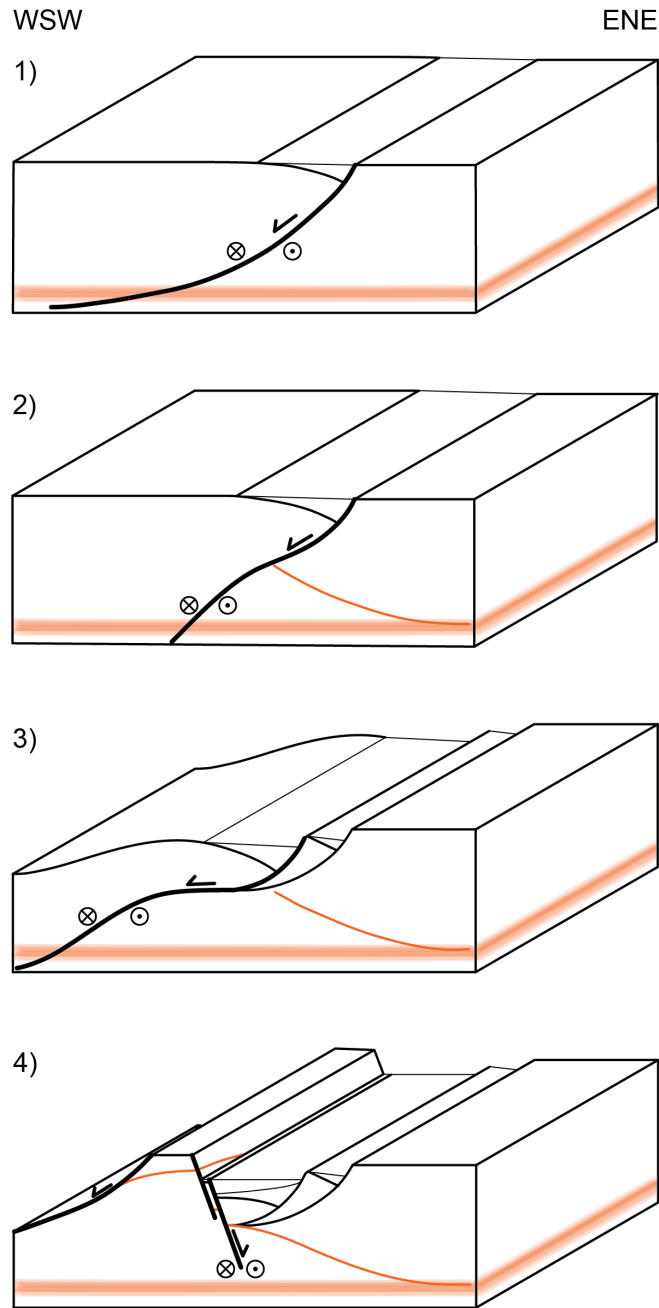


Fig. 59: Schematic evolution of the Forlandsundet Graben in a purely transtensional setting. The orange layer represents the mid-crustal detachment while the thin orange line stands for inactive and uplifted parts of the detachment. The model is based on the exhumation mechanisms proposed by Osmundsen and Péron-Pinvidic (2018).

Previous studies have reported that a population of the fold axes within the Paleogene strata on Prins Karls Forland trends predominantly NW-SE (Gabrielsen et al., 1992; Lepvrier, 1990), which would correspond to the orientation of transtensional folds on Sarsøyra (section 4.2.3). Also, folding and thrusting at a high angle towards the basin boundaries, as observed along the western margin of the Forlandsundet Graben (e.g. Gabrielsen et al., 1992; Lepvrier, 1990), can be associated with transtension (cf. Sanderson and Marchini, 1984). Therefore, it

cannot be ruled out that also the Paleogene sedimentary successions along the western basin margin were deformed under transtensional stress.

Heating of the western basin strata, as indicated by the coalification pattern, could have been supplied by hydrothermal fluids (Paech and Koch, 2001) or the juxtaposition of hot crust against the Paleogene sediments (e.g. Reston, 2007). Kleinspehn and Teyssier (1992) speculated that Prins Karls Forland might represent a metamorphic core complex. Recent studies by Barnes and Schneider (2018) and Schneider et al. (2018) document that parts of Prins Karls Forland represent deeper crustal levels that got exhumed later and faster than Oscar II Land and the rest of Spitsbergen's west coast (Fig. 57). Kleinspehn and Teyssier (1992) stipulated that such data were needed to justify a geological model that includes the exhumation of Prins Karls Forland along a low-angle detachment. However, the model has not been investigated further in recent publications (i.e. Barnes and Schneider, 2018; Blinova et al., 2009; Faehnrich et al., 2016; Kleinspehn and Teyssier, 2016; Schneider et al., 2018).

The recognition of metamorphic core complexes in extensional settings commonly requires the recognition of a low-angle detachment (e.g. Braathen et al., 2018; Hossack, 1984). During passive margin formation, metamorphic core complexes often evolve due to rotation of deep seated normal faults (Osmundsen and Péron-Pinvidic, 2018). Crane et al. (1991) anticipated that a steeply eastwards dipping detachment was located beneath Spitsbergen in Paleogene times but that would facilitate the exhumation of Spitsbergen's west coast as metamorphic core complex (cf. Kleinspehn and Teyssier, 1992). Blinova et al. (2009) interpreted a flat-lying seismic reflector beneath the Bellsund Graben as detachment surface. The Bellsund Graben is considered to represent the southern continuation of the Forlandsundet Graben but is fully submerged (Dallmann, 2015). Blinova et al. (2009) suggested that the detachment originated as a basal detachment within the basement involved deformation zone of the WSFB that was predicted from onshore studies (Bergh et al., 2000; Braathen et al., 1999; Braathen and Bergh, 1995a). The detachment was probably reactivated during subsequent extension since normal faults of the Bellsund Graben sole out into the detachment (Blinova et al., 2009). In the seismic lines from the Forlandsundet Graben (section 5.1.3) the detachment reflector is not evident, which Blinova et al. (2009) relate to the lower quality of the old seismic data. Thus, it is very likely that the detachment surface continues to the north into the Forlandsundet area where it may have constituted the detachment that enabled the exhumation a metamorphic core complex.

A basement window consisting of the mylonitic Pinkie unit has been documented on Prins Karls Forland (Faehnrich et al., 2016; Kościńska et al., 2017). The Pinkie unit exhibits a fault contact to the surrounding rocks of lower metamorphic grade (Schneider et al., 2018) and would therefore be an obvious candidate for a metamorphic core complex (e.g. Lister and Davis, 1989). Schneider et al. (2018) documented that these rocks experienced $>450\text{ }^{\circ}\text{C}$ during the Eurekan orogeny and were rapidly exhumed afterwards (cf. Barnes and Schneider, 2018). However, basement rocks c. 15 km south on Prins Karls Forland did not get heated above $\sim 240\text{ }^{\circ}\text{C}$ since the Cretaceous according to ZFT dating by Redfield (unpublished data). Thus, it is a possibility that the Pinkie unit represents the tip of a domal core complex structure that supplied heat to the adjacent rocks (Fig. 58). The so called Bouréefjellet fault zone that delineates the Pinkiefjellet unit, has been mapped as a westerly dipping thrust fault (Hjelle et al., 1999; Schneider et al., 2018). However, many of the kinematic indicators from that fault zone, imaged in Schneider et al. (2018), appear to exhibit a general top-to-the west movement direction. Consequently, the Bouréefjellet fault zone might represent an extensional fault, but since the area was not visited for this study, this interpretation remains speculative. Especially, because a westerly dipping foliation below the fault contact indicates top-to-the east transport (Schneider et al., 2018).

The eastern contact of the Pinkie unit is obscured by glaciers and glacial deposits while the basin-bounding fault of the Forlandsundet Graben runs through rocks of lower metamorphic grade where it is exposed (Hjelle et al., 1999). However, Hjelle et al., (1999) indicated that the basin-bounding fault crosscuts the Bouréefjellet fault zone, suggesting that today's western basin boundary postdates the exhumation of the potential metamorphic core complex. Therefore, at least three phases of transtensional deformation are suggested (Fig. 58):

1. Initiation of a western dipping normal fault soling out below a mid-crustal detachment of the WSFB.
2. Rotation of the normal fault, giving rise to the formation of a metamorphic core complex that exhumed the Pinkie unit from lower crustal levels.
3. Normal faulting along the western basin boundary that was probably associated with intrabasinal faulting and the deposition of the Sarstangen Formation.

6.2.4 Comparison of the basin models

Two end-member models for the evolution of the Forlandsundet Graben have been discussed in this study (sections 6.2.2 and 6.2.3). However, as they represent end-members, combinations of the models are possible, e.g. formation of a metamorphic core complex adjacent to a basin that was initiated in a transpressive setting.

Each of the models has strengths and weaknesses compared with the other. The deformation pattern is easily reproduced by the multi-stage model. In that case, the sediments along the western basin margin would have been deformed independently from the Sarsbukta Formation. However, the structures could have evolved under transtension too (cf. Fossen et al., 2013; Fossen and Tikoff, 1998; Sanderson and Marchini, 1984). The differences in deformation style throughout the basin would be attributed to the large variations in orientation of the boundary lineaments (i.e. Gabrielsen et al., 1992) towards the extensional stress, as the contractional component increases with the obliquity (e.g. Agostini et al., 2009; Fossen and Tikoff, 1998; Kristensen et al., 2017). At Sarsøyra for example, the obliquity in a northwest oriented stress field would have been lower compared to parts of the western boundary fault (i.e. Gabrielsen et al., 1992).

Also, the thermal imprint of the Paleogene strata in the Forlandsundet Graben can be explained with both models. In the multistage model, parts of the basin initiated before or during the WSFB and experienced burial due to overthrusting. But also, the exhumation of hot lower crust associated with a metamorphic core complex could have caused the gradient in thermal maturity along Prins Karls Forland. The domal shape of a metamorphic core complex (e.g. Osmundsen and Péron-Pinvidic, 2018) would have resulted in differential uplift of the basement, i.e. less exhumation with distance from the metamorphic core complex. The sedimentary units could have experienced heating from the hotter rocks in the footwall of the detachment (e.g. Reston, 2007). The suggestion of a metamorphic core complex on Prins Karls Forland remains speculative. However, the new thermochronology data from Barnes (2016), Schneider et al. (2018) and Redfield (unpublished data) award this possibility renewed relevance. It is possible that the detachment horizon under the Bellsund Graben (Blinova et al., 2009), extends northwards and facilitated the exhumation of the Pinkie unit. The fact that the detachment does not rise towards the potential metamorphic core complex (Blinova et al., 2009) could be due to the fact that the Molloy Fracture Zone delineates the Forlandsundet Graben from the Bellsund Graben (cf. Ohta, 1982).

A metamorphic core complex would also explain the significantly different uplift history of Prins Karls Forland compared with the west coast of Spitsbergen, since the formation of a metamorphic core complex is an efficient way to exhume deeper crustal levels and thin the crust (Osmundsen and Péron-Pinvidic, 2018). It is questionable whether the rapid exhumation of the Pinkie unit could have been facilitated by isostatic uplift of a horst structure, as suggested by Barnes and Schneider (2018). Future studies will have to evaluate the kinematics within the Pinkie unit to better constrain how it was emplaced and whether it is bordered by an extensional shear zone.

6.2.5 Regional Implications

On a regional scale, the results of this study confirm that contractional deformation was evident on Svalbard from 53.5 Ma (section 4.1.2), probably as a response to break up in the north Norwegian Sea (Engen et al., 2008; Faleide et al., 2015). Whether the subsequent WSFB was formed under transpression only (Braathen et al., 1999; Braathen and Bergh, 1995b; Faleide et al., 2008; Leever et al., 2011), or as the result of a compressional followed by strike-slip regime (CASE Team, 2001; Piepjohn et al., 2016), is not clearly resolved in the data. However, the contractional structures along the eastern basin boundary appear to be associated with a continuation of the SEDL and was proven to be active since 53.5 Ma (Schönenberger et al., 2019), i.e. the beginning of the Eurekan orogeny on Svalbard (Engen et al., 2008; Faleide et al., 2008; Piepjohn et al., 2016). The SEDL is considered to have accumulated mainly strike-slip and backthrusting within the WSFB (Maher et al., 1997) which would favor a strain-partitioned transpressional evolution.

The deposition of the Sarsbukta Formation during syn-sedimentary normal faulting along the eastern basin boundary (section 6.1.3) suggests that rifting began already before the Sarstangen Formation was deposited in Early Oligocene. Also, it implies that the rift process featured at least two phases; the first was characterized by lower subsidence than sedimentation rates (Sarsbukta Formation) while the second stage featured higher subsidence than sedimentation rates (Sarstangen Formation). Heine and Brune (2014) showed that two-stage kinematics can be related to a strength-velocity feedback. Rifting is slow in the beginning and rapidly accelerates once the crust is weakened enough, i.e. the plastic yield limit has been surpassed, to allow rupturing of the entire crust. In comparison with other rifted margins, the Svalbard margin developed over a relatively short time period (cf. Peron-

Pinvidic and Osmundsen, 2018). The high obliquity of the Svalbard margin might be the reason since oblique rifts require less strain and force to reach the plastic yield limit than orthogonal rifts (Brune et al., 2018, 2012; Heine and Brune, 2014).

The results of this study also corroborate that the spreading direction of the Molloy and Knipovich ridges (Curewitz et al., 2010) was established already during rifting, as suggested by Kleinspehn and Teyssier (2016).

6.2.6 The Forlandsundet Graben in the context of (transform) rifted margin evolution

Peron-Pinvidic et al. (2013) demonstrated that the temporal and spatial evolutions of rifted margins are closely linked. The Forlandsundet Graben is located in the so called necking domain of the Svalbard margin (Fig. 7), the zone where the continental crust tapers from 30 km to <10 km (e.g. Mohn et al., 2012, 2010; Peron-Pinvidic et al., 2013; Péron-Pinvidic and Manatschal, 2009). Within the necking domain, the mechanisms that facilitate thinning of the lithosphere as well as deformation coupling between the upper and lower crust tend to be preserved (Peron-Pinvidic et al., 2013).

Deformation coupling throughout the entire crust is facilitated by embrittlement of the mid-crustal ductile layer due to the decrease in pressure associated with crustal thinning (Pérez-Gussinyé et al., 2003; Pérez-Gussinyé and Reston, 2001; Reston, 2007). Thus, drastic thinning of the lithosphere can be provided by crustal-scale normal faults and characterizes the structural style of the necking domain (Osmundsen and Péron-Pinvidic, 2018; Peron-Pinvidic et al., 2013).

Osmundsen and Péron-Pinvidic (2018) presented a model for the evolution of metamorphic core complexes in the necking domain during the process of deformation coupling. Considering the evolution of Prins Karls Forland in association with a metamorphic core complex (section 6.2.3), the Forlandsundet Graben would have evolved above a late-to-post-orogenic as described in Osmundsen and Péron-Pinvidic (2018). The original detachment was abandoned in the area of the Forlandsundet Graben due to up-warping while faulting continued to be active towards the west of Prins Karls Forland (Fig. 59). Therefore, the eastern boundary fault of the Forlandsundet Graben, together with a detachment off the west coast of Prins Karls Forland, might constitute the inner necking break away complex of the

Svalbard margin (*sensu* Osmundsen and Péron-Pinvidic, 2018). This interpretation fits well with the location of the Forlandsundet Graben in respect to the crustal taper, as construed from seismic profiles (Faleide et al., 2008; Ritzmann et al., 2004), since it is located in the eastern part of the Svalbard margin where the crust is still more than 25 km thick (Fig. 7) (*cf.* Osmundsen and Péron-Pinvidic, 2018; Peron-Pinvidic et al., 2013). However, the cited literature refers to orthogonally rifted margins and might not directly apply to the Svalbard margin. Despite that, the structural domains proposed by Peron-Pinvidic et al. (2013) have previously been recognized in the oblique rifted margin of the gulf of Aden by Nonn et al. (2017), and indicate that a transfer of the concepts can be feasible.

According to Osmundsen and Péron-Pinvidic (2018), several normal fault splays have to successively initiate within the supradetachment basin to allow deformation coupling to continue despite the up-warping and subsequent abandonment of the initial detachment. Consequently, intrabasinal normal faulting and multiple syn-rift sediment packages can be expected within basins that are associated with metamorphic core complexes (*cf.* Osmundsen and Péron-Pinvidic, 2018). In the Forlandsundet Graben this process could explain the deposition of the Sarstangen Formation after the deposition of the Sarsbukta Formation in the same transtensional setting (section 6.2.3).

Another factor that could have introduced multistage rifting to the Forlandsundet Graben is strain partitioning. Agostini et al. (2009) showed that oblique rifts can exhibit a two-stage evolution under a stable stress field. First, the basin-bounding faults are initiated and accommodate mainly strike slip motion along with some normal offset. During the second stage, intrabasinal normal faults initiate and account for the bulk extension (Agostini et al., 2009). This two stage model would also fit with the proposed evolution of the Sarstangen and Sarsbukta Formations.

7 Conclusions

To conclude this study, the key findings are summarized below:

- The Sarsbukta Formation was deposited by marginal alluvial fans, interfingering with fluvial and floodplain deposits.
- The Sarstangen Formation consists of a marine clay stone, overlain by a footwall-derived proximal fan deposit.
- The sedimentary units along the eastern basin margin were probably both deposited under NW-SE oriented transtension.
- Deposition of the sedimentary units on Sarsøyra occurred over two stages; first the Sarsbukta Formation was deposited in a regime with lower subsidence than sedimentation rates. Afterwards, the Sarstangen Formation was deposited in Early to Middle Oligocene and subsidence exceeded the sediments supply.
- The deformation sequence on Sarsøyra during Paleogene includes reverse and strike slip faulting connected to the formation of the WSFB at 53.5 Ma. Subsequently, the stress field switched to NW-SE transtension before the deposition of the Sarstangen Formation in Early to Middle Oligocene. Rifting in the continental domain ceased with the establishment of the passive margin at 22 Ma.
- Two end-member models have been proposed for the evolution of the Forlandsundet Graben as a whole. One is based on a multiphase deformation history, consisting of compression followed by transtension while the other model explores a purely transtensional origin of the Forlandsundet Graben. However, more data is required to reconstruct the relationship between the sedimentary units along the eastern and western basin margin.
- The Forlandsundet Graben might have evolved in association with a metamorphic core complex on Prins Karls Forland, possibly consisting of the Pinkie unit. Further investigations are suggested to confirm whether or not this is the case.

References

- Agostini, A., Corti, G., Zeoli, A., Mulugeta, G., 2009. Evolution, pattern, and partitioning of deformation during oblique continental rifting: Inferences from lithospheric-scale centrifuge models. *Geochemistry, Geophysics, Geosystems* 10. <https://doi.org/10.1029/2009GC002676>
- Aksu, A.E., Calon, T.J., Hiscott, R.N., Yasar, D., 2000. Anatomy of the North Anatolian Fault Zone in the Marmara Sea, Western Turkey: Extensional Basins Above a Continental Transform. *GSA Today* 10, 3–7.
- Alexander, J., Leeder, M.R., 1987. Active Tectonic Control on Alluvial Architecture. *Recent Developments in Fluvial Sedimentology* 243–252. <https://doi.org/10.2110/pec.87.39.0243>
- Allen, P.A., 1981. Sediments and processes on a small stream-flow dominated, devonian alluvial fan, Shetland Islands. *Sedimentary Geology* 29. [https://doi.org/10.1016/0037-0738\(81\)90056-7](https://doi.org/10.1016/0037-0738(81)90056-7)
- Allmendinger, R.W., Cardozo, N.C., Fisher, D., 2013. *Algorithms: Vectors & Tensors*. Cambridge University Press.
- Atkinson, D.J., 1962. Tectonic Control of Sedimentation and the Interpretation of Sediment Alternation in the Tertiary of Prince Charles Foreland, Spitsbergen. *Geological Society of America Bulletin* 73.
- Barker, C.E., Pawlewicz, M.J., 1994. Calculation of Vitrinite Reflectance from Thermal Histories and Peak Temperatures. A comparison of Methods. Vitrinite reflectance as a maturity parameter: applications and limitations. 216–229. <https://doi.org/10.1021/bk-1994-0570.ch014>
- Barnes, C.J., 2016. Cretaceous-Paleogene low temperature history of the Southwestern Province, Svalbard, revealed by (U-Th)/He thermochronometry: implications for High Arctic tectonism. University of Ottawa.
- Barnes, C.J., Schneider, D., 2018. Late Cretaceous – Paleogene burial and exhumation history of the Southwestern Basement Province, Svalbard, revealed by zircon (U-Th)/He thermochronology. *Circum-Arctic Structural Events: Tectonic Evolution of the Arctic Margins and Trans-Arctic Links with Adjacent Orogens*: Geological Society of America Special Paper 541 541, 1–22.
- Basile, C., 2015. Transform continental margins — part 1: Concepts and models. *Tectonophysics* 661, 1–10. <https://doi.org/10.1016/j.tecto.2015.08.034>
- Bense, F.A., Wemmer, K., Löbens, S., Siegesmund, S., 2014. Fault gouge analyses: K-Ar illite dating, clay mineralogy and tectonic significance—a study from the Sierras Pampeanas, Argentina. *International Journal of Earth Sciences* 103, 189–218. <https://doi.org/10.1007/s00531-013-0956-7>
- Benvenuti, M., 2003. Facies analysis and tectonic significance of lacustrine fan-deltaic

- successions in the Pliocene-Pleistocene Mugello Basin, Central Italy. *Sedimentary Geology* 157, 197–234. [https://doi.org/10.1016/S0037-0738\(02\)00234-8](https://doi.org/10.1016/S0037-0738(02)00234-8)
- Bergh, S.G., Andresen, A., 1990. Structural development of the Tertiary fold-and-thrust belt in east Oscar II Land, Spitsbergen. *Polar Research* 8, 217–236. <https://doi.org/10.1111/j.1751-8369.1990.tb00385.x>
- Bergh, S.G., Braathen, A., Andresen, A., 1997. Interaction of basement-involved and thin-skinned tectonism in the Tertiary fold-thrust belt of central Spitsbergen, Svalbard. *AAPG Bulletin* 81, 637–661. <https://doi.org/10.1306/522B43F7-1727-11D7-8645000102C1865D>
- Bergh, S.G., Braathen, A., Karlson, F., Maher, H., 1998. Fault Motion Along the Eastern Margin of the Forlandsundet graben, Sarstangen, Svalbard. *Omaha*.
- Bergh, S.G., Maher, H.D., Braathen, A., Maher Jr, H.D., 2000. Tertiary divergent thrust directions from partitioned transpression, Broggerhalvoya, Spitsbergen. *Norsk Geologisk Tidsskrift* 80, 63–81. <https://doi.org/10.1080/002919600750042573>
- Bernet, M., 2005. Fission-track Analysis of Detrital Zircon. *Reviews in Mineralogy and Geochemistry* 58, 205–237. <https://doi.org/10.2138/rmg.2005.58.8>
- Best, J.L., Ashworth, P.J., Bristow, C.S., Roden, J., 2003. Three-Dimensional Sedimentary Architecture of a Large, Mid-Channel Sand Braid Bar, Jamuna River, Bangladesh. *Journal of Sedimentary Research* 73, 516–530. <https://doi.org/10.1306/010603730516>
- Betlem, P., Midttømme, K., Jochmann, M., Senger, K., Olaussen, S., 2018. Geothermal Gradients on Svalbard, Arctic Norway, in: *First EAGE/IGA/DGMK Joint Workshop on Deep Geothermal Energy*. pp. 9–11. <https://doi.org/10.3997/2214-4609.201802945>
- Betlem, P., Senger, K., Hodson, A., 2019. 3D thermobaric modelling of the gas hydrate stability zone onshore central Spitsbergen, Arctic Norway. *Marine and Petroleum Geology* 100, 246–262. <https://doi.org/10.1016/j.marpetgeo.2018.10.050>
- Bird, D., 2001. Shear margins: Continent-ocean transform and fracture zone boundaries. *The Leading Edge* 20, 150. <https://doi.org/10.1190/1.1438894>
- Blair, T.C., 2000. Sedimentology and progressive tectonic unconformities of the sheetflood-dominated Hell's Gate alluvial fan, Death Valley, California. *Sedimentary Geology* 132, 233–262. [https://doi.org/10.1016/S0037-0738\(00\)00010-5](https://doi.org/10.1016/S0037-0738(00)00010-5)
- Blair, T.C., McPherson, J.G., 1994. Alluvial Fans and their Natural Distinction from Rivers Based on Morphology, Hydraulic Processes, Sedimentary Processes, and Facies Assemblages. *SEPM Journal of Sedimentary Research* Vol. 64A, 450–489. <https://doi.org/10.1306/D4267DDE-2B26-11D7-8648000102C1865D>
- Blinova, M., Thorsen, R., Mjelde, R., Faleide, J.I., 2009. Structure and evolution of the Bellsund graben between Forlandsundet and Bellsund (Spitsbergen) based on marine seismic data. *Norsk Geologisk Tidsskrift* 89, 215–228.
- Bloom, L.A., 1964. Peat Accumulation and Compaction in a Connecticut Coastal Marsh.

SEPM Journal of Sedimentary Research Vol. 34, 599–603.
<https://doi.org/10.1306/74D710F5-2B21-11D7-8648000102C1865D>

- Blum, M.D., Marriott, S.B., Leclair, S.F., 2005. Fluvial Sedimentology VII, Special Publication Number 35 of the International Association of Sedimentologists.
<https://doi.org/10.1002/eqe.2783>
- Boggs, S.J., 2011. Principles of Sedimentology and Stratigraphy, Journal of Chemical Information and Modeling. <https://doi.org/10.1017/CBO9781107415324.004>
- Bourquin, S., Guillocheau, F., Péron, S., 2009. Braided rivers within an arid alluvial plain (example from the lower triassic, western german basin): Recognition criteria and expression of stratigraphic cycles. *Sedimentology* 56, 2235–2264.
<https://doi.org/10.1111/j.1365-3091.2009.01078.x>
- Bown, T.M., Kraus, M.J., 1981. Lower Eocene alluvial paleosols (Willwood Formation, Northwest Wyoming, U.S.A.) and their significance for paleoecology, paleoclimatology, and basin analysis. *Palaeogeography, Palaeoclimatology, Palaeoecology* 34, 1–30.
[https://doi.org/10.1016/0031-0182\(81\)90056-0](https://doi.org/10.1016/0031-0182(81)90056-0)
- Boyd, R., Dalrymple, R., Zaitlin, B.A., 1992. Classification of clastic coastal depositional environments. *Sedimentary Geology* 80, 139–150. [https://doi.org/10.1016/0037-0738\(92\)90037-R](https://doi.org/10.1016/0037-0738(92)90037-R)
- Braathen, A., Bergh, S.G., 1999. Application of a critical wedge taper model to the Tertiary transpressional fold-thrust belt on Spitsbergen, Svalbard 2–19.
- Braathen, A., Bergh, S.G., 1995a. Kinematics of Tertiary deformation in the basement-involved fold-thrust complex, western Nordenskiöld Land, Svalbard: tectonic implications based on fault-slip data analysis. *Tectonophysics* 249, 1–29.
[https://doi.org/10.1016/0040-1951\(95\)00036-M](https://doi.org/10.1016/0040-1951(95)00036-M)
- Braathen, A., Bergh, S.G., 1995b. Structural outline of a Tertiary Basement-cored uplift/inversion structure in western Spitsbergen, Svalbard: Kinematics and controlling factors. *Tectonics* 14, 95–119.
- Braathen, A., Bergh, S.G., Maher, H.D., 1999. Application of a critical wedge taper model to the tertiary transpressional fold-thrust belt on Spitsbergen, Svalbard. *Bulletin of the Geological Society of America* 111, 1468–1485. [https://doi.org/10.1130/0016-7606\(1999\)111<1468:AOACWT>2.3.CO;2](https://doi.org/10.1130/0016-7606(1999)111<1468:AOACWT>2.3.CO;2)
- Braathen, A., Bergh, S.G., Maher Jr., H.D., 1997. Thrust kinematics in the central part of the Tertiary transpressional fold-thrust belt in Spitsbergen. *Bulletin - Norges Geologiske Undersøkelse* 433, 32–33.
- Braathen, A., Osmundsen, P.T., Maher, H., Ganerød, M., 2018. The Keisarhjelmen detachment records Silurian–Devonian extensional collapse in Northern Svalbard. *Terra Nova* 30, 34–39. <https://doi.org/10.1111/ter.12305>
- Brandes, C., Tanner, D.C., 2014. Fault-related folding: A review of kinematic models and their application. *Earth-Science Reviews* 138, 352–370.

<https://doi.org/10.1016/j.earscirev.2014.06.008>

- Breivik, A.J., Mjelde, R., Faleide, J.I., Murai, Y., 2006. Rates of continental breakup magmatism and seafloor spreading in the Norway Basin–Iceland plume interaction. *Journal of Geophysical Research* 111, B07102. <https://doi.org/10.1029/2005JB004004>
- Brune, S., Popov, A.A., Sobolev, S. V., 2012. Modeling suggests that oblique extension facilitates rifting and continental break-up. *Journal of Geophysical Research: Solid Earth* 117, 1–16. <https://doi.org/10.1029/2011JB008860>
- Brune, S., Williams, S.E., Müller, R.D., 2018. Oblique rifting: the rule, not the exception. *Solid Earth Discussions* 1–26. <https://doi.org/10.5194/se-2018-63>
- Buiter, S.J.H., Torsvik, T.H., 2014. A review of Wilson Cycle plate margins: A role for mantle plumes in continental break-up along sutures? *Gondwana Research* 26, 627–653. <https://doi.org/10.1016/j.gr.2014.02.007>
- Burg, J.P., Harris, L.B., 1982. Tension fractures and boudinage oblique to the maximum extension direction: an analogy with lüders' bands. *Tectonophysics* 83, 347–363. [https://doi.org/10.1016/0040-1951\(82\)90027-0](https://doi.org/10.1016/0040-1951(82)90027-0)
- Cameron, C.C., Esterle, J., Palmer, C.A., 1989. The geology, botany and chemistry of selected peat-forming environment from temperate and tropical latitude. *Journal of Coal Geology* 12, 105–156. [https://doi.org/10.1016/0166-5162\(89\)90049-9](https://doi.org/10.1016/0166-5162(89)90049-9)
- CASE Team, 2001. The Evolution of the West Spitsbergen Fold-and-Thrust Belt. *Intra-Continental Fold Belts CASE 1: West Spitsbergen* 733–773.
- Čepek, P., 2001. Paleogene calcareous nannofossils from the Firkanten and Sarsbukta Formations on Spitsbergen, *Intra-Continental Fold Belts CASE 1: West Spitsbergen*.
- Čepek, P., Krutzsch, W., 2001. Conflicting interpretations of the Tertiary biostratigraphy of Spitsbergen and new palynological results. *Intra-Continental Fold Belts CASE 1: West Spitsbergen* 551–599.
- Corti, G., 2012. Evolution and characteristics of continental rifting: Analog modeling-inspired view and comparison with examples from the East African Rift System. *Tectonophysics* 522–523, 1–33. <https://doi.org/10.1016/j.tecto.2011.06.010>
- Crane, K., Sundvor, E., Buck, R., Martinez, F., 1991. Rifting in the northern Norwegian-Greenland Sea: Thermal tests of asymmetric spreading. *Journal of Geophysical Research* 96, 14529. <https://doi.org/10.1029/91JB01231>
- Crowell, J.C., 1957. Origin of pebbly mudstones. *Bulletin of the Geological Society of America* 68, 993–1010. [https://doi.org/10.1130/0016-7606\(1957\)68\[993:OOPM\]2.0.CO;2](https://doi.org/10.1130/0016-7606(1957)68[993:OOPM]2.0.CO;2)
- Curewitz, D., Okino, K., Asada, M., Baranov, B., Gusev, E., Tamaki, K., 2010. Structural analysis of fault populations along the oblique, ultra-slow spreading Knipovich Ridge, North Atlantic Ocean, 74°30'N–77°50'N. *Journal of Structural Geology* 32, 727–740. <https://doi.org/10.1016/j.jsg.2009.08.011>

- Dade, W.B., Friend, P.F., The, S., November, N., Dade, W.B., Friend, P.F., 1998. Grain - Size , Sediment - Transport Regime , and Channel Slope in Alluvial Rivers Published by : The University of Chicago Press Stable URL : <http://www.jstor.org/stable/10.1086/516052> Grain-Size , Sediment-Transport Regime , and Channel Slope in Alluvial. *The Journal of Geology* 106, 661–676.
- Dallmann, W.K., 2015. *Geoscience Atlas of Svalbard*. Norwegian Polar Institute, Tromsø. <https://doi.org/10.1086/624152>
- Dallmann, W.K., 1999. Lithostratigraphic lexicon of Svalbard: review and recommendations for nomenclature use: Upper Palaeozoic to Quaternary bedrock. Norwegian Polar Institute, Tromsø.
- De Paola, N., Holdsworth, R.E., McCaffrey, K.J.W., Barchi, M.R., 2005. Partitioned transtension: An alternative to basin inversion models. *Journal of Structural Geology* 27, 607–625. <https://doi.org/10.1016/j.jsg.2005.01.006>
- DeCelles, P.G., Gray, M.B., Ridgeway, K.D., Cole, R.B., Pivnik, D.A., Pequera, N., Srivastava, P., 1991. Controls on synorogenic alluvial-fan architecture, Beartooth Conglomerate (Palaeocene), Wyoming and Montana. *Sedimentology* 38, 567–590. <https://doi.org/10.1111/j.1365-3091.1991.tb01009.x>
- Dick, H.J.B., Lin, J., Schouten, H., 2003. An ultraslow-spreading class of ocean ridge. *Nature* 426, 405–412. <https://doi.org/10.1038/nature02128>
- Dill, H.G., Altangerel, S., Bulgamaa, J., Hongor, O., Khishigsuren, S., Majigsuren, Y., Myagmarsuren, S., Heunisch, C., 2004. The Baganuur coal deposit, Mongolia: Depositional environments and paleoecology of a Lower Cretaceous coal-bearing intermontane basin in Eastern Asia. *International Journal of Coal Geology* 60, 197–236. <https://doi.org/10.1016/j.coal.2003.09.008>
- Dimakis, P., Braathen, B.I., Faleide, J.I., Elverhøi, A., Gudlaugsson, S.T., 1998. Cenozoic erosion and the preglacial uplift of the Svalbard-Barents Sea region. *Tectonophysics* 300, 311–327. [https://doi.org/10.1016/S0040-1951\(98\)00245-5](https://doi.org/10.1016/S0040-1951(98)00245-5)
- Dörr, N.U., Clift, P.D., Lisker, F., Spiegel, C., 2013. Why is Svalbard an island? Evidence for two-stage uplift, magmatic underplating, and mantle thermal anomalies. *Tectonics* 32, 473–486. <https://doi.org/10.1002/tect.20039>
- Døssing, A., Hopper, J.R., Olesen, A. V., Rasmussen, T.M., Halpenny, J., 2013. New aerogravity results from the Arctic: Linking the latest Cretaceous-early Cenozoic plate kinematics of the North Atlantic and Arctic Ocean. *Geochemistry, Geophysics, Geosystems* 14, 4044–4065. <https://doi.org/10.1002/ggge.20253>
- Eidvin, T., Goll, R.M., Grogan, P., Smelror, M., Ulleberg, K., 1998. The Pleistocene to Middle Eocene stratigraphy and geological evolution of the western Barents Sea continental margin at well site 7316/5-1 (Bjørnøya West area) TOR. *Norosk Geologisk Tidsskrift* 78200002, 99–123.
- Eidvin, T., Riis, F., Rasmussen, E.S., 2014. Oligocene to Lower Pliocene deposits of the Norwegian continental shelf, Norwegian Sea, Svalbard, Denmark and their relation to

- the uplift of Fennoscandia: A synthesis. *Marine and Petroleum Geology* 56, 184–221. <https://doi.org/10.1016/j.marpetgeo.2014.04.006>
- Engen, Ø., Faleide, J.I., Dyreng, T.K., 2008. Opening of the Fram Strait gateway: A review of plate tectonic constraints. *Tectonophysics* 450, 51–69. <https://doi.org/10.1016/j.tecto.2008.01.00>
- Faehnrich, K., Manecki, M., Schneider, D., Czerny, J., Myhre, P.I., Majka, J., Kościńska, K., Barnes, C., Maraszewska, M., 2016. A tectonic window into the crystalline basement of Prins Karls Forland, Svalbard, in: *EGU General Assembly 2016*. Vienna.
- Faleide, J.I., Bjorlykke, K., Gabrielsen, R.H., 2015. Geology of the Norwegian Continental Shelf, in: *Petroleum Geoscience*. <https://doi.org/10.1007/978-3-642-02332-3>
- Faleide, J.I., Tsikalas, F., Breivik, J., Mjelde, R., Ritzmann, O., Engen, O., Wilson, J., Eldholm, O., 2008. Structure and evolution of the continental margin off Norway and the Barents Sea. *Episodes* 31, 82–91. <https://doi.org/10.1016/j.strusafe.2006.11.005>
- Faleide, J.I., Vågnes, E., Gudlaugsson, S.T., 1993. Late Mesozoic-Cenozoic evolution of the south-western Barents Sea in a regional rift-shear tectonic setting. *Marine and Petroleum Geology* 10, 186–214. [https://doi.org/10.1016/0264-8172\(93\)90104-Z](https://doi.org/10.1016/0264-8172(93)90104-Z)
- Feyling-Hanssen, R.W., Ulleberg, K., 1984. A Tertiary-Quaternary section at Sarsbukta, Spitsbergen, Svalbard, and its foraminifera. *Polar Research* 2, 77–106. <https://doi.org/10.1111/j.1751-8369.1984.tb00487.x>
- Fielding, C.R., 1986. Coal depositional model for deltaic and alluvial plain sequences. *Geology* 15, 661–664. [https://doi.org/10.1130/0091-7613\(1987\)15<661](https://doi.org/10.1130/0091-7613(1987)15<661)
- Fossen, H., 2010. *Structural Geology*. Cambridge University Press, Cambridge. <https://doi.org/https://doi.org/10.1017/CBO9780511777806>
- Fossen, H., Rotevatn, A., 2016. Fault linkage and relay structures in extensional settings-A review. *Earth-Science Reviews* 154, 14–28. <https://doi.org/10.1016/j.earscirev.2015.11.014>
- Fossen, H., Schultz, R.A., Shipton, Z.K., Mair, K., 2007. Deformation bands in sandstone: a review. *Journal of the Geological Society* 164, 755–769. <https://doi.org/10.1144/0016-76492006-036>
- Fossen, H., Teyssier, C., Whitney, D.L., 2013. Transtensional folding. *Journal of Structural Geology* 56, 89–102. <https://doi.org/10.1016/j.jsg.2013.09.004>
- Fossen, H., Tikoff, B., 1998. Extended models of transpression and transtension, and application to tectonic settings. *Geological Society, London, Special Publications* 135, 15–33. <https://doi.org/10.1144/GSL.SP.1998.135.01.02>
- Franke, D., 2013. Rifting, lithosphere breakup and volcanism: Comparison of magma-poor and volcanic rifted margins. *Marine and Petroleum Geology* 43, 63–87. <https://doi.org/10.1016/j.marpetgeo.2012.11.003>

- Friedman, M., Logan, J.M., 1973. Lüders' bands in experimentally deformed sandstone and limestone. *Bulletin of the Geological Society of America* 84, 1465–1476.
[https://doi.org/10.1130/0016-7606\(1973\)84<1465:LBIEDS>2.0.CO;2](https://doi.org/10.1130/0016-7606(1973)84<1465:LBIEDS>2.0.CO;2)
- Gabrielsen, R.H., Kløvjan, O.S., Haugsbø, H., Midbøe, P.S., Nøttvedt, A., Rasmussen, E., Skott, P.H., 1992. A structural outline of the Forlandsundet Graben, Prins Karls Forland, Svalbard. *Norsk Geologisk Tidsskrift* 72, 105–120.
- Gallagher, K., Brown, R., Johnson, C., 1998. Fission Track Analysis and Its Applications To Geological Problems. *Annual Review of Earth and Planetary Sciences* 26, 519–572.
<https://doi.org/10.1146/annurev.earth.26.1.519>
- Gawthorpe, R.L., Leeder, M.R., 2000. Tectono-sedimentary evolution of active extensional basins. *Basin Research* 12, 195–218. <https://doi.org/10.1111/j.1365-2117.2000.00121.x>
- Gloppen, T.G., Steel, R.J., 1981. The deposits, internal structure and geometry in six alluvial fan-fan delta bodies (Devonian-Norway)-A study in the significance of bedding sequence in conglomerates. *Society for Sedimentary Geology Special Publication* 31, 49–69.
- Goscombe, B.D., Passchier, C.W., 2002. Asymmetric boudins as shear sense indicators - an assessment from field data. *Journal of Structural Geology* 25, 1–15.
- Harland, W.B., Horsfield, W.T., Manby, G.M., Morris, A.P., 1979. An outline of pre-Carboniferous stratigraphy of central western Spitsbergen. *Norsk Polarinstitutt Skrifter* 167, 119–44.
- Harvey, A.M., Mather, A.E., Stokes, M., 2005. Alluvial fans: geomorphology, sedimentology, dynamics — introduction. A review of alluvial-fan research. *Geological Society, London, Special Publications* 251, 1–7. <https://doi.org/10.1144/GSL.SP.2005.251.01.01>
- Heine, C., Brune, S., 2014. Oblique rifting of the equatorial atlantic: Why there is no saharan atlantic ocean. *Geology* 42, 211–214. <https://doi.org/10.1130/G35082.1>
- Helland-Hansen, W., 1990. Sedimentation in Paleogene foreland basin, Spitsbergen. *American Association of Petroleum Geologists Bulletin* 74, 260–272.
- Henriksen, E., Ryseth, A.E., Larssen, G.B., Heide, T., Rønning, K., Sollid, K., Stoupakova, A. V., 2011. Chapter 10 Tectonostratigraphy of the greater Barents Sea: implications for petroleum systems. *Geological Society, London, Memoirs* 35, 163 LP-195.
<https://doi.org/10.1144/M35.10>
- Hirajima, T., Banno, S., Hiroi, Y., Ohta, Y., 1988. Phase petrology of eclogites and related rocks from the Motalafjella high-pressure metamorphic complex in Spitsbergen (Arctic Ocean) and its significance. *LITHOS* 22, 75–97. [https://doi.org/10.1016/0024-4937\(88\)90018-7](https://doi.org/10.1016/0024-4937(88)90018-7)
- Hjelle, A., Piepjohn, K., Saalman, K., Ohta, Y., Salvigsen, O., Thiedig, F., Dallmann, W.K., 1999. *Geological Map Svalbard 1:100,000, A7G Kongsfjorden*.
- Hossack, J.R., 1984. The geometry of listric growth faults in the Devonian basins of

- Sunnfjord, W Norway. *Journal of the Geological Society* 141, 629–637.
<https://doi.org/10.1144/gsjgs.141.4.0629>
- Hosseinpour, M., Müller, R.D., Williams, S.E., Whittaker, J.M., 2013. Full-fit reconstruction of the Labrador Sea and Baffin Bay. *Solid Earth* 4, 461–479. <https://doi.org/10.5194/se-4-461-2013>
- Jackson, J., McKenzie, D., 1983. The geometrical evolution of normal fault systems. *Journal of Structural Geology* 5, 471–482.
- Johansson, Å., Gee, D.G., Larionov, A.N., Ohta, Y., Tebenkov, A.M., 2005. Grenvillian and Caledonian evolution of eastern Svalbard - A tale of two orogenies. *Terra Nova* 17, 317–325. <https://doi.org/10.1111/j.1365-3121.2005.00616.x>
- Kanat, L., Morris, A., 1988. A working stratigraphy for central western Oscar II Land, Spitsbergen.
- Kapp, P., Taylor, M., Stockli, D.F., Ding, L., 2008. Development of active low-angle normal fault systems during orogenic collapse: Insight from Tibet. *Geology* 36, 7–10.
<https://doi.org/10.1130/G24054A.1>
- Kesper, J., 1986. Kartierung der tertiären Ablagerungen auf Sarsøyra (Svalbard). Universität Kiel.
- Kleinspehn, K.L., Teyssier, C., 2016. Oblique rifting and the Late Eocene–Oligocene demise of Laurasia with inception of Molloy Ridge: Deformation of Forlandsundet Basin, Svalbard. *Tectonophysics* 693, 363–377. <https://doi.org/10.1016/j.tecto.2016.05.010>
- Kleinspehn, K.L., Teyssier, C., 1992. Tectonics of the Paleogene Forlandsundet Basin, Spitsbergen - a Preliminary-Report. *Norsk Geologisk Tidsskrift* 72, 93–104.
- Kośmińska, K., Spear, F., Majka, J., 2017. P-T-t metamorphic evolution of highly deformed metapelites from the Pinkie unit of western Svalbard using quartz-in-garnet barometry, trace element thermometry, P-T-X-M diagrams and monazite in-situ dating, in: 19th EGU General Assembly. Vienna.
- Kralik, M., Klima, K., Riedmüller, G., 1987. Dating fault gouges. *Nature* 327, 315–317.
<https://doi.org/10.1038/327315a0>
- Krasil'scikov, A.A., Kubanskij, A.P., Ohta, Y., 1995. Surface Magnetic Anomaly Study on the Eastern Part of the Forlandsundet-Graben. *Polar Research* 14, 55–68.
- Kristensen, T.B., Rotevatn, A., Marvik, M., Henstra, G.A., Gawthorpe, R.L., Ravnås, R., 2017. Structural evolution of sheared margin basins: The role of strain partitioning. Sørvestsnaget Basin, Norwegian Barents Sea. *Basin Research* 1–23.
<https://doi.org/10.1111/bre.12253>
- Labrousse, L., Elvevold, S., Lepvrier, C., Agard, P., 2008. Structural analysis of high-pressure metamorphic rocks of Svalbard: Reconstructing the early stages of the Caledonian orogeny. *Tectonics* 27, 1–22. <https://doi.org/10.1029/2007TC002249>

- Leeder, M.R., Gawthorpe, R.L., 1987. Sedimentary models for extensional tilt-block/half-graben basins. Geological Society, London, Special Publications 28, 139–152. <https://doi.org/10.1144/GSL.SP.1987.028.01.11>
- Leever, K.A., Gabrielsen, R.H., Faleide, J.I., Braathen, A., 2011. A transpressional origin for the West Spitsbergen fold-and-thrust belt: Insight from analog modeling. *Tectonics* 30. <https://doi.org/10.1029/2010TC002753>
- Lehmann, U., Thiedig, F., Harland, W.B., 1978. Spitzbergen im Tertiär. *Polarforschung* 48, 120–138.
- Leleu, S., Hartley, A.J., Williams, B.P.J., 2009. Large-Scale Alluvial Architecture and Correlation in a Triassic Pebbly Braided River System, Lower Wolfville Formation (Fundy Basin, Nova Scotia, Canada). *Journal of Sedimentary Research* 79, 265–286. <https://doi.org/10.2110/jsr.2009.034>
- Lepvrier, C., 1992. Early Tertiary palaeostress distribution on Spitsbergen : implications for the tectonic development of the western fold-and-thrust belt. *Norsk Geologisk Tidsskrift* 72, 129–135.
- Lepvrier, C., 1990. Early Tertiary Paleostress History and Tectonic Development of the Forlandsundet Basin, Svalbard, Norway. *Norsk Polarinstitut Meddelelser* 112.
- Li, S., Li, S., Shan, X., Gong, C., Yu, X., 2017. Classification, formation, and transport mechanisms of mud clasts. *International Geology Review* 59, 1609–1620. <https://doi.org/10.1080/00206814.2017.1287014>
- Lister, G.S., Davis, G.A., 1989. The origin of metamorphic core complexes and detachment faults formed during Tertiary eontinental margins. *Geology* 14, 246–250. [https://doi.org/10.1016/0191-8141\(89\)90036-9](https://doi.org/10.1016/0191-8141(89)90036-9)
- Livsic, J., 1992. Tectonic history of Tertiary sedimentation of Svalbard. *Norsk Geologisk Tidsskrift* 72, 121–127.
- Livsic, J., 1974. Palaeogene deposits and the platform structure of Svalbard. *Norsk Polarinstitut Skrifter*.
- Lunt, I.A., Bridge, J.S., 2004. Evolution and deposits of a gravelly braid bar, Sagavanirktok River, Alaska. *Sedimentology* 51, 415–432. <https://doi.org/10.1111/j.1365-3091.2004.00628.x>
- Lyons, J.B., Snellenburg, J., 1971. Dating faults. *Bulletin of the Geological Society of America* 82, 1749–1752. [https://doi.org/10.1130/0016-7606\(1971\)82\[1749:DF\]2.0.CO;2](https://doi.org/10.1130/0016-7606(1971)82[1749:DF]2.0.CO;2)
- Magnus, S., 1986. Geologische kartierung tertiärer Sedimente auf Prins - Karls - Forland (Svalbard). Christian - Albrechts - Universität zu Kiel.
- Maher, H.D., Bergh, S.G., Braathen, A., Ohta, Y., 1997. Svartfjella, Eidembukta, and Daudmannsodden lineament: Tertiary orogen-parallel motion in the crystalline hinterland of Spitsbergen's fold-thrust belt. *Tectonics* 16, 88–106. <https://doi.org/10.1029/96TC02616>

- Manby, G., Lyberis, N., 1992. Tectonic evolution of the Devonian Basin of northern Svalbard. *Norsk Geologisk Tidsskrift* 72, 7–19.
- Manum, S.B., 1962. Studies in the Tertiary flora of Spitsbergen, with notes on Tertiary floras of Ellesmere Island, Greenland, and Iceland. *Norsk Polarinstitutts Skrifter* 125, 1–127.
- Manum, S.B., 1960. Some dinoflagellates and hystrichosphaerids from the Lower Tertiary of Spitsbergen. *Nytt Magasin for Botanikk* 8, 17–21.
- Manum, S.B., Thronsen, T., 1986. Age of Tertiary formations on Spitsbergen. *Polar Research* 4, 103–131. <https://doi.org/10.1111/j.1751-8369.1986.tb00526.x>
- Martin, C.A.L., Turner, B.R., 1998. Origins of massive-type sandstones in braided river systems. *Earth Science Reviews* 44, 15–38. [https://doi.org/10.1016/S0012-8252\(98\)00019-1](https://doi.org/10.1016/S0012-8252(98)00019-1)
- McLelland, S.J., Ashworth, P.J., Best, J.L., Roden, J., Klaassen, G.J., 1999. Flow Structure and Transport of Sand-Grade Suspended Sediment around an Evolving Braid Bar, Jamuna River, Bangladesh. *Fluvial Sedimentology* VI. <https://doi.org/10.1002/9781444304213.ch4>
- Mercier De Lépinay, M., Loncke, L., Basile, C., Roest, W.R., Patriat, M., Maillard, A., De Clarens, P., 2016. Transform continental margins – Part 2: A worldwide review. <https://doi.org/10.1016/j.tecto.2016.05.038>
- Miall, A.D., 1985. Architectural-Element Analysis: A New Method of Facies Analysis Applied to Fluvial Deposits. *Earth-Science Reviews Elsevier Science Publishers B.V* 22, 261–308. [https://doi.org/10.1016/0012-8252\(85\)90001-7](https://doi.org/10.1016/0012-8252(85)90001-7)
- Miall, A.D., 1977a. A Review of the Braided-River Depositional Environment 13.
- Miall, A.D., 1977b. Lithofacies types and vertical profile models in braided river deposits: a summary. *Fluvial Sedimentology* 5, 597–600.
- Mills, H.H., 1979. Downstream Rounding of Pebbles--A Quantitative Review. *Journal of Sedimentary Research* 49, 295–302. <https://doi.org/10.1306/212F7720-2B24-11D7-8648000102C1865D>
- Mohn, G., Manatschal, G., Beltrando, M., Masini, E., Kuszniir, N., 2012. Necking of continental crust in magma-poor rifted margins: Evidence from the fossil Alpine Tethys margins. *Tectonics* 31, 1–28. <https://doi.org/10.1029/2011TC002961>
- Mohn, G., Manatschal, G., Müntener, O., Beltrando, M., Masini, E., 2010. Unravelling the interaction between tectonic and sedimentary processes during lithospheric thinning in the Alpine Tethys margins. *International Journal of Earth Sciences* 99, 75–101. <https://doi.org/10.1007/s00531-010-0566-6>
- Moran, K., Backman, J., Brinkhuis, H., Clemens, S.C., Cronin, T., Dickens, G.R., Eynaud, F., Gattacceca, J., Jakobsson, M., Jordan, R.W., Kaminski, M., King, J., Koc, N., Krylov, A., Martinez, N., Matthiessen, J., McInroy, D., Moore, T.C., Onodera, J., O'Regan, M., Pälke, H., Rea, B., Rio, D., Sakamoto, T., Smith, D.C., Stein, R., St John, K., Suto, I.,

- Suzuki, N., Takahashi, K., Watanabe, M., Yamamoto, M., Farrell, J., Frank, M., Kubik, P., Jokat, W., Kristoffersen, Y., 2006. The Cenozoic palaeoenvironment of the Arctic Ocean. *Nature* 441, 601–605. <https://doi.org/10.1038/nature04800>
- Mosar, J., 2003. Scandinavia's North Atlantic passive margin. *Journal of Geophysical Research* 108, 2360. <https://doi.org/10.1029/2002JB002134>
- Mosar, J., Eide, E. a., Osmundsen, P.T., Sommaruga, A., Torsvik, T.H., 2002. Greenland-Norway separation: a geodynamic model for the North Atlantic. *Norwegian Journal of Geology* 82, 281–298.
- Müller, D.R., Spielhagen, R.F., 1990. Evolution of the Central Tertiary Basin of Spitsbergen: towards a synthesis of sediment and plate tectonic history. *Palaeogeography, Palaeoclimatology, Palaeoecology* 80, 153–172. [https://doi.org/10.1016/0031-0182\(90\)90127-S](https://doi.org/10.1016/0031-0182(90)90127-S)
- Nanson, G.C., Croke, J.C., 1992. A genetic classification of floodplains. *Geomorphology*. <https://doi.org/10.2113/gsecongeo.3.7.611>
- Nemec, W., Postma, G., 1993. Quaternary alluvial fans in southwestern Crete: sedimentation processes and geomorphic evolution, in: Marzo, M., Puigdefabregas, C. (Eds.), *Alluvial Sedimentation*. pp. 235–276.
- Nemec, W., Steel, R.J., 1984. Alluvial and coastal conglomerates: their significant features and some comments on gravelly mass-flow deposits. *Sedimentology of Gravels and Conglomerates* 10, 1–31. <https://doi.org/>
- Nilsen, T.H., 1982. Alluvial Fan Deposits. *AAPG Memoir 31: Sandstone Depositional Environments* 49–86.
- Nonn, C., Leroy, S., Khanbari, K., Ahmed, A., 2017. Tectono-sedimentary evolution of the eastern Gulf of Aden conjugate passive margins: Narrowness and asymmetry in oblique rifting context. *Tectonophysics* 721, 322–348. <https://doi.org/10.1016/j.tecto.2017.09.024>
- Norwegian Polar Institute, 2018. Sarstangen [WWW Document]. Place names in Norwegian polar areas. URL placenames.npolar.no (accessed 5.8.18).
- Oakey, G.N., Chalmers, J.A., 2012. A new model for the Paleogene motion of Greenland relative to North America: Plate reconstructions of the Davis Strait and Nares Strait regions between Canada and Greenland. *Journal of Geophysical Research: Solid Earth* 117, 360–363. <https://doi.org/10.1029/2011JB008942>
- Oakey, G.N., Stephenson, R., 2008. Crustal structure of the Inuitian region of Arctic Canada and Greenland from gravity modelling: Implications for the Palaeogene Eurekan orogen. *Geophysical Journal International* 173, 1039–1063. <https://doi.org/10.1111/j.1365-246X.2008.03784.x>
- Ohta, Y., 1994. Caledonian and precambrian history in Svalbard: a review, and an implication of escape tectonics. *Tectonophysics* 231, 183–194. [https://doi.org/10.1016/0040-1951\(94\)90129-5](https://doi.org/10.1016/0040-1951(94)90129-5)

- Ohta, Y., 1982. Morpho-tectonic studies around Svalbard and the northernmost Atlantic. *Arctic Geology and Geophysics Memoir* 8, 415–428.
- Ohta, Y., Kraslikov, A.A., Lepvrier, C., Teben'kov, A.M., 1995. Northern continuation of Caledonian high-pressure metamorphic rocks in central-western Spitsbergen. *Polar Research* 14, 303–316. <https://doi.org/10.1111/j.1751-8369.1995.tb00717.x>
- Olsson, W.A., 2000. Origin of Lüders' bands in deformed rock. *Journal of Geophysical Research* 105, 5931–5938. <https://doi.org/10.3109/17453674.2010.492765>
- Orton, G.J., Reading, H.G., 1993. Variability of deltaic processes in terms of sediment supply, with particular emphasis on grain size. *Sedimentology* 40, 475–512.
- Osmundsen, P.T., Andersen, T.B., 2001. The middle Devonian basins of western Norway: Sedimentary response to large-scale transtensional tectonics? *Tectonophysics* 332, 51–68. [https://doi.org/10.1016/S0040-1951\(00\)00249-3](https://doi.org/10.1016/S0040-1951(00)00249-3)
- Osmundsen, P.T., Péron-Pinvidic, G., 2018. Crustal-Scale Fault Interaction at Rifted Margins and the Formation of Domain-Bounding Breakaway Complexes: Insights From Offshore Norway. *Tectonics* 37, 935–964. <https://doi.org/10.1002/2017TC004792>
- Osmundsen, P.T., Redfield, T.F., Ganerød, M., Appleyard, T., Peron-Pinvidic, G., Schaaf, N., 2017. From transpression to transtension along the west Barents margin : the, in: 19th EGU General Assembly. p. 4100.
- Paech, H.-J., Koch, J., 2001. Coalification in Post-Caledonian Sediments on Spitsbergen, Intra-Continental Fold Belts CASE 1: West Spitsbergen.
- Passchier, C.W., Simpson, C., 1986. Porphyroclast system as kinematic indicators. *Journ. Struct. Geol.* 8, 831–843.
- Passchier, C.W., Trouw, R.A.J., 2005. *Microtectonics*, Springer.
- Pérez-Gussinyé, M., Ranero, C.R., Reston, T.J., Sawyer, D., 2003. Mechanisms of extension at nonvolcanic margins: Evidence from the Galicia interior basin, west of Iberia. *Journal of Geophysical Research: Solid Earth* 108, 1–19. <https://doi.org/10.1029/2001JB000901>
- Pérez-Gussinyé, M., Reston, T.J., 2001. Rheological evolution during extension at nonvolcanic rifted margins: Onset of serpentinization and development of detachments Leading To Continental Breakup. *Journal of Geophysical Research* 106, 3961–3975.
- Péron-Pinvidic, G., Manatschal, G., 2009. The final rifting evolution at deep magma-poor passive margins from Iberia-Newfoundland: A new point of view. *International Journal of Earth Sciences* 98, 1581–1597. <https://doi.org/10.1007/s00531-008-0337-9>
- Peron-Pinvidic, G., Manatschal, G., Osmundsen, P.T., 2013. Structural comparison of archetypal Atlantic rifted margins: A review of observations and concepts. *Marine and Petroleum Geology* 43, 21–47. <https://doi.org/10.1016/j.marpetgeo.2013.02.002>
- Peron-Pinvidic, G., Osmundsen, P.T., 2018. The Mid Norwegian - NE Greenland conjugate margins: Rifting evolution, margin segmentation, and breakup. *Marine and Petroleum*

- Geology 98, 162–184. <https://doi.org/10.1016/j.marpetgeo.2018.08.011>
- Piepjoh, K., 2000. The Svalbardian-Ellesmerian deformation of the Old Red Sandstone and the pre-Devonian basement in NW Spitsbergen (Svalbard). Geological Society, London, Special Publications 180, 585–601. <https://doi.org/10.1144/GSL.SP.2000.180.01.31>
- Piepjoh, K., von Gosen, W., Tessensohn, F., 2016. The Eureka deformation in the Arctic: an outline. Journal of the Geological Society 173. <https://doi.org/10.1144/jgs2016-081>
- Pimentel, N.L.V., 2002. Pedogenic and early diagenetic processes in Palaeogene alluvial fan and lacustrine deposits from the Sado Basin (S Portugal). Sedimentary Geology 148, 123–138. [https://doi.org/10.1016/S0037-0738\(01\)00213-5](https://doi.org/10.1016/S0037-0738(01)00213-5)
- Postma, G., Nemeč, W., Kleinspehn, Karen, L., 1988. Large floating clasts in turbidites a me. Sedimentary Geology 58, 47–61. <https://doi.org/10.1128/JVI.80.6.2631>
- Rahn, P.H., 1967. Sheetfloods, streamfloods, and the formation of pediments. Annals of the Association of American Geographers 57, 593–604. <https://doi.org/10.1111/j.1467-8306.1967.tb00624.x>
- Reinfelds, I., Nanson, G., 1993. Formation of braided river floodplains, Waimakariri River, New Zealand. Sedimentology 40, 1113–1127. <https://doi.org/10.1111/j.1365-3091.1993.tb01382.x>
- Reston, T.J., 2007. The formation of non-volcanic rifted margins by the progressive extension of the lithosphere: the example of the West Iberian margin. Geological Society, London, Special Publications 282, 77–110. <https://doi.org/10.1144/SP282.5>
- Rickenmann, D., Weber, D., 2003. Erosion by debris flows in field and laboratory experiments. Debris-Flow Hazards Mitigation: Mechanics, Prediction, and Assessment 883–894.
- Ritzmann, O., Jokat, W., Czuba, W., Guterch, A., Mjelde, R., Nishimura, Y., 2004. A deep seismic transect from Hovgård Ridge to northwestern Svalbard across the continental-ocean transition: A sheared margin study. Geophysical Journal International 157, 683–702. <https://doi.org/10.1111/j.1365-246X.2004.02204.x>
- Rodine, J.D., Johnson, A.M., 1976. The ability of debris, heavily freighted with coarse clastic materials, to flow on gentle slopes. Sedimentology 23, 213–234. <https://doi.org/10.1111/j.1365-3091.1976.tb00047.x>
- Rohais, S., Eschard, R., Ford, M., Guillocheau, F., Moretti, I., 2007. Stratigraphic architecture of the Plio-Pleistocene infill of the Corinth Rift: Implications for its structural evolution. Tectonophysics 440, 5–28. <https://doi.org/10.1016/j.tecto.2006.11.006>
- Rosgen, D.L., 1994. A classification of natural rivers. Catena.
- Rust, B.R., 1977a. Depositional models for braided Alluvium. Fluvial Sedimentology 5, 605–625.
- Rust, B.R., 1977b. A CLASSIFICATION OF ALLUVIAL CHANNEL SYSTEM. Fluvial

Sedimentology Memoir 5.

- Rust, B.R., 1972. Structure and Process in a Braided River. *Sedimentology* 18, 221–245.
<https://doi.org/10.1111/j.1365-3091.1972.tb00013.x>
- Rye-Larsen, M., 1982. Forlandsundet Graben - Sedimentasjon og tektonisk utvikling av et basseng ved en transform plategrense. University of Bergen.
- Sanderson, D.J., Marchini, W.R.D., 1984. *Transpression* 6, 449–458.
[https://doi.org/10.1016/0191-8141\(84\)90058-0](https://doi.org/10.1016/0191-8141(84)90058-0)
- Schlische, R.W., 1995. Geometry and origin of fault-related folds in extensional settings. *American Association of Petroleum Geologists Bulletin* 79, 1661–1678.
<https://doi.org/10.1306/7834DE4A-1721-11D7-8645000102C1865D>
- Schneider, D., Faehrich, K., Majka, J., Manecki, M., 2018. Ar / ³⁹Ar geochronologic evidence of Eureka deformation within the West Spitsbergen Fold and Thrust Belt. *Circum-Arctic Structural Events: Tectonic Evolution of the Arctic Margins and Trans-Arctic Links with Adjacent Orogens: Geological Society of America Special Paper* 541 2541, 1–16.
- Scholz, C.H., 1987. Wear and gouge formation in brittle faulting. *Geology* 15, 493–495.
[https://doi.org/10.1130/0091-7613\(1987\)15<493:WAGFIB>2.0.CO;2](https://doi.org/10.1130/0091-7613(1987)15<493:WAGFIB>2.0.CO;2)
- Schönenberger, J., van der Lelij, R., Xie, R., Schaaf, N.W., Osmundsen, P.T., 2019. Unravelling the timescales and conditions of clay forming processes with X-Ray diffraction and K-Ar analysis, in: *Geological Society of Norway, Winter Conference 2019*. Bergen.
- Schultz, R.A., Fossen, H., 2008. Terminology for structural discontinuities. *AAPG Bulletin* 92, 853–867. <https://doi.org/10.1306/02200807065>
- Seiler, C., Fletcher, J.M., Quigley, M.C., Gleadow, A.J.W., Kohn, B.P., 2010. Neogene structural evolution of the Sierra San Felipe, Baja California: Evidence for proto-gulf transtension in the Gulf Extensional Province? *Tectonophysics* 488, 87–109.
<https://doi.org/10.1016/j.tecto.2009.09.026>
- Sellevoll, M.A., Duda, S.J., Guterch, A., Pajchel, J., Perchuc, E., 1991. Crustal structure in the Svalbard region from seismic measurements. *Tectonophysics* 189, 55–71.
- Senger, K., Tveranger, J., Ogata, K., Braathen, A., Planke, S., 2014. Late Mesozoic magmatism in Svalbard: A review. *Earth-Science Reviews* 139, 123–144.
<https://doi.org/10.1016/j.earscirev.2014.09.002>
- Sewall, J.O., Sloan, L.C., 2004. Less ice, less tilt, less chill: The influence of a seasonally ice-free Arctic Ocean and reduced obliquity on early Paleogene climate. *Geology* 32, 477–480. <https://doi.org/10.1130/G20295.1>
- Singhal, B.B.S., Gupta, R.P., 2010. *Fractures and discontinuities*, second. ed, Applied Hydrogeology of Fractured Rocks. Springer Dordrecht Heidelberg London New York, London. <https://doi.org/10.1007/978-90-481-8799-7>

- Skogseid, J., Planke, S., Faleide, J.I., Pedersen, T., Eldholm, O., Neverdal, F., 2000. NE Atlantic continental rifting and volcanic margin formation, Geological Society, London, Special Publications. <https://doi.org/10.1144/GSL.SP.2000.167.01.12>
- Smelror, M., Petrov, O. V., Larssen, G.B., Werner, S.C., 2009. Atlas Geological History of the Barents Sea. Trondheim.
- Smith, D.G., 1987. MEANDERING RIVER POINT BAR LITHOFACIES MODELS: MODERN AND ANCIENT EXAMPLES COMPARED DERALD. The Society of Economic Paleontologists and Mineralogists.
- Smith, N.D., 1974. Sedimentology and Bar Formation in the Upper Kicking Horse River, a Braided Outwash Stream. *The Journal of Geology* 82, 205–223. <https://doi.org/10.1086/627959>
- Smith, N.D., 1972. Flume Experiments on the Durability of Mud Clasts. *Journal of Sedimentary Petrology* 42, 378–383. <https://doi.org/10.1306/74D72559-2B21-11D7-8648000102C1865D>
- Sohn, Y.K., Rhee, C.W., Kim, B.C., 1999. Debris Flow and Hyperconcentrated Flood-Flow Deposits in an Alluvial Fan, Northwestern Part of the Cretaceous Yongdong Basin, Central Korea. *The Journal of Geology* 107, 111–132. <https://doi.org/10.1086/314334>
- Sperling, V., 1990. Kartierung der tertiären Ablagerungen auf Sarsøyra, Oscar II Land, Spitsbergen, Svalbard. Universität Hamburg.
- Spielhagen, R.F., Tripathi, A., 2009. Evidence from Svalbard for near-freezing temperatures and climate oscillations in the Arctic during the Paleocene and Eocene. *Palaeogeography, Palaeoclimatology, Palaeoecology* 278, 48–56. <https://doi.org/10.1016/j.palaeo.2009.04.012>
- Srivastava, S.P., 1985. Evolution of the Eurasian Basin and its implications to the motion of Greenland along Nares Strait. *Tectonophysics* 114, 29–53. [https://doi.org/10.1016/0040-1951\(85\)90006-X](https://doi.org/10.1016/0040-1951(85)90006-X)
- Steel, R.J., Dalland, A., Kalgraff, K., Larsen, V., 1981. The Central Tertiary Basin of Spitsbergen; sedimentary development of a sheared-margin. *Geology of the North Atlantic borderlands*. 7, 647–664.
- Steel, R.J., Gjelberg, J.G., Helland-Hansen, W., Kleinspehn, K., Nøttvedt, A., Rye-Larsen, M., 1985. The Tertiary Strike-Slip Basins and Orogenic Belt of Spitsbergen, in: *Society for Economic Paleontology and Mineralogy*. pp. 339–359.
- Steel, R.J., Thompson, D.B., 1983. Structures and textures in Triassic braided stream conglomerates ('Bunter' Pebble Beds) in the Sherwood Sandstone Group, North Staffordshire, England. *Sedimentology* 30, 341–367. <https://doi.org/10.1111/j.1365-3091.1983.tb00677.x>
- Steel, R.J., Worsley, D., 1984. Svalbard's post-Caledonian strata - an atlas of sedimentational patterns and palaeogeographic evolution. *Petroleum Geology of North European Margin* 109–135. https://doi.org/10.1007/978-94-009-5626-1_9

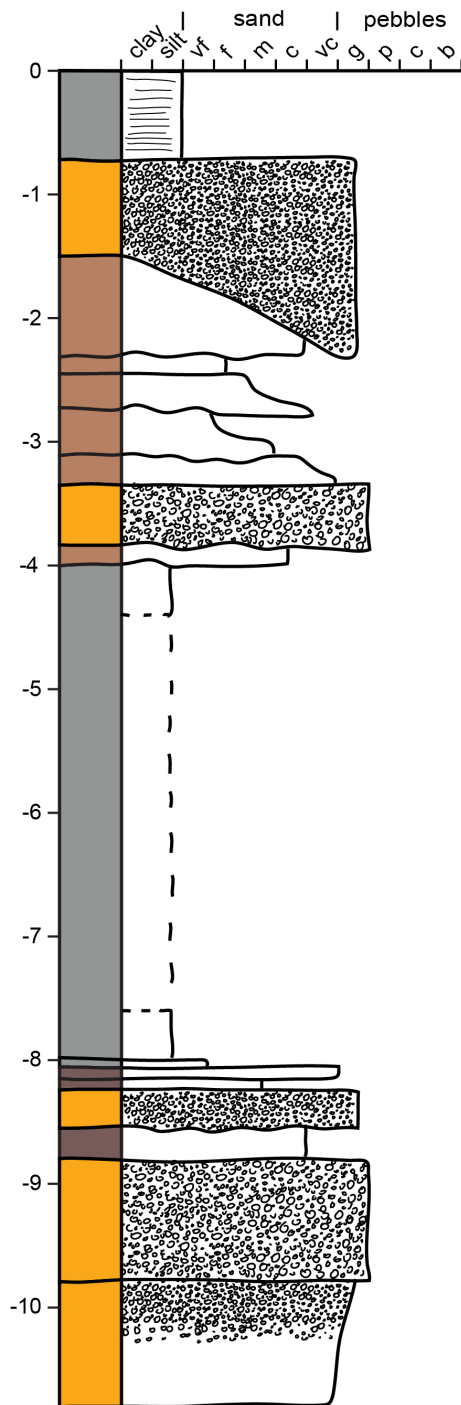
- Sylvester, A.G., 1988. Strike-slip faults. *Geological Society of America Bulletin* 100, 1666–1703.
- Talwani, M., Eldholm, O., 1977. Evolution of the Norwegian-Greenland Sea. *Bulletin of the Geological Society of America* 88, 969–999. [https://doi.org/10.1130/0016-7606\(1977\)88<969:EOTNS>2.0.CO;2](https://doi.org/10.1130/0016-7606(1977)88<969:EOTNS>2.0.CO;2)
- Tanner, L.H., Hubert, J.F., 1991. *Basalt Breccias and Conglomerates* 61, 15–27.
- Tavani, S., Storti, F., Lacombe, O., Corradetti, A., Muñoz, J.A., Mazzoli, S., 2015. A review of deformation pattern templates in foreland basin systems and fold-and-thrust belts: Implications for the state of stress in the frontal regions of thrust wedges. *Earth-Science Reviews* 141, 82–104. <https://doi.org/10.1016/j.earscirev.2014.11.013>
- Tessensohn, F., Piepjohn, K., 2000. Eocene compressive deformation in Arctic Canada, North Greenland and Svalbard and its plate tectonic causes. *Polarforschung* 68, 121–124.
- Traverse, A., 2007. *Paleopalynology*. Springer, Dordrecht, The Netherlands.
- Venkat-Ramani, M., Tikoff, B., 2002. Physical models of transtensional folding. *Geology* 30, 523–526. [https://doi.org/10.1130/0091-7613\(2002\)030<0523:PMOTF>2.0.CO](https://doi.org/10.1130/0091-7613(2002)030<0523:PMOTF>2.0.CO)
- Vogt, P.R., Parrish, M., 2012. Driftwood dropstones in Middle Miocene Climate Optimum shallow marine strata (Calvert Cliffs, Maryland Coastal Plain): Erratic pebbles no certain proxy for cold climate. *Palaeogeography, Palaeoclimatology, Palaeoecology* 323–325, 100–109. <https://doi.org/10.1016/j.palaeo.2012.01.035>
- von Gosen, W., Peach, H.J., 2001. Structures in the Tertiary sediments of the Forlandsundet Graben. Edited by F. Tessensohn. *Geologisches Jahrbuch (Polar Issue No. 7)*, B 475–502.
- Vrolijk, P., Van Der Pluijm, B.A., 1999. Clay gouge. *Journal of Structural Geology* 21, 1039–1048. [https://doi.org/10.1016/S0191-8141\(99\)00103-0](https://doi.org/10.1016/S0191-8141(99)00103-0)
- Walker, R.G., Cant, D.J., 1984. Sandy fluvial systems. *Facies Models* 71–89.
- Watkins, R., 1992. Sedimentology and paleoecology of Pliocene shallow marine conglomerates, Salton Trough region, California. *Palaeogeography, Palaeoclimatology, Palaeoecology* 95, 319–333. [https://doi.org/10.1016/0031-0182\(92\)90148-X](https://doi.org/10.1016/0031-0182(92)90148-X)
- Weidinger, J.T., Korup, O., Munack, H., Altenberger, U., Dunning, S.A., Tippelt, G., Lottermoser, W., 2014. Giant rockslides from the inside. *Earth and Planetary Science Letters* 389, 62–73. <https://doi.org/10.1016/j.epsl.2013.12.017>
- Withjack, M.O., Olsen, J., Peterson, E., 1990. Experimental models of extensional forced folds. *AAPG Bulletin* 74, 1038–1054.
- Woodcock, N.H., Mort, K., 2008. Classification of fault breccias and related fault rocks. *Geological Magazine* 145, 435–440. <https://doi.org/10.1017/S0016756808004883>
- Worsley, D., 2008. The post-Caledonian development of Svalbard and the western Barents Sea. *Polar Research* 27, 298–317. <https://doi.org/10.1111/j.1751-8369.2008.00085.x>

Worsley, D., 1986. The geological history of Svalbard: evolution of an Arctic archipelago.
Den norske stats oljeselskap as.

Appendix

Logs (northern beach)

Northeastern log

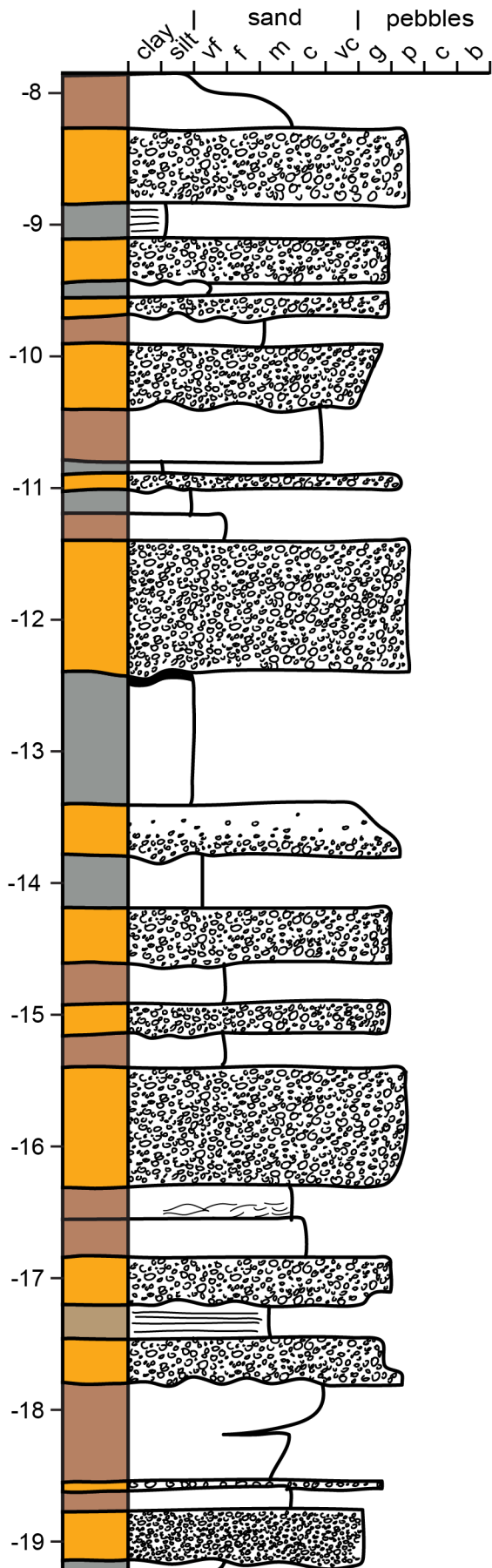


Notes

bedding 100/20

bedding 082/20

scree covered



Notes

dark organic rich layer

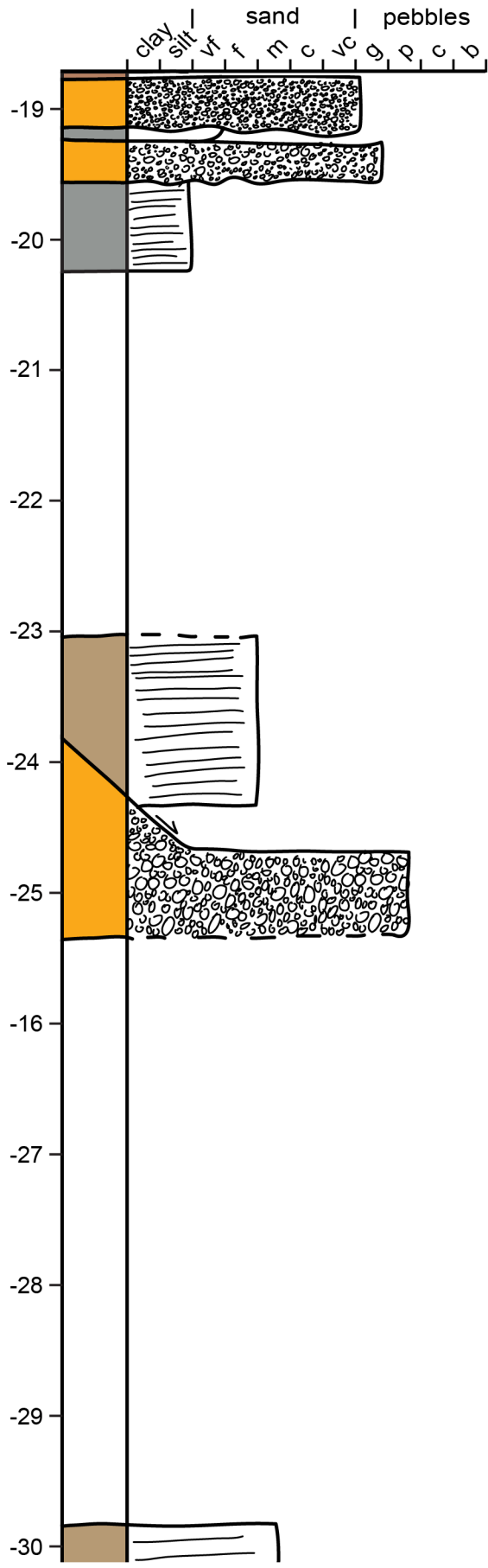
bedding 098/21

lithified

dark organic rich layer

bedding 041/17

dark organic rich layer



Notes

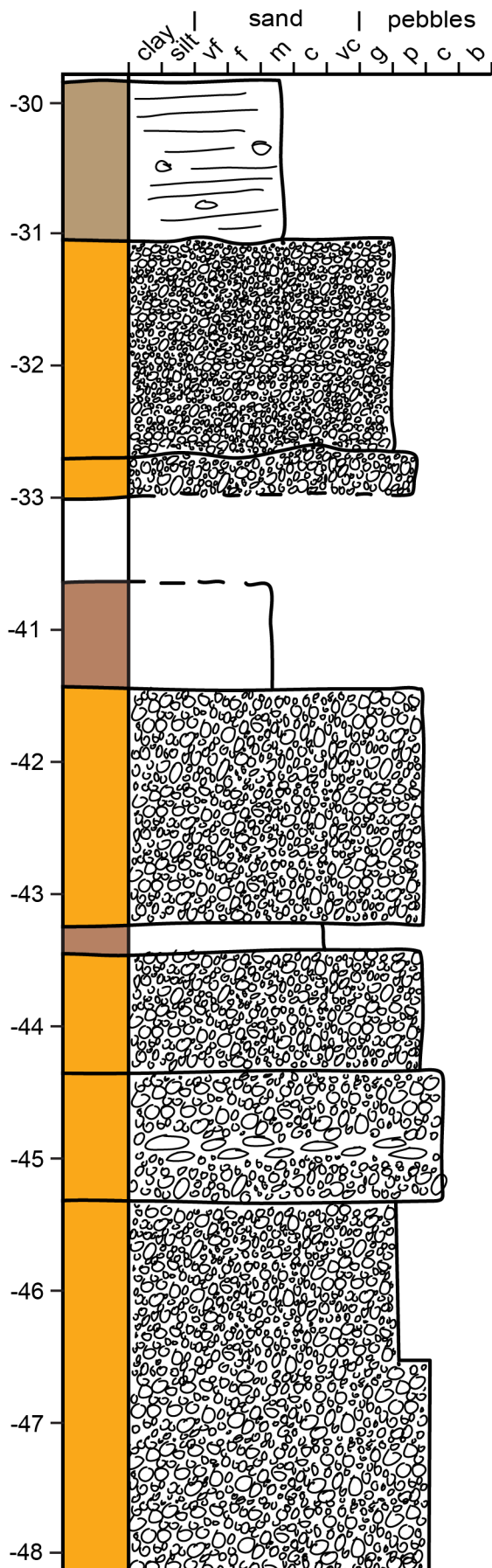
bedding 098/10

scree covered

normal fault, offset unclear

generally many smaller normal faults

scree covered



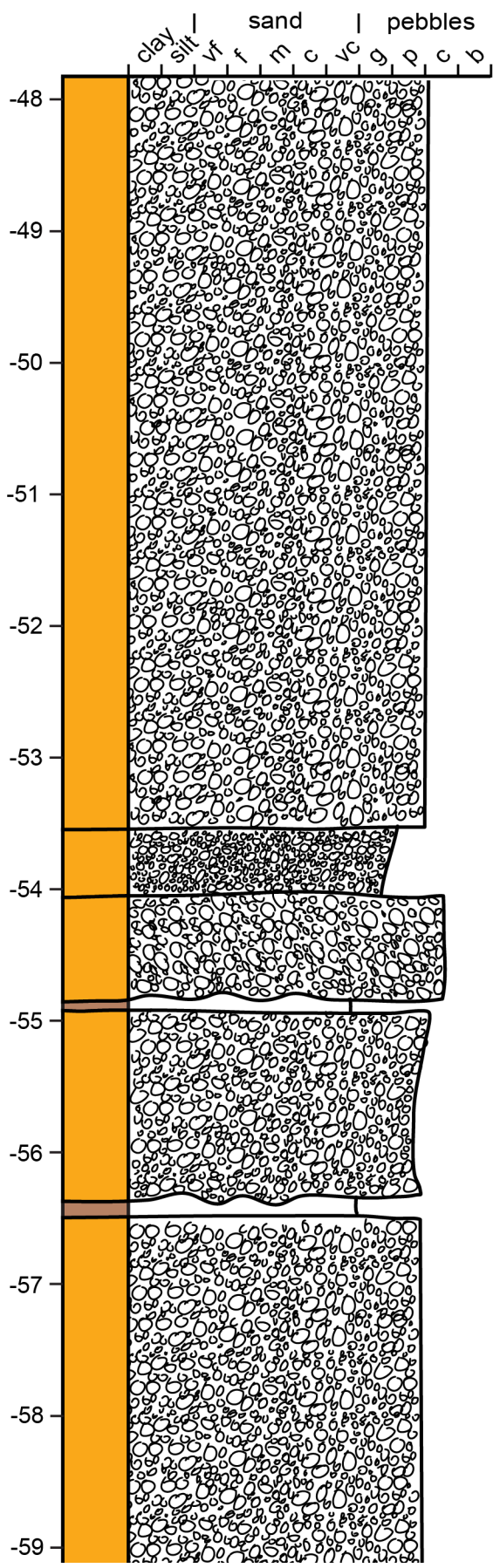
Notes

coal stringers

heavily fractures

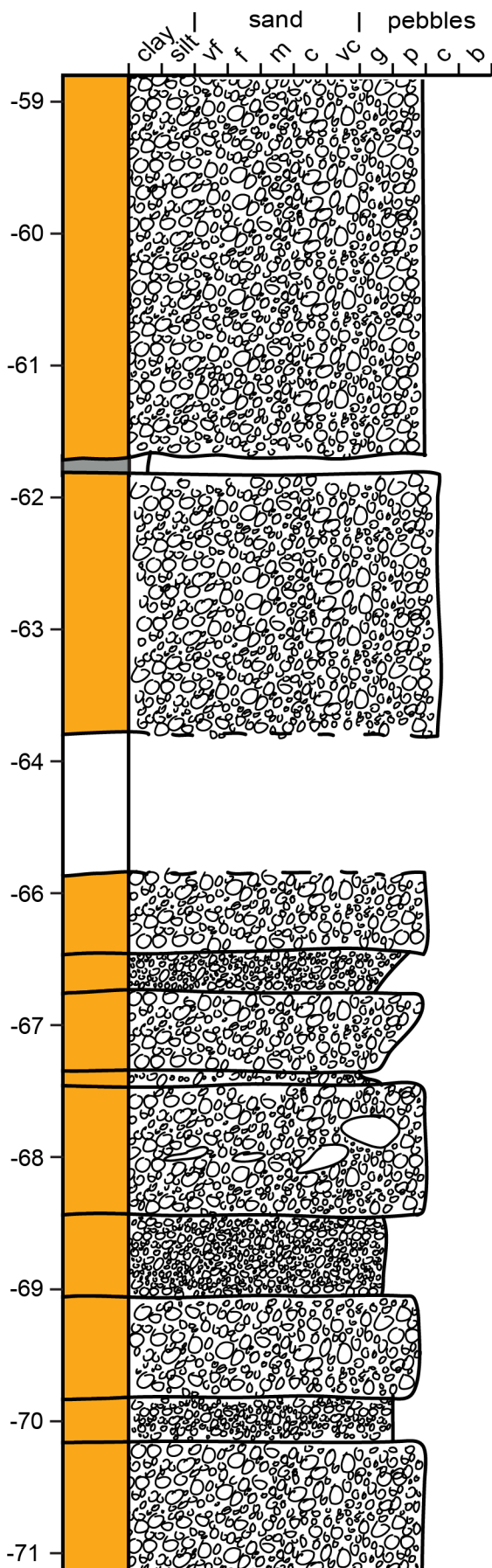
fractured cobbles

bedding 097/26



Notes

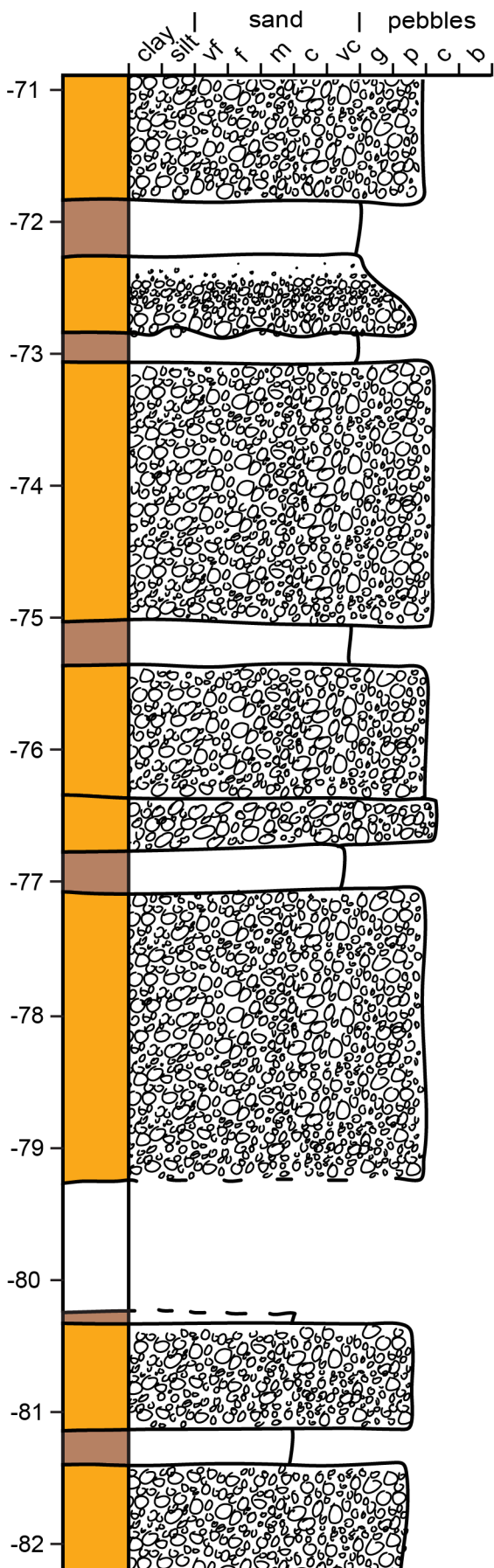
many minor normal faults



Notes

well stratified

well stratified

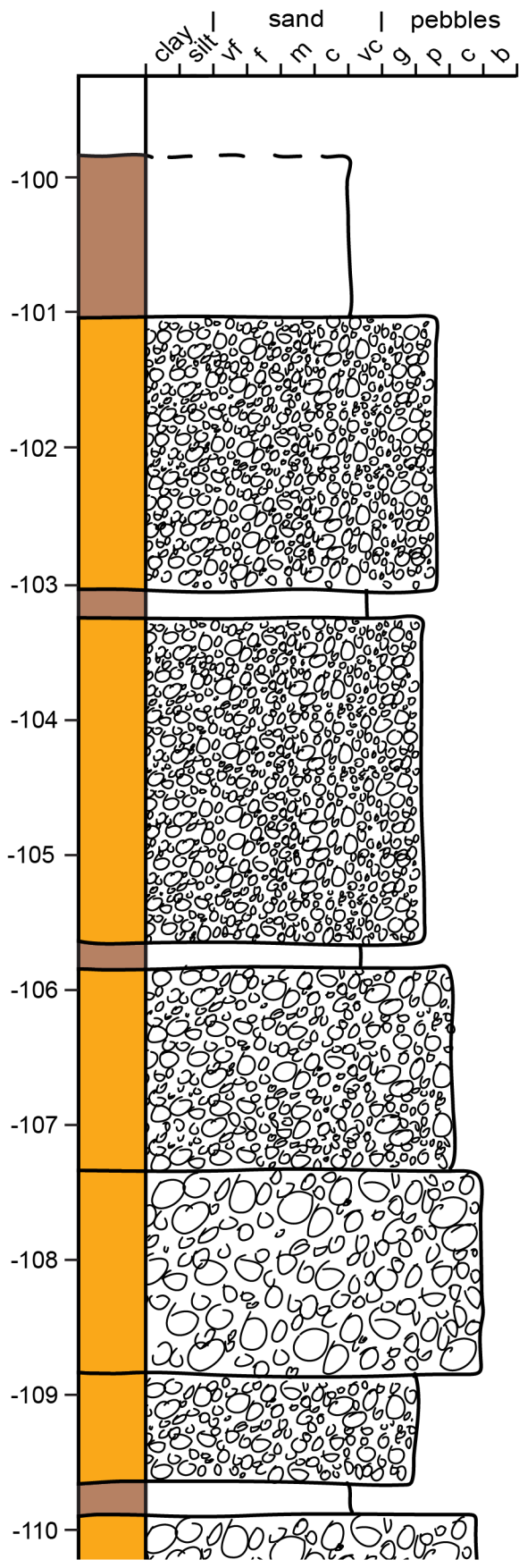


Notes

abundant normal faulting

scree covered well stratified

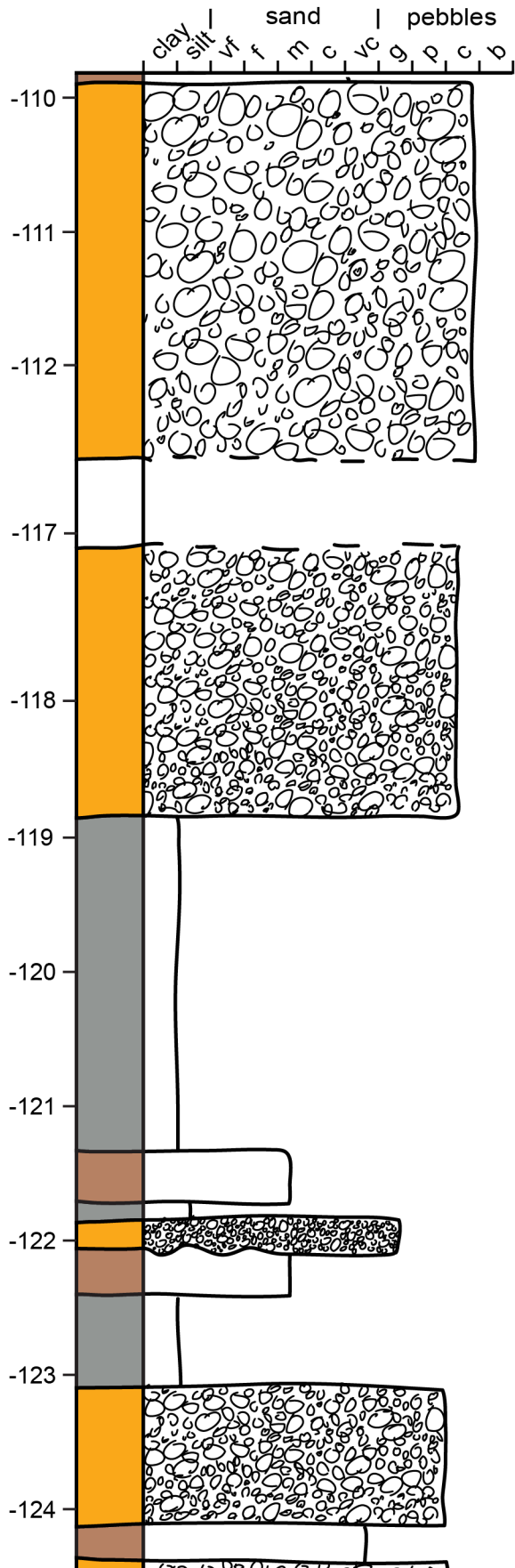
bedding 103/32



Notes

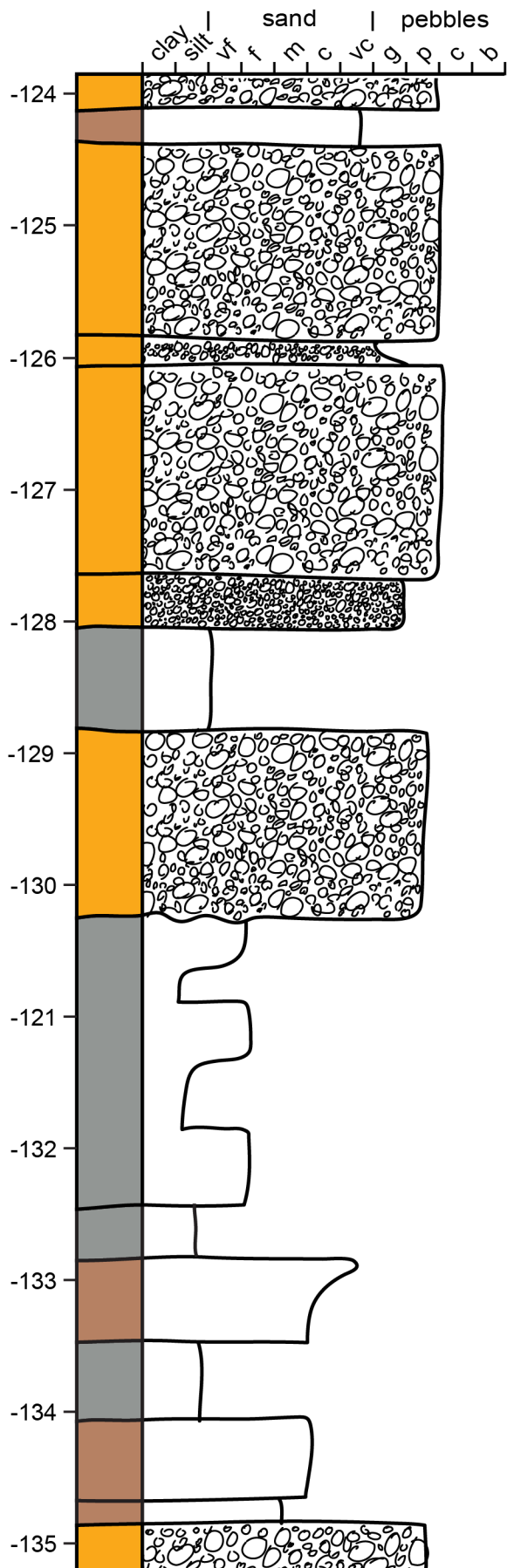
covered by scree

abundant detrital coal clasts



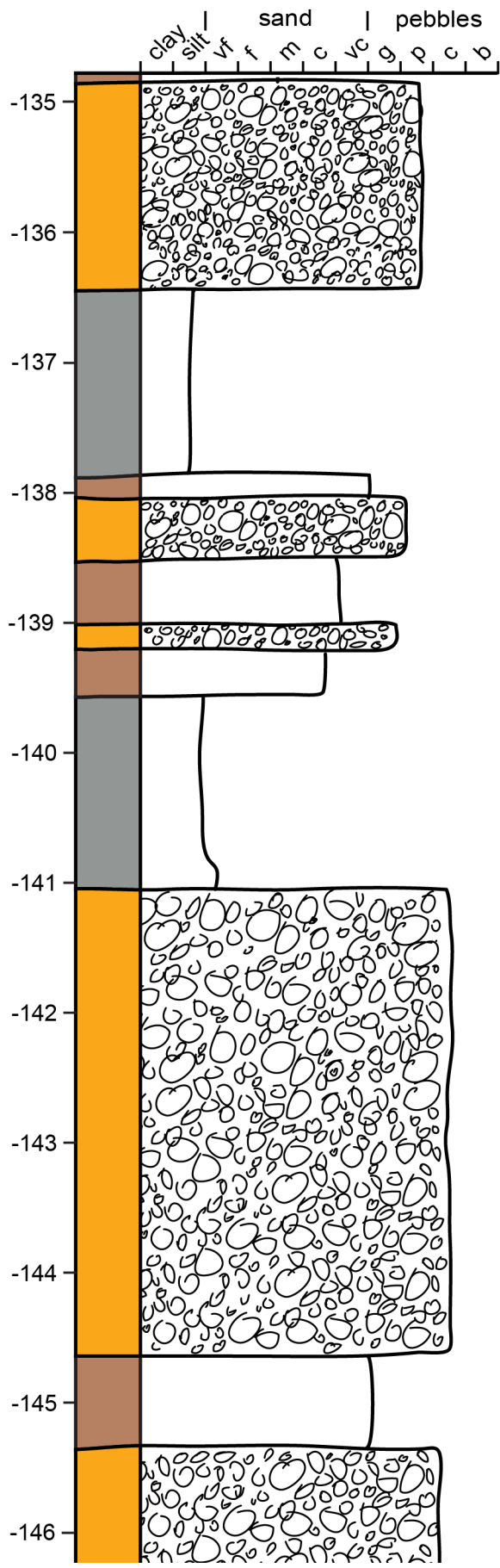
Notes

scree covered, might cover
fine grained deposits

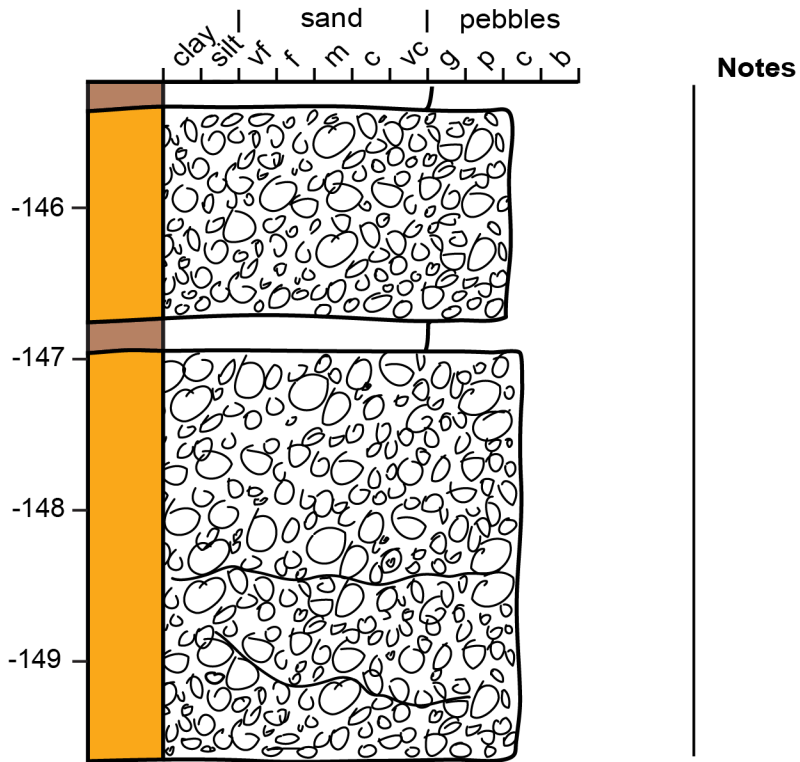


Notes

dark sand & silt stone interlayered

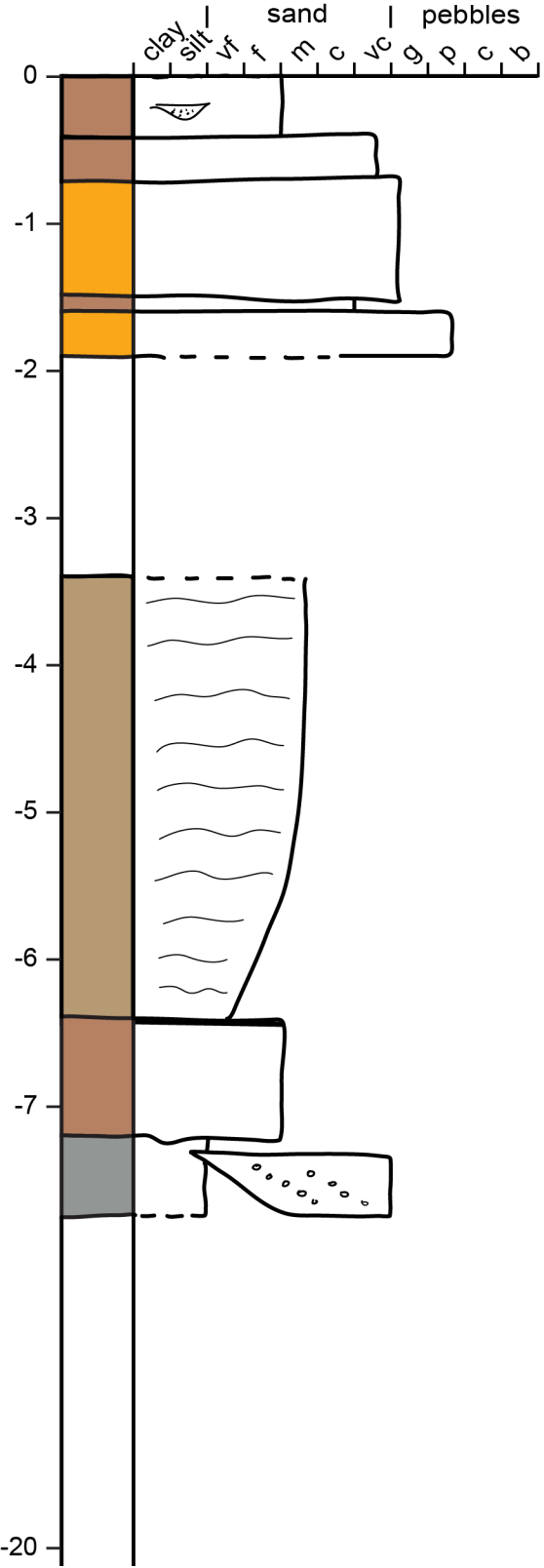


Notes



Appendix 1: Log from the northeastern part of the northern beach. For the legend see Table 2, for location see Fig. 22.

Middle log



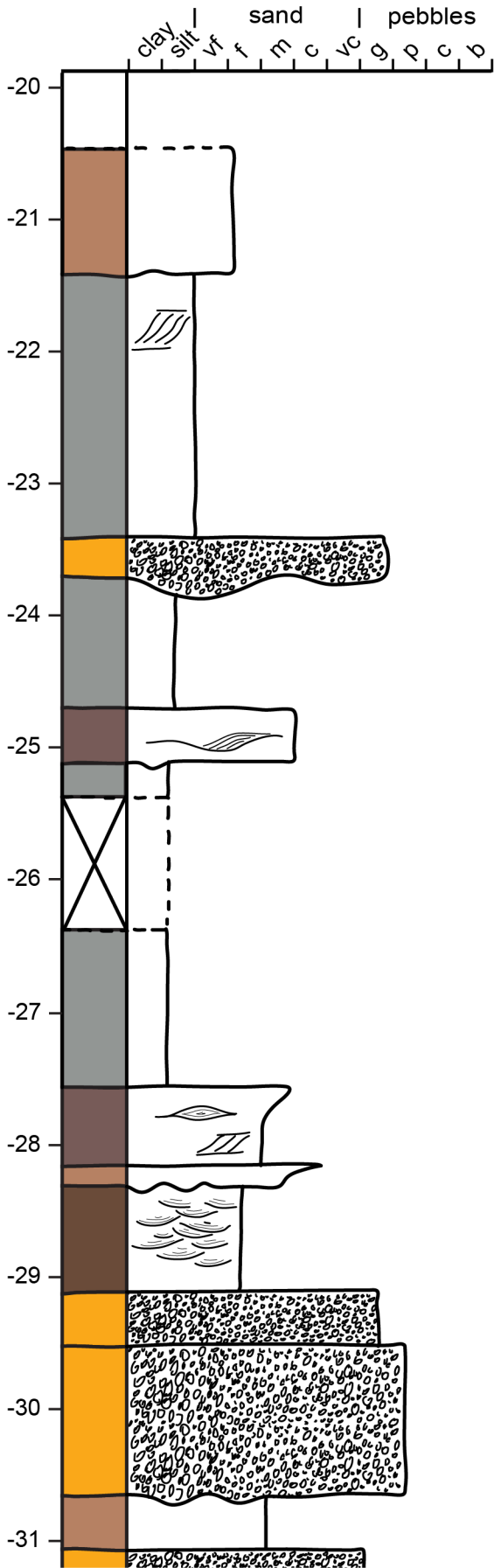
Notes

bedding subhorizontal

bedding 338/27

dark organic rich layer

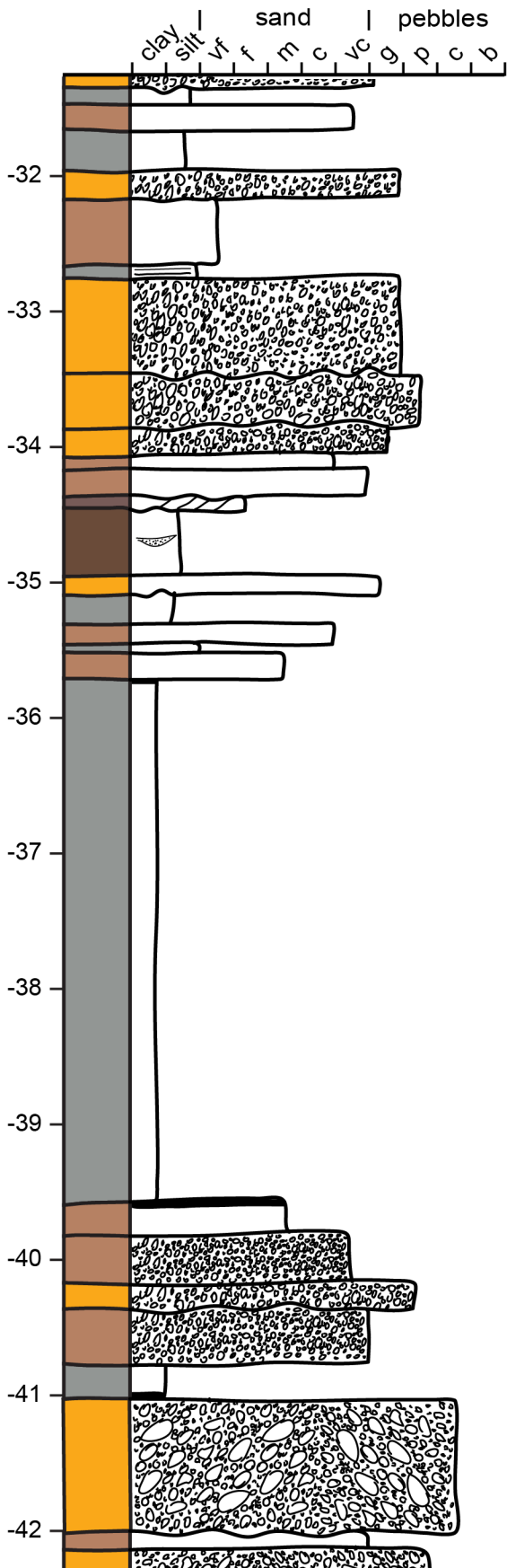
100 m of covered outcrop
approx. 13 m of stratigraphy



Notes

planar crossbeds 280/15

lithified (only this bed)



Notes

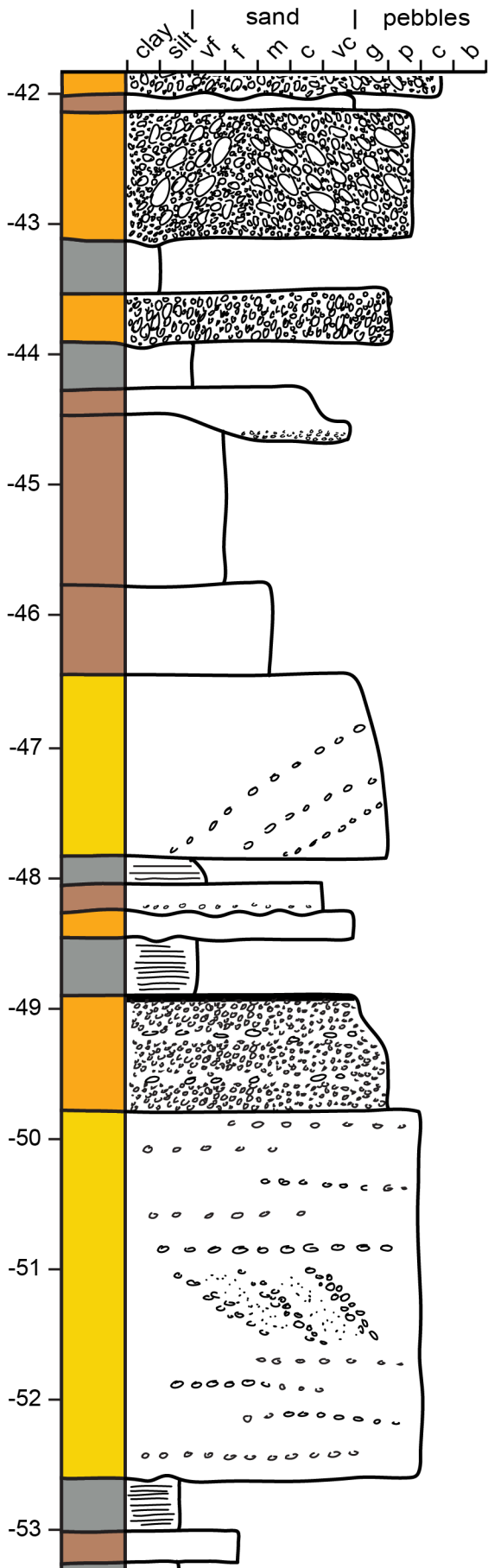
dark organic rich layer

planar crossbed 268/30

dark organic rich layer

dark organic rich layer

dark organic rich layer

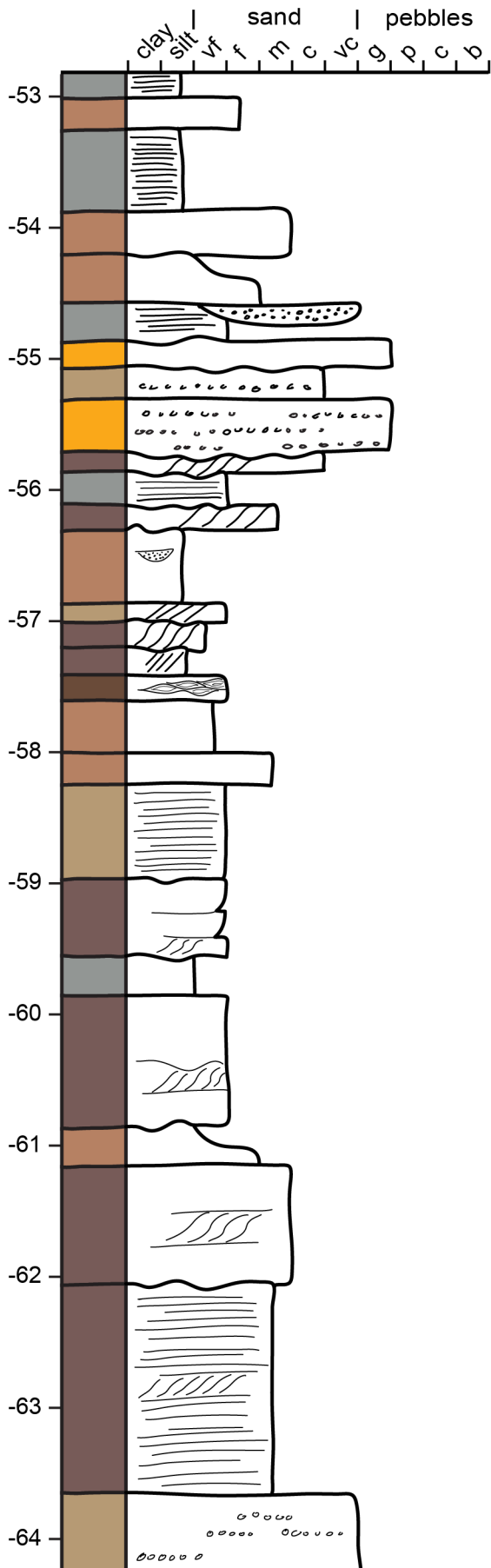


Notes

coal stringers

dark organic rich layer

planar crossbed 263/45



Notes

bedding 263/10

planar crossbed 317/40

planar crossbed 295/42

planar crossbed 236/40

planar crossbed 279/43

planar crossbed 306/52

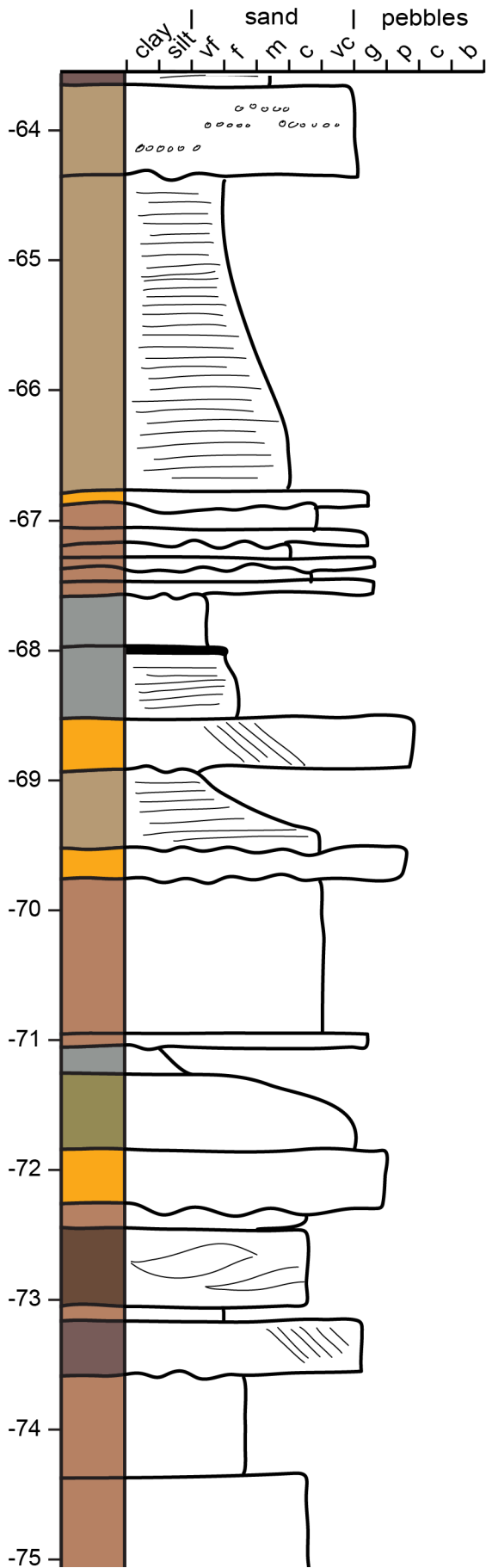
planar crossbed 253/52

planar crossbed 278/50

planar crossbed 244/40

planar crossbed 294/45

pebbly, stratified



Notes

pebbly, stratified

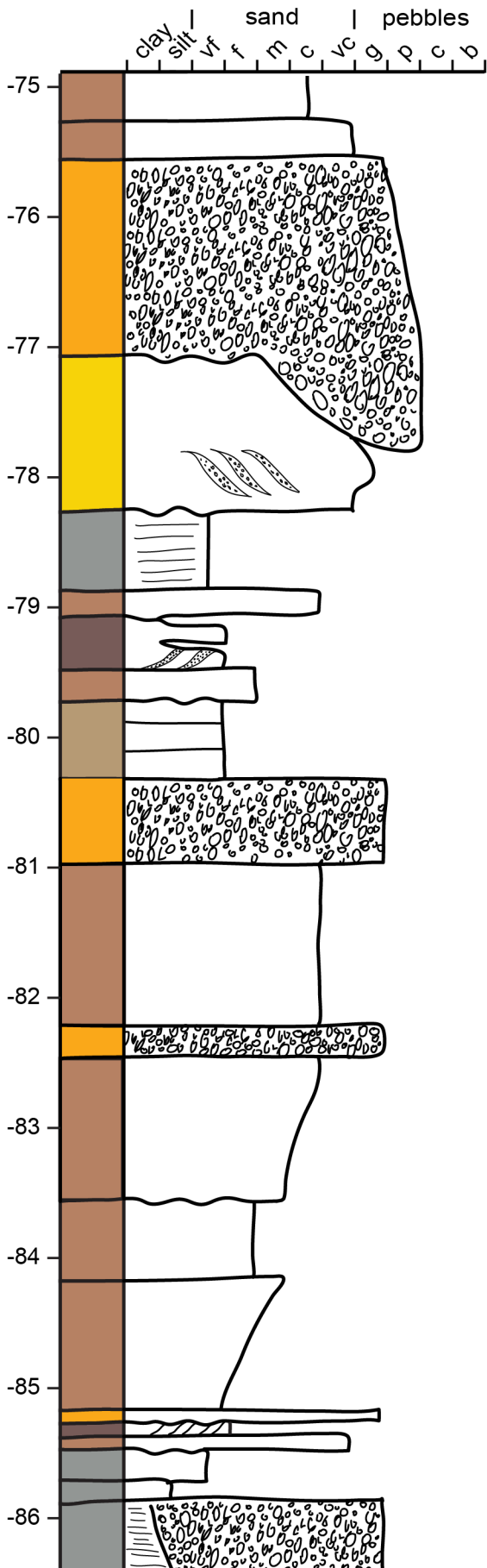
very soft

dark organic rich layer

very loose

rootlets

dark organic rich layer



Notes

stratified

planar crossbeds 318/35

planar crossbeds 313/42

planar crossbeds 259/40

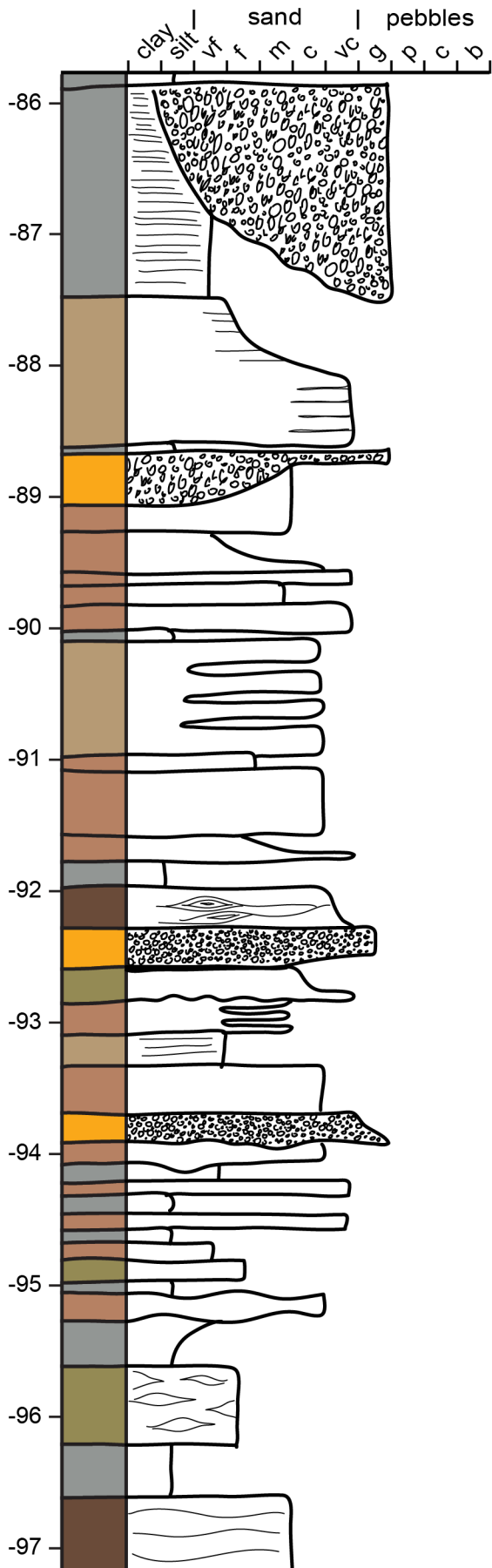
two dark organic rich layers

location of channel that is assessed in detail

coalified plant print

planar crossbeds 319/37

smaller coal fragments



Notes

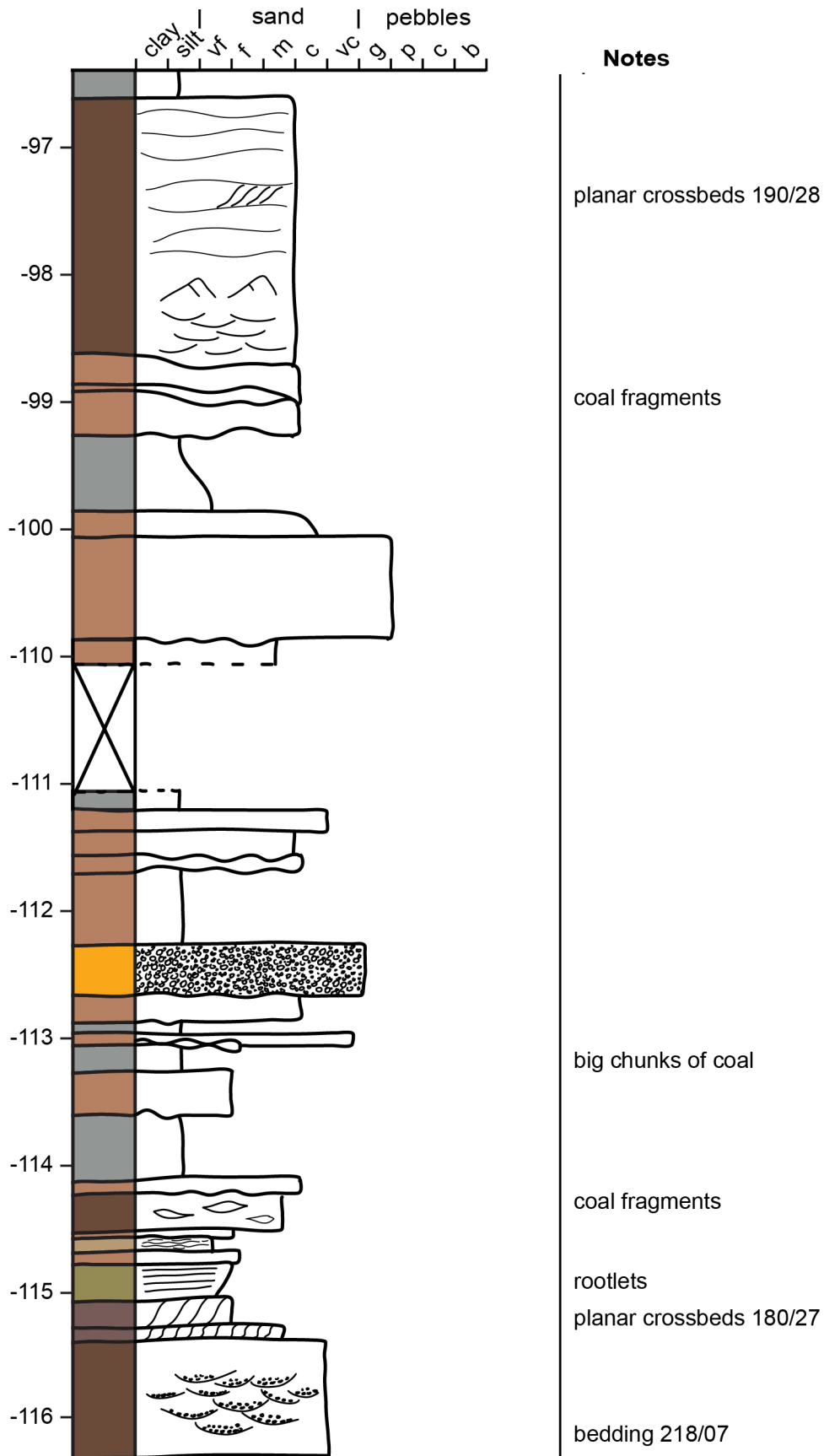
smaller coal fragments

larger stems that appear to have been deformed, dewatering?

many rootlets

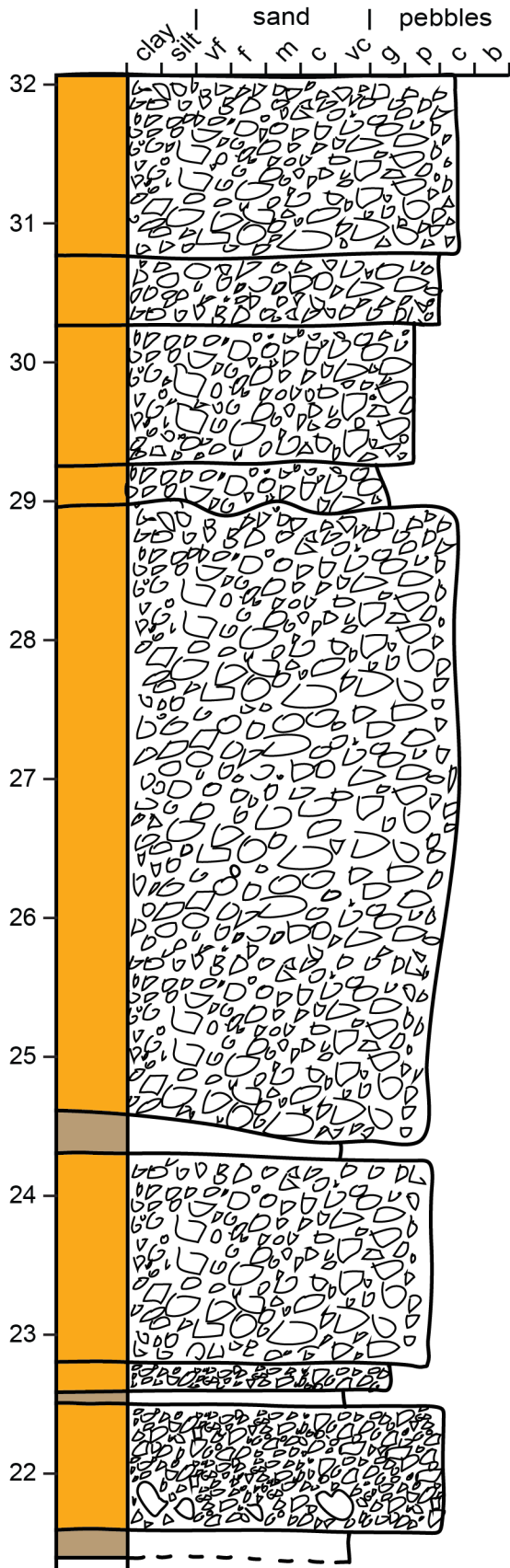
rootlets

rootlets & plant fossils



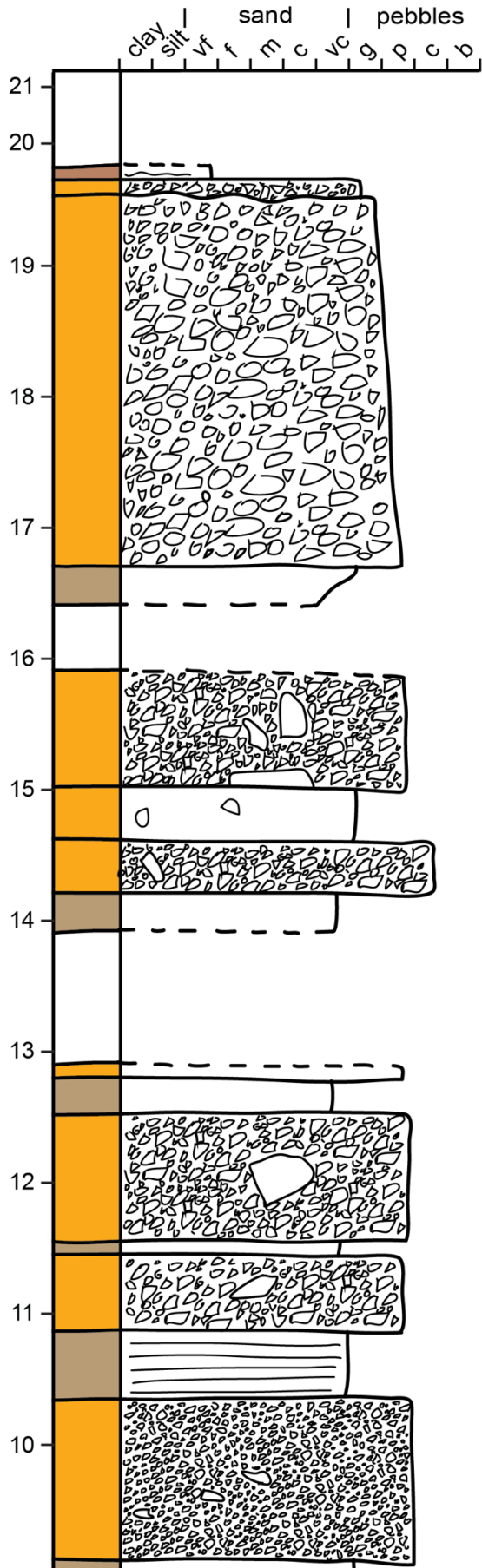
Appendix 2: Log from the middle part of the northern beach. For the legend see Table 2, for location see Fig. 22.

Southwestern log



Notes

sandy matrix

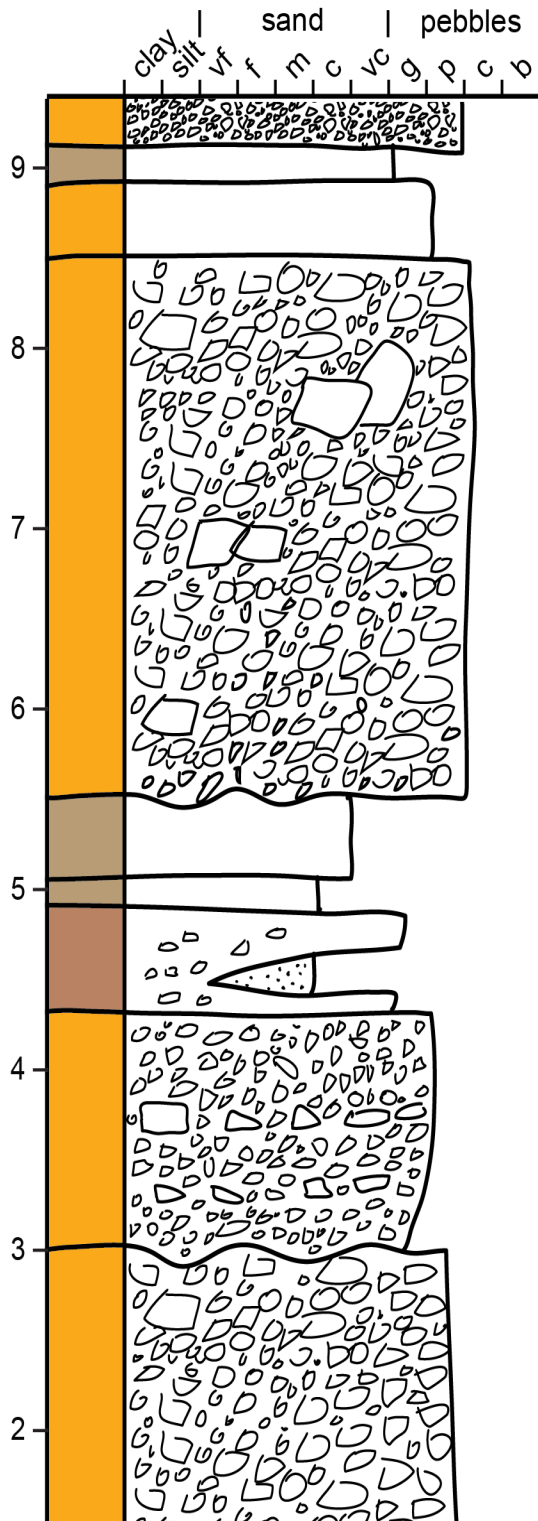


Notes

outside cobbles

outside boulders

outside cobbles



Notes

bedding 202/24

outsize boulders ~30m

Appendix 3: Log from the southwestern part of the northern beach. For the legend see Table 2, for location see Fig. 22.

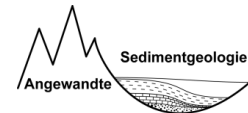
Paleolimnology

Institut für Angewandte Geowissenschaften
Fachgebiet Angewandte Sedimentgeologie
PD Dr. Olaf Lenz



Olaf Lenz, 12.07.2018

**Report on palynostratigraphic analysis of sediment samples
OSL-17-13 to OSL-17-23**



The scope of the study

The aim of the study is to determine the age of sediment samples by using pollen-analytical (palynological) investigations. The identification, distribution and abundance of palynomorphs can be used to provide chronological control for sedimentary sequences and to correlate sedimentary sequences of any age. Especially sporomorphs respectively their parent plants evolved at times very rapidly during the Phanerozoic since the Devonian, with the result that sporomorphs are characteristic of a fairly narrow time range and hence are very useful for stratigraphic studies (Traverse, 2007). Therefore, stratigraphic palynology is an accepted and widely used method, because the morphological diversity, for example, of pollen and spores as well as the rapid evolution of their parent plants predestinate such microfossils as index fossils.

A stratigraphic classification of samples and a distinction between the different Paleogene and Neogene series and stages at Spitsbergen based on pollen and spores should be possible, because the global climatic changes with warming and cooling periods which occurred during this time interval have led to significant changes within the composition and diversity of Spitsbergens vegetation. This is directly reflected in the pollen rain, which is therefore stratigraphically usable. In addition, elements of the marine phytoplankton, in particular dinoflagellate cysts, are excellently suited as stratigraphic markers. Nevertheless, the prerequisite is that an appropriate number of palynomorphs of sufficient quality is present in the samples, which unfortunately is not the case in most of the 10 samples (Tab. 1) that are studied here.

The stratigraphic classification presented in this report is largely based on the detailed palynological studies of Manum (1962) and Cepek and Krutzsch (2001) who described samples from the Tertiary record of Spitsbergen between the Upper Cretaceous and the Oligocene(?).

Sample preparation

Following standard procedures as described by Kaiser and Ashraf (1974) all samples were successively treated with hydrochloric acid (HCl), hydrofluoric acid (HF) and potassium hydroxide (KOH). The residue was sieved with a mesh size of 10 μm and slightly oxidized with diluted hydrogen peroxide (H_2O_2) to remove flocculating organic matter and to improve the transparency of the palynomorphs.

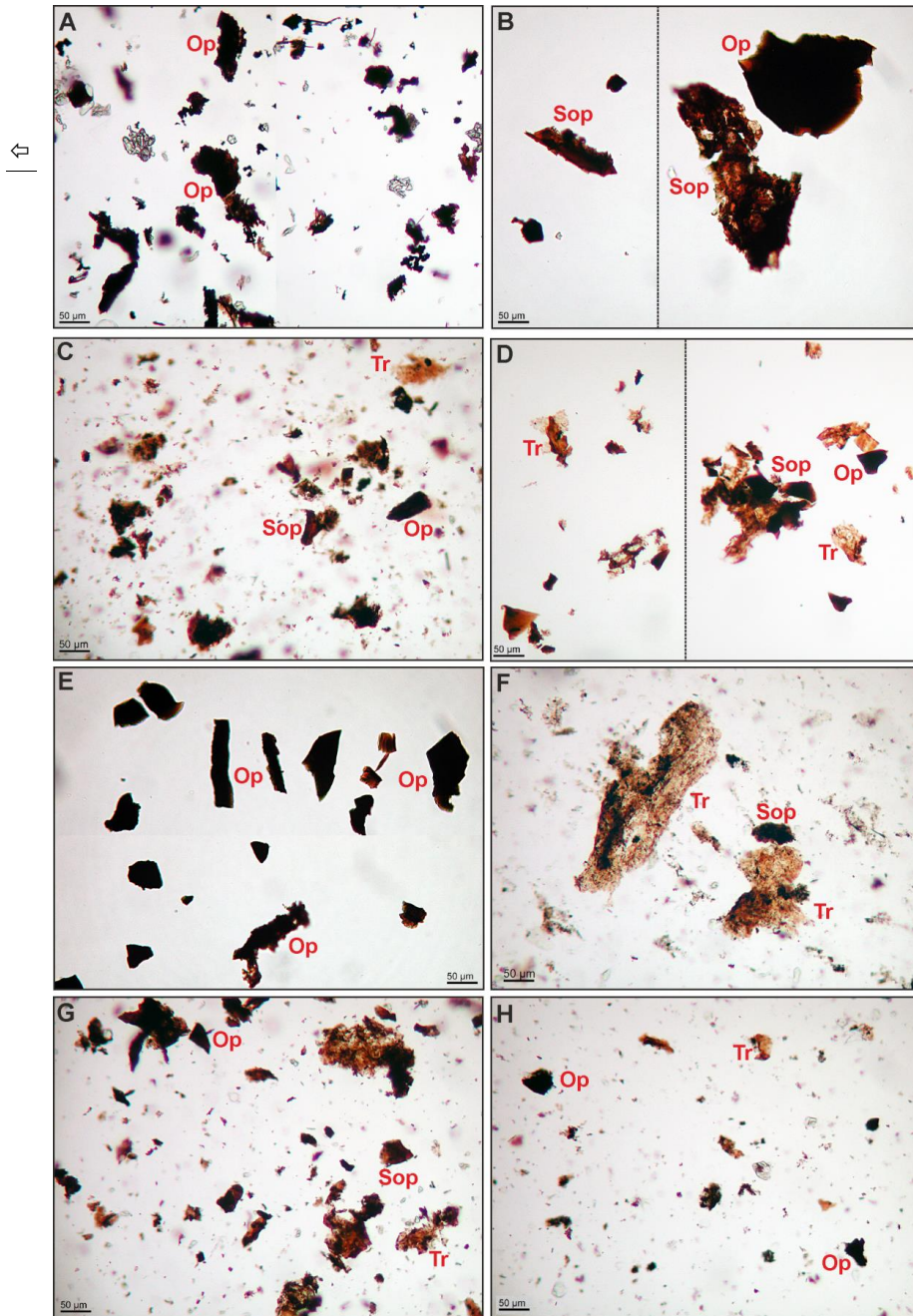
| Sample No. | Description |
|------------|----------------------|
| OSL-17-13 | coal |
| OSL-17-15 | coal |
| OSL-17-16 | coal |
| OSL-17-17 | coal |
| OSL-17-18 | coal |
| OSL-17-19 | sandstone |
| OSL-17-20 | siltstone |
| OSL-17-21 | siltstone |
| OSL-17-22 | sandstone, siltstone |
| OSL-17-23 | sandstone |

Tab. 1: Sample list

The organic content

Basically, the organic content is very high in the studied samples. However, predominantly phytoclasts, mostly woody residues or cuticles, are present, but only few or no palynomorphs. The samples OSL-17-15, OSL-17-17, OSL-17-18 and OSL-17-23 are completely barren of palynomorphs, whereas samples OSL-17-13, OSL-17-19, OSL-17-20 and OSL-17-22 contain only single pollen grains in bad preservation, which prevents an accurate determination. In sample OSL-17-16 palynomorphs are nearly absent, but diatoms occur regularly. Only in sample OSL-17-21 a rich and diverse pollen flora is included along with some diatoms. The overview photos in Figs. 1 and 2 present the palynofacies types of the different samples.

⇒ **Fig. 1:** Palynofacies of samples: (A) OSL-17-13 with a characteristic content of large (>100µm) opaque equidimensional phytoclasts, (B) OSL-17-15 with very large equidimensional and blade-shaped semi-opaque to opaque phytoclasts (up to 500µm), (C) OSL-17-16 with a mixture of medium-sized (c. 50 µm) opaque, semi-opaque and translucent equidimensional phytoclasts, (D) OSL-17-17 with a composition of large (up to 250 µm) and mainly translucent to semi-opaque phytoclasts, (E) OSL-17-18 with a characteristic content of medium-sized (c. 50 µm) equidimensional and large (> 100µm) blade-shaped opaque phytoclasts, (F) OSL-17-19 with few but large (up to 500µm) equidimensional and blade-shaped translucent to semi-opaque phytoclasts, (G) OSL-17-20 with a composition of small- to medium-sized (10 to 100 µm) equidimensional opaque, semi-opaque and translucent phytoclasts, (H) OSL-17-21 with few mainly equidimensional translucent to opaque phytoclasts (c. 50 µm); Sop: semi-opaque phytoclast, Tr: translucent phytoclast, Op: opaque phytoclast.



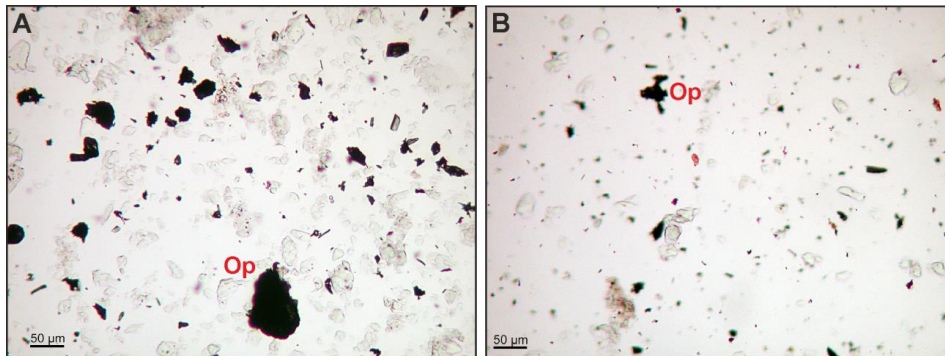


Fig. 2: Palynofacies of samples: (A) OSL-17-22 with a characteristic content of generally small (< 50µm) equidimensional opaque phytoclasts, (B) OSL-17-23 with very small equidimensional opaque phytoclasts (< 10µm); Op: opaque phytoclast

Samples OSL-17-15, OSL-17-17, OSL-17-18, OSL-17-23:

The samples are barren of palynomorphs and contain mainly opaque phytoclasts (Figs. 1, 2). Therefore, a stratigraphic analysis based on palynomorphs is not possible.

Sample OSL-17-13:

A single pollen grain that is poorly preserved was found in this sample (Fig. 3). Because of preservation, an obvious botanical assignment is not possible. However, the pollentype, probably a tetrad, has strong similarities to Ericaceae pollen. Similar morphotypes are described by Manum (1962) as *Ericipites* sp., Type C. Ericaceae played a notable role in the vegetation of Spitsbergen and are important elements within swamp environments during the Paleogene (Manum 1962). Nevertheless, as facies elements the ericaceous pollen have minor stratigraphic relevance. Ericaceae have been found in the Lower to Middle Eocene of Spitsbergen (Cepek and Krutsch 2001), but mostly in younger records from the Oligocene and Miocene (Livšić 1974, Boulter and Manum, 1996).

The sample is dominated by various diatom species of the genus *Stephanopyxis* (Figs 4 A, B), a diatom that is common in Eocene to Oligocene records in the northern Norwegian-Greenland Sea (Scherer and Koç 1996) but also abundant around the Paleocene/Eocene boundary in the North Sea basin (Mitlehner 1996).

A stratigraphic classification of the sample due to palynomorphs and diatoms beyond a general Paleogene dating is therefore not possible

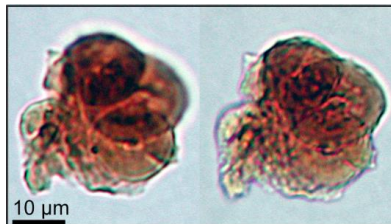


Fig. 3: Badly preserved palynomorph from sample OSL-17-13 representing possibly a tetrad of an ericaceous pollen (*Ericiptes* sp.)

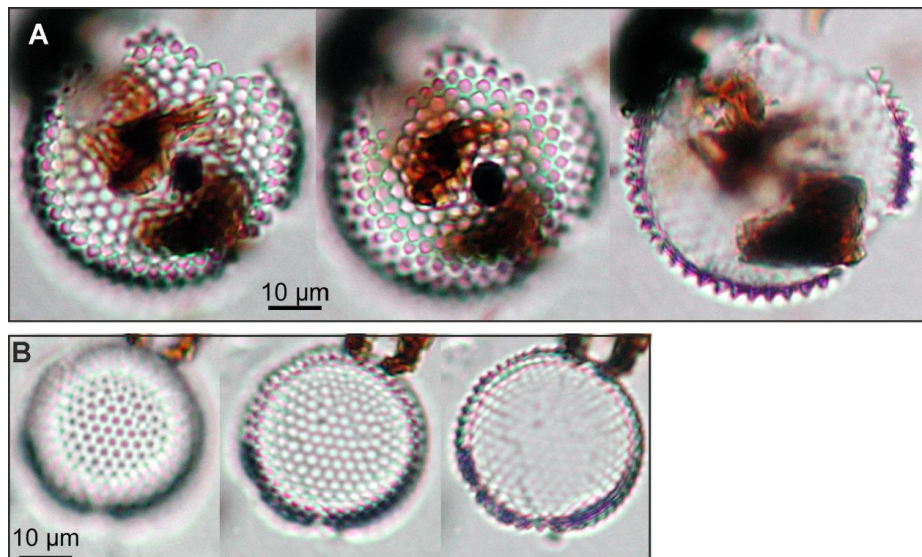


Fig. 4: Two diatoms of the genus *Stephanopyxis* from sample OSL-17-13

Sample OSL-17-16:

Sample OSL-17-16 is a typical example for the very poor preservation of palynomorphs and other microfossils in the studied samples.. Unfortunately, their preservation does not allow a precise identification. Characteristic examples are presented in Fig. 5. Two of the palynomorphs (Figs. 5 B, C) show the typical oval-elliptical shape and possibly also the characteristic dehiscence slit (laesura) of monolete fern spores but they are very small. Furthermore, characteristic features of the spore wall such as sculpturing patterns are not identifiable. Therefore, the morphological features are too weak to get

clear evidence of the mother plants. Thus, based on these palynomorphs stratigraphic statements are not possible.

A third grain (Fig. 5 D) is possibly an inaperturate pollen of the Cupressaceae. They have been described by Cepek and Krutzsch (2001) from the Renardodden area and were dated as Middle to Upper Eocene. Nevertheless, palynological studies of intrabasaltic sediment layers in the lower volcanic series from ODP Leg 104 outer Vøring Plateau Hole 642E Cores 102 through 109 in the Norwegian Sea, which were dated as Upper Paleocene to Lower Eocene, show also a dominance of pollen of Cupressaceae (Boulter and Manum 1989). Mathiesen (1932) described several species of such conifers as well as angiosperm leaf megafossils from Kap Dalton and other localities in East Greenland and deduced an Early Tertiary (Paleocene-Eocene) age of these deposits.

Some fragments of diatoms have been found in the sample (Fig. 5A), which can be identified as *Coscinodiscus* or *Stephanopyxis*. Especially *Coscinodiscus* occurs with a number of different species at the Paleocene/Eocene boundary in the North Sea basin (Oreshkina 2012). After Gradstein et al. (1988) *Coscinodiscus* spp. has a special stratigraphic position, because within the foraminiferal stratigraphy of the Tertiary in the North Sea these diatoms are eponymous for the *Coscinodiscus* zone, which marks the Paleocene/Eocene boundary during a time of limited distribution of foraminifers. *Stephanopyxis* can be found in marine records between the Paleocene and the Oligocene (Mitlehner 1996, Scherer and Koç 1996).

In summary, based on the available palynological evidence, the assemblage of palynomorphs and diatoms may indicate an **Upper Paleocene to Upper Eocene** age of

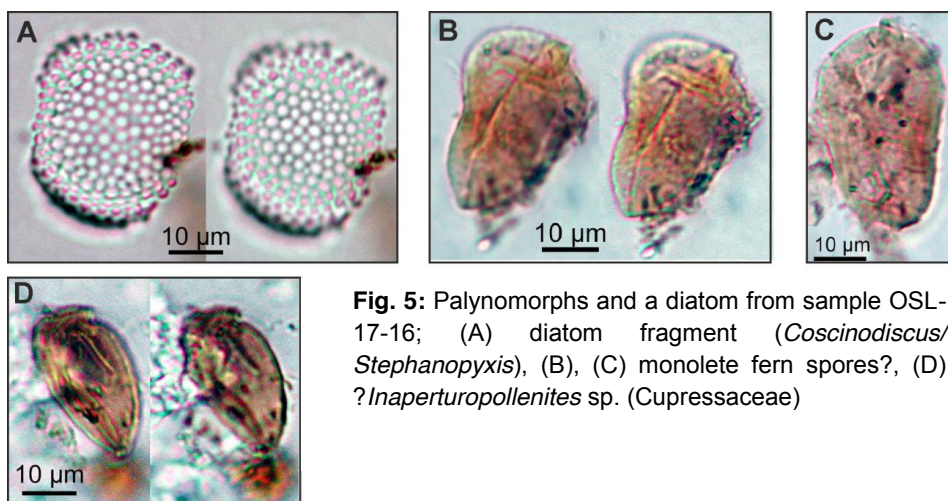


Fig. 5: Palynomorphs and a diatom from sample OSL-17-16; (A) diatom fragment (*Coscinodiscus*/*Stephanopyxis*), (B), (C) monolete fern spores?, (D) ?*Inaperturopollenites* sp. (Cupressaceae)

the sample, but due to the weak evidence that is based on mainly badly preserved microfossils, this statement must be considered with caution.

Samples OSL-17-19, OSL-17-20:

In each of the two samples only a single pollen grain has been found. Both grains are probably inaperturate pollen of the Cupressaceae (*Taxodium*- or *Glyptostrobus*-type, *Inaperturopollenites* sp.), whereas especially the poor preservation of the pollen in sample OSL-17-19 is too bad to allow an exact botanical assignment (Fig. 6). In contrast, the pollen grain in sample OSL-17-20 is relatively well preserved and can be identified as a cupressaceous pollen (Fig. 7).

Taxodium/*Glyptostrobus* are distributed in Spitsbergen during the complete Paleogene Livšic (1974), but especially in the Upper Paleocene and Lower Eocene they are dominating elements in the vegetation (Cepek and Krutzsch 2001, see also sample OSL-17-16). Nevertheless, the single grains that were found in the two samples do not allow a more precise dating than Paleogene.

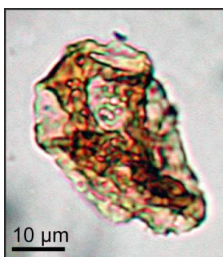


Fig. 6: Sample OSL-17-19:
?Inaperturopollenites sp.

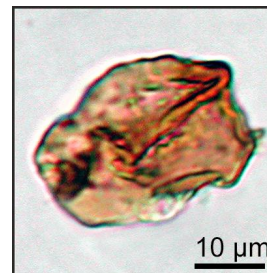


Fig. 7: Sample OSL-17-20:
Cupressaceae (*Taxodium*,
Glyptostrobus, *Inaperturopollenites* sp.)

Sample OSL-17-21

Among the studied samples OSL-17-21 shows the richest palynoflora and additionally some diatoms (Fig. 8). However, the preservation is due to taphonomic processes mostly poor (Fig. 8B). Therefore, an exact determination of palynomorphs on species level is often impossible. Nevertheless, the assemblage allows a stratigraphic classification of the sample.

The assemblage is dominated by pollen of gymnosperms which are present in high diversity. The Pinaceae occur with pollen of *Pinus* or *Cathaya* (*Pityosporites labdacus*, (Figs. 8 A-C). Frequent is also the pollen of *Tsuga* (Fig. 8 D). Manum (1962) described these pollen as *Tsugaepollenites viridifluminipites* from Spitsbergen. Nearly identical *Tsuga* pollen are described as *Zonalapollenites neogenicus* from the Oligocene and

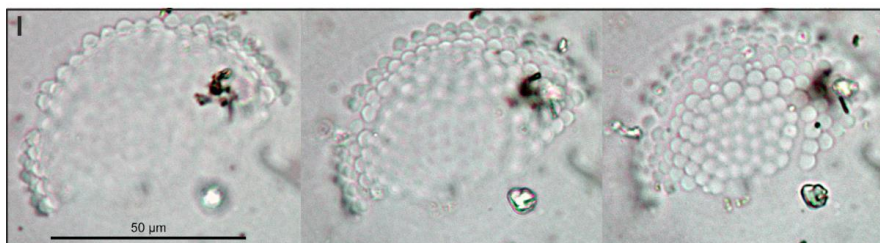
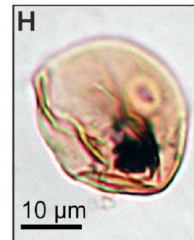
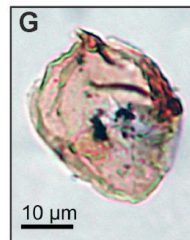
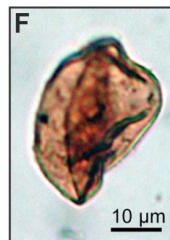
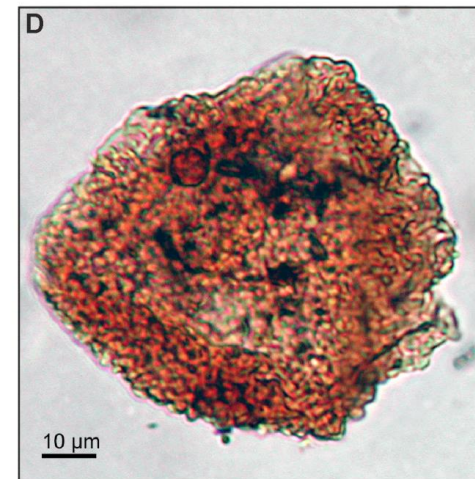
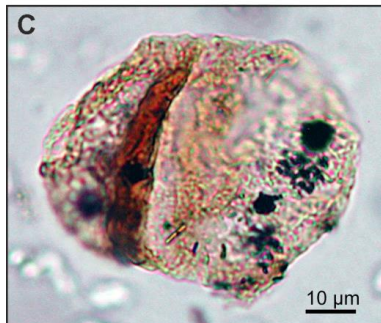
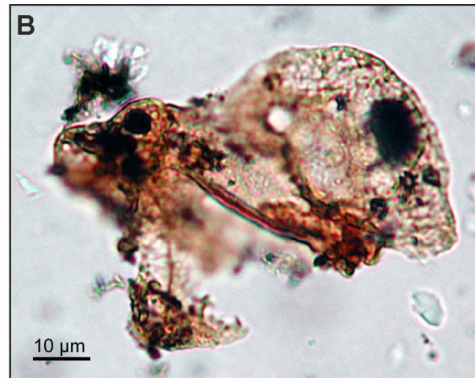
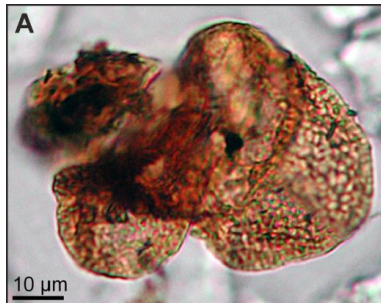
Miocene of the western and central Parathethys (Hochuli 1978). The Cupressaceae are also represented with different species. In addition to the pollen of *Taxodium/Glyptostrobus* (*Inaperturopollenites* sp., Fig. 8 F) *Sequoia* (*Sequoiapollenites* sp., Fig. 8G) is present in the sample.

Compared to the gymnosperm pollen the fern spores and pollen grains of angiosperms are rare in the sample. Among the spores *Leiotriletes* sp. (Schizaeaceae, Fig. 8 E) occurs regularly, whereas angiosperms are represented only by a single pollen grain (Fig. 8 H). It is a monoporate pollen of the Poaceae. Such pollen are so far unknown from the Paleogene of Spitsbergen. This may indicate a contamination of the sample with an extant pollen or indicates an Oligocene to Miocene age of the sample, since fossil records of Poaceae in Scandinavia have only been known since that time (e.g., Larsson et al. 2009). Nevertheless, due to a possible contamination this pollen grain should not be considered for stratigraphic statements.

Generally, in the Arctic region it can be distinguished between forests of the older Paleogene (Paleocene/Eocene) and forests of the younger Paleogene to Neogene (Oligocene/Miocene). The latter are composed of conifers related to *Pinus*, *Picea*, *Tsuga* and *Taxodium*, with a minor element of angiosperms but relatively common ferns (Boulter and Manum 1996). This composition is different from the Paleocene/Eocene floras that were also rich in conifers, but had a richer and more diverse angiosperm element and especially lacked *Tsuga* relatives (Boulter and Manum 1996).

Livšić (1974) has analyzed Paleogene deposits on Spitzbergen and provided a fairly accurate compilation of pollen assemblages from the Paleocene to the Oligocene. In his compilation the fern spores are diverse in all Paleogene deposits and therefore cannot be used as stratigraphically relevant fossils. Among the pollen of gymnosperms *Taxodium* pollen are distributed in the complete Paleogene, but especially in the Upper Paleocene and Lower Eocene in high numbers. In sample OSL-17-21 they are present, but are not among the dominating elements. Pollen of *Tsuga* are restricted to the younger Paleogene and Miocene (Boulter and Manum 1996). Because of the lack of a characteristic equatorial fringe the *Tsuga* pollen in sample OSL-17-21 and the *Tsuga* pollen described by Manum (1962) from the Sarsbukta locality on Spitsbergen are nearly identical.

⇒**Fig. 8:** Palynomorphs and a diatom from sample OSL-17-21: (A) – (C) Pinaceae *Pinus* or *Cathaya* (*Pityosporites labdacus*), (D) Pinaceae, *Tsuga* (*Tsugaepollenites viridifluminipites*), (E) Schizaeaceae (*Leiotriletes* sp.), (F) Cupressaceae (*Taxodium*-, *Glyptostrobus*-type, *Inaperturopollenites* ssp.), (G) Cupressaceae, *Sequoia* (*Sequoiapollenites* sp.), (H) Poaceae (*Graminidites* sp.), (I) diatom fragment



The pollen assemblage of Sarsbukta was dated by Boulter and Manum (1996) as Middle Oligocene and by Cepek and Krutzsch (2001) as Upper Eocene to Lower Oligocene. Today, *Tsuga* lives in cool, dark and humid conditions and favored therefore the climate conditions of the high Arctic during the Oligocene and Miocene (Boulter and Manum 1996). They were not distributed in Spitsbergen during the relatively warm climatic optima of the Upper Paleocene and Lower and Middle Eocene.

Among the Angiosperm pollen especially pollen of *Ulmus*, *Corylus* and *Erica* are according to Livšic (1974) restricted to the Oligocene. The relative diverse mixed forest on Spitsbergen for Paleogene and Eocene times, which has been described by Cepek and Krutzsch (2001), is composed of Normapolles elements such as *Trudopollis* or *Triatriopollenites* in the Paleocene and of *Alnus*, *Juglans*, *Carya*, *Pterocarya* and further elements which are represented by diverse tricolpate and tricolporate pollen during the Eocene. An occurrence of Poaceae in the older and younger forest communities has not been described so far. Therefore, stratigraphically relevant angiosperm pollen are not included in the sample.

In conclusion, especially the occurrence of *Tsuga* pollen and the abundant evidences of other conifer pollen strongly indicate a **Lower to Middle Oligocene age** of the sample. Nevertheless, the absence of angiosperm pollen should be mentioned, which would have significantly supported an exact dating.

Sample OSL-17-22:

Similar as in sample OSL-17-19 only a single poorly preserved pollen of the Cupressaceae (Taxodium- or Glyptostrobus-type, *Inaperturopollenites* sp.) has been recognized. *Taxodium/Glyptostrobus* are distributed in Spitsbergen during the complete Paleogene (Livšic 1974), Therefore, the single grain does not allow a more precise dating than Paleogene



Fig. 9: Sample OSL-17-22: ?*Inaperturopollenites* sp.

Overall view of the results

The sediments from the Paleogene of Spitsbergen are often barren of palynomorphs or contain only a few, often poorly preserved, taxa, which do not allow a precise stratigraphic assignment that is more detailed than a general Paleogene classification (Cepek and Krutzsch 2001). Accordingly, four of the samples, which were studied here, are completely barren of palynomorphs and another five samples are characterized by such a small number of palynomorphs that an exact stratigraphic dating is hardly possible. Only one of the samples, sample OSL-17-21, is characterized by a diverse

palynoflora. The assemblage points clearly to a stratigraphic age of the sample between the Lower and Middle Oligocene. This sample would also allow a detailed quantitative study of the pollen and spore inventory for a detailed reconstruction of the paleoenvironment of a coastal vegetation.

References

- Boulter, M. C. and Manum, S. B. (1989). The Brito-Arctic Igneous Province flora around the Paleocene/Eocene boundary. In: Eldholm, O; Thiede, J; Taylor, E; et al. (eds.), *Proceedings of the Ocean Drilling Program, Scientific Results*. 104, 663 – 680.
- Cepek, P. and Krutzsch, W. (2001). Conflicting Interpretations of the Tertiary Biostratigraphy of Spitsbergen and New Palynological Results. *Geologisches Jahrbuch B* 91, 551-599.
- De Jonghe, A., Hart, M. B., Grimes, S. T., Mitlehner, A. G., Price, G. D. and Smart, C. W. (2011). Middle Eocene diatoms from Whitecliff Bay, Isle of Wight, England: stratigraphy and preservation. *Proceedings of the Geologists' Association* 122, 472–483
- Gradstein, F. M., Kaminski, M. A. and Berggren, W. A. (1988). Cenozoic foraminiferal biostratigraphy of the Central North Sea. *Abhandlungen der Geologischen Bundesanstalt* 41, 97-108.
- Hochuli, P. A. (1978). Palynologische Untersuchungen im Oligozän und Untermiozän der Zentralen und Westlichen Paratethys. *Beiträge Paläont. Österreich* 4, 1-132.
- Kaiser, M. L. and Ashraf, R. (1974). Gewinnung und Präparation fossiler Pollen und Sporen sowie anderer Palynomorphae unter besonderer Berücksichtigung der Siebmethode. *Geologisches Jahrbuch, Reihe A* 25, 85–114.
- Larsson, L.M., Vajda, V., Dybkjær, K. 2009. Vegetation and climate in the latest Oligocene–earliest Miocene in Jutland, Denmark. *Review of Palaeobotany and Palynology* 159, 166-176
- Livšic, J. J. (1974). Paleogene deposits and the platform structure of Svalbard. *Norsk Polarinstitut Skrifter* 159.
- Manum, S. (1962). Studies in the Tertiary Flora of Spitzbergen, with notes on Tertiary floras of Ellesmere Island, Greenland, and Iceland: a palynological investigation. *Norsk Polarinstitut Skrifter* 125.
- Mathiesen, J. (1932): Notes on some fossil plants from east Greenland. *Medd. om Greenland* 85, 4.
- Mitlehner, A.G. (1996). Palaeoenvironments in the North Sea Basin around the Paleocene-Eocene boundary: evidence from diatoms and other siliceous microfossils. In: Knox, R. W. O'B., Corfield, R. M. & Dunay, R. E. (eds), *Correlation of the Early*

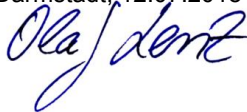
Paleogene in Northwest Europe, Geological Society Special Publication No. 101, pp. 255-273.

Oreshkina, T. V. (2012). Evidence of Late Paleocene - Early Eocene hyperthermal events in biosiliceous sediments of Western Siberia and adjacent areas. *Austrian Journal of Earth Sciences* 105, 145-153.

Scherer, R.P. and Koç N. (1996): Late Paleogene diatom biostratigraphy and paleoenvironment of the northern Norwegian-Greenland Sea. In: Thiede, J., Myhre, A.M., Firth, J.V., Johnson, G.L., and Ruddiman, W.F. (Eds.), *Proceedings of the Ocean Drilling Program, Scientific Results*. 151, 75-99.

Traverse, A. (2007): *Paleopalynology*. Second Edition. Springer, Dordrecht, The Netherlands, 813 p.

Darmstadt, 12.07.2018



K-Ar dating of the fault gouge



 NORGES
 GEOLOGISKE
 UNDERSØKELSE

7491 TRONDHEIM
 Tlf.: 73 90 40 00
 E-mail: lab@ngu.no

K-Ar dating
 GEOLOGICAL MATERIAL
 CONTRACT nr. 2017.0207

Contract 2017.0207
Project 360900
Customer Per Terje Osmundsen / Morgan Ganerød
Number of samples 5
Sample type Clay Size fractions from a fault gouge

Quality Control Ar-analysis

Comment All analyses ran normally.

| Standards run in same batch | Standard | Measured Age (Ma) | 1 σ (Ma) | Reference age (Ma) | Reference |
|-----------------------------|----------|-------------------|------------------|--------------------|-----------|
| | HD-B1 | 24.13 | ± 0.17 | 24.13 ± 0.17 | |
| HD-B1 | 24.13 | ± 0.17 | 24.13 ± 0.17 | | |
| HD-B1 | 24.10 | ± 0.17 | 24.13 ± 0.17 | | |

| Ar measurements in same batch | n | ⁴⁰ Ar/ ³⁹ Ar | 1 σ | ³⁹ Ar/ ³⁹ Ar | 1 σ |
|-------------------------------|---|------------------------------------|------------|------------------------------------|------------|
| | | 50 | 299.2852 | ± 0.014 | 0.189988 |

K-analyses completed by: Ruikai Xie
PHD, Analyst ICP-OES Date: 25/07/18

Ar-analyses completed by: Roelant van der Leijl
PHD, Analyst mass spectrometry Date: 28/05/18

Report completed by: Roelant van der Leijl
PHD, Senior Engineer Geochronology Date: 06/08/18

| | |
|---|---|
| Sample weighing and loading | Air dried, homogenized clay materials and standards were wrapped in molybdenum envelopes, and the net mass of the aliquots was determined using a Mettler Toledo XPE26DR microbalance fitted with an antistatic ionizer. The microbalance has resolution of 2 µg and a measured reproducibility of 4 µg (1σ). The samples and standards were left overnight in a drying oven at 105 ± 3°C, and weighed again to determine the dry weight and relative humidity loss. The molybdenum envelopes were subsequently loaded into an ultra high vacuum extraction line, and baked at a maximum temperature of 120°C to eliminate excess water following the recommendations of Clauer and Chaudhuri (1995). |
| Argon extraction and purification | Argon was extracted from the aliquots in a Pond Engineering double vacuum resistance furnace. During heating, bulk sample gas was expanded directly into a stainless steel vessel housing a freshly activated Titanium Sublimation Pump, to strip the sample gas from a majority of reactive gases including H ₂ O, N ₂ , O ₂ , CO and CO ₂ (O'Hanlon, 2005). A known molar amount of pure ³⁹ Ar spike (Schumacher, 1975) was prepared using a 0.2 cc gas pipette attached to a 4 litre reservoir, and was mixed with the purified sample gas. The gas mixture was subsequently isolated in a second cleanup stage and exposed for 10 minutes to two SAES GP50 getter cartridges with ST101 Zr-Al alloy, one of which was kept at 350°C and one at room temperature, to remove residual reactive gases including H ₂ and CH ₄ . |
| Sample degas conditions | Furnace 20 minutes 1400± 10°C |
| Determination of radiogenic ⁴⁰Ar* | Argon isotopes were determined on an IsotopX NGX multicollector noble gas mass spectrometer using faraday cups fitted with 10 ¹² Ω amplifiers, except for ⁴⁰ Ar which was measured using a faraday fitted with a 10 ¹¹ Ω amplifier. Time-zero beam intensities were measured for 30 cycles of 20 1-second integrations, and time-zero intensities were calculated using exponential regressions back to gas inlet time. Furnace blanks were run regularly between samples, and generally had Ar compositions close to atmospheric argon. Instrument mass discrimination was determined using aliquots of argon purified from air, and compared with the reference value of 298.56±0.31 (Lee et al., 2006). The ³⁹ Ar spike pipette was calibrated using GA-1550 biotite with ⁴⁰ Ar* = 1.342±0.007 x 10 ⁻⁹ mol/g (McDougall and Wellman, 2011) and HD-B1 biotite (Fuhrmann et al., 1987) with a ⁴⁰ Ar* = 3.351±0.01 x 10 ⁻¹⁰ mol/g (Charbit et al., 1998). The overall standard deviation of the pooled spike calibrations by combined GA1550 and HD-B1 is <0.3 %. The accuracy of the ⁴⁰ Ar* determinations was monitored within batch by HD-B1 biotite. |
| Detector scan time | 30 cycles with 20 1-second integrations |
| Determination of K | Potassium concentration was determined by digesting a sample aliquot of 10-30 mg sample material in Li ₂ B ₄ O ₇ flux at a temperature of 1000±50 °C in palladium crucibles. The resulting glass was subsequently dissolved in HNO ₃ , and analysed on a Perkin Elmer Optima 4300 DV ICP-OES. 1σ uncertainties are estimated from the reproducibility of a range of standards with K concentrations between 0.19%K and 8.3%K and take into account the signal strength of K during analysis. Mean standard deviations of all measured standards overlap with published reference values, and their published standard deviations. |
| Age calculations | K-Ar ages were calculated using the ⁴⁰ K decay constants, abundance and branching ratio of Steiger and Jaeger (1977). Atmospheric argon corrections were performed using the relative abundances of ³⁹ Ar, ³⁸ Ar and ³⁶ Ar of Lee et al. (2006; ³⁹ Ar/ ³⁶ Ar = 298.56±0.31). Uncertainties were estimated using the error equation for multicollector isotope dilution measurements from Halas and Wojtowicz (2014) modified to take into account the uncertainty on mass discrimination. |
| References | <ul style="list-style-type: none"> • Charbit, S., Guillou, H., Turpin, L., 1998. Cross calibration of K-Ar standard minerals using an unspiked Ar measurement technique. <i>Chemical Geology</i> 150, 147–159. • Clauer, N., Chaudhuri, S., 1995. Clays in crustal environments. Isotope tracing and dating. Berlin, Springer-Verlag. • Fuhrmann, U., Lippolt, H., Hess, J.C., 1987. HD-B1 Biotite reference material for K-Ar chronometry. <i>Chemical Geology</i> 66, 41–51. • Halas, S., Wojtowicz, A., 2014. Propagation of error formulas for K/Ar dating method. <i>Geochronometria</i> 41, 202–206. • Lee, J.-Y., Marti, K., Severinghaus, J.P., Kawamura, K., Yoo, H.-S., Lee, J.B., Kim, J.S., 2006. A redetermination of the isotopic abundances of atmospheric Ar. <i>Geochimica et Cosmochimica Acta</i> 70, 4507–4512. • McDougall, I., Wellman, P., 2011. Calibration of GA1550 biotite standard for K/Ar and 40 Ar/39 Ar dating. <i>Chemical Geology</i> 280, 19–25. • Odin, G.S., 1982. Numerical dating in stratigraphy. John Wiley & Sons. • O'Hanlon, J.F., 2005. A user's guide to vacuum technology. John Wiley & Sons. • Schumacher, E., 1975. Herstellung von >99,9997% 38Argon für die 40K-40Ar Geochronologie. <i>Chimia</i> 29, 441–442. • Steiger, R.H., Jäger, E., 1977. Subcommittee on geochronology: convention on the use of decay constants in geochronology and cosmochronology. <i>Earth and Planetary Science Letters</i> 36, 359–362. |

Apatite and zircon fission track

| Sample | Long | Lat | m | ASI | Analysis | Comment |
|--------|----------|----------|----|----------|----------|---|
| SI05 | 12.92800 | 78.53440 | 0 | AFT/Prag | 0 | Fine to medium grained metagabbro; Good prospects |
| SI09 | 13.07381 | 78.51284 | 10 | AFT | 0 | Medium grained quartzite; hopeful possibility |
| KKF04 | 11.26030 | 78.55260 | 0 | AFT | 0 | Indurated sandstone |
| KKF11 | 11.38530 | 78.54750 | 0 | AFT | 0 | Indurated sandstone |
| KKF18 | 11.22900 | 78.58690 | 0 | AFT | 0 | Dirty sandstone just below conglomerate layer |

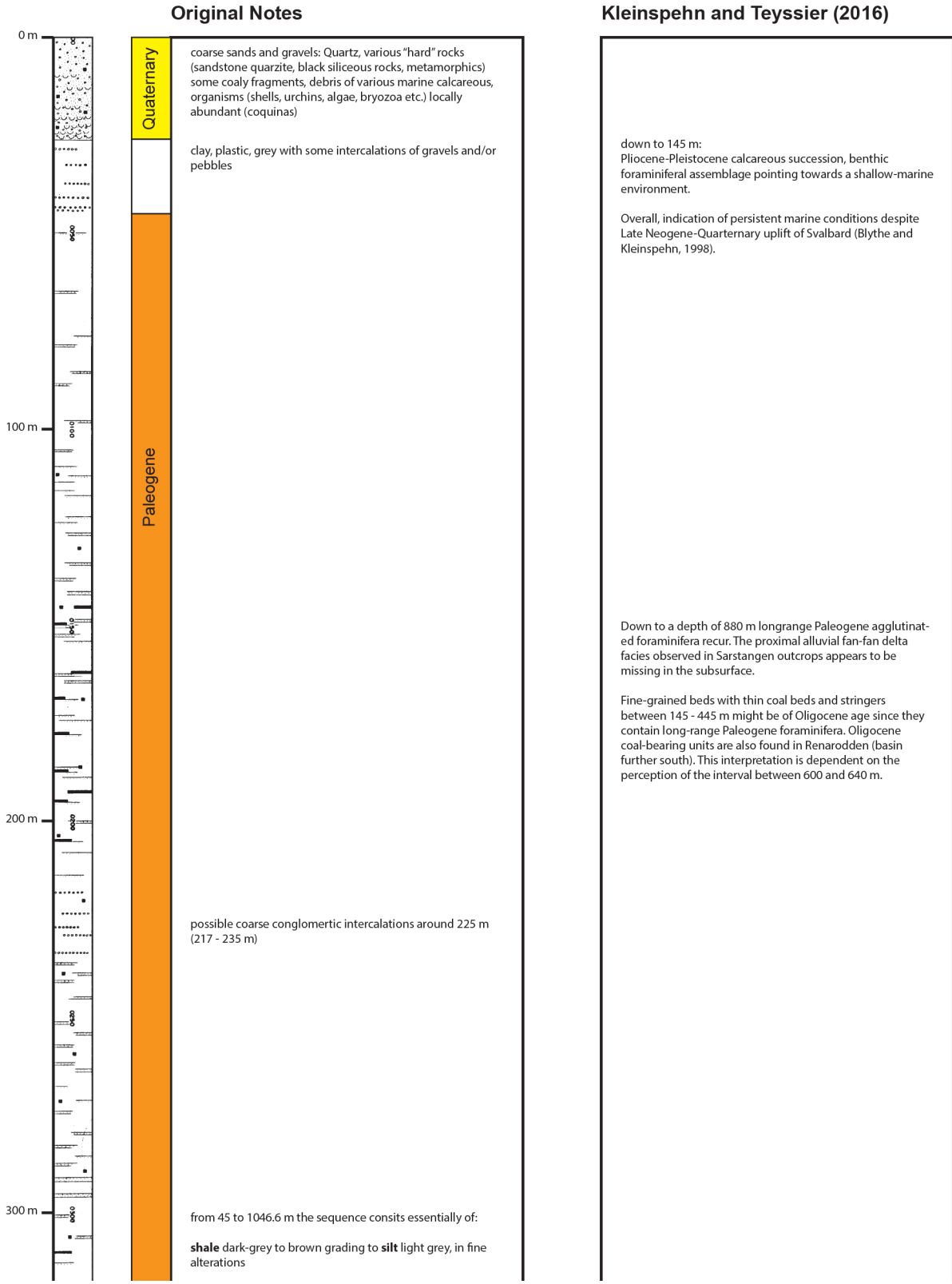
| ZFT Results | | Pool'd ZFT | | 95% conf | | 95% conf | | Rho | | Rho 1 sigma | | Chi2 | | mean U pp | | mean TH p | | mean Sm ppm | |
|-------------|----------|------------|----------|----------|-------|----------|----------|----------|-------|-------------|----------|----------|----------|-----------|----------|-----------|----------|-------------|----------|
| Age (Ma) | Interval | Age (Ma) | Interval | Interval | spots | Tracks | Rho | Interval | spots | Tracks | Interval | spots | Tracks | Interval | spots | Tracks | Interval | spots | Tracks |
| 11.26030 | 78.55260 | 175.03 | 17.87 | 19.87 | 20 | 2972 | 6.72E-07 | 3.33E-08 | 20 | 4744 | 6.08E-07 | 2.98E-08 | 111.1543 | 168102.4 | 228371.5 | 3.78 | 4.88 | 172282 | 212277.3 |
| 11.38530 | 78.54750 | 305.49 | 29.72 | 32.84 | 20 | 4744 | 6.08E-07 | 2.98E-08 | 20 | 5576 | 8.32E-07 | 3.8E-08 | 56.0556 | 178161.1 | 189450.5 | 3.39 | 3.78 | 178161.1 | 189450.5 |
| 11.22900 | 78.58690 | 263.17 | -24.3 | 26.72 | 20 | 5576 | 8.32E-07 | 3.8E-08 | 20 | 5576 | 8.32E-07 | 3.8E-08 | 56.0556 | 178161.1 | 189450.5 | 3.39 | 3.78 | 178161.1 | 189450.5 |

| AFT Results | | Pool'd AFT | | 95% conf | | 95% conf | | Rho | | Rho 1 sigma | | Chi2 | | mean U pp | | mean TH p | | mean Sm p | | MTL | | Std err | | Std dev | | tracks | | mean Dpar | | | |
|-------------|----------|------------|----------|----------|-------|----------|----------|----------|-------|-------------|----------|----------|----------|-----------|--------|-----------|----------|-----------|--------|----------|-------|---------|----------|---------|--------|----------|-------|-----------|----------|-------|--------|
| Age (Ma) | Interval | Age (Ma) | Interval | Interval | spots | Tracks | Rho | Interval | spots | Tracks | Interval | spots | Tracks | Interval | spots | Tracks | Interval | spots | Tracks | Interval | spots | Tracks | Interval | spots | Tracks | Interval | spots | Tracks | Interval | spots | Tracks |
| 12.92800 | 78.53440 | 125.62 | 8.84 | 9.5 | 40 | 1021 | 6.66E-05 | 6.24E-07 | 40 | 1021 | 6.66E-05 | 6.24E-07 | 116.6027 | 2.16 | 6.78 | 24.11 | 200.22 | 13.69 | 0.17 | 1.63 | 94 | 1.99 | | | | | | | | | |
| 13.05840 | 78.51340 | 39.9 | 20.11 | 40.4 | 40 | 48 | 9.92E-06 | 3.17E-06 | 40 | 48 | 9.92E-06 | 3.17E-06 | 41.2384 | 2.39 | 50.9 | 49.72 | 342.01 | 13.81 | 0.28 | 1.67 | 36 | 2.05 | | | | | | | | | |
| 11.26030 | 78.55260 | 122.5 | 27.24 | 34.93 | 23 | 65 | 4.35E-06 | 8.75E-08 | 23 | 65 | 4.35E-06 | 8.75E-08 | 17.3285 | 2.3 | 194.71 | 3285.58 | 325.02 | 14.09 | 0.33 | 1.13 | 13 | 1.92 | | | | | | | | | |
| 11.38530 | 78.54750 | 26.43 | 3.66 | 4.51 | 39 | 170 | 5.31E-05 | 4.36E-07 | 39 | 170 | 5.31E-05 | 4.36E-07 | 132.8229 | 2.15 | 20.39 | 162.1 | 242.55 | 14.11 | 1.8 | 1.55 | 42 | 1.87 | | | | | | | | | |
| 11.22900 | 78.58690 | 34.38 | 3.9 | 4.4 | 40 | 306 | 7.34E-05 | 6.8E-07 | 40 | 306 | 7.34E-05 | 6.8E-07 | 287.592 | 2.29 | 84.29 | 836.81 | 265.05 | 13.96 | 0.29 | 1.51 | 28 | 1.94 | | | | | | | | | |

means there are far too few data...

Appendix 6: Summary of the apatite and zircon fission track results, provided by Tim Redfield (NGU).

Composite log of the 7811/5-1 Sarstangen petroleum exploration well





from 45 to 1046.6 m the sequence consists essentially of:

shale dark-grey to brown grading to **silt** light grey, in fine alterations

with

occasional streaks of thin beds of **sandstones**, generally coarse to microconglomeratic, poorly sorted, pyritic, probably with shale laminations.

conglomerates with various elements of "old, hard" rocks such as quartz, quartzite, siltstone, siliceous black rock, metamorphics (phyllite, micashist), dolomite (?)

mica and **pyrite** frequent to abundant, both in shale and in sandstone

frequent traces of coal (probable thin coaly streaks in the intervals 145 - 205 and 310 - 480 m)

presence of **dispersed carbonaceous matter** in the whole sequence

occasional traces of calcite (veinlets? nodules?)

presence of foraminifera (F)

@ 394 and 396 m few fragments of calcite (veinlet, nodule?) impregnated with **live oil** (see shows column)

between 545 and 770 m, the "sandy" intercalations are relatively frequent and well developed

below the 7 5/8 casing shoe, the logs provide a better definition of the sandy beds.

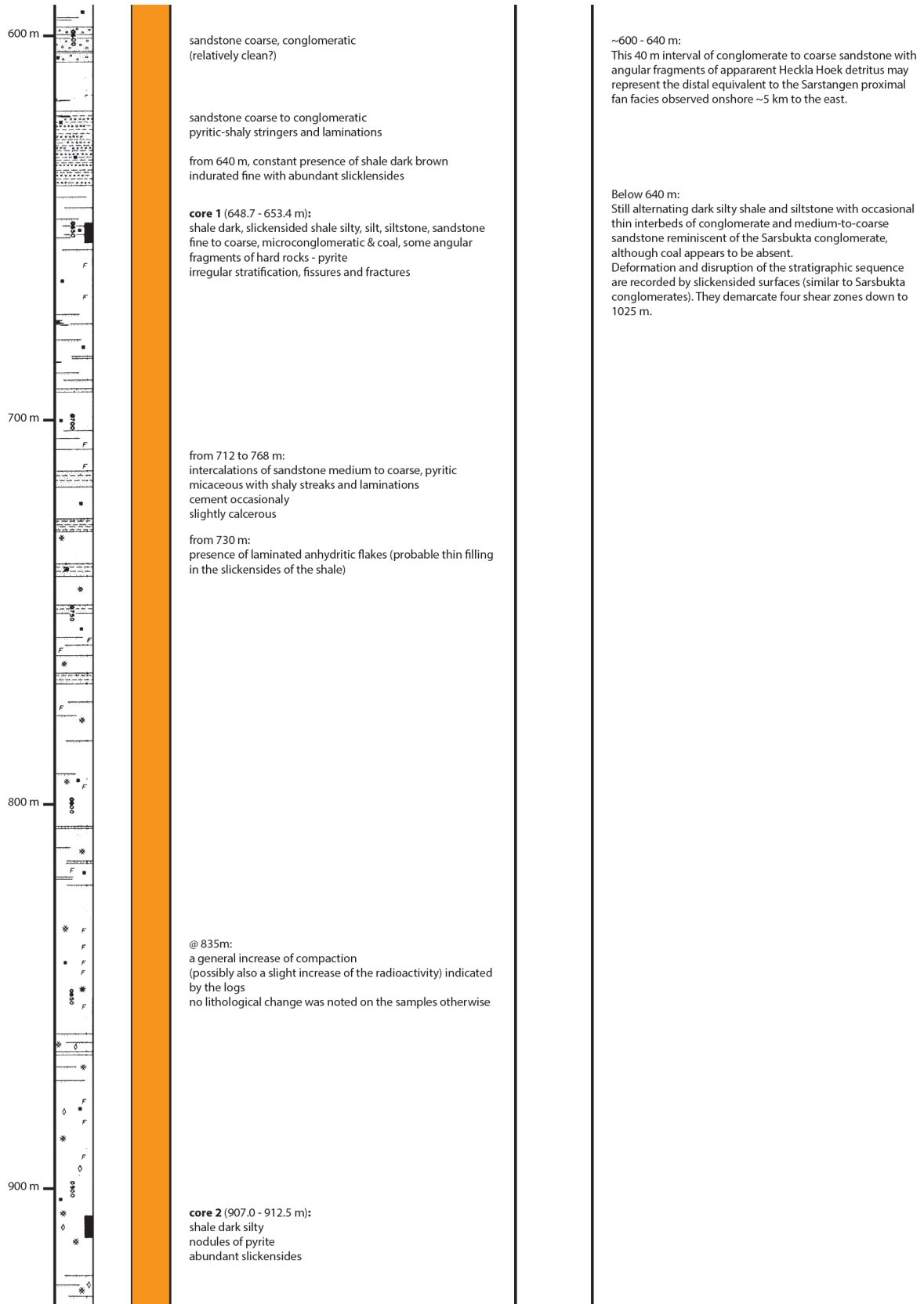
sandstones coarse, conglomeratic with stringers and laminations of shale

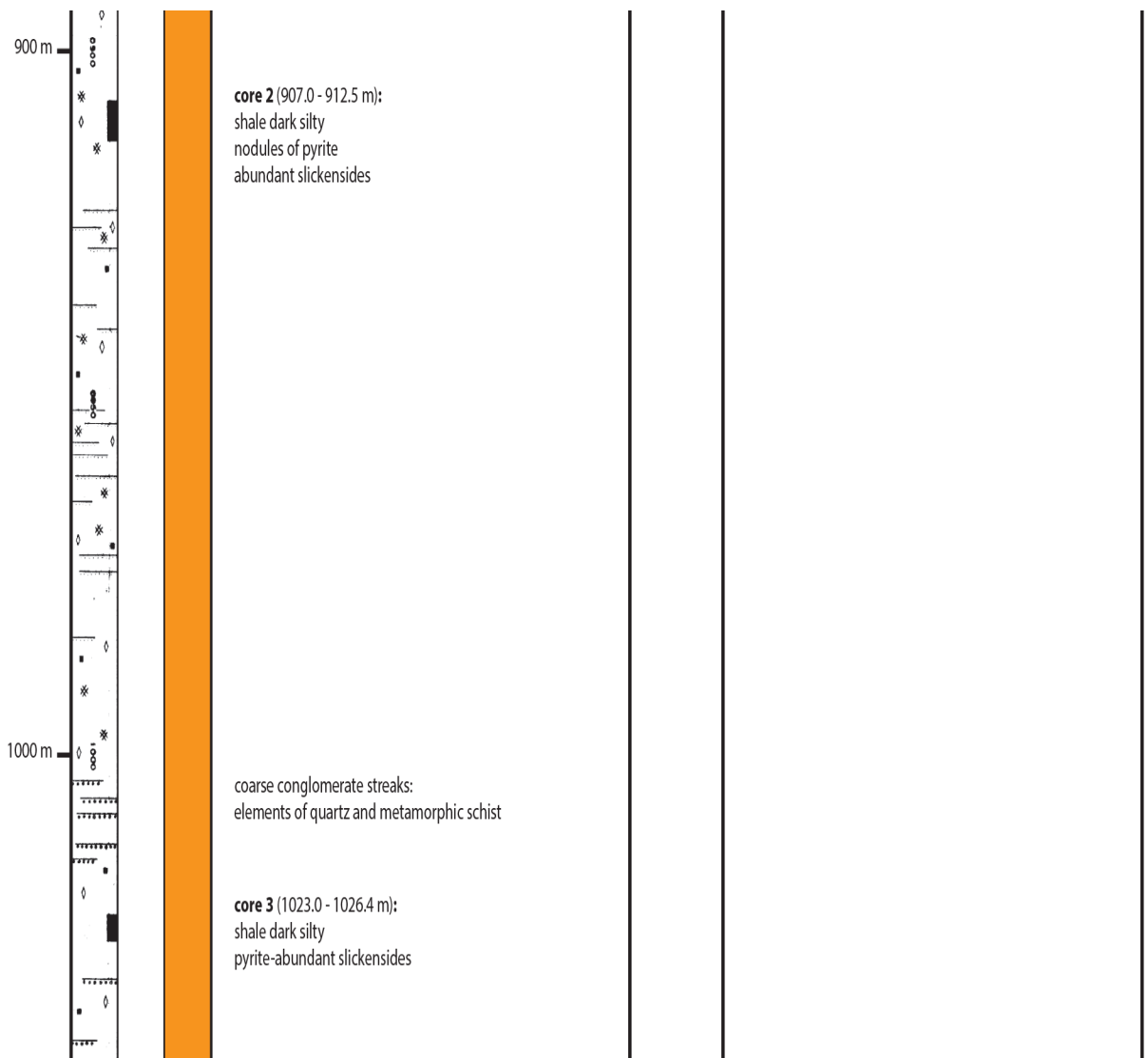
fragments of pyritized wood

sandstone coarse, conglomeratic (relatively clean?)

sandstone coarse to conglomeratic pyritic-shaly stringers and laminations

~600 - 640 m:
This 40 m interval of conglomerate to coarse sandstone with angular fragments of apparent Heckla Hoek detritus may represent the distal equivalent to the Sarstangen proximal fan facies observed onshore ~5 km to the east.





Appendix 7: Lithological log of the 7811/5-1 Sarstangen petroleum exploration well drilled by Norsk Polar Navigasjon AS with original annotations and the interpretation from Kleinspehn and Teyssier (2016). Raw data kindly provided by Asbjørn Skotte.

Abstract NGF wintermeeting 2019

Norwegian Geological Society – Winter Conference 2019

Tectono-stratigraphic evolution of the Forlandsundet Graben – new insights from Sarsøyra, Western Svalbard, Arctic Norway

Schaaf, Niklas W.^{1,2}, Osmundsen, Per Terje^{3,1}, Schönenberger, Jasmin⁴, van der Lelij, Roelant⁴, Lenz, Olaf⁵, Senger, Kim²

¹ Department of Geosciences, University of Oslo, niklas.schaaf@posteo.de

² Department of Arctic Geology, The University Centre in Svalbard

³ Department of Geoscience and Petroleum, Norwegian University of Science and Technology

⁴ NGU Laboratory, Geological Survey of Norway

⁵ Senckenberg Society for Nature Research, Frankfurt am Main

During the Paleogene, the western Svalbard margin evolved from a fold-and-thrust-belt into a sharply tapered transtensional margin. The Forlandsundet Graben represents a unique opportunity to study this transition. It is situated between Spitsbergen and Prins Karls Forland, along the inner border of a very narrow necking domain between the West Svalbard orogen and the Molloy and Knipovitch spreading ridges.

We report new structural, sedimentological and geochronological data, collected during two field seasons at Sarsøyra on the eastern margin of the Forlandsundet Graben. The basin is bounded in the east by a N-S trending fault zone, exhibiting a graben to half-graben geometry. Crosscutting relationship of the basin-bounding oblique normal faults with structures of the Paleocene-Eocene West Spitsbergen fold-and-thrust-belt favor an Oligocene age, albeit age-relationships are debated. New paleontological data support an Oligocene age for at least parts of the basin.

We describe the contact relationships to metamorphic basement along the eastern basin margin, and provide new kinematic data from the basement as well as from the basin fill (~400 measurements). A gouge from a deformed zone in the basement close to the contact was dated, using K-Ar geochronology. The basin fill comprises coarse continent-derived siliciclastics and finer marine deposits. We document facies relationships in the eastern parts of the basin in detail (~370m logs), including a previously poorly described fluvial succession in the northern part of the study area. We also provide new paleocurrent data (>100 measurements). Based on field observations and the revision of existing subsurface data, we discuss the implications of our results on alternative basin models, including deposition in a piggy back basin with subsequent transtensional basin formation. We further discuss whether Prins Karls Forland might represent a metamorphic core complex. We propose that the outcrops along the eastern basin margin represent successions deposited under dextral NW-SE transtension.